

Impacts of rudder configurations on inland vessel manoeuvrability

Liu, Jialun

DOI

[10.4233/uuid:bef6c12f-5804-407b-a4c6-f7949541f21c](https://doi.org/10.4233/uuid:bef6c12f-5804-407b-a4c6-f7949541f21c)

Publication date

2017

Document Version

Final published version

Citation (APA)

Liu, J. (2017). *Impacts of rudder configurations on inland vessel manoeuvrability*. [Dissertation (TU Delft), Delft University of Technology]. <https://doi.org/10.4233/uuid:bef6c12f-5804-407b-a4c6-f7949541f21c>

Important note

To cite this publication, please use the final published version (if applicable).
Please check the document version above.

Copyright

Other than for strictly personal use, it is not permitted to download, forward or distribute the text or part of it, without the consent of the author(s) and/or copyright holder(s), unless the work is under an open content license such as Creative Commons.

Takedown policy

Please contact us and provide details if you believe this document breaches copyrights.
We will remove access to the work immediately and investigate your claim.

Impacts of Rudder Configurations on Inland Vessel Manoeuvrability

Jialun LIU

Impacts of Rudder Configurations on Inland Vessel Manoeuvrability

Proefschrift

ter verkrijging van de graad van doctor
aan de Technische Universiteit Delft,
op gezag van de Rector Magnificus prof. ir. K. C. A. M. Luyben,
voorzitter van het College voor Promoties,
in het openbaar te verdedigen
op maandag 27 februari 2017 om 12:30 uur

door

Jialun LIU

Master of Science, Wuhan University of Technology, China
geboren te Fushun, Liaoning, China.

This dissertation has been approved by the

promotor: Prof. ir. J. J. Hopman
copromotor: Dr. ir. R. G. Hekkenberg

Composition of the doctoral committee:

Rector Magnificus, chairperson
Prof. ir. J. J. Hopman, Delft University of Technology, promotor
Dr. ir. R. G. Hekkenberg, Delft University of Technology, copromotor

Independent members:

Prof.dr.-ing. B. O. el Moctar, University of Duisburg-Essen
Prof. dr. H. Yasukawa, Hiroshima University
Prof. dr. ir. R. H. M. Huijsmans, Delft University of Technology
Prof. dr. D. J. E. M. Roekaerts, Delft University of Technology
Dr. ir. H. J. de Koning Gans, Delft University of Technology

The author of this thesis was financially supported by the China Scholarship Council (CSC) under Grant 201206950025.



Published and distributed by: Jialun Liu

Contact: jialunliu@outlook.com

Homepage: <http://www.jialunliu.com>

Keywords: inland vessels, inland vessel manoeuvrability, ship manoeuvrability, rudder configurations, manoeuvring simulations, rudder profiles, rudder parameters, rudder design, rudder hydrodynamic characteristics, Computational Fluid Dynamics

Copyright © 2017 by JialunLiu.

All rights reserved. No part of the material protected by this copyright notice may be reproduced or utilised in any form or by any means, electronic or mechanical, including photocopying, recording or by any information storage and retrieval system, without the prior permission of the author.

ISBN 978-94-6233-5622

An electronic version of this dissertation is available at <http://repository.tudelft.nl>.

*To my fiancée Shijie,
my muse.*

Jialun Liu

Preface

Finally, it is the time for me to write a summary of the journey to my doctoral title. When I look back, I feel grateful for everything that happened in the last four years, no matter good nor bad, because all these experiences made me a better man. I would like to thank all the people that helped, encouraged, and accompanied me and apologise for my mistakes, careless, and rudeness. See you sometime somewhere. I believe what Karel Čapek (1890 – 1938) said, “*Life is not to have fun, it is to suffer, be enchanted, be amazed.*” When misfortune happens, people cherish more of what they have had and work harder for a better future. And that is how I accomplished my PhD.

I would like to thank my daily supervisor Dr. ir. Robert Hekkenberg. It was you that helped me out of the chaos at the start of my study. You did not only teach me how to do research but also how to think as a researcher. You never criticised my mistakes, which I surely made a lot, but encouraged and inspired me. Thank you for helping me to improve. I am very grateful to my promoter Prof. ir. Hans Hopman. Thank you for all your help and support. Your excellent guidance and valuable comments clarified my ideas and pushed me in the right direction.

I am sincerely thankful to Ir. Frans Quadvlieg from Maritime Research Institute Netherlands (MARIN). Thank you for sharing your wisdom with me. It was hard to catch you for a discussion but that was what I really looking forward to. Your great experience and knowledge helped me to gain insights into the world of manoeuvring. I would like to thank Dr. ir. Hank de Koning Gans. It was fun and fruitful to have discussions with you. Many thanks for your assistance in my study.

Special gratitudes must be made to my master promoter Prof. Mingjun Liu. Thank you so much for your guidance and support. I would like to thank Prof. Yanmin Xu that gave me the very first lecture of ship manoeuvrability and encouraged me to continue studying. I would like to express my thanks to Prof. Junmin Mou who encouraged me to apply for the scholarship at the very last minute. That is where the whole story began. In addition, I gratefully acknowledge the grant from China Scholarship Council (CSC).

Furthermore, I would like to thank all my colleagues in the section of Ship Design, Production, and Operation. I would like to express my gratitude to Ir. Erik Rotteveel, Dr. ir. Etienne Duchateau, Ir. Peter de Vos, and Dr. Milinko Godjevac. Many thanks for helping me to settle down and know around. You all helped me a lot in many ways, such as coding in MATLAB, handling with LaTeX, writing in English, and understating the engines.

I would like to say thank you to Qu Hu, Xiao Liang, and Wenhua Qu. Thanks for joining in the adventures in Iceland and around the Mount Blanc. Many thanks go to Fangliang Xiao, Yang Zhou, Yamin Huang, and Linying Chen. With your accompany, I can still feel Wuhan even though I am thousands of miles away. I thank all my friends that are always so kind to me, not only in the Netherlands but also in China. I might not be a good friend of keeping in contact, but you all know that I am always willing to help.

I would like to thank my parents, Jianzhang Liu and Fengjun Zhang, for their endless

love and support. You taught me to be good, honest, and humbled and I would not let you down. Finally, I would like to thank my fiancée, Dr. Shijie Li. I am proud of you and grateful for everything that you have done for me. Words cannot describe how lucky I am to have you in my life. Let's explore the world, hand in hand.

Jialun Liu
Delft, February 2017.

Summary

Ship manoeuvrability is fundamental for the navigation safety of ships. Furthermore, through the equipment used for manoeuvring, it also affects investment, operation, and maintenance cost of these ships. Ships are primarily designed from an economic point of view. To ensure and improve the maritime efficiency, research on inland vessel manoeuvrability deserves more attention than the present situation. Most of the research on manoeuvrability has been performed for seagoing ships. Since sailing conditions and ship particulars between seagoing ships and inland vessels are different, the impacts of these differences on manoeuvring prediction and evaluation should be carefully considered.

Inland vessels should be designed in such a way that they should always be capable of manoeuvring without significantly harming the cost-effectiveness of operations. One of the biggest differences between seagoing ships and inland vessels is the rudder configuration. Conventionally, seagoing ships have similar single-rudder configurations while inland vessels have more complex multiple-rudder configurations. Although multiple-rudder configurations can have a positive effect on manoeuvrability, they often have a negative effect on resistance and, therefore, also a negative effect on the fuel consumption.

Quantitative impacts of the rudder configuration on ship manoeuvrability have not been fully understood, especially for multiple-rudder configurations with complex rudder profiles. These differences in the rudder configuration may significantly change the ship manoeuvring behaviours and, therefore, should require further research. Moreover, to compare and evaluate the manoeuvring performance of inland vessels with different configurations, the existing manoeuvring tests and standards for inland vessels are less elaborate than those for seagoing ships. The above-mentioned considerations formulate the following main research question:

What are the proper rudder configurations to achieve well manoeuvrable inland vessels without significant loss of navigation efficiency?

The main research question of this thesis can be answered through resolving four key research questions as follows:

- Q1. *What are the practical manoeuvres to evaluate and compare the manoeuvring performance of inland vessels?*
- Q2. *How does the rudder configuration affect the rudder hydrodynamic characteristics?*
- Q3. *How do changes in the rudder configuration affect the ship manoeuvrability in specific manoeuvres?*
- Q4. *How to choose a proper rudder configuration according to the required manoeuvring performance?*

An accurate estimation of rudder forces and moments is needed to quantify the impacts of the rudder configurations on ship manoeuvring performance. This thesis applied Reynolds-Averaged Navier-Stokes (RANS) simulations to obtain rudder hydrodynamic characteristics and integrated the RANS results into manoeuvring models. Additionally, new manoeuvres and criteria have been proposed for prediction and evaluation of inland vessel manoeuvrability. Simulations of ships with various rudder configurations were conducted to analyse the impacts of rudder configurations on ship manoeuvrability in different classic and proposed test manoeuvres. Accordingly, guidance on rudders for inland vessel manoeuvrability has been summarised for practical engineers to make proper design choices.

Through the research presented in this thesis, it is clear that different rudder configurations have different hydrodynamic characteristics, which are influenced by the profile, the parameters, and the type of a specific configuration. New regression formulas have been proposed for naval architects to quickly estimate the rudder induced forces and moments in manoeuvring. Furthermore, an integrated manoeuvring model has been proposed and validated for both seagoing ships and inland vessels. Using the proposed regression formulas and manoeuvring model, the impacts of rudder configurations on inland vessel manoeuvrability have been studied.

The manoeuvring performance of a typical inland vessel can be improved by 5% to 30% by changing the rudder configuration. The rudder configuration should be capable of providing sufficient manoeuvring forces and then optimised to reduce the rudder induced resistance. In general, well-streamlined profiles are good for efficiency but not as good as high-lift profiles for effectiveness. As a summary, the ship manoeuvring performance can be improved by using effective profiles, enlarging the total rudder area, accelerating the rudder inflow velocity, increasing the effective rudder aspect ratios, and enlarging the spacing among multiple rudders.

Contents

Preface	vii
Summary	ix
Contents	xiv
Glossary	xxi
1 Introduction	1
1.1 Research background	1
1.1.1 Applied terminologies	1
1.1.2 Inland waterway transport	2
1.1.3 Inland vessel manoeuvrability	3
1.1.4 Inland vessel rudder design	4
1.1.5 Concluding remarks	4
1.2 Problem statement	4
1.3 Research questions	6
1.4 Research boundaries	7
1.5 Thesis structure	7
2 Literature Review on Inland Vessel Manoeuvrability and Ship Rudders	11
2.1 Impact factors on inland vessel manoeuvrability	11
2.1.1 External environment factors	12
2.1.2 Internal design factors	13
2.1.3 Concluding remarks	15
2.2 Hydrodynamic force analysis	16
2.2.1 Captive model tests	16
2.2.2 Free-running tests	16
2.2.3 Open water tests	16
2.2.4 Numerical methods	17
2.2.5 Concluding remarks	17
2.3 Rudder working conditions	17
2.3.1 Reynolds numbers	19
2.3.2 Angles of attack	19
2.3.3 Concluding remarks	20
2.4 Rudder design choices	20
2.4.1 Rudder profiles	21
2.4.2 Rudder parameters	24
2.4.3 Rudder types	27
2.4.4 Relative positions	28
2.4.5 Multiple rudders	29

2.4.6	Concluding remarks	30
2.5	Rudder performance	31
2.5.1	Ship manoeuvrability	31
2.5.2	Fuel consumption	32
2.5.3	Rudder cavitation.	32
2.6	Synthesis.	33
3	Test Manoeuvres and Criteria for Inland Vessel Manoeuvrability	35
3.1	Existing manoeuvrability standards	35
3.1.1	International Maritime Organization	37
3.1.2	American Bureau of Shipping	38
3.1.3	Central Commission for the Navigation of the Rhine	38
3.1.4	European Commission	38
3.1.5	Bureau Veritas	39
3.1.6	Concluding remarks	39
3.2	Existing test manoeuvres	39
3.2.1	Existing turning circle test	39
3.2.2	Existing zigzag test.	40
3.2.3	Existing evasive action test	41
3.2.4	Existing stopping test.	42
3.2.5	Concluding remarks	43
3.3	Proposed test manoeuvres	43
3.3.1	Proposed turning circle test	43
3.3.2	Proposed hard turning test	45
3.3.3	Proposed T-junction test	45
3.3.4	Proposed lane changing test	47
3.3.5	Proposed stopping with rudder correction test.	48
3.3.6	Proposed stopping with clam shell angles test.	48
3.4	Synthesis.	50
4	Hydrodynamic Characteristics of Ship Rudders	51
4.1	Applied RANS methods	51
4.1.1	Turbulence modelling	52
4.1.2	Boundary conditions	54
4.1.3	Applied domains and meshes.	55
4.1.4	Numerical solvers	56
4.1.5	Grid independence	58
4.2	Validation of the RANS methods	59
4.2.1	Validation of the 2D RANS method.	59
4.2.2	Validation of the 3D RANS method.	60
4.3	2D RANS study on rudder hydrodynamics	61
4.3.1	Impacts of Reynolds numbers on rudder hydrodynamics	62
4.3.2	Impacts of profiles on single-rudder hydrodynamics.	63
4.3.3	Impacts of spacing on twin-rudder hydrodynamics	65
4.3.4	Impacts of profiles on twin-rudder hydrodynamics	68
4.3.5	Impacts of spacing on quadruple-rudder hydrodynamics	70

4.4	3D RANS study on rudder hydrodynamics	75
4.5	Regression study on rudder hydrodynamic coefficients	77
4.5.1	Regression study on single-rudder hydrodynamic coefficients	77
4.5.2	Regression study on twin-rudder hydrodynamics coefficients	77
4.5.3	Limitations of the regression formulas	85
4.6	Synthesis	85
5	Mathematical Modelling of Ship Manoeuvrability	87
5.1	Introduction to modelling of inland vessels	87
5.1.1	Degrees of freedom	87
5.1.2	Types of manoeuvring models	88
5.1.3	Challenges of the multiple-propeller multiple-rudder model	89
5.2	Reference ships	89
5.3	Mathematical models of ship motions	91
5.3.1	Coordinate systems	91
5.3.2	Dynamic equations	92
5.4	(Added) mass and (added) moment of inertia	93
5.4.1	Mass and moment of inertia	93
5.4.2	Added mass and added moment of inertia	94
5.5	Hull forces and moments	94
5.6	Propeller forces and moments	96
5.6.1	Propeller wake fraction	97
5.6.2	Propeller thrust deduction factor	98
5.7	Rudder forces and moments	99
5.7.1	Rudder force components	100
5.7.2	Rudder hydrodynamic coefficients	100
5.7.3	Rudder inflow velocity components	102
5.7.4	Additional parameters	105
5.8	Selection of the methods for hull forces and moments	106
5.9	Validation of the manoeuvring model	109
5.9.1	Validation using the seagoing KVLCC2 tanker	109
5.9.2	Validation using the inland 6700 t bulk carrier	113
5.9.3	Validation using the inland 3500 t tanker	119
5.10	Synthesis	125
6	Impacts of Rudder Configurations on Ship Manoeuvring Performance	127
6.1	Rudder profiles	127
6.1.1	Impacts of rudder profiles on turning	128
6.1.2	Impacts of rudder profiles on zigzag	130
6.1.3	Impacts of rudder profiles on hard turning	132
6.1.4	Impacts of rudder profiles on lane changing	134
6.1.5	Concluding remarks	135

6.2	Spacing between twin rudders	137
6.2.1	Impacts of spacing between twin rudders on turning	137
6.2.2	Impacts of spacing between twin rudders on zigzag	137
6.2.3	Impacts of spacing between twin rudders on hard turning	140
6.2.4	Impacts of spacing between twin rudders on lane changing	140
6.2.5	Concluding remarks	141
6.3	Spacing among quadruple rudders	142
6.3.1	Impacts of spacing among quadruple rudders on turning	142
6.3.2	Impacts of spacing among quadruple rudders on zigzag	142
6.3.3	Impacts of spacing among quadruple rudders on hard turning	142
6.3.4	Impacts of spacing among quadruple rudders on lane changing	142
6.3.5	Concluding remarks	146
6.4	Synthesis	147
7	Guidance on Rudder Configurations	149
7.1	Working conditions	149
7.2	Rudder profiles	149
7.3	Rudder parameters	150
7.4	Rudder types	150
7.5	Ship manoeuvrability	151
7.6	Ship resistance	151
7.7	Design flow	161
7.8	Synthesis	163
8	Conclusions and Recommendations	165
8.1	Answers to research questions	165
8.2	Recommendations for future research	167
	Bibliography	169
	Curriculum Vitae	193

Glossary

Abbreviations

ABS	American Bureau of Shipping
BV	Bureau Veritas
CCNR	Central Commission for the Navigation of the Rhine
CCS	China Classification Society
CFD	Computational Fluid Dynamics
COG	Centre of Gravity
DNS	Direct Numerical Simulation
DOF	Degree of freedom
EC	European Commission
EEDI	Energy Efficiency Design Index
EU	European Union
HSVA	Hamburgische Schiffbau Versuchsanstalt GmbH
IFS	Institute für Schiffbau
NACA	National Advisory Committee for Aeronautics
IMO	International Maritime Organization
IWT	Inland Waterway Transport
LES	Large Eddy Simulation
MARIN	Maritime Research Institute Netherlands
OSA	Overshoot angle
PMM	Planar Motion Mechanism
QPI	Inner rudder of the port side twin-rudder unit
QPO	Outer rudder of the port side twin-rudder unit
QSI	Inner rudder of the starboard side twin-rudder unit

QSO	Outer rudder of the starboard side twin-rudder unit
RANS	Reynolds-Averaged Navier-Stokes
RPS	Revolutions per second
SPSR	Single-propeller single-rudder
SPTR	Single-propeller twin-rudder
TPQR	Twin-propeller quadruple-rudder
TPTR	Twin-propeller twin-rudder
TSS	Traffic Separation Scheme

Greek Symbols

α	Angle of attack	(rad)
α_0	Incidence for zero lift	(rad)
α_R	Effective rudder angle	(rad)
$\bar{\delta}$	Average applied rudder angle	(rad)
β	Ship drift angle on midship	(rad)
β_P	Drift angle at propeller position	(rad)
β_R	Drift angle at rudder position	(rad)
δ	Applied rudder angle	(rad)
Δ	Relative difference	(%)
δ_h	Hydrodynamic inflow angle of the rudder	(rad)
$\dot{\delta}$	Rudder turning rate	(rad s ⁻¹)
ε	Dissipation of the turbulent energy	(—)
ε_R	Ratio of wake fraction of propeller to wake fraction of rudder	(—)
η	Ratio of rudder consumed power to the total power consumed by the hull and the rudder	(—)
η_R	Ratio of propeller diameter to rudder span, $\eta_R = D_P/B_R$	(—)
k_P	Impact factor of the propeller slipstream on the rudder hydrodynamics	(—)
k_R	Impact factor of the end plates on the rudder hydrodynamics	(—)
γ_R	Flow straightening coefficient of the rudder	(—)

κ_R	Experimental constant for expressing u_R	(—)
λ	Model scale	(—)
Λ_E	Rudder effective aspect ratio	(—)
Λ_G	Rudder geometric aspect ratio	(—)
μ	Dynamic viscosity of water	(Ns m ⁻²)
∇	Ship displacement volume	(m ³)
ω	Specific rate of dissipation of turbulence kinetic energy	(—)
ψ	Heading angle	(rad)
ψ_{O1}	First overshoot angle	(rad)
ψ_{O2}	Second overshoot angle	(rad)
ρ	Density of water	(kg m ⁻³)
σ	Root mean squared error (standard error) of the regression coefficients	(—)
σ_T	Average absolute deviation of the turning criteria	(—)
σ_Z	Average absolute deviation of the zigzag criteria	(—)

Roman Symbols

A_D	Advance in the turning manoeuvre, $A'_D = A_D/L$	(m)
a_H	Rudder force increase factor	(—)
A_m	Ship midship section area	(m ²)
A_R	Rudder lateral area without the horn part	(m ²)
A_{RP}	Rudder lateral area in the propeller slipstream	(m ²)
T_D	Tactical diameter of turning circle test, $T'_D = T_D/L$	(m)
B	Ship width at water level	(m)
B_R	Rudder span	(m)
C_b	Block coefficient	(—)
C_D	Drag coefficient	(—)
C_L	Lift coefficient	(—)
C_L/C_D	Lift to drag ratio	(—)
C_N	Normal force coefficient	(—)

C_R	Rudder chord length	(m)
C_T	Axial force coefficient	(—)
C_{D_0}	Drag coefficient at zero angle of attack	(—)
C_{L_0}	Lift coefficient at zero angle of attack	(—)
$C_{YR\alpha}$	Gradient of the rudder induced side force coefficient	(—)
C_{YR}	Rudder induced side force coefficient	(—)
D_P	Propeller diameter	(m)
d_R	Clearance between rudder tip and bottom of waterway, $d'_R = d_R/B_R$	(m)
F_D	Rudder drag force	(N)
F_L	Rudder lift force	(N)
F_N	Rudder normal force	(N)
F_R	Rudder resultant force	(N)
F_T	Rudder tangential force	(N)
F_X	Longitudinal component of rudder induced forces	(N)
F_Y	Lateral component of rudder induced forces	(N)
Fr	Froude number	(—)
H	Water depth	(m)
I_z	Moment of inertial	(kgm ²)
J_P	Propeller advance ratio, $J_P = V_P/nD_P$	(—)
J_z	Added moment of inertial	(kgm ²)
k	Turbulent kinetic energy	(—)
k^{CD}	Regression coefficients of twin-rudder drag coefficients	(—)
k^{CL}	Regression coefficients of twin-rudder lift coefficients	(—)
k_Λ	Impact factor of the rudder aspect ratio on the rudder hydrodynamics	(—)
K_T	Propeller thrust coefficient	(—)
L	Ship length between perpendiculars	(m)
m	Ship's mass	(kg)
m_x	Ship's added mass in x -direction	(kg)

m_y	Ship's added mass in y -direction	(kg)
N	Total hydrodynamic moment acting on the ship	(Nm)
n	Propeller revolution rate	(s^{-1})
N_H	Hydrodynamic moment due to hull acting on the ship	(Nm)
N_P	Hydrodynamic moment due to propeller acting on the ship	(Nm)
n_P	Number of propellers	(—)
N_R	Hydrodynamic moment due to rudder acting on the ship	(Nm)
n_R	Number of rudders	(—)
n_T	Number of performed turning manoeuvres	(—)
n_Z	Number of performed zigzag manoeuvres	(—)
P	Power consumed by the rudder induced resistance	(kW)
$P(\delta)$	Probability distribution of each applied rudder angle	(—)
\dot{r}	Yaw acceleration around midship	(rad s^{-2})
r	Yaw rate around midship	(rad s^{-1})
R^2	R-squared (coefficient of determination) of the regression coefficients	(—)
r_C	Yaw rate in steady turn	(rad s^{-1})
Re	Reynolds number	(—)
S	Wetted surface	(m)
T	Ship draught	(m)
t	Rudder profile section thickness	(m)
T_P	Propeller thrust	(N)
t_P	Propeller thrust deduction	(—)
t_R	Steering resistance deduction factor	(—)
t_{O1}	Time to the first overshoot angle	(s)
t_{O2}	Time to the second overshoot angle	(s)
\dot{u}	Ship acceleration in x -direction	(m s^{-2})
u	Forward speed in x -direction, $u = V \cos \beta$	(m s^{-1})
u_R	Longitudinal velocity of the inflow to rudder	(m s^{-1})

\dot{v}	Ship acceleration in y -direction	(ms^{-2})
V	Ship velocity on midship, $V = \sqrt{u^2 + v^2}$	(ms^{-1})
v	Lateral speed in y -direction on midship, $v = -V \sin \beta$	(ms^{-1})
V_A	Propeller advance speed	(ms^{-1})
V_C	Speed in steady turn	(ms^{-1})
V_P	Propeller advance speed	(ms^{-1})
V_R	Rudder inflow velocity	(ms^{-1})
v_R	Lateral velocity of the inflow to rudder	(ms^{-1})
V_S	Service speed	(ms^{-1})
w_P	Wake factor at propeller position in manoeuvring	(—)
w_R	Wake factor at rudder position in manoeuvring	(—)
w_{P_0}	Wake factor at propeller position in straight moving	(—)
X	Total hydrodynamic force acting on midship in x -direction	(N)
x_G	Longitudinal position of centre of gravity in o - xyz	(m)
X_H	Hydrodynamic force due to hull acting on midship in x -direction	(N)
x_H	Longitudinal position of acting point of additional lateral force	(m)
X_P	Hydrodynamic force due to propeller acting on midship in y -direction	(N)
x_P	Longitudinal position of propeller in o - xyz	(m)
X_R	Hydrodynamic force due to rudder acting on midship in x -direction	(N)
x_R	Longitudinal position of rudder in o - xyz	(m)
x_{PR}	Longitudinal propeller-rudder separation	(m)
Y	Total hydrodynamic force acting on midship in y -direction	(N)
y^+	Non-dimensional wall distance	(—)
y_i	Distance from the wall to the first mesh point in mesh generation	(—)
Y_R	Hydrodynamic force due to rudder on midship in y -direction	(N)
y_R	Relative position of the rudder to the propeller shaft	(m)
y_{PR}	Lateral propeller-rudder separation	(m)
y_{TR}	Spacing between the twin rudders	(m)

y_{TU} Spacing between the two twin-rudder units (m)

z_{PR} Vertical propeller-rudder separation (m)

Subscripts

AH Route from Antwerp, Belgium to Vlaardingen, the Netherlands

H Hull

P Propeller

R Rudder

VH Route from Vlaardingen, the Netherlands to Hamm, Germany

Superscripts

Exp Experiment

P Port side

S Starboard Side

Sim Simulation

TP Port side of a twin-rudder configuration

TS Starboard side of a twin-rudder configuration

Chapter 1

Introduction*

“A man without a goal is like a ship without a rudder.”

Thomas Carlyle (1795 – 1881)

Inland shipping plays an important role in transport. In order to maintain and further develop this important role, safe and efficient inland vessels are prerequisites. Inland vessels should always be capable of safe manoeuvring without significantly harming the cost-effectiveness of operations. Options to influence manoeuvrability through the design of inland vessels, such as the hull form and the main dimensions, are commonly constrained due to the limits of inland waterways. One of the possibilities that are left to improve ship manoeuvrability is to optimise rudder configurations. Additionally, practical engineers and authority officers necessitate test manoeuvres and related criteria to predict and evaluate ship manoeuvrability for design and management.

This chapter presents the significance and motivation of this research. Section 1.1 introduces the applied terminologies and the research background. Section 1.2 states the research problems to be resolved through this thesis. Section 1.3 proposes the research questions for improving inland vessel manoeuvrability. Section 1.4 addresses the research boundaries. In the end, Section 1.5 explains the structure of this dissertation and describes the content of each chapter.

1.1. Research background

1.1.1. Applied terminologies

When considering terms like design and performance, many definitions appear in literature and general use. To avoid ambiguity, in this thesis, the following definitions have been chosen:

- An **inland vessel** is a self-propelled motor ship that sails in inland waterways, such as rivers, canals, and lakes.
- **Ship manoeuvrability** is the ability of a ship to react to certain navigation orders, which include, but not limited to, turning, evading, yaw checking, course keeping, and stopping.

*This chapter is based on Liu and Hekkenberg [177] and Liu et al. [180].

- A **test manoeuvre** is the scenario that describes the test conditions to start and end a specific manoeuvring test. Different test manoeuvres emphasise different aspects of ship manoeuvrability.
- A **rudder configuration** is the combination of rudder design choices related to the rudder profile, the rudder parameters, the rudder type, the number of rudders, the rudder end plate, and the relative positions to the hull, the propeller, and other rudders.
- A **rudder profile** is the 2D sectional shape of a rudder.
- A **rudder parameter** is one of the rudder design values, such as area, thickness, span, chord, and aspect ratios.
- A **rudder type** depends on the structure, the position of the rudder stock (unbalanced, semi-balanced, or balanced), and the structural rudder-hull connection (the number of pintles, no skeg, semi-skeg, or full-skeg).
- **Rudder effectiveness** is judged by the amount of rudder induced manoeuvring force. For open water rudder hydrodynamics, the rudder effectiveness is evaluated by the normal force coefficient.
- **Rudder efficiency** is defined as the ratio of the rudder induced useful force (lift in open water or lateral force in manoeuvring) to useless force (drag in open water or longitudinal force in manoeuvring). In this thesis, the lift to drag ratio is taken as an indicator of the rudder efficiency for open water tests.

1.1.2. Inland waterway transport

Inland waterway transport (IWT) plays a significant role in the modal split of transport for a long time and still does [95, Section 1.1]. It takes a large modal split in countries, including, but not limited to, Brazil (the Paraguay-Paraná inland waterway), Bulgaria and Romania (the Danube), China (the Yangtze River), Germany and the Netherlands (the Rhine), and United States of America (the Mississippi) [67, 96, 199]. More specifically, China has over 110000 km navigable inland waterways, most of which are wide, stable, and ice-free all year around, with flourishing IWT [7, 128, 299]. In the Yangtze River, the total cargo increased from 690 million tonnes in 2000 to 1160 million tonnes in 2006, and it is expected to reach 2350 million tonnes in 2020 [199].

The Netherlands, Germany, and Belgium are European countries with the largest capacity of inland waterway transport. Over half of the international country flows for transport are loaded and unloaded among these three countries [68]. The inland shipping sector is indispensable for the Netherlands, taking a modal split share of more than 35 % of the Dutch freight [67]. In Germany, up to 240 million tonnes of bulk goods are transported per year via inland waterways, which almost equals 75 % of the goods transported by railway [70]. Based on the data from 2005 to 2013, the IWT of Belgium increased from 14.5 % to 20.5 %, which were larger than the modal split share of railway [67]. Additionally, the annual volume of the IWT in the United States is about 600 million tonnes [300].

The European Union (EU) sets an objective of shifting traffic from roads to rail and water-borne transport for cost savings, reducing pollution, and increasing transport safety

[64]. However, according to the European Court of Auditors [66], the EU inland waterway transport strategies have not been effectively implemented and policy objective has not been achieved yet. Therefore, projects that provide benefits for inland waterway transport are highly encouraged [66]. To further develop inland navigation, on the one hand, infrastructure bottlenecks in waterways should be eliminated, on the other hand, inland vessels themselves should be capable of sailing safely and efficiently. Safety and efficiency of inland vessels justify significant research attention.

1.1.3. Inland vessel manoeuvrability

Developments and innovations enable cost reduction, improvement of environmental performance, access niche markets, and compliance with new regulations [96]. The safety of the ship is a prerequisite for efficient and reliable inland waterway transport. Nevertheless, ships have been primarily designed from an economic point of view [228]. Due to the potentially high cost of improving manoeuvrability, a wise, well-balanced, compromise between performance and interest has to be made [21]. Furthermore, the reasons why the manoeuvrability of inland vessels deserves special attention are as follows:

- Inland waterways are often narrow, bendy, and shallow. Artificial structures, such as bridges, wharfs, and locks, also put limits on the navigational area. In addition, strong currents may happen in conjunctions of channels, especially in flood seasons. Thus, ship manoeuvring performance is crucial to ensure safe navigation.
- Inland waterways are frequently busy, making the navigation situation complex. A lot of encountering and overtaking may happen in day-to-day operations which require inland vessels to be well manoeuvrable. More specifically, inland vessels should be able to quickly and effectively respond to the orders of the skippers.
- Unlike seagoing ships which may get assistance from tugs in hard manoeuvring situations, inland vessels sail independently most of the time. Additional consideration on low-speed manoeuvrability should be taken into account. Furthermore, the enhancement of low-speed manoeuvrability should not harm the cruising-speed performance.
- Inland vessels customarily equip multiple rudders with a large variety of profiles, parameters, types, and relative positions. Impacts of these rudder choices on ship manoeuvrability have not been sufficiently understood yet. Furthermore, a rudder may increase the total resistance by 1% at the neutral position and 2% to 6% at moderate angles [5]. Correspondingly, optimising the rudder profile and type can reduce the total resistance by 2% to 8%. [98].

There are many ways to improve ship manoeuvrability, such as increasing rudder area, upgrading thrust power, reducing ship weight, and applying active steering devices. In practice, inland vessels have few choices in main particulars and hull forms because the main particulars are constrained by the width and depth of waterways, canals, and, especially, locks. In Europe, for each class of inland waterways, the dimensions of inland vessels are regulated [65]. Additionally, to maximise the capacity of the ships, hull forms of inland vessels typically have similar large block coefficients (C_b), length to ship width ratios (L/B), and ship width to draught ratios (B/T) [228]. Therefore, one of the remaining possibilities

to significantly improve ship manoeuvrability without changing the main dimensions and hull forms is to optimise rudder configurations.

In general, rudders have significant impacts on ship manoeuvring performance as well as an underestimated potential for fuel savings [98]. Molland and Turnock [206, p. 86] concluded the role of rudders in manoeuvring as follows:

“The rudder has to be able to develop sufficient side force to maintain the ship on a straight course at typical service speeds, to change course at service speed, and to manoeuvre at slower speeds. In the case of course keeping, interest is centred on minimising deviations from the set course. In the cases of changes in course or manoeuvring, interest centres on the ease and rapidity with which a ship takes up a new course. The effectiveness of the rudder in these two situations will depend on the directional stability of the ship” [206, p. 86].

1.1.4. Inland vessel rudder design

Commonly, the effectiveness and efficiency of the rudders are evaluated by the amount of the rudder induced side force (Y_R) and the ratio of Y_R to the rudder induced resistance respectively. In open water tests, the effectiveness and the efficiency are commonly presented by the lift coefficient (C_L) and the lift to drag ratio (C_L/C_D). For manoeuvring simulations, only rudder normal force (N_R) is considered in the calculation of Y_R and rudder tangential force is neglected. Furthermore, N_R is routinely estimated based on the Fujii’s formula [72, 73, 73], which does not take the above-mentioned design choices into account. Thus, research on rudder design choices is especially needed for inland vessels that have a large range of variety of rudder configurations.

1.1.5. Concluding remarks

Section 1.1 has discussed the importance of inland shipping. It is desirable to properly estimate ship manoeuvrability in the ship design process to ensure safe and efficient navigation. In the limited options for inland vessel design, optimising the rudder configuration is feasible to improve ship manoeuvring performance and possible to reduce fuel consumption. The above discussions inspire this research to analyse the impacts of rudder configurations on inland vessel manoeuvrability and generate guidance for naval architects to make proper choices.

1.2. Problem statement

Thus far, research in the field of ship manoeuvrability has been primarily focused on seagoing ships [34]. However, interest in inland shipping is growing [236]. Generally, inland vessels have more complex arrangements than seagoing ships. An example of common inland vessel rudder and propulsion arrangements is shown in Figure 1.1, which has a hull tunnel in front of ducted twin propellers and quadruple rudders. The complex arrangements also make studies on the manoeuvrability of inland vessels harder to tackle than those of seagoing ships. Furthermore, sailing in a complex navigation environment, inland vessels are expected to be more manoeuvrable than seagoing ships to ensure navigation safety. In

order to ensure a good performance in practice, accurate methods of prediction are needed to link the design parameters to manoeuvring performance. Additionally, relevant requirements on manoeuvrability should be established for designers and authorities.



Figure 1.1: An inland vessel with a hull tunnel, ducted twin propellers, and quadruple rudders.

To evaluate the manoeuvring performance of ships, standard test manoeuvres and related criteria are needed. Manoeuvrability standards issued by the International Maritime Organization [111, 112] are widely applied. However, these test manoeuvres and criteria are intended for seagoing ships in deep water. Central Commission for the Navigation of the Rhine [32], European Commission [63], and Bureau Veritas [27] published regulations for inland vessels that define required evasive action and stopping capacity. In addition, China Classification Society [38] set up more test manoeuvres, including turning circle, $15^\circ/15^\circ$ zigzag, stopping, pull-out, and course keeping tests. ITTC Manoeuvring Committee [120] gave a review of the standards in use for inland vessels, encouraging more test scenarios and criteria.

Considering the above-mentioned research challenges and gaps in knowledge, there are several open issues related to inland vessel manoeuvrability:

- **The adaptability of the previous research, intended for seagoing ships, to inland vessels has not been examined yet.** Existing research on ship manoeuvrability has been primarily performed for seagoing ships. However, inland vessels and seagoing ships are different in design options, rudder configurations, and navigation environment. These differences make it questionable to apply seagoing ship based results directly to inland vessels. It is worthwhile to study the critical differences between inland vessels and seagoing ships and their impacts on ship manoeuvring performance.
- **Impacts of design choices in rudder configurations, namely the rudder profile, the rudder parameters, the number of rudders, and the spacing among multiple rudders, on ship manoeuvrability are not clear.** Current empirical formulas are established from the research on seagoing ships which commonly use a single NACA

rudder while inland vessels may have more options. Even for seagoing ships, twin rudders and high-lift profiles are also applied owing to the ship enlargement and the requisite for improvement of ship manoeuvrability. Therefore, it is necessary to set up guidance for naval architects to make proper choices of rudder configurations.

- **Existing test manoeuvres and criteria for inland vessels are not as elaborate as those for seagoing ships.** For seagoing ships, turning, zigzag, and stopping tests are mandatory while additional spiral (direct, reverse, and simplified), pull-out, and very small zigzag are suggested [111, 112]. For inland vessels, only tests of evasive action and stopping capacity are regulated [63]. Furthermore, the existing manoeuvres are insufficient to present ship manoeuvring performance in complex navigation environment. More practical and handy manoeuvres are needed to evaluate inland vessel manoeuvrability and compare the performance of various inland vessel designs.

1.3. Research questions

In Section 1.2, practical problems in inland vessel manoeuvrability were identified. There is a lack of knowledge in the prediction methods of inland vessel manoeuvrability. The impacts of rudder configurations on ship manoeuvrability are not clear. The existing test manoeuvres for inland vessels are not sufficient. Following these problems, this thesis aims to resolve the following main research question:

What are the proper rudder configurations to achieve well manoeuvrable inland vessels without significant loss of navigation efficiency?

This main research question leads to the following four key research questions:

- Q1. *What are the practical manoeuvres to evaluate and compare the manoeuvring performance of inland vessels?*

When the above question is answered, new manoeuvres and related criteria will be proposed. The proposed manoeuvres and criteria focus on day-to-day inland vessel operations, such as the hard turning in bent waterways and the lane changing in narrow channels.

- Q2. *How does the rudder configuration affect the rudder hydrodynamic characteristics?*

Answers to the above key research question will provide insights into the impacts of the rudder profile, the rudder parameters, the number of rudders, and the spacing among multiple rudders on rudder hydrodynamic characteristics, which can be applied to the mathematical model for manoeuvrability prediction.

- Q3. *How do changes in the rudder configuration affect the ship manoeuvrability in specific manoeuvres?*

By integrating the rudder hydrodynamic characteristics into ship motion models, the rudder design choices will be directly related to ship manoeuvring performance. The manoeuvring performance of reference inland vessels with various rudder design will be evaluated and compared through test manoeuvres proposed in the first key research question.

Q4. *How to choose a proper rudder configuration according to the required manoeuvring performance?*

Answering this question summaries guidance on the rudder configurations for inland vessel manoeuvrability. To ensure certain manoeuvring performance in the proposed manoeuvres, suggestions on rudder design choices are given.

When the main and key research questions are answered, a further insight into the rudder impacts on inland vessel manoeuvrability will be obtained. Guidance on rudders will become available for naval architects. With such guidance, designers may have a better estimation of the ship manoeuvring performance with their choices of rudder configurations. Additionally, designers can optimise their rudder design towards a more manoeuvrable ship.

1.4. Research boundaries

In this thesis, the study of inland vessel manoeuvrability is based on the assumption that the manoeuvrability of a vessel can be judged by its manoeuvring trajectories and indices in specified test manoeuvres. Owing to the availability of data, reference ships are taken from Chinese and Dutch fleets. Lengths of these ships are around 110 m. Small vessels are not explicitly included in the presented research. Only conventional self-propelled motor vessels are considered. Due to the above-mentioned research assumptions, this thesis has the following research boundaries:

- Shallow water effects on ship manoeuvrability and resistance are not explicitly studied.
- Service-speed manoeuvrability of the reference ships is evaluated while slow-speed manoeuvring performance is not considered.
- Bow and stern thrusters are not considered.
- Hydrographic and meteorological conditions, including the current and the wind, are not considered.
- Channel characteristics, such as the width and the slope of the bank, are not included.
- Ship-ship interactions and ship-bank interactions are not included.
- Human factors are not included.

1.5. Thesis structure

To answer the identified research problems and questions, the impacts of rudder configurations on inland vessel manoeuvrability will be analysed and guidance on rudder design choices will be proposed. Figure 1.2 describes the structure of this thesis and indicates the read before relations of the chapters. This thesis is organised as follows:

- **Chapter 2** presents background information and reviews state-of-the-art literature on inland vessel manoeuvrability and ship rudders to clarify the research topic. The literature review leads to the applied methods and studied parameters.

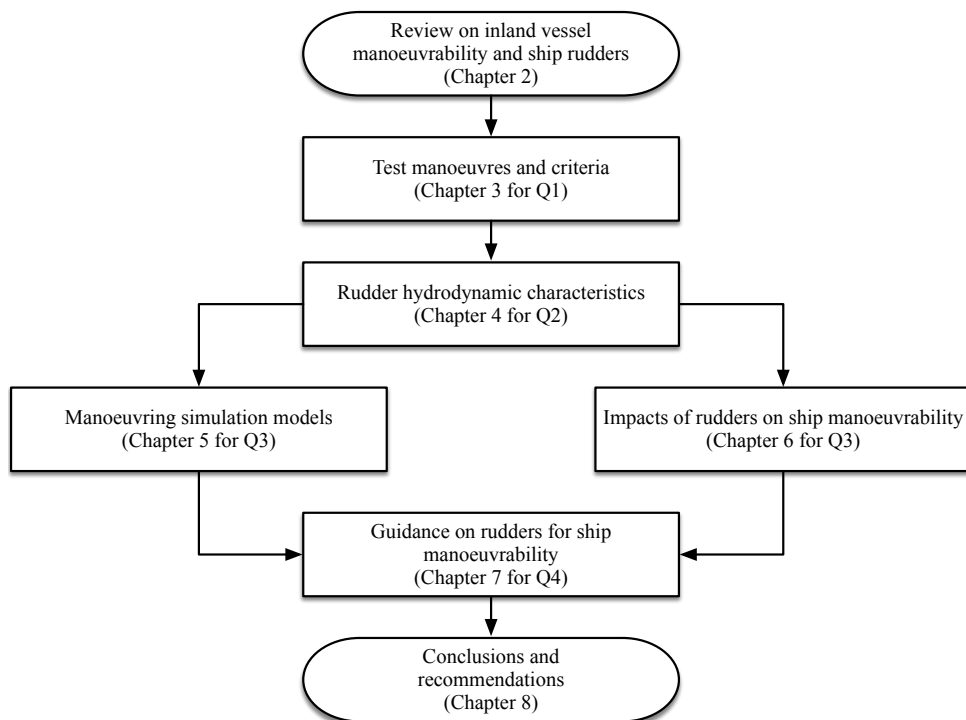


Figure 1.2: Thesis structure.

- **Chapter 3** describes classic and proposed test manoeuvres and related criteria for inland vessels. These test manoeuvres and criteria are used to evaluate inland vessel manoeuvrability and compare the manoeuvring performance of ships with various rudder configurations. This chapter answers the key research question 1 (Q1).
- **Chapter 4** introduces the applied Computational Fluid Dynamics (CFD) methods. Then, these CFD methods are applied to obtain the hydrodynamic characteristics of various rudder configurations. The impacts of the rudder profile, the rudder parameters, the number of rudders, and the relative position of rudders on the hydrodynamic coefficients of single, twin, and quadruple rudders are analysed. This chapter answers the key research question 2 (Q2).
- **Chapter 5** presents mathematical manoeuvring models and modelling approaches. Using the hydrodynamic characteristics obtained in **Chapter 4**, new regression formulas are proposed to calculate the rudder force in manoeuvring. This chapter partly answers the key research question 3 (Q3).
- **Chapter 6** studies the impacts of rudder configurations on ship manoeuvrability. Integrating the results of **Chapter 4** into the mathematical models described in **Chapter 5**, manoeuvring simulations of the reference ships are carried out. The simulations are done in test manoeuvres that are proposed in **Chapter 3**. This chapter partly answers the key research question 3 (Q3).
- **Chapter 7** provides guidance on rudder design choices. For certain manoeuvring performance, the possible design choices of rudders are listed. This chapter answers the key research question 4 (Q4).
- **Chapter 8** summarizes the conclusions of this thesis and outlines the recommendations for further research.

Chapter 2

Literature Review on Inland Vessel Manoeuvrability and Ship Rudders*

“The more I read, the more I acquire, the more certain I am that I know nothing.”

Voltaire (1694 – 1778)

The manoeuvrability of seagoing ships has been studied extensively, but several factors make it doubtful to directly apply the seagoing ship oriented research to inland vessels. These factors relate to the environmental conditions in which inland vessels operate and the particulars of the vessels. Given the impact factors on ship manoeuvrability and the differences between seagoing ships and inland vessels, Section 2.1 describes the extra impact factors to be addressed for inland vessel manoeuvrability and identifies the rudder configuration as a crucial difference.

To analyse the impacts of the rudder configuration on ship manoeuvring performance, the rudder induced forces need to be determined. Section 2.2 introduces the methods of hydrodynamic force analysis in captive model tests, free-running tests, open water tests, and numerical methods. Among these methods, the Computation Fluid Dynamics (CFD) method is applied in this thesis as it does not require sophisticated test facilities. To achieve reasonable results, CFD simulations of rudders should be carried out at relevant Reynolds numbers and angles of attack, which are discussed in Section 2.3.

The rudder induced manoeuvring forces and moments are affected by, including, but not limited to, the rudder profile, the rudder parameters, the rudder type, the number of rudders, the spacing between rudders, and the relative positions among the hull, the propeller, and the rudder. The key factors are identified through a review on each of the above-mentioned impacts on the rudder hydrodynamics in Section 2.4, which are further studied through CFD simulations in Chapter 4. To judge the quality of the rudder design, Section 2.5 presents the evaluation perspectives of the rudder performance in ship manoeuvrability, fuel consumption, and rudder cavitation. In the end, Section 2.6 draws the conclusions of this chapter.

2.1. Impact factors on inland vessel manoeuvrability

Impact factors on inland vessel manoeuvrability are roughly characterised into two aspects: external environment and internal design. The external factors are set by the environment in which the ship sails while the internal factors are determined by the ship design and

*This chapter is based on Liu and Hekkenberg [177] and Liu et al. [180].

operation profiles. This section reviews the literature on the impact factors and highlights the differences between inland vessels and seagoing ships.

2.1.1. External environment factors

The following paragraphs provide a review on two main impact factors of the navigation environment on the manoeuvrability of inland vessels, namely shallow-water and ship-ship/ship-bank interactions. External impacts are determined by the characteristics of the waterways while naval architects cannot control them.

Shallow-water effects

As a consequence of scale enlargement in ships [49, 79, 157], the ship manoeuvring performance in constrained channels is no longer only a concern for inland vessels but also crucial for seagoing ships. The performance of seagoing ships in shallow water is still considered to be less important because seagoing ships sail in deep water most of the time. On the contrary, for inland vessels which commonly sail in shallow water, shallow-water effects are very critical [100]. The ratio of the water depth to the ship draught (H/T) is typically larger than 4 for seagoing ships, but it is commonly smaller than 2.5 for inland vessels, especially in the dry period. The influence of water depth begins noticeable in medium deep water ($1.5 < H/T < 3.0$), becomes significant in shallow water ($1.2 < H/T < 1.5$), and dominates in very shallow water ($H/T < 1.2$) [288].

The limited water depth influences ship resistance [274], which is the main component of the hull induced forces in the longitudinal direction (X_H). Meanwhile, in constrained waterways, the horizontal restrictions also have an influence on the resistance, which is the so-called blockage effect [141, 264]. At the same advance speed, a decrease of H/T results in impacts in the ship squat and the wave height [121], leading to impacts in X_H . Gronarz [85] and [86] proposed a shallow-water manoeuvring model and indicated that the influence of shallow water on the hull dominates and that on the propeller and the rudder can be neglected. For inland vessels, Rotteveel [239] compared the existing models for ship resistance, proposed shallow water corrections for manoeuvring, and pointed out that the current estimation methods do not clearly represent the shallow-water effects in extremely shallow water.

Considering the lateral forces and moments, Eloot and Vantorre [60] reported impacts in the course keeping ability, leading to a larger tactical diameter in shallow water than in deep water for a slender seagoing container ship. ITTC Manoeuvring Committee [118] also presented impacts in the tactical diameters due to an increment of the hull damping force, which is a widely known shallow water effect. However, Yoshimura and Sakurai [314] and Yasukawa and Kobayashi [303] found that the tactical diameter is smaller in shallow water than in deep water for twin-propeller wide-width ships. Kijima and Nakiri [135] and Lee and Lee [162] showed that shallow-water effects on the tactical diameters and advances vary with ship types. Lee and Lee [162] reported that the tactical diameter increases while the advance almost remains the same on the port side turning, but both the tactical diameter and the advance increase on the starboard side turning. In contrast to the above findings, Koh and Yasukawa [146] found that a pusher-barge system may have a smaller turning circle and a worse course keeping ability in shallow water than in deep water.

Above all, research on shallow-water effects has been primarily done for large seagoing ships, manoeuvring in ports or entering harbours, rather than for inland vessels [60, 135,

162, 303, 314]. Shallow-water effects on the inland vessel manoeuvrability are still unclear. It should be noted that inland vessels have similar characteristics to the twin-propeller wide-width ship applied by Yoshimura and Sakurai [314] and Yasukawa and Kobayashi [303], which means shallow-water effects on inland vessels could be different from typical large seagoing ships. To further study the ship manoeuvrability in shallow water, Landsburg et al. [157] suggested applying more accurate full-scale trials and mathematical modelling techniques.

Ship-ship and ship-bank interactions

Inland waterways feature many artificial structures, such as locks, terminals, and bridge pillars along or in the channel, restricting the navigable area [178]. Thus, knowledge of ship behaviour in horizontally and vertically restricted areas helps to reduce infrastructure and operation cost and enhance the navigation safety [60]. Inland vessels suffer far less from the strong wind and waves than seagoing ships. However, in natural waterways, currents may lead to very different sailing conditions for the upstream and downstream directions. In many cases, seagoing ships are requested to use additional manoeuvring assistance like tugs in mandatory pilotage areas. On the contrary, inland vessels have to manoeuvre independently almost all the time. Consequently, inland vessels should meet higher manoeuvrability standards than seagoing ships to ensure safe navigation.

Due to the high density of traffic in inland waterways, inland vessels have to pass and meet each other at a close range much more frequently than seagoing ships. When a ship moves into the proximity of other ships, lateral force and yaw moment are induced due to the asymmetrical flow around the ship. For seagoing ships, both numerical [37, 172, 185] and experimental [62, 159, 160, 290] methods were applied to analyse these interactions and their impacts on ship manoeuvrability. However, for inland vessels, no systematic research was found.

Ship handling is also affected by the ship-bank interactions [61, 164]. The minimum channel width to the ship's width ratio may be as small as 4, 3, or 2 for double-lane, narrow-double lane, or single-lane channels respectively [237, 238]. Lee and Lee [163] researched the transverse distance and the maximum rudder angle for safe passing. Vantorre et al. [291] proposed an empirical formula to predict the ship-bank interaction forces through model tests. De Koning Gans [48], Lo [185], and Zou and Larsson [318] investigated the sinkage and trim caused by ship-ship and ship-bank interactions through CFD simulations. Similar to the research on shallow-water effects, the scenarios for ship-ship and ship-bank interactions were primarily assumed for a large seagoing ship, for instance, the KVLCC2 tanker [318], in a narrow channel.

2.1.2. Internal design factors

Analysing the navigation environment, naval architects may adapt ship particulars to compensate the negative influences of the external disturbances. Four main features of inland vessels, which are different from seagoing ships, specifically slow speed, hull forms, propulsion, and rudder configurations, are addressed in the following paragraphs.

Slow speed

The cruising speed of inland vessels (8 km h^{-1} to 28 km h^{-1}) is often slower than that of seagoing ships (18 km h^{-1} to 36 km h^{-1}). To compare the velocity among ships, the

Froude number (Fr) is commonly used. Considering the range of ship dimensions and velocities, inland vessels commonly have smaller Fr than seagoing ships, leading to lower wake-making resistance. Moreover, slow speed also means a slow incidence velocity to the propeller and the rudder, affecting their performance. Even though slow-speed manoeuvring is not the central concern for the design of most seagoing ships, their crucial impacts on safe operations deserve attention [46, 109].

Inland vessels that consistently sail at a slower speed than seagoing ships should be optimised to improve their slow-speed performance. ITTC Manoeuvring Committee [118] raised the necessity of standards for slow-speed manoeuvring. Additionally, ITTC Manoeuvring Committee [119] presented an overview of the existing slow-speed manoeuvring models for seagoing ships. Oh [220] compared the effectiveness of typical slow-speed manoeuvring models. In sum, Eloot and Vantorre [59] concluded the opportunities and limitations of slow-speed models, emphasising the differences between low-speed and ordinary-speed manoeuvring.

Hull forms

Inland vessels include motor vessels, pusher-barge systems, and towed-barge systems. Compared with the hull forms of seagoing ships, inland motor vessels in Europe commonly have larger block coefficients (C_b), much larger length to width ratios (L/B), and much larger width to draught ratios (B/T) due to the limits imposed on the draught (T), the length (L), and the width (B) of the ship [228]. These differences in hull forms greatly influence the ship resistance and other hull-generated hydrodynamic forces and moments in manoeuvring.

Pusher-barge and towed-barge systems are widely used in inland waterways all around the world. They are superior to motor vessels regarding transport capacity in shallow water. A significant amount of research has been conducted on the hydrodynamics of pusher-barge systems. Luo and Zhang [189], Koh et al. [147], Koh et al. [148], Koh et al. [149], Maimun et al. [190], and Koh and Yasukawa [146] presented manoeuvring research on pusher-barge systems through numerical or experimental methods. Tabaczek et al. [262] and Tabaczek [261] analysed the resistance and planar motions of a twin-screw inland vessel with different bow forms.

Propulsion

The propulsion of inland vessels is affected by the ship propulsors and appendages. Since propellers are not far from the free surface, inland motor vessels are commonly designed with a tunnel at the aft ship to improve the propeller inflow and prevent the propeller ventilation. In the process of model tests for ships with appendages, scale effects were found by Clement [41] and Gregory and Beach [80] in determining the resistance. To relate test results to practical ships, Holtrop [105] covered the extrapolation methods of ships with multiple appendages and complex propulsors. As the propeller diameter of inland vessels is constrained by the water depth, multiple propellers, especially twin-propellers, are commonly installed. Kim et al. [144] reported worse turning but better course keeping and course changing abilities of a twin-propeller ship compared to a single-propeller ship at sea. For inland vessels, further research is necessary to determine the impacts of the propulsion on ship manoeuvrability.

Rudder configurations

Compared to a common value of 2 for seagoing ships [142], the aspect ratio of inland vessel rudders is limited by the water depth to 1 to 2. Meanwhile, rudder orders for course corrections are more frequently called in inland waterways than at sea. To obtain sufficient manoeuvring forces and moments, a configuration of multiple rudders per propeller is commonly used to increase the total rudder area. Additionally, inland vessels feature a larger range of rudder profiles, for instance, the Schilling rudder with additional end plates on the root and tip. The rudder profile largely affects the rudder hydrodynamic characteristics and has further impacts on manoeuvrability. However, the impacts of the rudder design choices like profiles, parameters, types, and interactions among multiple rudders are not fully considered in the existing studies.

Nagarajan et al. [213] demonstrated a superior course keeping ability of a VLCC tanker with Schilling rudders to conventional Mariner rudders at constant engine torque under various encounter angles of the wind. Vantorre [287] carried out comprehensive model tests to determine the open water characteristics of several rudder configurations in a shallow water towing tank. Last but not least, inland vessels may use large rudder angles larger than 35° , which is the common maximum angle for seagoing ships, in hard manoeuvring situations. When side movement is needed at slow speed, the rudder angles may reach 90° . Currently, most of the research on propeller and rudder performance has been done for deep water [228]. The necessity to adjust the existing propeller and rudder models for shallow water was proposed by Eloot and Vantorre [59].

2.1.3. Concluding remarks

In the external design factors, the shallow water has significant effects on hull forces, in particular for the resistance, but not much for the rudder forces. Since the shallow-water effects become significant when $H/T < 1.5$ and the presented reference vessels in this thesis (Table 5.1) are primarily designed for the deep downstream of the Rhine and the Yangtze River, the shallow-water effects on ship manoeuvrability are not explicitly studied. Furthermore, there is no validation data publicly available for shallow water mathematical modelling of inland vessels. The ship-ship and ship-bank interactions are important for safe operations but not thoroughly studied as this thesis focuses on the design of individual inland vessels.

In the internal design factors, slow-speed manoeuvring is critical for hard manoeuvring situations in port areas. The ranges of inland vessel particulars are different from those of seagoing ships. Thus, extra care should be given to the usability of seagoing oriented empirical formulas for hull forces and moments, which will be further discussed in Chapter 5. Propulsion impacts are relatively minor on the ship manoeuvrability. Thus, it is out of the scope of this thesis. Last but not least, the rudder configuration of a ship is important for its manoeuvring performance. Furthermore, the rudder configuration is one of the most critical differences between inland vessels and seagoing ships, which has not been fully considered as yet.

Section 2.1 has addressed the additional impact factors on inland vessel manoeuvrability besides those for seagoing ships. Above all, existing estimation methods for hull forces are based on seagoing ships. They may not give proper results for inland vessels and result in a bad prediction of manoeuvrability. Therefore, future research is suggested to consider

the differences between seagoing ships and inland vessels while this thesis focuses on the impacts of rudder configurations on inland vessel manoeuvrability.

2.2. Hydrodynamic force analysis

2

To study the impacts of rudder configurations on ship manoeuvrability, the rudder induced forces and moments need to be analysed. This section reviews the contemporary hydrodynamic force analysis methods to gather coefficients that are used to solve the equations of ship motions. These methods are captive model tests, free-running tests, open water tests, and numerical tests.

2.2.1. Captive model tests

Captive model tests are primarily used to determine the hydrodynamic coefficients of ships [280]. These tests are commonly carried out with Planar Motion Mechanism (PMM) or Computerised Planar Motion Carriage. The ship model (bare hull or equipped with a propeller, a rudder, and an electrical motor for propulsion) is attached to the towing carriage. Hydrodynamic coefficients are then obtained through testing in straight lines and harmonic tests. With the obtained hydrodynamic coefficients, other tests that are not suitable for the size of the towing basin, such as pull-out manoeuvres and spiral tests, can be numerically simulated. Another kind of captive model tests, the so-called rotating-arm test, is designed to obtain stationary turning coefficients. The ship model is attached to a rotating arm which is set at the centre of the basin turning at a constant velocity.

2.2.2. Free-running tests

Static towing tests are done at constant drift angles and rudder angles, which means that the motion is decoupled in the horizontal plane, so additional corrections have to be applied to the decoupling effects [280]. To directly obtain the manoeuvring characteristics, free-running tests are applied to solve the uncoupled problems as it can generate a series of coefficients associated with positions [110]. International Towing Tank Conference [116] presented the standard procedure of free-running tests. System identification techniques are commonly correlated with the free-running model tests for hydrodynamic force coefficients [10, 22, 84, 307, 308]. Oltmann [222] gave an example of how to create a mathematical model from a series of zigzag tests. However, free-running tests are constrained by the dimension of the towing tank. Thus, these tests are regularly carried out on a rather small scale with high scaling errors.

2.2.3. Open water tests

In addition to tests for ship manoeuvrability, open water tests for propeller thrust, torque, and efficiency are usually performed in towing tanks or cavitation tunnels [116]. Furthermore, open water tests are also used to obtain rudder open water characteristics [287]. In contrary to the highly non-uniform ship wake in practice, these tests are carried out in uniform inflow. Considering the size of the towing tank, test models are commonly built in a range between 2 m to 9 m in length [117]. Due to the differences of vortex shedding and flow separation, errors exist in scaling model test results to full scales [19]. Thus, Holtrop [105] and Oyan [225] developed an extrapolation method to transfer model-scale results to

full-scale applications [117].

2.2.4. Numerical methods

Even though ship model tests are regarded as the most reliable solutions [286, 289], numerical methods are also widely applied. In practice, naval architects need simple prediction tools with reasonable accuracy. To design a new ship, coefficients may be obtained from one parent ship or a series of hull forms through empirical constants or regression formulas. Extensive tests are needed to build up these empirical databases. Longo et al. [187], Todd [270, 271], and Toda et al. [269] described the procedure of tests on Series 60 and presented the results in different perspectives, such as wave profiles, wave elevations, mean velocities, pressure field distribution, and scale effects. As the computation power increases dramatically, numerical calculation through CFD methods is becoming more and more popular [276]. Chau [36] applied Multi-block Finite Volume Method to study the free-stream characteristics of rudders.

El Moctar [56] applied RANS methods for rudders and propellers in uniform and oblique flow, rudder-propeller interaction, and forces on the ship hull in manoeuvring. Morgan and Lin [209] gave an introduction to the historical development of the hydrodynamic prediction. Furthermore, it is possible to use CFD methods for model-scale or full-scale tests [11, 29, 140, 266] in virtual tanks. CFD methods have been proved to be useful and more insights can be gained if additional work can be done on the verification and validation of the complex simulations as suggested by Rotteveel [239], Stern et al. [253], Stern et al. [254], and Wilson et al. [298]. In order to compensate the time-consuming CFD calculation and high-cost model tests, system identification methods were applied by Abkowitz [3], Araki et al. [10], Yoon and Rhee [307], and Zhang and Zou [316].

2.2.5. Concluding remarks

After reviewing the existing methods, manoeuvrability prediction methods can be roughly divided into two aspects: free running model tests and computer simulations based on mathematical models. Due to the high cost and uncontrollable test conditions, full-scale tests are rarely used in predictions. Hence, the model test is still considered as the most reliable measurement, which is commonly used as a final check before the ship construction. Computer simulations based on mathematical models are more flexible at the initial design stage. To obtain coefficients for the mathematical models, Section 2.2 presents literature on the contemporary hydrodynamic force analysis methods. The Computation Fluid Dynamics (CFD) method is selected because it does not require sophisticated physical test facilities. Furthermore, it can provide sufficiently accurate results at relatively low cost.

2.3. Rudder working conditions

To obtain reasonable results, the rudder hydrodynamic characteristics should be analysed in practical conditions. This section inspects two key elements of the working conditions, i.e. the Reynolds number (Re) and the angle of attack (α), to set up proper test cases for the CFD simulations in Chapter 4. Under certain working conditions, rudders generate lift (F_L) and drag (F_D), based on which normal force (F_N) and tangential force (F_T) can be calculated according to the rudder angle (δ) or the angle of attack (α). Figure 2.1 illustrates

the applied terminology of rudder forces in this thesis.

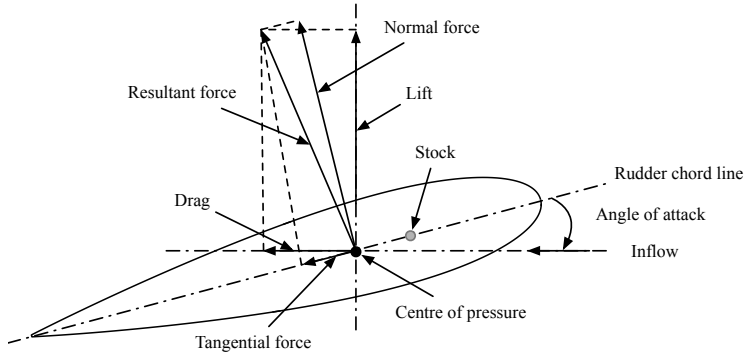


Figure 2.1: Rudder induced forces. Adapted from Molland and Turnock [206, p. 73].

Lift is mainly generated by the pressure difference between the two surfaces. It is the component of the resultant force that acts perpendicular to the inflow direction. Lift nearly increases as a linear function of the angle of attack before the stall angle, which is the critical angle of attack at which maximum lift occurs. Normally, stall angles of rudders in open water are in the range of 15° to 20° , and the practical stall angles in the propeller slipstream would be larger. Furthermore, the stall angle is also affected by the rudder aspect ratio and other parameters. In astern conditions, the lift curve slope reduces to 75 % to 85 % of the ahead condition, the stall angle decreases by 5° to 10° , and the maximum lift coefficient is about 45 % to 75 % of the ahead case [206, p. 99].

Drag is the rudder force component along the incidence flow direction, which consists of skin friction drag and form drag. It increases parabolically with the angle of attack. The friction drag is caused by the frictional shear stress and determined by the size of the wetted surface. The form drag, also known as viscous pressure drag or pressure drag, primarily depends on the shape of the rudder. The friction drag is almost the same for rudders with the same wetted area while the form drag is relatively small. At a Re of 2.4×10^5 , Reichel [234] concluded that under small rudder angles (up to 5°) almost all the tested six types of rudders with the same lateral area but different profiles and constructions have the same drag coefficients.

Routinely, non-dimensional coefficients are used to compare the rudder hydrodynamic performance with various design choices. Two main hydrodynamic characteristics are the lift coefficient (C_L) and the drag coefficient (C_D) based on which the stall angle, the maximum lift coefficient, the normal force coefficient (C_N), the tangential force coefficient (C_T), and the lift to drag ratio (C_L/C_D) are identified. These parameters are non-dimensionalised and calculated as follows:

$$\begin{aligned}
 C_L &= F_L / (0.5 \rho V_R^2 A_R) \\
 C_D &= F_D / (0.5 \rho V_R^2 A_R) \\
 C_N &= C_L \cos \alpha + C_D \sin \alpha \\
 C_T &= C_D \cos \alpha - C_L \sin \alpha,
 \end{aligned} \tag{2.1}$$

where ρ is the water density, α is the angle of attack, V_R is the rudder inflow speed, A_R is the rudder area. Whicker and Fehlner [295], Abbott and Von Doenhoff [1], Thieme [267], and Molland and Turnock [206] provided further information about these coefficients.

2.3.1. Reynolds numbers

The Reynolds number (Re) is the ratio of the momentum force to the viscous force of a flow, expressing the relative importance of these two types of forces. Rudders may have different hydrodynamic characteristics at low Re (laminar flow) and high Re (turbulent flow). Based on the chord length (C_R), full-scale Re of a rudder range from about 5×10^5 for a small yacht up to about 1×10^8 for a large fast ship [206, p. 34]. For complete dynamic similarity of the flow conditions, Re has to be the same for both model-scale and full-scale in experimental and numerical tests. However, Re as high as 1×10^8 is commonly not achievable in contemporary physical model test facilities.

In practice, Re_M is one order smaller than Re_F . The difference in Re violates the similarity of the rudder force in model-scale and full-scale manoeuvring motions. Accordingly, Ueno et al. [278] and Ueno and Tsukada [277] proposed corrections of the rudder effectiveness and the speed to transfer model-scale results to full-scale. In general, an increase in Re leads to an increase in the lift coefficient and a decrease in the drag coefficient [176]. Furthermore, the drag coefficient is more sensitive to the change of Re than the lift coefficient [176]. Whicker and Fehlner [295] indicated that Re influences are significant in the range of 1×10^6 to 3×10^6 and insignificant above 3×10^6 . Ladson [155] noted little variations of the coefficients above Re of 6×10^6 . Detailed information about impacts of Reynolds numbers on rudder hydrodynamics was given by Loftin and Smith [186].

To obtain insights into the rudder performance at high Re from actual low Re physical experiments, roughness strips are commonly attached near the model leading edge to generate turbulent flow instead of laminar flow. In practice, rudders nearly always work in fully turbulent flow due to the propeller rotation. CFD methods can study the full-scale open water rudder hydrodynamics at high Re . Fach and Bertram [69] reported the progress of CFD applications in simulations of rudder flows. However, the required simulation time and computation resource increase dramatically with the model size.

2.3.2. Angles of attack

The angle of attack (α) or the effective rudder angle (α_R) significantly affects the amount and the direction of the rudder induced forces. α_R is closely related to the rudder angle (δ) and the ship drift angle (β), which is commonly expressed as $\alpha_R = \delta - \beta$ [304]. Greitsch [82] and Greitsch et al. [83] applied operation profiles, including the frequency distributions of rudder angles and ship speeds in rudder shape optimisation, cavitation risk analysis, and ship design. Brix [24] indicated that the rotation caused by the propeller may induce an incidence of 10° to 15° to the rudder and a 10% increase in the rudder resistance. Therefore, it is beneficial to have the maximum lift to drag ratio and the minimal drag coefficient within this range to reduce the fuel consumption.

Records of rudder angles were taken on a 110 m long inland vessel by students supervised by the author. Figure 2.2 presents the probability distributions of rudder angles during the one journey from Antwerp, Belgium to Vlaardingen, the Netherlands and the other journey from Vlaardingen, the Netherlands to Hamm, Germany. It shows that the

most frequently used rudder angles are in the range of -15° to 15° . This finding is quite similar to the frequency distributions published by Greitsch [82] and Greitsch et al. [83], which are rudder angles used by a ferry in the North Sea.

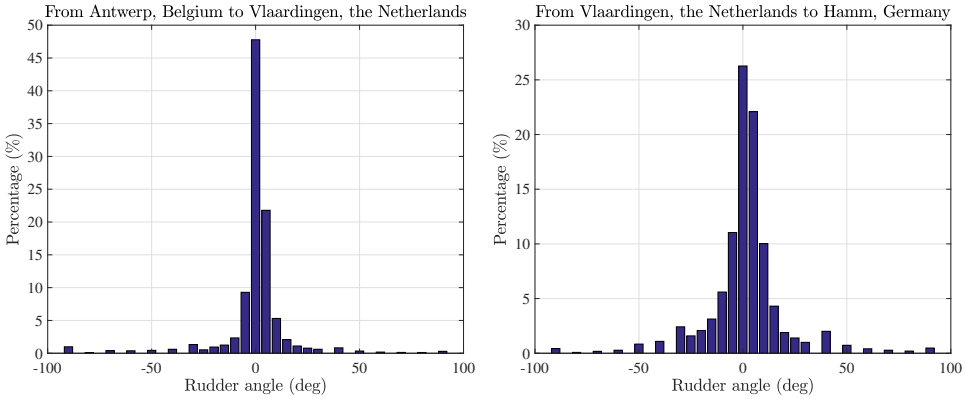


Figure 2.2: Probability distributions of the applied rudder angles in the range of -90° to 90° .

In Figure 2.2, large rudder angles up to 90° also applied at relatively slow speed. These operations are typical for inland vessels in hard manoeuvring situations but rarely seen on seagoing ships which have a customary maximum rudder angle of 35° . Inland vessels, which commonly do not have assistance for birthing or hard manoeuvring, apply the rudders at 90° with bow thrusters to crab or turn on the spot. However, few studies have been made on the rudder performance at large angles of attack. Since this research is intended for primary ship design at service speed, the manoeuvres with large rudder angles are not explicitly studied. Further research is suggested for slow-speed manoeuvring modelling with related parameters to study the performance of crabbing, birthing, and turning with large rudder angles.

2.3.3. Concluding remarks

Considering the Re effects, it is suggested to test a model as large as possible at a sufficiently but not extensively large Re to have a balance of computational cost and accurate results. Therefore, in this thesis, CFD simulations are performed at Re of 6×10^6 above which lift and drag coefficients are not significantly affected. For the angles of attack, this thesis presents CFD simulations with angles of attack in the range of 0° to 35° to have a full vision of the tendency of the rudder hydrodynamic coefficients. Manoeuvring with large rudder angles are important but not studied in this thesis as it is only performed at very low speed and commonly with bow thrusters.

2.4. Rudder design choices

A rudder design needs to consider aspects, including, but not limited to, working conditions (Reynolds numbers and angles of attack), profiles (sectional shapes), parameters (area, thickness, span, chord, and aspect ratios), types (the position of the stock and the structural

rudder-hull connection), and interactions (among the hull, the propeller, and the rudder). These design choices determine the amount and the direction of rudder forces, resulting in different rudder performance. This section presents the state-of-the-art of studies on these choices.

2.4.1. Rudder profiles

Rudder profiles are rudder sectional shapes. The profile is usually described by the rudder camber, the position of the maximum camber, the rudder thickness, the position of the maximum thickness, and the nose radius. Figure 2.3 illustrates the terminology to be used later. Various distributions of the camber and the thickness formulate different rudder series or families.

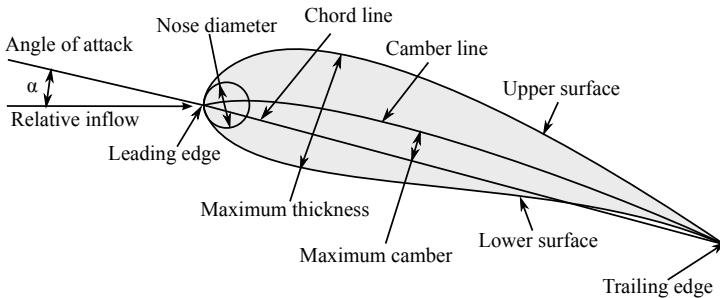


Figure 2.3: Rudder profile terminology. Adapted from Cleynen [42].

Typical rudder profiles applied in practice are presented in Figure 2.4. Most of the existing rudder profiles are originally designed for aerofoils like the NACA series. There are also profiles designed particularly for ship rudders such as the IFS and HSVA series [267]. Other profiles include flat-plate, wedge-tail, fishtail, and flapped rudders. Various rudder profiles have different hydrodynamic characteristics, leading to a different performance in ship manoeuvrability, fuel consumption, and rudder cavitation.

Flat-plate

Flat-plate profiles are normally rectangles in 2D (square head in Figure 2.4). They are the simplest flow deflecting devices to design, the easiest profiles to produce, and the cheapest rudders to buy. To reduce the form drag, flat-plate profiles may have semi-circle or triangular leading and trailing edges with faired tips (round head in Figure 2.4). However, the flat-plate profile may encounter stiffness issues when a large area is required, resulting in limitations of applications.

Thieme [267] indicated that the flat-plate profiles may achieve high efficiency in straight-ahead condition. However, this high efficiency only appears at small angles of attack, up to approximately 5° , after which the flat-plate profile stalls and its lift-to-drag ratio collapses. At present, flat-plate rudders are frequently seen on small boats and antique inland vessels but not common for modern seagoing ships.

NACA

NACA profiles, which are developed by National Advisory Committee for Aeronautics (NACA), are the most widely applied rudder profiles [142] (Figure 2.4). They are also ap-

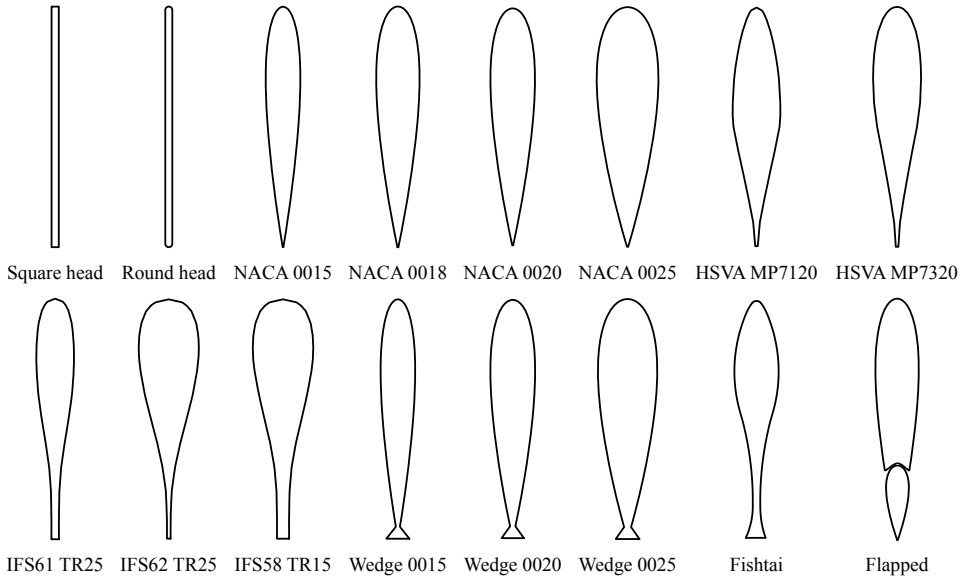


Figure 2.4: Common rudder profiles.

plied to other foil-shaped structures such as, propellers [263], propeller ducts [145, 305], marine current turbines [14, 15, 78, 208], fins [233, 259, 260], and wind turbines [18, 268]. Furthermore, the NACA series is the most thoroughly investigated aerofoil family. Therefore, it is commonly taken as a benchmark case for both aerodynamic and hydrodynamic studies. The geometry of the NACA series was described by Ladson et al. [156].

Wind tunnel test results for aerofoils at small Mach numbers, which means the air is almost incompressible like water, are applicable for ship rudders [1, 81, 155, 186, 195]. Especially, characteristics of aerofoils with low aspect ratios [71, 226, 242, 272] are quite close to those of common ship rudders. Whicker and Fehlner [295] and Thieme [267] further discussed applications of the NACA profiles to shipping. In general, NACA profiles can generate sufficient manoeuvring force with high efficiency.

HSVA

HSVA profiles were specially developed for ship rudders by Hamburg Ship Model Basin (Hamburgische Schiffbau Versuchsanstalt GmbH, Hamburg, Germany). Considering the rudder working conditions, the HSVA series is designed to have a good pressure distribution that reduces the onset cavitation [151]. Bertram [19, p. 271] provided offsets of two main HSVA profiles, namely HSVA MP7120 and HSVA MP7320. Thieme [267] and Brix [24] presented hydrodynamic characteristics of the HSVA profiles in detail. According to Hollenbach and Friesch [102], high-lift HSVA profiles may reduce the rudder area, achieving 1 % fuel saving.

IFS

IFS profiles were developed by Institute für Schiffbau, Hamburg, Germany to achieve a steep lift curve slope, a large stall angle, and a high maximum lift coefficient, as shown in Figure 2.4. Bertram [19, p. 271] showed the offsets of three main IFS profiles, which are

IFS58 TR15, IFS61 TR25 and IFS62 TR25. Thieme [267] presented wind tunnel tests of the IFS profiles. Compared to the HSVA profiles, IFS profiles may generate slightly more lift, induce more drag, and suffer less cavitation [19, p. 297].

Fishtail

Fishtail profiles (Figure 2.4), also known as Schilling rudders [243, 244], are normally developed based on conventional NACA, HSVA, and IFS profiles with trailing tails. The concave part, where the original profile connects with the tail, is smoothed to have a better pressure distribution that delays stalling. Fishtail rudders can effectively generate lift, improving the ship manoeuvrability. Therefore, they are frequently used on inland vessels.

Van Nguyen and Ikeda [281, 282] developed high-lift fishtail profiles by optimising the maximum rudder thickness and the trailing edge thickness. Hasegawa et al. [93] and Nagarajan et al. [213] discussed the superiority of the fishtail rudder to the conventional Mariner rudder of the course keeping ability in windy conditions. However, very few studies have examined the fishtail profiles by experimental tests. In addition, offsets of the fishtail profiles are not publicly available.

Wedge-tail

Wedge-tail profiles are simplified fishtail profiles (Figure 2.4), which normally have a sharp concave point. Van Nguyen and Ikeda [283] indicated that the hydrodynamic characteristics of wedge-tail rudders are related to the size of the tail and the profile thickness. Through CFD simulations, Liu and Hekkenberg [173] presented that the tested wedge-tail profiles can generate more lift than the tested flat-plate and NACA profiles at the cost of additional drag. Since no standard offsets of wedge-tail profiles are found, it is hard to compare the performance of wedge-tail rudders in literature.

Flapped

A flapped profile has a movable flap which changes the profile camber (Figure 2.4). Therefore, flapped profiles can improve ship manoeuvring performance without significantly affecting its cruising characteristics. The disadvantages of flapped rudders are large hinge moments, high mechanical complexity, and potential maintenance difficulties [224]. Two main parameters of a flapped rudder are the flap-linkage ratio (the flap angle relative to the rudder chord line divided by the rudder angle) and the flap-area ratio (the sectional area of the flap divided by the total sectional area). Olson [221] indicated that an increase in either the flap-linkage ratio or the flap-area ratio increases the lift coefficient, reduces the rudder efficiency, and shifts the centre of pressure to the rear in ahead condition while for the astern condition, the lift coefficient is decreased.

Bertram [19, p. 284] described that flapped rudders may provide a much higher lift curve slope and 60 % to 70 % higher maximum lift compared to a conventional rudder of the same shape, size, and area. Olson [221] reported that a 30 % flap NACA 0018 profile using a 1.5 flap-linkage ratio can generate 50 % higher lift than an all-movable rudder of equal area. Kerwin et al. [129, 130, 131] and Oppenheim [224] indicated that a 20 % flap NACA 66 profile may achieve 59 % higher lift than the original NACA 66 profile. Kerwin et al. [129] showed that the drag coefficient at zero lift increases with the flap size and concluded that even a small flap can significantly increase the maximum lift coefficient. Additionally, the size of the flap in a range of 20 % to 50 % of the total rudder area does not influence the maximum lift coefficient [129].

However, the increase in maximum lift is achieved at the expense of a large increase in the drag and the hinge moment [129, 131]. The flap balance may reduce the flap moment but it also significantly reduces the rudder induced side force [130]. Thus, Kerwin et al. [130] suggested that a rudder with small, unbalanced flap might achieve a balance of the improvement over the all-movable rudder and the practical structural requirement. Champlain [35] analysed the effects of the flap gap (the distance between the trailing edge of the skeg and the leading edge of the flap with zero flap deflection) on rudder hydrodynamic characteristics indicating that a larger open gap may achieve a better overall performance.

2.4.2. Rudder parameters

After a selection of the profile, detailed design of rudder parameters should be considered. To avoid ambiguity, the rudder parameters are illustrated in Figure 2.5. These parameters affect the rudder hydrodynamic characteristics and determine the rudder effectiveness and efficiency. Main parameters discussed in this thesis are the area, the thickness, the span, the chord length, and the aspect ratios. These parameters are determined as the key parameters and examined in Chapter 4.

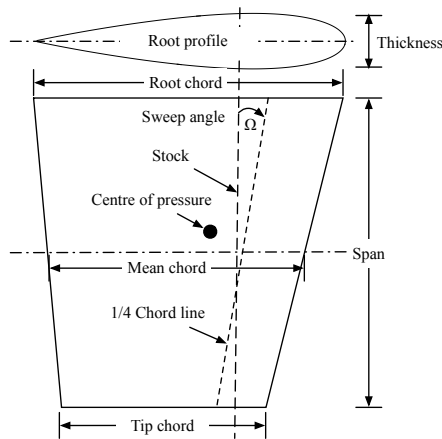


Figure 2.5: Rudder parameter terminology. Adapted from Molland and Turnock [206, p. 72].

Sweep angles, taper ratios, and tip shapes have relatively small influences on the rudder hydrodynamic characteristics [206], therefore, they are only briefly introduced here. The sweep angle slightly affects the maximum lift coefficient and the stall angle [205, p. 79]. An increase in the taper ratio leads to an increase in the lift curve slope, the maximum lift coefficient, and the stall angle [206, p. 90].

A faired tip shape may reduce the minimum drag at zero angle of attack but it decreases the stall angle by 2° to 3° [295]. Hoerner [99] and Molland and Turnock [206] concluded that the square tip is better than the faired tip because the small advantage of the faired tip in the reduction of drag at small rudder angles is gained at the expense of large hydrodynamic losses at large rudder angles.

Area

The rudder area (A_R) affects the amount of lift and drag induced by the rudder. To generate required manoeuvring forces and moments, rudders (one or more) should have a sufficient total area. Multiple rudders are applied when the area of a single rudder is insufficient to turn the ship at the required rate. One reason why the rudder cannot have the required area is because the draught of the ship is small, for instance, inland vessels. However, a larger rudder area normally means larger rudder induced resistance.

The rudder area or the total rudder area, if more than one rudder is applied, is commonly expressed as a ratio of the ship lateral underwater area (LT), where L is the ship length between perpendiculars and T is the loaded ship draught. The value of A_R/LT is normally first estimated based on similar ships or empirical formulas, and then optimised through iterations [142]. Table 2.1 summaries the reference A_R/LT values found in literature [13, 142, 206].

Table 2.1: Reference ratios of the rudder area to the ship lateral underwater area for different ship types.

Ship types	A_R/LT (%)
Container ships	1.2 to 1.7 [13, p. 88]
Passenger liners	1.2 to 1.7 [13, 142, p. 88]
General cargo ships	1.5 [13, p. 88]
Single-propeller merchant ships	1.6 to 1.8 [206, p. 189]
Twin-propeller merchant ships	1.6 to 2.2 [206, p. 189]
Small cargo ships	1.7 to 2.3 [142]
Large cargo ships	2.0 to 2.8 [142]
Oil tankers and bulk carriers	2.0 [13, p. 88]
Lake steamers	2.0 [13, p. 88]
Cross channel ferries (RoRo ships)	2.0 to 3.0 [13, p. 88]
Coastal vessels	2.0 to 3.3 [13, p. 88]
Warships	2.4 to 2.8 [206, p. 189]
Pilot vessels	2.5 to 4.0 [13, p. 88]
Tugs	3.0 to 4.0 [206, p. 189]
Trawlers	3.0 to 4.0 [206, p. 189]
Inland cargo vessels in non-rapid flow segment	2.0 to 3.0 [38, p. 11]
Inland cargo vessels in rapid flow segment	4.5 to 5.0 [38, p. 11]

Reference values in Table 2.1 indicate that the ships which have high requirements of manoeuvrability, such as warships, pilot vessels, tugs, and trawlers, need a large rudder area. For rudders working directly behind propellers, Det Norske Veritas [50] suggested that A_R/LT should not be less than:

$$\frac{A_R}{LT} = 0.01 \left[1 + 50C_b^2 \left(\frac{B}{L} \right)^2 \right], \quad (2.2)$$

where C_b is the ship block coefficient. Additional 30 % area should be added if the rudder does not work directly behind a propeller [50].

To ensure a quick response to helm for broad ships, Schneekluth and Bertram [245, p. 62] advised relating the rudder area (A_R) to the ship midship section area (A_m) and A_R should not be less than 12 % of A_m . To satisfy a particular turning index, Clarke et al. [40] reported that as C_b increases A_R increases slightly while as B/L increases A_R increases significantly, especially above B/T larger than 3. Thus, inland vessels which typically have larger block coefficients, much larger L/B ratios, and extremely much larger B/T ratios than seagoing ships [228] should carefully consider the size of each rudder and the number of rudders to have sufficient total area.

Thickness

The rudder thickness is commonly expressed as a ratio of the rudder chord length. It needs to satisfy the structural needs and, furthermore, affects the minimum drag, the stall angle, and the maximum lift coefficient [206, p. 92]. Commonly, thinner profiles have higher efficiency, more specifically a higher lift to drag ratio, than thicker profiles. Van Beek [279] indicated that a slim rudder profile may increase the propulsive efficiency by 1 % to 3 %. A rudder may have a span-wise different thickness, for instance, a thin profile at the tip and linearly increases to a thick rudder profile at the root. This configuration may provide a balance of the structural requirement and the hydrodynamic efficiency.

Span and chord length

The rudder span or rudder height (B_R) is the distance between the rudder root and tip sections. Normally, the span is expected to be as large as possible, which may ensure a large geometric rudder aspect ratio for high effectiveness and efficiency. However, the span is commonly constrained by ship particulars (ship draught) and operational profiles (water depth).

From observation and experience, for inland vessels, a normal value of the rudder span is around the size of the propeller diameter. The rudder chord length (C_R) is the distance between the leading and trailing edges. The chord length is commonly determined according to the rudder area, the geometric aspect ratio, and the span. For unbalanced rudders, a large chord length is not favourable as it may put an excessive burden on the steering gear.

Geometric and effective aspect ratios

Rudder aspect ratios have the most significant influence on rudder hydrodynamic characteristics [206, p. 89]. It includes two concepts: the geometrical aspect ratio (Λ_G) and the effective aspect ratio (Λ_E). Λ_G is commonly expressed as $\Lambda_G = B_R/C_R$ or $\Lambda_G = B_R^2/A_R$. The effective aspect ratio (Λ_E) is the actual aspect ratio applied to hydrodynamic force calculation.

In general, a rudder with a larger geometric aspect ratio can generate larger lift at lower drag [295]. However, a small geometric aspect ratio may enhance the manoeuvrability with a large stall angle [206, p. 64]. Confirmed by a rudder manufacturer, a common range of geometric aspect ratios for seagoing ships is 1.5 to 3 while the common range of aspect ratios for inland vessels is 1 to 2.

To compare the hydrodynamic characteristics of profiles, an infinite geometric aspect ratio (an infinite span), is commonly assumed in experimental and numerical studies [89, 195]. Such an approach associates the hydrodynamics only with the parameters of the 2D profile rather than the 3D shape of the rudder. Thus, it is useful for investigating the profile drag, the pressure distribution, and theoretical application [206, p. 41].

In practice, the rudder has a finite span and a finite aspect ratio. A finite span has a downward flow along and behind the rudder, which is the so-called downwash. This downwash is combined with the inflow leading to a smaller effective angle of attack than the deflected rudder angle. Therefore, small geometric aspect ratios have a larger reduction of effective rudder angles due to larger downwash leading to a larger stall angle.

The effective aspect ratio (Λ_E) is commonly estimated based on the geometric aspect ratio (Λ_G). When the rudder root is sufficiently close to a flat surface, such as a large end plate or a flat hull, Λ_E/Λ_G is close to 2 owing to the ideal mirror image effect [206, p. 183]. Considering the gap effects, Brix [24, p. 97] provided reference values of Λ_E/Λ_G . Root and tip end plates may increase the effective aspect ratio and cause notable drag. From observation, seagoing ship rudders normally do not have end plates while inland vessel rudders tend to have both root and tip plates.

2.4.3. Rudder types

Rudder types are classified based on two aspects: the position of the stock (unbalanced, semi-balanced, or balanced) and the structural rudder-hull connection (the number of pintles, without a skeg, semi-skeg, or full-skeg). The choice of the rudder type depends on the ship type, the ship main dimensions, the shape of the stern, and the required rudder size [206, p. 13]. This section reviews four common rudder types, namely unbalanced, fully-balanced, spade, and semi-skeg, which are shown in Figure 2.6.

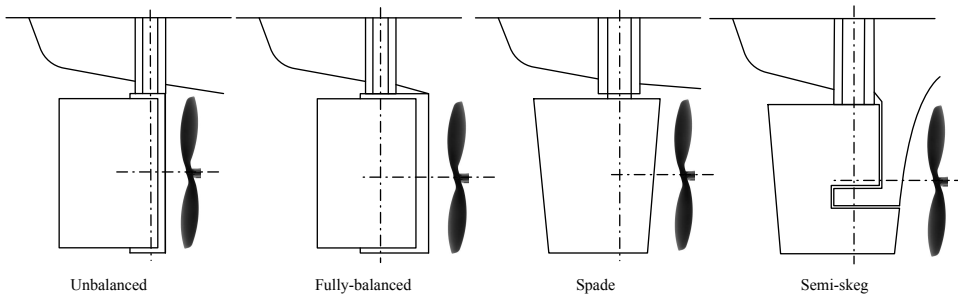


Figure 2.6: Common rudder types. Adapted from Molland and Turnock [206, p. 15].

Unbalanced

Unbalanced rudders have their stocks at the leading edge, as a result of which, the entire rudder area is located after their stocks (Figure 2.6). The steering gear has to provide all the rudder turning torque. It implies that this solution only works for rudders with a limited area. Otherwise, the rudder cannot be steered properly. To compensate for the large bending moment, this type of rudder has two pintles on top and bottom. Currently, unbalanced rudders are not widely used for modern single-propeller ships, but they are still popular for small crafts and fishing vessels as the unbalanced rudders are easy and cheap to produce [19, p. 282].

Fully-balanced

Fully-balanced rudders have their rudder stocks at 20% to 40% chord length from the leading edge (Figure 2.6). The water force acting on the aft part of the rudder is partially

or, at some rudder angles, completely compensated by the force acting on the forward part of the rudder. Therefore, the rudder turning torque and the required capacity of the steering gear for fully-balanced rudders are far less than that for unbalanced rudders. Since the action point of the force changes with the rudder angle, it is not feasible to maintain the balance over a complete range of rudder angles. Fully-balanced rudders are extensively applied to single-propeller merchant ships and gradually superseded by semi-balanced skeg rudders [206, p. 14].

Spade

Spade rudders are balanced rudders with a taper ratio (the ratio of the root chord to the tip chord) as shown in Figure 2.6. Rudders with a large taper ratio may reduce the rudder drag or even generate thrust [28]. Due to the large bending moment, spade rudders are commonly designed with a large stock diameter and a large rudder thickness. According to Bertram [19, p. 283], spade rudders are not feasible if the required stock diameter is larger than 1 m. Commonly, spade rudders consume less energy to be operated than the unbalanced rudders.

According to Bertram [19, p. 272], spade rudders are more favourable than unbalanced or fully-balanced rudders. From hydrodynamic and cavitation points of view, spade rudders are better than semi-skeg rudders. At an optimum relative position to the propeller (about 30 % to 35 % of the propeller diameter), a spade rudder shows about 1.6 % gain of power against a semi-skeg rudder [198]. Unlike semi-skeg or full-skeg rudders, spade rudders do not have gap cavitation, reducing the time and cost for maintenance. Nowadays, spade rudders are widely applied to all ship types.

Semi-skeg

Semi-skeg rudders, also called horn rudders, or Mariner rudders, are semi-balanced rudders, more specifically unbalanced root part with a skeg and balanced tip part without a skeg (Figure 2.6). The location of the pintle is supposed to be in the vicinity of the centre of pressure, affecting the response and torque characteristics of the rudder. The horn provides structural support for the span-wise bearing moment, making a large rudder area possible. In addition, semi-skeg rudders require less turning torque than unbalanced rudders and have less bending moment than spade rudders. Nowadays, semi-skeg rudders tend to be favourable for newly built large ships despite the hydrodynamic advantages of spade rudders [188].

Through series of free-stream wind-tunnel tests, Molland [200, 201] found that a semi-skeg rudder has a little smaller maximum lift, a smaller lift to drag ratio, and a significantly smaller lift curve slope than an all-movable rudder of the same size. Thus, semi-skeg rudders are less effective than spade rudders for manoeuvring [19, p. 283]. These changes in lift and drag coefficients are mainly caused by the rudder horn. Even though the rudder horn itself does not incline, it still significantly affects the lift and drag of the rudder [188].

2.4.4. Relative positions

The relative positions of the propeller and the rudder are described by longitudinal (x_{PR}), lateral (y_{PR}), and vertical (z_{PR}) separations. The relative positions determine the proportion of the rudder area in the propeller slipstream, which influences the rudder induced side force [202]. Stierman [255, 256] indicated that the dominant impact factors on the propeller-

rudder interaction are the propeller pitch ratio, the rudder thickness, and the longitudinal propeller-rudder separation.

The longitudinal separation (x_{PR}) is the distance between the rudder stock and the propeller rotating plane. It determines the diameter of the propeller slipstream that arrives at the rudder and the velocity distribution within it [275]. According to Molland and Turnock [202], x_{PR} has little impacts on the rudder side force. Oppenheim [224] concluded that the steady forces on the rudder are completely independent of x_{PR} in the range of $0.5D_P$ to $1.0D_P$.

Under some extraordinary conditions, the rudder may generate thrust, reducing the overall resistance of the ship [28]. At various ship speeds, Reichel [234] tested six rudders at x_{PR} of $0.59D_P$, $0.65D_P$ and $0.71D_P$ and concluded that the best rudder location is the closest to the propeller. Minchev et al. [198] tested spade and semi-skeg rudders at x_{PR} of $0.456D_P$, $0.371D_P$ and $0.272D_P$ and showed that the optimum x_{PR} for a single-propeller single-rudder bulk carrier could be in the range of $0.30D_P$ to $0.35D_P$.

The lateral separation (y_{PR}) is the distance between the rudder stock and the propeller shaft. When the number of propellers and the number of rudders are the same, the rudder central plane commonly aligns with the propeller shaft. A change in y_{PR} leads to a shift in the rudder incidence for zero lift while the hydrodynamic characteristics are not greatly affected [122, 203, 204]. Additionally, this shift increases with an increase in the propeller working load [207].

The vertical separation (z_{PR}) is the distance between the rudder tip and the propeller shaft. A change of z_{PR} alters the proportion of the rudder span in the propeller slipstream leading to a shift in the incidence of zero lift. In general, the vertical separation has relatively small influences on the rudder performance.

2.4.5. Multiple rudders

When multiple rudders are applied, the interaction among the rudders should be considered. Multiple-rudder ships may have different starboard-side and port-side manoeuvring behaviours. The asymmetrical behaviours are notable for single-propeller twin-rudder ships [25, 51, 87, 92, 125, 214]. According to Yoshimura and Sakurai [314], hydrodynamic characteristics of a twin-propeller twin-rudder are not so much different from those of a single-propeller single-rudder ship. Quite a few studies have been done for twin-propeller twin-rudder ships [22, 43, 53, 54, 123, 132–134, 144, 165, 261, 306, 314]. Additionally, hydrodynamic characteristics of each rudder in twin-rudder configurations are also affected by the interaction between the rudders [77].

For twin-rudder ships, the distance between the rudder stocks and the coupling of the rudder angles may have significant impacts on ship manoeuvrability. By setting both rudders outwards at 75° , covering the gap between the leading edges, a twin-rudder ship may reduce the stopping distance by 50% compared to a conventional reverse engine stopping [16, p. 41]. These outwards rudder angles are called clam shell angles as shown by Hamamoto and Enomoto [87] and discussed by Hasegawa et al. [91].

Hamamoto and Enomoto [87] proposed analytical formulas of the ship forward speed drop, the stopping time, and the stopping distance when a ship stops with the clam shell angles. Although the above studies invested the manoeuvrability of some twin-rudder seagoing ships, no reference in the literature described the manoeuvring performance of multiple-

rudder inland vessels. In fact, inland vessels are more commonly equip twin rudders or even quadruple rudders than seagoing ships.

2.4.6. Concluding remarks

Section 2.4 has reviewed the common rudder profiles, namely flat-plate, NACA, HSVA, IFS, fishtail, wedge-tail, and flapped. The flat-plate profile is effective with small rudder angles but limited by stiffness issues in the rudder area. Considering the enlargement of inland vessels, the flat-plate profile is not suitable and thus not considered in this thesis. The NACA series has been widely applied and systematically studied. Therefore, it is chosen as the benchmark profile and applied to CFD validation in Chapter 4. The IFS series is taken as a representative of the rudder oriented profiles.

Fishtail and wedge-tail rudders are both designed to have high lift coefficients. Since no publicly available offsets of these profiles were found, the author designed a series of wedge-tail profiles based on the NACA profiles of the same thickness. The flapped profile may have superior performance to the classic whole-body profiles but it has disadvantages of hinge moments, mechanical complexity, and maintenance difficulties. The flapped profile is a good alternative for ships that require high performance such as tugs, working boats, and cruise ships. In summary, this thesis chooses the NACA, the IFS, and the wedge-tail profiles as reference profiles.

Key design parameters in a rudder design, more specifically the area, the thickness, the span, the chord length, and the aspect ratios, should be considered as a whole to find the most suitable combination. In general, the area should be sufficiently large. The thickness should be as thin as possible with the prerequisite of satisfying the structural requirements. The span and chord length should be optimised to ensure large aspect ratios. This thesis does not vary these detailed design parameters in each tested rudder configuration but provides an integrated manoeuvring model (Chapter 5) which makes it possible to analyse the impacts of each parameter.

Based on the above-mentioned literature and daily observation of the inland vessels in the Netherlands waterways, it is concluded that the spade type rudder is still the most suitable for commercial motor vessels because the spade rudders are superior to other types with regard to the overall performance of hydrodynamics, cavitation, and maintenance. Considering enlargement of inland vessels and inland-seagoing combined vessels, the semi-skeg type is a good alternative which enables a large rudder area. In this thesis, the impacts of rudder configurations on ship manoeuvrability are analysed based on the spade type rudder, but the results are also applicable to other rudder types.

The interaction between the propeller and the rudder is primarily determined by their relative positions. Longitudinal and lateral separations affect the incidence angles and speeds while the vertical operation has little influence. Inland vessels commonly feature multiple-rudder configurations and the interactions among rudders should be carefully considered. Impacts of spacing among twin and quadruple rudders are analysed in Chapter 4 and their influences on inland vessel manoeuvrability are further discussed in Chapter 6.

2.5. Rudder performance

Good performance in ship manoeuvrability, fuel consumption, and rudder cavitation is the goal of a rudder design. Above all, rudders should be capable of inducing sufficient manoeuvring forces to ensure navigation safety, especially for ships which frequently sail in constrained waterways or severe conditions. The rudder should also be efficient, which means minimum drag at the required lift. Last but not least, rudder cavitation should be considered to reduce the time and cost of maintenance.

2.5.1. Ship manoeuvrability

The rudder effectiveness in ship manoeuvrability is commonly evaluated by the amount of the rudder induced side force (Y_R), which is the component of the rudder resultant force normal to the ship centreline [24, p. 96]. Y_R can be calculated as the following:

$$Y_R = 0.5\rho V_R^2 A_R C_{YR}, \quad (2.3)$$

where C_{YR} is the rudder side force coefficient and is normally estimated based on the gradient of the side force coefficient $C_{YR\alpha}$ as $C_{YR} = \alpha C_{YR\alpha}$. Normally, $C_{YR\alpha}$ is available from experimental results or empirical formulas as the following:

$$C_{YR\alpha} = \frac{1.8\pi\Lambda_E}{\sqrt{\Lambda_E^2 + 4 + 1.8}}, \text{ by Mandel [191];} \quad (2.4)$$

$$C_{YR\alpha} = \frac{2\pi\Lambda_E(\Lambda_E + 1)}{(\Lambda_E + 2)^2}, \text{ by Söding [250].} \quad (2.5)$$

More frequently, the rudder side force is calculated by the rudder normal force (F_N), neglecting the rudder tangential force (F_T) [138, 304] as the following:

$$Y_R = -(1 + a_H)F_N \cos \delta, \quad (2.6)$$

where a_H is the rudder force increase factor due to the hull. The rudder normal force (F_N) is expressed as:

$$F_N = 0.5\rho V_R^2 A_R f_\alpha \sin \alpha, \quad (2.7)$$

where $f_\alpha \sin \alpha$ stands for the rudder normal force coefficient (C_N). According to Fujii [72] and Fujii and Tsuda [73, 74], f_α is commonly estimated as the following:

$$f_\alpha = \frac{6.13\Lambda_G}{\Lambda_G + 2.25}. \quad (2.8)$$

However, Equation 2.8 does not account the effects of the rudder profile and the number of rudders on the rudder hydrodynamic coefficients.

2.5.2. Fuel consumption

A rudder may increase total resistance by about 1% in the neutral position and 2% to 6% at moderate angles [5]. Aiming to cut CO₂ emissions, International Maritime Organization [113, 114] requires that all ships larger than 400 gross tonnage reduce Energy Efficiency Design Index (EEDI) by up to 30% after 2025. To achieve such a goal, more efficient rudders, which can induce sufficient lift with minimum drag, are helpful. Furthermore, minimised rudder torque can also reduce the fuel consumed by the steering gear. In general, 2% to 8% saving can be achieved by optimising the rudder configuration in terms of profiles, types, and efficiency-improving devices [98].

Hochkirch and Bertram [98] pointed out that the rudder has an underestimated potential for fuel reduction, for instance, reducing the rudder size (weight and resistance) by improving the rudder profile or changing to a highly efficient flapped rudder. Lehmann [169] summarised that an efficient rudder system should have a slim and low drag rudder profile, generate high lift at small rudder angles, have a smooth surface, be tuned with the propeller, be light weighted, and be easy to maintain. Hollenbach and Friesch [102] listed possible maximum gains of fuel reduction by optimising the arrangement and shape of the propeller-rudder system.

Lehmann [169] suggested optimising the propeller-rudder system and reducing the rudder weight to save fuel. Lehmann [169] indicated that it is important to integrate rudder design with propeller and hull form design. Van Beek [279] and Lehmann [169] applied a torpedo shaped bulb on the rudder as a streamlined continuation of the propeller hub. Similarly, Hollenbach and Reinholz [103] found that the ships with a bulb fitted rudder require 4% less power than those with the standard rudder. Sarasquete et al. [241] showed a 12% reduction of power demand for a fishing vessel by modifying the propeller hub and rudder shapes.

Reducing drag due to rotating incidence flow, a twisted rudder may enhance the overall propulsive efficiency. Commonly for a clockwise rotating propeller, the leading edge of the rudder above the shaft centre is twisted port and below the shaft is twisted starboard. A twisted rudder with a Costa bulb may have 4% less fuel consumption [102]. Kim et al. [143] reported that a Z-twisted rudder, which has a Z-shape leading edge, with and without a fin may reduce the fuel consumption by 2.35% and 2.95% respectively. Due to a decrease in the effective angle of attack, the lift and drag of twisted rudders may be smaller than those of common spade rudders [143]. Yang et al. [302] further studied the rudder forces of a twisted rudder.

2.5.3. Rudder cavitation

Rudders are placed in the high-speed propeller slipstream. Cavitation happens when the pressure in the flow is as low as the water vapour pressure. Brennen [23, Section 3.6] explained that the cavitation damage is caused by the repetition of cavitation bubble collapse in the vicinity of a solid surface. This collapse generates highly localised and transient surface stresses, which causes local surface fatigue failure and eventually develops to erosion. Due to repair or replacement of the eroded rudder, maintenance cost increases and operational time decreases [246]. Meanwhile, rudder cavitation also causes an increase in drag, hull vibration, and radiated noise [246].

The enlargement of ships and the impacts in ship speed lead to higher speed and lower

pressure in the propeller slipstream. Rudder cavitation has become more and more serious [4, 88]. However, service speed tends to be decreased to save fuel and meet the EEDI requirements [98, 102, 169]. Thus, the cavitation may become less significant in the future. As Rhee et al. [235] showed, Figure 2.7 illustrates typical areas of cavitation damage on a semi-skeg rudder. The damages are mainly due to the high speed near the horn and pintle section gaps, the propeller tip and hub vortex, and the propeller sheet.

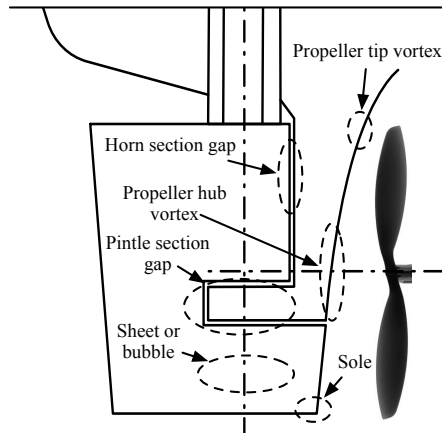


Figure 2.7: Typical areas of cavitation damage on a semi-skeg rudder. Adapted from Rhee et al. [235].

Cavitation causes cavity drag. The cavity drag increases sharply with an increase in ship speed [246]. Thus, a reduction of ship resistance is expected if the rudder can be operated without cavitation, especially for high-speed vessels. Lübke [188] showed that the cavitation effects cause a 10 % decrease in lift and a 20 % increase in drag. According to Shen et al. [247], Mewis and Klug [197], and Ahn et al. [4], twisted spade rudders can reduce the cavitation and improve the propulsion efficiency. Ahn et al. [4] reported an X-Twisted rudder which can reduce the rudder cavitation and improve the overall manoeuvrability.

2.6. Synthesis

Chapter 2 has reviewed the literature on two main aspects: inland vessel manoeuvrability and ship rudders. Ship manoeuvrability deserves more attention in ship design compared to the previous economic point of view [231], especially for inland vessels. The research on ship manoeuvrability is increasing, but still mainly focusing on seagoing ships rather than inland vessels. Main challenges for inland vessel manoeuvrability analysis are how to estimate the hydrodynamic forces with given ship particulars in a specified waterway and how to evaluate their performance according to manoeuvrability criteria required by the navigation environment of that waterway. Gaps in knowledge need to be filled for inland vessels at slow speed in shallow water considering complex configurations, especially multiple rudders.

Clear differences exist in the external environment factors and internal design factors on ship manoeuvrability between inland vessels and seagoing ships (Section 2.1). Accordingly,

design differences should be carefully considered in inland vessel manoeuvrability studies. Since shallow-water effects become significant when $H/T < 1.5$ and the reference vessels in this thesis primarily sail in channels deeper than this value, it is decided not to explicitly study the shallow-water effects. Furthermore, the ship-ship and ship-bank interactions are not considered as they are not the primary design concerns for an initial design. This thesis provides a modular type manoeuvring model in Chapter 5, which allows further research to put new impacts into consideration, such as shallow water, ship-ship, and ship-bank effects.

The rudder configuration has been identified as one of the most critical differences and pointed as the main research topic of this thesis. A good rudder configuration should be effective in manoeuvring force generation, ensuring ship navigation safety. Considering fuel consumption, the rudder should also be efficient, more specifically induce minimum resistance with sufficient manoeuvring force. To analyse the hydrodynamic forces, the common methods are captive model tests, free-running tests, open water tests, and numerical methods (Section 2.2). With the fast development of computer science, Computational Fluid Dynamics (CFD) techniques are increasingly popular in manoeuvrability research for hydrodynamic coefficients and force prediction. Thus, CFD methods, which are validated with experimental test data, are selected to analyse the rudder forces in Chapter 4.

Rudder hydrodynamics are closely related to the working conditions, i.e. Reynolds numbers and angles of attack (Section 2.3). From literature, the Reynolds number for CFD simulations is determined to be 6×10^6 above which the rudder hydrodynamics are not significantly affected by the Reynolds number. Even though inland vessels often applied large rudder angles at slow-speed hard-manoevring situations, rudder angles in the range of -35° to 35° are primarily applied at service speed (Figure 2.2). Future study is recommended for the rudder hydrodynamic characteristics at large angles of attack, which can also be integrated into the proposed mathematical model in Chapter 5 for manoeuvring with clam shell angles.

Rudder design choices of profiles, parameters, and types determine the rudder hydrodynamic performance (Section 2.4). Considering the features of the profile families, the accessibility of profile offsets, and the availability of the validation data, the NACA, IFS, and wedge-tail series are selected as the reference profiles. The rudder parameters are tested as they are for the reference inland vessels but not varied individually in this thesis. The spade type rudder is selected as the reference rudder type not only because it is the original design of the reference ships but also because of its superior hydrodynamic and cavitation performance to other rudder types.

In this thesis, the rudder performance is primarily evaluated in ship manoeuvrability (rudder effectiveness) and fuel consumption (rudder efficiency). The rudder cavitation is not examined as inland vessels normally sail at slow speed and have less significant cavitation than high-speed seagoing ships (Section 2.5). To evaluate and compare the manoeuvring performance of ships with various design, practical test manoeuvres and related criteria are needed. Existing manoeuvrability standards and new test manoeuvres for inland vessels are discussed and proposed in Chapter 3.

Chapter 3

Test Manoeuvres and Criteria for Inland Vessel Manoeuvrability*

“Only a man’s character is the real criterion of worth.”

Eleanor Roosevelt (1884 – 1962)

As discussed in Chapter 2, inland vessels are different from seagoing ships in the external environment and internal design factors. These differences should be considered in test manoeuvres and related criteria because improper tests may lead to a wrong judgement of the manoeuvring performance in reality. The test manoeuvres are designed to evaluate the ship’s capability of accomplishing certain manoeuvring behaviour, such as turning in a constrained area, collision avoidance in an emergency, and stopping in a limited distance. Thus, the manoeuvres to be designed as practical as possible. However, existing manoeuvrability standards for inland vessels are not satisfactory.

Factors that constrain inland vessel manoeuvrability such as limited channel breadth and shallow water are not addressed explicitly in the initial ship design. The difficulties of considering the ship behaviour in shallow water are commonly ignored on the understanding that if the ship’s performance is improved in deep water then it will likely also be better in shallow water. In addition, standard parameters and manoeuvres for design and testing of inland vessel manoeuvrability are still not as elaborate as the IMO standards for seagoing ships [111, 112]. Thus, guidance and criteria are required to enable naval architects to ensure good manoeuvrability for navigation safety and economic benefits.

For the purpose of achieving more realistic judgement on manoeuvrability, benchmark manoeuvres and related criteria are proposed in this chapter. Section 3.1 introduces the existing manoeuvrability standards. Accordingly, the contemporary test manoeuvres for seagoing ships and inland vessels are presented in Section 3.2. After analysing the definitions in existing standards and manoeuvres, Section 3.3 proposes new manoeuvres and criteria for inland vessels. Some of these manoeuvres are tested in Chapter 6 and summarised in Chapter 7. Section 3.4 presents the conclusions of this chapter.

3.1. Existing manoeuvrability standards

Presently, the most common standards for ship manoeuvrability are issued by International Maritime Organization (IMO). These standards should be applied to “ships of all

*This chapter is based on Liu et al. [179] and Liu et al. [180].

rudder and propulsion types, of 100 m in length and over, and chemical tankers and gas carriers regardless of the length” [111, 112]. In the IMO standards, the ship type, either seagoing or inland, is not clearly stated. However, the applicable condition of the standards is described as deep, unconstrained water ($H/T > 4$). It is, therefore, rational to suppose that the IMO standards are intended for seagoing ships, but also valuable as guidance for inland vessels.

Regulations for inland vessels are normally proposed by regional authorities [32, 33, 63] and classification societies [27]. Compared to the IMO standards for seagoing ships, these regional requirements have fewer test manoeuvres and criteria. According to Gray et al. [79], it is still doubtful if the existing standards lead to adequate manoeuvrability in shallow, restricted, and congested waterways. Therefore, in either case of inland vessels or seagoing ships, new test manoeuvres and procedures for shallow and restricted water operations are required to properly predict and evaluate ship manoeuvrability [157, 179].

In order to improve maritime safety and enhance marine environmental protection, standards for ship manoeuvrability should be used in ship design, construction, and operation [21]. Due to the lack of uniform manoeuvring standards, some ships have been built with very poor manoeuvring qualities, which may result in casualties and pollution [52, 217]. Hence, elaborate and uniform criteria should be established for safety [227]. ITTC Manoeuvring Committee [120] gave a review of the criteria in use for inland vessels, fast ships, and dedicated low-speed manoeuvres. More requirements are necessary for other scenarios like constrained waterways and port areas. The necessity of more critical requirements for specific situations was discussed by Li et al. [171].

Table 3.1 compares the existing manoeuvrability standards. From this table, it is concluded that more elaborate criteria for different navigational conditions, especially for inland waterways, should be issued to define the minimum performance. Furthermore, emergency situations, such as engine failure, strong wind, currents, and waves, should be examined to predict the worst manoeuvring cases.

Table 3.1: Overview of existing standards and criteria for ship manoeuvrability [6, 33, 63, 111, 112].

Abilities	Manoeuvres	IMO	ABS	CCNR and European Commission	Bureau Veritas
Turning	35° turning	Advance $< 4.5 L$. Tactical diameter $< 5 L$.	Not rated $R_{td} \geq 1$	The turning capacity of vessels and convoys whose length does not exceed 86 m and width does not exceed 22.90 m shall be considered sufficient.	
Initial turning	10°/10° zigzag	Distance ship travelled $\leq 2.5 L$ by the time the heading has changed by 10° from the original heading.	$R_{ti} \geq 1$		
Yaw checking and course keeping	10°/10° zigzag	First overshoot angle: $< 10^\circ (L/V < 10 \text{ s});$ $< (5+0.5 L/V)^\circ (10 \text{ s} \leq L/V < 30 \text{ s});$ $< 20^\circ (L/V \geq 30 \text{ s}).$	Rated ≥ 1	Evasive manoeuvres with a rudder angle of 20° and 45° to starboard and port shall be checked by yaw rate and maximal period instead of overshoot angles for zig-zag manoeuvres. Criteria vary for different ship dimensions and water depth.	Requirements are put on stopping capacity, astern trials, capacity of taking evasive actions, and turning capacity of inland vessels.
		Second overshoot angle: $< 25^\circ (L/V < 10 \text{ s});$ $< (17.5 + 0.75 L/V)^\circ (10 \text{ s} \leq L/V < 30 \text{ s});$ $< 40^\circ (L/V \geq 30 \text{ s}).$	Not rated		
20°/20° zigzag	First overshoot angle $\leq 25^\circ$	$R_{in20} \geq 1$			
Stopping	Full astern stopping	Track reach $< 15 L$. None for head reach.	Not rated $R_{ts} \geq 1$	In flowing or standing water, stopping distance changes with the ship length.	

Due to the differences in navigation conditions and ship particulars between inland vessels and seagoing ships as discussed in Section 2.1, the standards for manoeuvrability are

expected to be ‘different’ in the aspects of the test manoeuvres and criteria. A summary of existing standards, namely International Maritime Organization (IMO), American Bureau of Shipping (ABS), European Commission (EC), Central Commission for the Navigation of the Rhine (CCNR), and Bureau Veritas (BV) is given in the succeeding paragraphs to find the gaps to improve inland vessel standards. After discussing the existing manoeuvrability standards, the required full-scale test conditions and contents are proposed.

3.1.1. International Maritime Organization

The most widely accepted criteria for ship manoeuvrability are issued by International Maritime Organization (IMO), including turning ability, initial turning ability, yaw checking and course keeping ability, and stopping ability [111, 112]. Daidola et al. [45] described how these IMO standards were defined and improved. However, these standards are specified for ships longer than 100 m in deep unconstrained water. Shorter ships and vessels with unconventional propulsion systems, for instance, azimuth thrusters, are not subject to the IMO standards. Based on the opinion of the administration, current rules can be taken as reference for unconventional ships.

To comply with the requirements of authorities, the manoeuvrability criteria should be evaluated under specified test conditions and procedures [116]. For seagoing ships, the trial should be conducted in deep unconstrained sea water to eliminate the effects of the waterway bottom, banks, and other external objects. The deep water here means that the depth of water should be more than 4 times of the mean draught [112]. The trial speed should be set to at least 90 % of the ship’s speed corresponding to 85 % of the maximum engine output. The test ships should be loaded to the design dead weight and even keel within 5 % deviation.

Three manoeuvres are needed for sea trials: the turning circle manoeuvre (turning and initial turning ability), the zigzag manoeuvre (yaw checking and course keeping abilities), and the stopping test (stopping ability) [111, 112]. For example, the zigzag test, which is specially developed for towing tank tests but also popular for full-scale tests [19], can show the manoeuvring capacities of initial turning and yaw checking ability. Brix [24] carried out series of model tests, yielding the typical values of ship zigzag indices. Since the test environment described in the IMO standards is open deep water, there is a need to consider ship’s manoeuvring capacities in shallow constrained areas, such as harbour entrance channels and ports [79, 109, 157].

The existing manoeuvres may also lead to misunderstanding of the actual manoeuvring performance. Yoshimura et al. [315] pointed out that an evaluation based on the second overshoot angle of a 10°/10° zigzag test and the first overshoot angle of a 20°/20° zigzag test may regard poor manoeuvrability as good. At present, hydrodynamic (constrained water), meteorological (the wind, the wave, and the current), and navigational (other ships, artificial constructions) impacts are not covered in the existing IMO standards. The need to formulate criteria for off service speed (slow speed) and water depth (shallow water) was recognised by Dand [46], Gray et al. [79], Hwang et al. [109], Landsburg et al. [157], and Quadvlieg and Van Coevorden [231].

Besides the standards specified for ship manoeuvrability, there are other requirements of IMO for navigation safety, which indirectly affect the ship manoeuvring performance. For example, International Maritime Organization [114] states, “The main steering gear and

rudder stock should be capable of putting the rudder over from 35° on one side to 35° on the other side with the ship at its deepest seagoing draught and running ahead at maximum ahead service speed and, under the same conditions, from 35° on either side to 30° on the other side in not more than 28 s". This rule requires a minimal rudder turning rate, which affects the turning related manoeuvring abilities.

3.1.2. American Bureau of Shipping

In most of the cases, ship designers only want to meet the minimum requirements of the authorities [231]. In order to enhance navigation safety instead of just meeting the minimum criteria, American Bureau of Shipping [6] (ABS) built a rating system to evaluate the overall manoeuvring capacity, which provides information on implementation and application of the IMO standards. Biancardi [21] developed a set of performance indices based on full-scale trial results. Spyrou [252] applied a rating procedure based on a synthesised manoeuvrability index. Belenky and Falzarano [17] compared the IMO requirements [111, 112], the rating system established by Barr et al. [12], and ABS Guide for Vessel Manoeuvrability [6].

3.1.3. Central Commission for the Navigation of the Rhine

Even though there are no universal criteria such as IMO standards for inland vessels, requirements have been set up as regional regulations. To maintain a safe and smooth flow of traffic on the Rhine, manoeuvring criteria and assessment approaches were proposed by Dijkhuis et al. [52]. Central Commission for the Navigation of the Rhine [32] (CCNR) stated the required inland vessel manoeuvrability in terms of the forward speed, the stopping capacity, the manoeuvrability while going astern, the capacity to take evasive actions, and the turning capacity. Only the evasive manoeuvre (similar to zigzag tests but checked by yaw rates instead of heading angles) and the stopping test are mandatory [33]. However, as seen in Table 3.1, these criteria are not as elaborate as the IMO standards. Since inland vessels commonly sail in more complex situations than seagoing ships, they may need more test manoeuvres and criteria in detail to ensure navigation safety.

Considering the differences between the open sea and inland waterways (Section 2.1), inland trials should be carried out in representative inland waterways. For ships in the Rhine, tests should be performed in areas of the Rhine or other inland waterways with similar conditions [33]. The area should be straight not less than 2 km and sufficiently wide, in flowing or standing water. The under keel clearance should be at least 20 % of the water depth and not less than 0.5 m [32]. The test load condition should be 70 % to 100 % of full load and even keel. The ship velocity relative to the water is at least 13 km. Vessels and convoys proceeding downstream should be able to stop in good time while remaining sufficiently manoeuvrable. Turning capacity should be demonstrated by upstream turning manoeuvres.

3.1.4. European Commission

European Commission [63] (EC) states that the technical requirements related to the capacity of taking evasive action and turning. For changes in speed, it concerns the forward speed, the stopping capacity, and the capacity of going astern. Accordingly, the manoeuvring capacities are tested by evasive action test and full astern test [33, 63]. Furthermore,

these requirements are also applied to coupling systems in a rigid assembly and vessels with active steering devices. At least four evasive action manoeuvres are requested, i.e. port and starboard side tests with rudder angles of 20° and 45°. The test conditions are similar to those of the CCNR standards in Section 3.1.3.

3.1.5. Bureau Veritas

Bureau Veritas [27] (BV) put requirements of inland vessel manoeuvrability on the stopping capacity, the astern trials, the capacity of taking evasive actions, and the turning ability of inland vessels. The ships classified by Bureau Veritas should be checked by all navigation tests in areas designated by the ship classification society. Similar to the European Commission standards, the stopping capacity test for ships which are not longer than 86 m and not wider than 22.9 m can be replaced by turning manoeuvres [27]. The requirements on ship manoeuvrability in the Bureau Veritas are less elaborate than other standards as their focus is mainly on the structure and the equipment of the ship.

3.1.6. Concluding remarks

After reviewing the existing standards, it is clear that the expected differences between regulations for inland vessels and seagoing ships exist, but the requirements have not always been specified in detail. Thus, based on the existing standards, new manoeuvres and parameters are needed to have a deeper insight into the manoeuvring performance of inland vessels. Furthermore, the existing methods of the full-scale test are also insufficient for ships in shallow/constrained water. In order to help naval architects to evaluate inland vessel manoeuvring performance, more elaborate criteria are needed. Since navigation conditions and ship particulars are different for inland vessels and seagoing ships, evaluation manoeuvres and related criteria should be adjusted. The existing test manoeuvres are reviewed in Section 3.2. Additionally, new test manoeuvres are proposed in Section 3.3.

3.2. Existing test manoeuvres

The main contemporary test manoeuvres for seagoing ships and inland vessels are regulated by International Maritime Organization [111, 112], European Commission [63], and Central Commission for the Navigation of the Rhine [33]. For seagoing ships, the test manoeuvres are turning circle, zigzag, and stopping [111, 112]. In addition, International Maritime Organization [111, 112] suggests additional manoeuvres, including spiral, reverse spiral, simplified spiral, pull-out, and very small zigzag manoeuvres, to further investigate the dynamic stability characteristics of the ship. For inland vessels, the test manoeuvres are evasive action and stopping [33, 63]. The test conditions have been described in Section 3.1. The following paragraphs present these test manoeuvres and discuss the insufficiency of applying them to inland manoeuvrability test.

3.2.1. Existing turning circle test

As requested by International Maritime Organization [111, 112], the turning circle manoeuvre should be performed on both starboard and port sides with 35° or the maximum design rudder angle permissible at the test speed when the ship is approaching at zero yaw rate. International Towing Tank Conference [115] indicated that a turning circle of at least

540° is necessary to determine the main turning indices while International Maritime Organization [112] recommended that a 720° turn should be completed to fully assess the environmental effects. Figure 3.1 shows the terminologies used on the turning circle test.

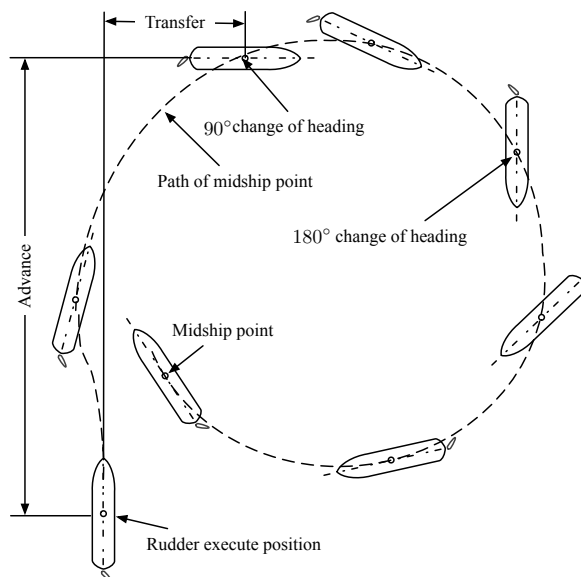


Figure 3.1: Terminologies used on existing turning circle tests. Adapted from International Maritime Organization [112].

International Maritime Organization [112] lists the tactical diameter, the advance, and the transfer as the essential parameters during a turning test. Besides these three parameters, International Towing Tank Conference [115] suggested to additionally obtain the loss of speed in a steady turn, the time to change heading 90° and 180°, the maximum advance, and the maximum transfer. However, International Maritime Organization [111] only takes the tactical diameter and advance as criteria for turning ability. It should be noted that there is no turning circle manoeuvre or criterion specified for inland vessels.

3.2.2. Existing zigzag test

The zigzag manoeuvre is performed to evaluate the yaw checking and course keeping abilities. Figure 3.2 illustrates the definition used on 20° (the heading angle ψ)/20° (the rudder angle δ) zigzag test. International Maritime Organization [111, 112] requests 10°/10° and 20°/20° zigzag test with both starboard and port rudder angles to identify the environmental effects. Moreover, International Towing Tank Conference [115] indicated that the turning and the yaw tracking abilities are of special interest as the emergency turns should be carried out to starboard. Values of first and second overshoot angles in 10°/10° zigzag are given while only the limit of the first overshoot angle in 20°/20° is set [111, 112].

Besides the overshoot angles, International Towing Tank Conference [115] defines additional results of the zigzag test, including the initial turning time, the time to check yaw, the reach, the time of a complete cycle, the angular speed, and the unit time. To express

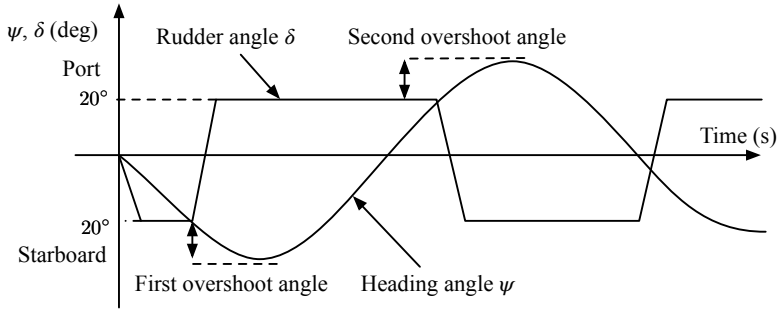


Figure 3.2: Terminologies used on existing $20^\circ/20^\circ$ zigzag tests. Adapted from International Maritime Organization [112].

the course keeping ability in conditions similar to practice, modified zigzag [115] and very small zigzag [112] were proposed, which may have the execute heading angle as small as 1° with the rudder angle being 5° or 10° . Nevertheless, the zigzag test might not be sufficient for ships in constrained waterways, especially for the case of inland vessels. For instance, the maximum deviation from the original course during the zigzag manoeuvring is valuable to ensure that inland vessels do not hit the bank in emergency collision avoidance.

3.2.3. Existing evasive action test

The evasive action test is used to prove that the tested inland vessel can take emergency avoidance in good time [33, 63]. Figure 3.3 presents the terminologies used on the evasive action test. The procedure of the evasive action test is similar to the zigzag test, but the criteria are different. The evasive action test evaluates the required yaw rate (r_1 and r_3) and the time to reach the second zero yaw rate (t_4) instead of the overshoot angles. r_1 and r_3 are different for the various dimensions of vessels or convoys. Furthermore, the limit value of t_4 depends on the ratio of the water depth to the ship draught (H/T). More information is achievable from this test, such as the reach from t_0 to t_4 , the maximum deviation from the original course, and the deviations from the original course when r_1 and r_3 are achieved, but these values are not evaluated in the contemporary standards.

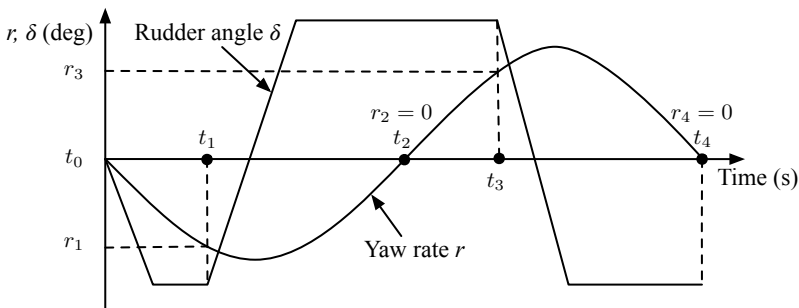


Figure 3.3: Terminologies used on existing evasive action tests. Adapted from European Commission [63].

3.2.4. Existing stopping test

Stopping ability is tested by the full astern stopping. The test procedure described by International Maritime Organization [111, 112], European Commission [63], and Central Commission for the Navigation of the Rhine [33] are basically the same. Figure 3.4 shows the terminologies used on the stopping test. It should be noted that the rudder angle is requested to be maintained at neutral position during the trial. In these regulations, only the track reach, which is the distance (relative to the ground) travelled by the midship, is checked. Rules for inland vessels [33, 63] consider the current (flowing or standing water) and the ship dimensions (length and width) while those for seagoing ships only mention that the track reach may be modified by the administration.

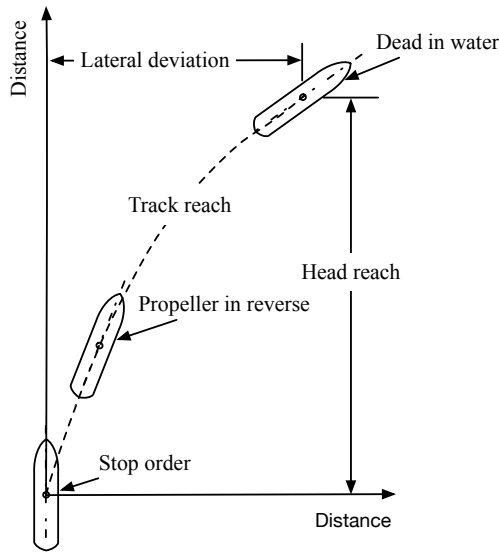


Figure 3.4: Terminologies used on existing stopping tests. Adapted from International Maritime Organization [112].

Ships can be very directionally unstable during the stopping manoeuvre, so that the trajectory is, to a large extent, determined by the initial conditions and environmental disturbances [112, 115]. That is the main reason why the lateral deviations are of interest but not evaluated. However, these lateral deviations are more crucial for inland vessels in narrow channels than seagoing ships in the open sea. Furthermore, the ambient disturbances, mainly about the wind, on inland vessels are also far less significant than those for seagoing ships. Therefore, it might be meaningful to include the lateral deviations into the criteria. Moreover, instead of maintaining a neutral rudder position, proper rudder angles may be applied to reduce the lateral deviations.

3.2.5. Concluding remarks

Section 3.1 has reviewed the existing manoeuvres for inland vessels (evasive action and stopping) and seagoing ships (turning, zigzag, and stopping). The deficiency of these manoeuvres and the missing criteria has been discussed. The existing test manoeuvres set a regulatory framework to address the fundamental manoeuvring abilities of ships. However, the existing criteria and manoeuvres for inland vessels are not as elaborate as those for seagoing ships. Furthermore, the existing criteria do not present the impacts of ship manoeuvrability on navigation efficiency.

Due to the differences in sailing conditions, the parameters that are not important for seagoing ships can be crucial for inland vessels, such as the lateral deviations in the zigzag test and the stopping test. Additionally, high-level data can be abstracted from the existing manoeuvres, such as the speed drop and the operation time, to show the impacts of manoeuvring on daily operations. Following this discussion, new manoeuvres and standards for inland vessels are proposed in Section 3.3.

3.3. Proposed test manoeuvres

As discussed in Section 3.2, test manoeuvres need to be adapted to the actual sailing conditions on restricted water. Furthermore, for both seagoing ships and inland vessels, it is possible to obtain more information from the existing test manoeuvres than those are regulated by the current standards. Accordingly, this section proposes test manoeuvres and related manoeuvring parameters for inland vessels. These manoeuvres and parameters are then applied in Chapter 6 and further summarised in Chapter 7.

3.3.1. Proposed turning circle test

As previously mentioned, the turning circle test is not mandatory for inland vessels. Due to the dimensions of the inland waterways, large inland vessels may not make the full turning circle at the cruising speed, for instance, 110 m inland vessels in the Rhine. In some circumstances, the turning circle manoeuvre is possible for small vessels or inland vessels in large rivers like the downstream of the Yangtze River. However, these full turning manoeuvres are strictly limited or even not allowed in some area. In practice, inland vessels with bow and stern thrusters can turn on a spot. However, the bow and stern thrusters are only effective at slow speed (under 6 km h^{-1}).

Regarding the limits of the turning circle test for inland vessels, it is still an effective way to evaluate a ship's turning ability. For vessels that sail in relatively narrow waterways where a full turning circle is not possible, the turning circle test is not necessary. Then, the turning ability of these vessels should be checked by other test manoeuvres. For inland vessels in large rivers, the turning circle is recommended and new parameters are proposed based on the existing turning circle test (Section 3.2.1) as illustrated in Figure 3.5.

More specifically, the proposed parameters are explained as follows:

- The **advance**, the **transfer**, and the **tactical diameter** are defined as the same as the current standards.
- The **lateral deviation** is the distance from the position at which a starboard rudder

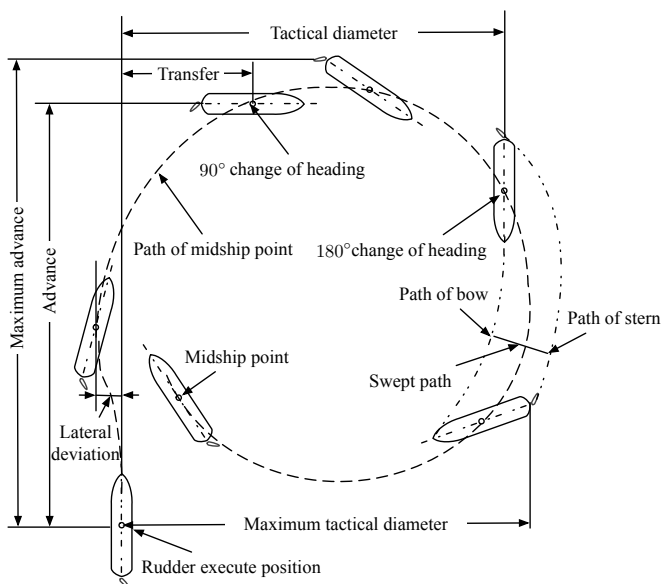


Figure 3.5: Terminologies used on the proposed turning circle test for inland vessels.

angle is given to the maximum port side deviation of the midship point of a vessel in a starboard side turning circle, and vice versa.

- The **maximum advance** is the distance travelled by the stern of a vessel from the position at which the rudder angle is given to the position at which the ship speed in the direction of the original course is zero.
- The **maximum tactical diameter** is the distance travelled by the stern of a ship from the position at which the rudder angle is given to the position at which the heading has changed 180° from the original course.
- The **maximum swept path** is the maximum difference between the trajectories of the bow and the stern.
- The **differences of the tactical diameters and advances** between the starboard side and port side turning circle tests should be studied to present the asymmetry behaviours of the ships.

Even though the classic turning manoeuvre can give a good representation of ship turning ability, the full circle turning test requires so much space that sometimes it is not feasible to be carried out for operation in real inland navigation. Furthermore, it is not a manoeuvre that an inland vessel is likely to make. Additionally, inland vessels are more commonly configured with multiple rudders and the maximum rudder angles for inland vessels can be 75° or even 90° instead of the customary 35° for seagoing ships. Therefore, the applied rudder angle should be clearly specified. Otherwise, the non-dimensional turning indices of inland vessels can be quite different from those of seagoing ships. Considering that it is

not possible to use the turning circle test in narrow waterways, a hard turning manoeuvre is proposed in the Section 3.3.2.

3.3.2. Proposed hard turning test

Hard turning test is proposed to present the turning ability of ships in bendy waterways. For a hard turning manoeuvre, the inland vessel needs to alter its course by a large angle with a specific rudder angle and then keep the new course. The extreme case of changing the course by 90° is just the first quarter of a turning circle as shown in Figure 3.6. More frequently, inland vessels need to change the course by 45° to 60° . The target performance parameters are the lateral deviation, the advance, and the transfer, which are defined as the same as the terminologies defined in Section 3.5. Furthermore, the operation time and the speed drop are meaningful to evaluate the ship response to the applied rudder angle. For cases where the turning circle test is not applicable, this hard turning manoeuvre can be an alternative to evaluate the ship turning ability.

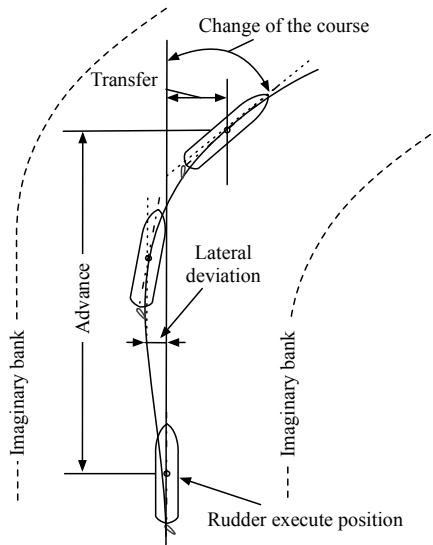


Figure 3.6: Terminologies used on proposed hard turning circle tests for inland vessels.

3.3.3. Proposed T-junction test

The confluences of rivers, channels, and canals are challenges for inland vessel navigation. Near the confluences, more encountering situations happen, increasing the density of the traffic flow. In addition, the speed and the direction of the current may change sharply, affecting the ship manoeuvrability. Furthermore, observation of the skippers may be affected by the natural or artificial obstacles. All in all, inland vessels should be capable of making a proper motion in the junction area and, moreover, have sufficient manoeuvring margin in case of emergency.

The T-junction manoeuvre can be taken as hard turning with extra constraints, such as the safe distance from the banks and the remaining yaw rate and the resultant drift angle

after the operation. Thus, the parameters used for hard turning tests, such as the advance and the transfer, can also be applied to the T-junction manoeuvres. In this section, example trajectories of a large inland vessel or an inland vessel that has poor manoeuvrability on single-lane and double-lane T-junctions are shown in Figure 3.7.

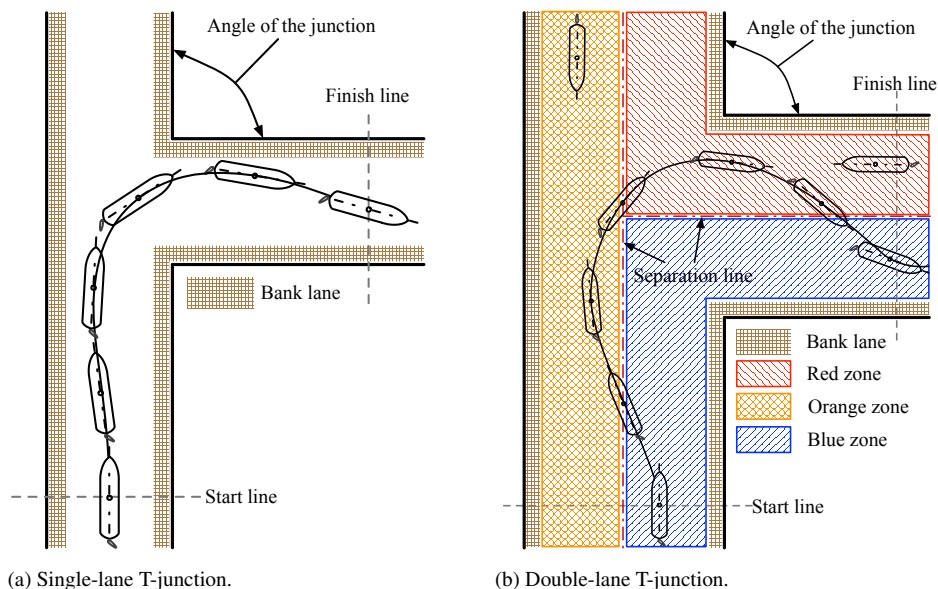


Figure 3.7: Terminologies used on proposed T-junction tests for inland vessels.

According to Rijkswaterstaat [237, p. 39], the width in the plane of the waterway bottom and the width in the keel plane of single-lane waterways must be at least twice the width of the reference ship. Double-lane waterways are divided as normal profile and narrow profile. The width in the plane of the waterway bottom for both double-lane profiles should be at least 2 times of the width of the reference ship. The width in the keel plane of the loaded reference vessel must be at least 4 and 3 times the width of the reference vessel in the normal profile and narrow profile respectively [237, p. 39].

The proposed single-lane T-junction test starts when the midship point of the ship passes the imaginary start line and finishes when the midship point of the ship reaches the finish line. The start and end speeds should be recorded to calculate the speed drop. The duration of the operation is used to show the quickness of the vessel to the turning order. Furthermore, the remaining drift angle and the resultant yaw rate at the end point are used to present the required manoeuvring margin to turn the vessel back to the straight course and avoid entering the bank lane. In general, vessels with smaller parameters, namely the speed drop, the operation time, the remaining yaw rate, and the resultant drift angle, have better manoeuvring performance.

The double-lane T-junction is more complex than the single-lane one because encountering situations may happen while the ship is turning. In some area, a strict Traffic Separation Scheme (TSS) is issued, where the vessel is not allowed to cross the separation line. Taking the separation line as an imaginary bank, the double-lane is the same as the single

lane. To fully use the capacity of the waterway, large vessels may be allowed to cross the separation line with extra care. For waterways where the TSS is not applied, double-lane T-junction is suggested

The navigable area of the double-lane channel is divided into three zones, i.e. blue, orange, and red. The blue zone is the safe zone for the own vessel. A vessel with good manoeuvrability is expected to be capable of passing the T-junction in the blue zone. The orange and red zones are lanes for the incoming vessels. Therefore, it is dangerous for the own ship to enter these zones. In addition, the red zone is more dangerous than the orange zone because the incoming ship in the red zone needs to make its own T-junction and has a relatively small vision due to the corner of the channels.

Similar to the case of the single-lane T-junction, the vessel is not allowed to enter the bank lane. In addition, the safety of the manoeuvre is judged by calculating the area between the ship trajectory and the separation line in each zone. The larger area in the orange and the red zones, the more dangerous the manoeuvre is. Furthermore, the manoeuvring performance of the vessel is evaluated based on the velocity, the drift angle, and the yaw rate at the time point when the ship enters or leaves each zone. For instance, the operation time in the orange zone and the red zone should be minimised.

To quantify the manoeuvring performance of a ship, the previously described turning, hard-turning, lane-changing tests are more fundamental than the proposed T-junction test. The properties of the T-junction tests depends on the waterway that ships sail on. For simplicity, the T-junction turning manoeuvre can be regarded as turning or hard-turning with additional boundaries. These boundaries should be considered by the naval architects for specified situations. In the rest of the thesis, the T-junction is not discussed explicitly, but the performance of ships in turning and hard-turning can show some insights of the possible behaviours in T-junction tests.

3.3.4. Proposed lane changing test

One of the most important aspects of the inland vessel manoeuvrability is the capability to change lanes in ship encountering and overtaking [52]. However, the lane changing ability is not covered in the existing standards. The capability of changing lanes is related to the initial turning ability and yaw checking ability, which can roughly be presented by the classic zigzag test. However, zigzag tests may lead to a wrong estimation of ship manoeuvring performance. The large overshoot angle may be caused by the large inertia of large ships or by the large rate of turn of small ships.

Dijkhuis et al. [52] proposed a revised zigzag test, which is based on the change of the rate of turn. Nevertheless, it is more realistic to emphasise the capability of a single lane changing test instead of continuous manoeuvres like the zigzag test. An example of the proposed lane changing test in an overtaking situation is illustrated in Figure 3.8. The distance before overtaking, the distance after overtaking, and the lateral distance should be expressed in non-dimensional forms of both ships properties and parameters of the channel.

Considering the small relative speed in the overtaking operations, it may be less critical than the cases of ship encountering. In more serious situations of collision avoidance, ships have to make large course altering to avoid the obstacles and correct the course as soon as possible to prevent grounding or ship-bank collision. In that case, large angles of lane changing tests are needed, for instance, $35^\circ/35^\circ$ or even larger lane changing tests .

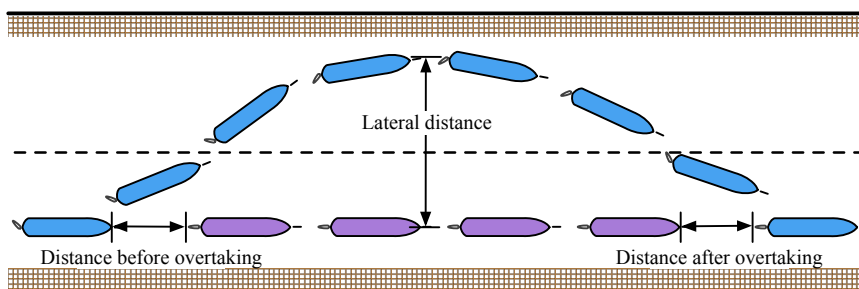


Figure 3.8: Terminologies used on proposed lane changing tests in an overtaking situation.

To evaluate the effectiveness of the large lane changing tests, further understanding of the rudder performance is needed.

3.3.5. Proposed stopping with rudder correction test

Stopping ability in a straight channel is important for emergency operations. As the channel is constrained in width, the stopping scenario for inland vessels is different from that for seagoing ships. The basic IMO requirement of the stopping ability is that the track reach should be smaller than 15 ship lengths (except impracticable cases for large displacement ships) in the full astern stopping test. To avoid a collision, seagoing ships commonly choose the more efficient operation of hard turning while, due to the constraints of the waterways, inland vessels have to carry out the crash stopping.

In the existing standards, there is no description about the rudder in the stopping test. The rudder angle is commonly taken as zero during the whole operation, more specifically from the time when the full astern order is given till the ship stops in the water. However, for inland ships, both the advance and the lateral deviation should be considered. To reduce the lateral deviation, inland vessels may use the rudder correction force as the proposed manoeuvre in Figure 3.9. In this case, there is the question of when to start this correction rudder order and when to stop it.

3.3.6. Proposed stopping with clam shell angles test

Twin-rudder inland vessels can set their rudders both outwards to reduce the crash stopping distance. Unlike seagoing ships that normally have a maximum rudder angle of 35° and operate both rudders in the same direction, inland vessels may apply rudder angles of nearly 90° to both sides. These outwards rudder angles are named as clam shell angles as shown in Figure 3.10.

An increase in the clam shell angle reduces the gap between the leading edges of the twin rudders. Therefore, more resistance, which is good for stopping, is induced by the rudders. The stopping distance can be reduced by 50% with the clam shell angles [16, p. 41]. In addition to the track reach required in the current standards, both the transfer and the head reach should be recorded as they are critical for inland vessel safety.

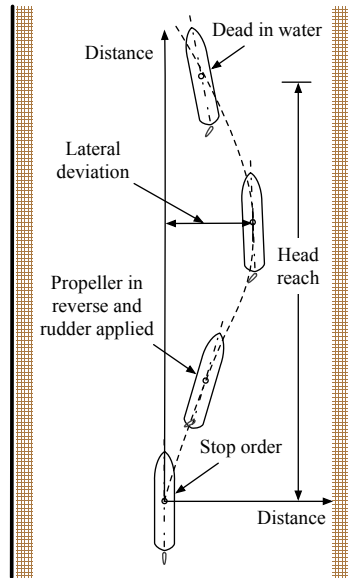


Figure 3.9: Terminologies used on proposed stopping with rudder correction tests.

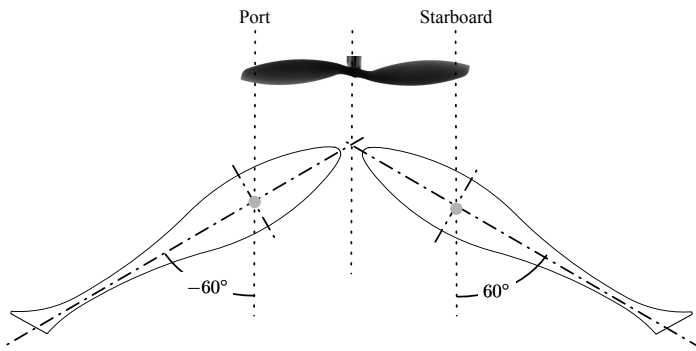


Figure 3.10: An example of the rudder clam shell angles

3.4. Synthesis

In Chapter 2, the main impact factors on manoeuvring performance were reviewed. Through this analysis, clear differences were found in the navigation environment and ship configurations between inland vessels and seagoing ships. In this chapter, standards of manoeuvres and criteria on ship manoeuvrability have been compared. There is a lack of knowledge of suitable manoeuvres to evaluate the manoeuvring performance of inland vessels in real-world navigation. Therefore, new benchmark manoeuvres have been proposed for further discussion. After all, following conclusions are drawn to answer the first research question in Section 1.3: *What are the practical manoeuvres to evaluate and compare the manoeuvring performance of inland vessels?*

1. Test manoeuvres and related criteria for inland vessels are less elaborate than those for seagoing ships. The current test manoeuvres have certain insufficiency to present the manoeuvring performance of day-to-day operations in inland waterways.
2. Besides the manoeuvring indices in the current standards, additional parameters can be obtained from the existing test manoeuvres. It is possible to have further insight into the ship manoeuvrability with the classic manoeuvring tests.
3. Inland vessels have more difficult manoeuvring situations like the T-junction than seagoing ships. Furthermore, inland vessels have extraordinary operation profiles like stopping with clam shell angles. These differences require extra care to ensure navigations safety.

Due to the possibilities of nautical operations, interest in manoeuvres for seagoing ships and inland vessels is not always the same. For instance, in the case of an imminent collision, a seagoing ship may either initiate a crash stopping or a turning manoeuvre while inland vessels can only make a crash stopping due to the limits of waterways. This highlights the importance of the crash stopping ability for inland vessels. All these different impact factors and interests in the manoeuvring performance request further research on the mechanisms of ship motions for more accurate manoeuvrability prediction [19].

Based on the existing test manoeuvres and practical operations, new parameters and manoeuvres have been proposed to evaluate inland vessel manoeuvrability in this chapter. From a perspective of initial design, classic turning and zigzag tests and proposed hard-turning and lane-changing manoeuvres are used to compare the manoeuvring performance of inland vessels with various rudder configurations in Chapter 6. The proposed T-junction, stopping with rudder correction, and stopping with clam shell angles can be carried out with specified safety margins to authorities' requirements.

In Chapter 4, hydrodynamic characteristics of rudders with various profiles and parameters are studied through CFD simulations. These hydrodynamic characteristics are then integrated into the manoeuvring model built in Chapter 5. With this integrated manoeuvring model, inland vessels with different rudder configurations are tested in the proposed test manoeuvres.

Chapter 4

Hydrodynamic Characteristics of Ship Rudders*

“Nature always tends to act in the simplest way.”

Daniel Bernoulli (1700 – 1782)

As discussed in Chapter 2, inland vessels have more complex rudder configurations than seagoing ships. Currently, the rudder profile, the number of rudders, and the spacing between rudders are not considered in the empirical methods for rudder force calculation. To analyse the impacts of the rudder configurations on inland vessel manoeuvrability, the hydrodynamic characteristics, for instance, lift and drag coefficients, of each configuration need to be calculated specifically. Considering the scaling effects and high cost of model tests, one of the Computational Fluid Dynamic (CFD) methods, the Reynolds-Averaged Navier-Stokes (RANS) method is applied to analyse the hydrodynamics of rudders in different configurations.

Section 4.1 describes the applied 2D and 3D RANS methods which are then used in Section 4.3 and Section 4.4 respectively. Section 4.2 validates the presented RANS methods against experimental and numerical test data. Section 4.3 uses the 2D RANS method to study the impacts of the Reynolds numbers, the rudder profiles, the spacing between twin rudders, and the spacing among quadruple rudders. Section 4.4 analyses the impacts of the effective aspect ratio and shallow water on rudder hydrodynamics through 3D RANS simulations. The obtained hydrodynamic characteristics are applied to manoeuvring simulations in Chapter 5 and Chapter 6. Finally, Section 4.6 draws the conclusions of this chapter.

4.1. Applied RANS methods

Conventional methods to study rudder hydrodynamics are wind-tunnel and open water tests. Due to the high cost and the scale effects of the model tests, the Computational Fluid Dynamics (CFD) method is considered as an increasingly attractive alternative (Section 2.2). CFD methods are roughly classed in a hierarchy of lifting-line, boundary element, Reynolds-Averaged Navier-Stokes (RANS), Large Eddy Simulation (LES), and Direct Numerical Simulation (DNS) methods.

*This chapter is based on Liu and Hekkenberg [173], Liu and Hekkenberg [174], Liu and Hekkenberg [175], Liu and Hekkenberg [177], Liu et al. [181], and Liu et al. [184].

The lifting-line method and similar potential flow based approaches describe the velocity field as the gradient of a scalar potential function. Assuming the flow is irrotational, the flow vorticity is expressed as a Laplace equation. With these assumptions, the lifting-line method has the advantages of implementation and computational time. However, the application of lifting-line methods can only be applied to high aspect ratios while ship rudders typically have a geometric aspect ratio in the range of 1 to 3.

Due to the assumption of potential flow, the lifting-line methods and boundary element methods cannot model the viscous flow effects, such as frictional drag, flow separation, and stall [206, p. 237]. The LES method simulates the large-scale eddies individually to reduce the length scale ranges of the solution, reducing the cost of computation while the DNS method presents all the flow motion. However, both LES and DNS methods require a very fine mesh and small time steps, making them expensive in engineering applications.

The presented RANS method uses a time-averaged Reynolds decomposition, which assumes that all the components of the flow velocity and pressure consist of a mean value and a bounded fluctuation to represent turbulence. Compared to the above mentioned CFD methods, the RANS method cannot only analyse the induced lift and drag of a rudder with a complex geometry, but also model the flow separation, and the stall angle with much fewer requirements of calculation resources than the LES and DNS methods. To obtain reliable CFD results, the simulations should be carefully configured in the turbulence modelling (Section 4.1.1), the boundary conditions (Section 4.1.2), the mesh generation (Section 4.1.3), and the numerical solver (Section 4.1.4).

4.1.1. Turbulence modelling

Due to the complexity and vast computer resources needed for solving full unsteady governing equations, the Reynolds-Averaged Navier-Stokes (RANS) method is widely applied to capture the essence of physics with the minimum amount of complexity. Turbulence models are developed to express the mean effects of the turbulent stresses. The turbulent characteristics of the flow play a crucial role in the determination of the fractional drag, the flow separation, the laminar to turbulent transition, and the thickness of boundary layers. No single turbulence model can be universally applied to any turbulent flow simulations [206, p. 248].

To utilise the RANS method for studies of rudder hydrodynamics, the turbulence model has to be chosen according to its suitability to the flow properties, such as the Reynolds number and the angle of attack as discussed in Section 2.3. The transition from laminar to turbulent flow mainly depends on the Reynolds number, the body roughness, and the turbulence existing in the income flow. The transition threshold of the Reynolds number is about 0.5×10^6 , which is much smaller than the practical range of ship rudders.

Owing to the shallow water, currents, ship making waves, and roughness of the rudder body, rudders are mainly operated in highly turbulent flows. Furthermore, the high turbulence model also poses requirements on the applied mesh, which in turns affects the accuracy and the cost of the simulations. In engineering applications, the turbulence model is commonly chosen from SpalartAllmaras (SA), Standard $k-\varepsilon$, RNG $k-\varepsilon$, Realisable $k-\varepsilon$, Standard $k-\omega$, and $k-\omega$ SST models. Table 4.1 summarises the applied and compared turbulence models in literature. The theory behind these models is briefly introduced in the following sections.

Table 4.1: Applied or compared turbulence models for RANS simulations in literature.

Year	Literature	Applied or compared models
2004	Stuck et al. [258]	SA, Standard $k-\varepsilon$, and RNG $k-\varepsilon$
2010	Wasberg and Reif [294]	SA
2011	Krasilnikov et al. [152]	$k-\omega$ SST
2011	Castro et al. [30]	$k-\omega$ SST
2012	Eleni et al. [57]	SA, Realisable $k-\varepsilon$, and $k-\omega$ SST
2012	Karim and Ahmmed [126]	RNG $k-\varepsilon$
2013	Broglia et al. [25]	SA
2013	Van Nguyen and Ikeda [281]	$k-\omega$ SST
2014	Van Nguyen and Ikeda [283]	$k-\omega$ SST
2014	Van Nguyen and Ikeda [284]	$k-\omega$ SST
2014	Shenoi et al. [248]	$k-\omega$ SST
2014	Wang and Zou [293]	RNG $k-\varepsilon$
2015	Van Nguyen and Ikeda [285]	Standard $k-\varepsilon$
2015	Tezdogan et al. [266]	Standard $k-\varepsilon$
2015	Badoe et al. [11]	$k-\omega$ SST
2015	Broglia et al. [26]	SA
2016	Dubbioso et al. [55]	SA
2016	Bhattacharyya et al. [20]	$k-\omega$ SST

SpalartAllmaras turbulence model

The SpalartAllmaras (SA) model is an one-equation model that solves the transport equation for the turbulent kinematic viscosity [251]. Compared with the Standard $k-\varepsilon$ and RNG $k-\varepsilon$ models, Stuck et al. [258, p. 22] confirmed that, for large angles of attack, only the SA model can predict the flow detachment while the other two models can at most show the flow stagnates without detaching. The SA model is originally designed for wall bounded aerodynamic flows. The original SA model is effective for low-Reynolds-number applications, requiring the viscous affected region of the boundary layer to be properly resolved [57].

Standard $k-\varepsilon$, RNG $k-\varepsilon$, and Realisable $k-\varepsilon$ turbulence models

The Standard $k-\varepsilon$ model was first given by Launder and Spalding [161]. It is a two-equation model that includes two additional transported variables k and ε , where k is the turbulent kinetic energy per mass and ε is the rate of dissipation of k , to represent the turbulent properties of the flow. In addition, ε specifies the scale of the turbulence and k determines the energy in the turbulence. The Standard $k-\varepsilon$ model is widely used in industry flow and heat transfer simulations owing to its robustness, economy, and accuracy for a wide range of turbulent flows [57]. In addition, Quérard et al. [232] noted that the Standard $k-\varepsilon$ model can save nearly 25 % CPU time compared to the Standard $k-\omega$ model.

Date [47] concluded the weaknesses of applying the Standard $k-\varepsilon$ model to rudder applications are the over-predicted turbulent kinetic energy and the under-predicted flow separation, particularly concerning flow stagnation, stall, and reattachment phenomena. MARNET-CFD [192] indicated that the Standard $k-\varepsilon$ is generally applicable only to high-Reynolds-number flows and suggested to only use the Standard $k-\varepsilon$ for preliminary assessments of steady ship flows. Molland and Turnock [206, p. 249] further pointed that the

Standard $k-\varepsilon$ is not able to capture laminar and transitional flows, which is an important drawback in the prediction of the rudders that are often operating at a transitional Reynolds number.

To overcome the shortcomings of the Standard $k-\varepsilon$ model, Yakhot et al. [301] introduced the RNG $k-\varepsilon$ model and Shih et al. [249] developed the Realisable $k-\varepsilon$ model. The RNG model has a modified equation of the dissipation rate to account for different scales of motion while the Realisable $k-\varepsilon$ model consists of a new model dissipation rate equation and a new realisable eddy viscosity formulation. The Realisable $k-\varepsilon$ is more widely applied than the RNG $k-\varepsilon$ model in engineering applications. Through the review of the applied turbulence models in Table 4.1, it is noted that the Standard $k-\varepsilon$ model and its variations commonly require less computation time and resources than the $k-\omega$ SST model, especially for 3D simulations.

Standard $k-\omega$ and $k-\omega$ SST turbulence models

The standard $k-\omega$ model is based on the Wilcox [296, 297] methods. It is a two-equation model that uses k and ω to predict turbulence, where k is as the same as that for $k-\varepsilon$ models while ω is the specific rate of dissipation of the turbulence kinetic energy (k) into internal thermal energy. The standard $k-\omega$ model incorporates low-Reynolds-number effects, compressibility, and shear flow spreading [57]. Menter [196] developed the $k-\omega$ SST model which effectively combines the strengths of the standard $k-\omega$ in the near-wall region and the Standard $k-\varepsilon$ in the far field. Therefore, the $k-\omega$ SST model can achieve more accurate and reliable results than the standard $k-\omega$ model. For simulations of the NACA 0012 profile, Eleni et al. [57] indicated that the $k-\omega$ SST model is more appropriate than the SA model and the Realisable $k-\varepsilon$ model.

Applied turbulence models

As a summary, the $k-\omega$ SST model is applied for 2D simulations in Section 4.3 because it gives better results than other models with affordable computation requirements. The Realisable $k-\varepsilon$ model is used for 3D simulations in Section 4.4 owing to its superiority in computation time and resources to other models, which is only especially important for 3D simulations that have a large number of cells. The SA model is effective for low-Reynolds-number applications and thus not suitable for the high-Reynolds-number simulations of rudders. Standard $k-\varepsilon$, RNG $k-\varepsilon$, and Standard $k-\omega$ models are not considered as they are gradually superseded by the $k-\omega$ SST and Realisable $k-\varepsilon$ models.

4.1.2. Boundary conditions

Boundary conditions are needed to define the initial and boundary states of variables for the governing equations and the turbulence models. Correct selections of the boundary conditions are crucial to the physical implementation, the calculation accuracy, and the convergence time. The following paragraphs introduce the applied boundary conditions in this thesis, specifically velocity inlet, pressure outlet, wall, and symmetry.

Velocity inlet

The velocity inlet specifies the direction and the value of the income flow to the rudder. For open water simulations of rudders, the inlet velocity can be set according to the test Reynolds number. In this thesis, a Reynolds number of 6×10^6 is taken as the threshold value above which the rudder hydrodynamics are not significantly affected as discussed

in Section 2.3. Otherwise, the inlet velocity is calculated according to the test Reynolds number specified in the validation data.

Pressure outlet

The pressure outlet condition defines the static pressure at the outlet boundary, which is as the same as the static pressure of the environment into which the flow exhausts. The static pressure is assumed to be constant at the outlet and atmospheric. Furthermore, the position of the outlet should be sufficiently far away from the region of interest to avoid backflow, which affects the accuracy of the results.

Wall

The wall condition defines that the tangential velocity of the fluid equals to the wall velocity and the normal velocity of the fluid is zero. Considering the viscous effects, the near wall flow is roughly divided into to a laminar layer, a buffer layer, and a turbulent layer. The non-dimensional wall distance (y^+) is commonly used to express the fineness of the mesh for the boundary layers. Different turbulence models have different suitable ranges of y^+ . Thus, the value of y^+ has to be carefully considered in the mesh generation.

A rule of thumb is to set y^+ around 1 or in the range of 30 to 200, considering the structure of the turbulent flow. In order to obtain the desired y^+ , the initial cell height (y_i), which is the distance from the wall to the first mesh point, needs to be determined. For Re smaller than 1×10^9 , y_i can be estimated as the following:

$$y_i = \frac{\sqrt{2}C_R y^+}{Re} (2 \log_{10} Re - 0.65)^{1.15}, \quad (4.1)$$

where C_R is the rudder chord length for open water studies of the rudder hydrodynamics. In this thesis, y^+ for the $k-\omega$ SST model is smaller than 1 and y^+ for the Realisable $k-\epsilon$ model is around 35.

Symmetry

The symmetry condition assumes that same physical processes exist on both sides of the boundary. No flow or scalar flux can cross the symmetry boundary. If the viscous effect is out of interest, the symmetry condition can be applied as an alternative of the wall condition to reduce computational effort. In that case, the symmetry condition is actually a no shear wall condition.

Applied boundary conditions

The applied boundary conditions for 2D and 3D simulations are shown in Figure 4.1. Velocity inlet configures the velocity of the uniform inflow for open water tests. Pressure outlet is set as the same as the static pressure of the environment. The wall boundary specifies the geometry of the rudder and accounts for the viscous effects of the rudder and the bottom of the domain in the validation study of the 3D RANS method. The symmetry boundary (no shear wall) is used for the side walls.

4.1.3. Applied domains and meshes

A mesh presents the physical model in a discrete form on which the governing equations can be resolved numerically. To obtain reliable CFD solutions, the mesh has to be sufficiently refined in the area where high gradients of fluid characteristics exist. Section 4.1.3

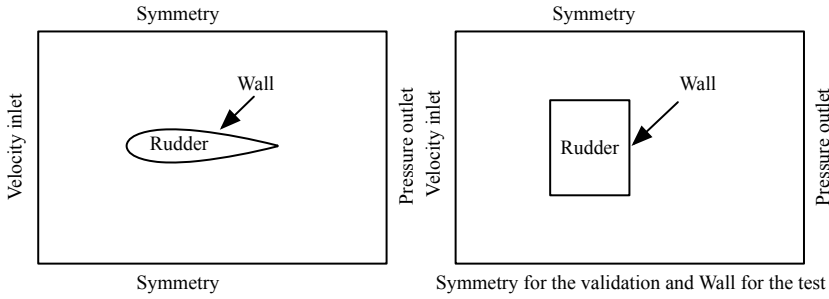


Figure 4.1: Applied boundary conditions in 2D (left) and 3D (right) simulations.

discusses the applied hybrid meshes, which have structured inflation layers around the profile and unstructured cells in the rest of the domain. Hybrid meshes are easier to generate and converge than structured meshes. Furthermore, hybrid meshes can better simulate the viscous effects than pure unstructured meshes. In addition, for all the simulations in this thesis, the fluid material is incompressible water.

2D domain and meshes

Figure 4.2 illustrates the 2D meshes for a NACA 0012 profile which are used for the validation of the 2D RANS method in Section 4.2. Meshes for other tested profiles are generated with the same strategy. The test Reynolds number is 6×10^6 . Above this value, small impacts of Re on the lift and drag coefficients are found (Section 2.3.1). Corresponding to the Re , the inflow speed is 6.0289 m s^{-1} for a rudder model with chord length of 1 m. The inflow is kept normal to the inlet boundary. Furthermore, the angle of attack is configured by rotating the profile rather than modifying the direction of the inflow.

2D meshes are implemented in a rectangular domain of $60 C_R$ in width and $90 C_R$ in length. The profile is located towards the front of the domain, with $30 C_R$ to left, top and bottom, and $59 C_R$ to right respectively. This domain is sufficiently large to minimise the influence of the boundary locations on the rudder hydrodynamics while not excessively large. As illustrated in Figure 4.1, an inner domain is defined to improve the accuracy of the solution and capture the wake area around the rudder.

3D domain and meshes

Similar to the 2D meshes, the presented 3D meshes are set up in a cuboid domain. The dimensions of the domain, the topology of the mesh, and the applied boundary conditions are illustrated in Figure 4.3, where d_R is the clearance between the rudder tip and the bottom of the waterway. Additionally, d_R is non-dimensionalised as $d'_R = d_R/B_R$. An inner domain is built to refine the necessary cells around the rudder. The velocity inlet condition defines the inflow velocity according to the tested Reynolds number (6×10^6 in water) or the value specified in the validation experiment (20 m s^{-1} in air). The pressure outlet condition sets the pressure as constant and atmospheric.

4.1.4. Numerical solvers

To represent the conservation principles, differential equations are needed in a discretization form on given meshes. Discretization techniques, such as the finite difference method, the finite element method, and the finite volume method, are applied to transform

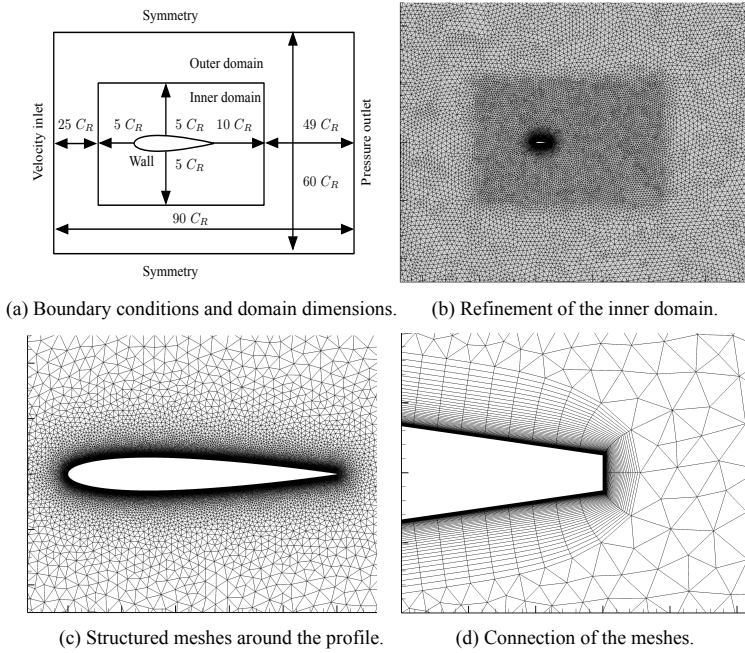


Figure 4.2: 2D mesh topology, boundary conditions, and domain dimensions.

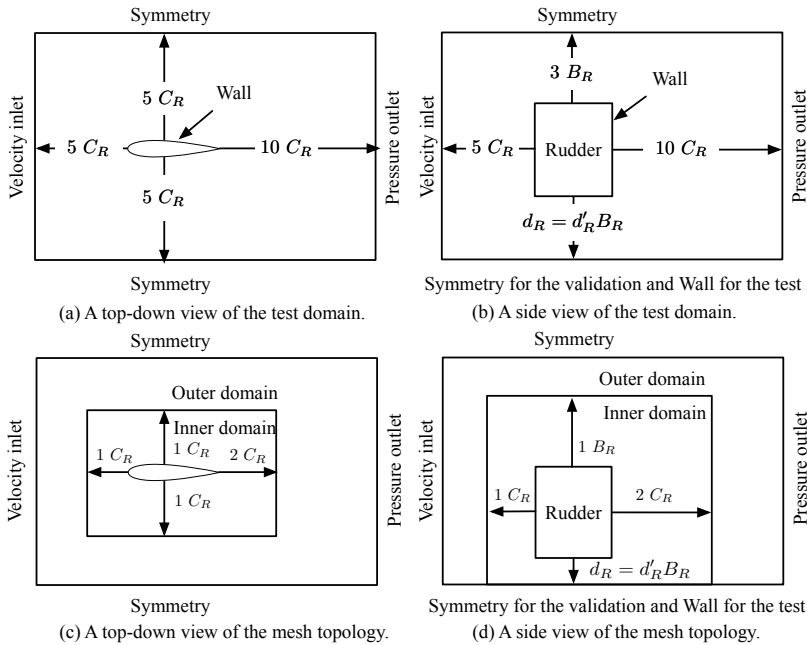


Figure 4.3: 3D mesh topology, boundary conditions, and domain dimensions.

each item in the differential equations to a set of algebraic equations for numerical solvers. In this thesis, the finite volume method is chosen as it is by far the most common approach in current CFD codes [192]. Details of the finite volume method are presented by Versteeg and Malalasekera [292]. Both pressure-based and density-based solvers are implemented in the commercial package ANSYS Fluent. The density-based solver has the advantage in presenting the shock effects for high-speed compressible fluid over the pressure-based solver. For incompressible viscous water, the pressure-based solver is recommended. The pressure-based solver is separated into segregated and coupled algorithms. The segregated scheme solves the governing equations sequentially while the coupled scheme solves them in a coupled way.

Since the segregated algorithm stores and solves the equations of each variable in the memory one at a time, it is more memory efficient than the coupled solver which has to put all the relevant equations in the memory at the same time. However, the advantage of memory efficiency is obtained at the expense of slow convergence. Kelecy [127] shows that the coupled solver requires more memory, resulting in a longer time for each iteration than the segregated one, but the coupled solver may achieve convergence with much fewer iterations than the segregated solver. Additionally, as the interest of the presented simulations is in the performance of the system, namely the hydrodynamics characteristics of rudders, rather than specific changing behaviours, for example, vortex shedding and turbulent studies, steady simulations are favourable than unsteady ones, considering the cost of computational time and resources. All in all, this thesis uses a pressure-based coupled steady solver with the finite volume method.

4.1.5. Grid independence

A grid independence test shows that the solutions are independent of the change in grids. This thesis refines meshes based on the chord-wise element size along the rudder profile, which determines the aspect ratio of the boundary layer elements. This parametric refinement addresses the crucial impact factors on the mesh quality and avoids waste of cells by overall refinement [253]. Wasberg and Reif [294] showed that the accuracy of the drag coefficients depends on the domain size and the turbulent flow conditions. Furthermore, the domain size mainly affects the prediction of the drag while its impacts on the lift are less significant. Comparing to wind-tunnel tests [155], an example of the grid independence is performed with a NACA 0012 profile at the angle of attack of 10° as shown in Figure 4.4.

As the first cell height is $4.46 \times 10^{-6} C_R$, the chord-wise element size is tested in a range of 2.68×10^{-3} to $2.23 \times 10^{-4} C_R$. The corresponding range of aspect ratios is 600 to 50 at an interval of 50. Figure 4.4 confirms that the accuracy of the drag coefficient is more sensitive to the number of cells than that of the lift coefficients. Through the mesh independence study, a mesh of 400000 cells is deemed sufficient to keep the results independent from the grid for a 2D single rudder. Similar procedures are taken for twin-rudder and quadruple-rudder configurations in 2D and single-rudder configurations in 3D. More specifically, the aspect ratio of the first layer of the structured mesh around the profile in 2D and 3D is about 100 and the chord-wise size is about $4.46 \times 10^{-5} C_R$. For these three cases, the number of cells at which mesh independence is achieved are 700000, 1200000, and 3000000 respectively.

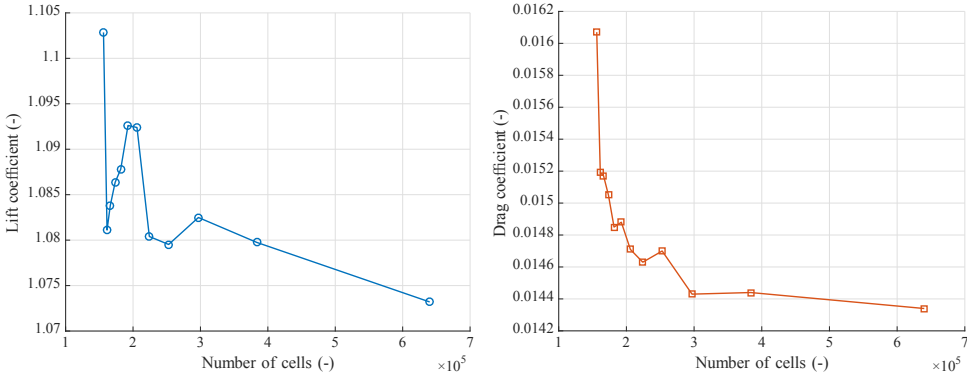


Figure 4.4: Grid independence study of the lift and drag coefficients at an angle of attack of 10° .

4.2. Validation of the RANS methods

4.2.1. Validation of the 2D RANS method

To validate the RANS method, a classic validation profile NACA 0012 is analysed under angles of attack in a range of 0° to 15° at an interval of 1° . The lift and drag coefficients are compared to one experimental dataset [155] and three independent CFD results [158], which are CFL3D (NASA LaRC, USA), FUN3D (NASA LaRC, USA), and NTS (NTS, Russia), as shown in Figure 4.5. These three benchmark CFD cases were carried out with structured meshes in a domain of $500 C_R$ around the profile. Each CFD case has three data points at angles of attack of 5° , 10° , and 15° .

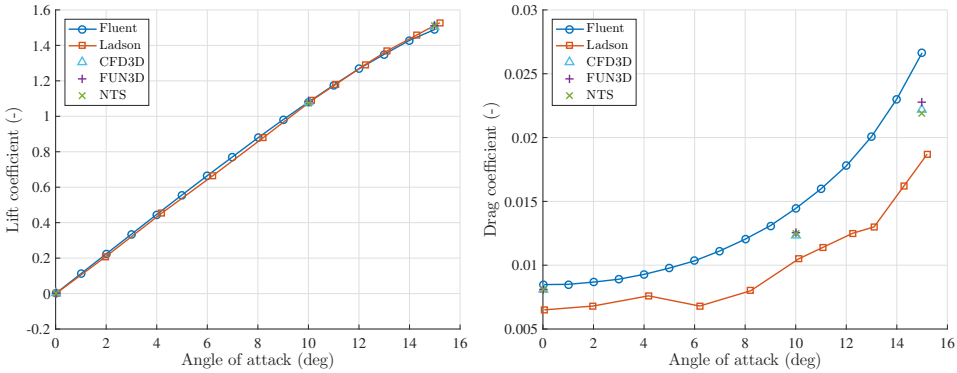


Figure 4.5: Comparison of the 2D Fluent results to the numerical and experimental tests.

The comparison in Figure 4.5 shows that the 2D RANS method with hybrid meshes predicts the lift coefficient well but overestimates the drag coefficient. The difference in the lift prediction is mainly due to numerical diffusion. The applied 2D RANS method has a larger overestimation of the drag coefficients than the CFD benchmarks because hybrid meshes introduce larger discretization errors than the structured meshes applied in the

benchmark cases. The accuracy of the drag coefficient can be improved by using fully-structured meshes, a larger domain, or more advanced CFD methods like Large Eddy Simulations or Direct Numerical Simulations (DNS). However, these improvements are quite expensive in computation resource and time. Since the drag coefficient is a relatively small value, which contributes to the normal force coefficient much less than the lift coefficient, the inaccuracy of the drag coefficients is deemed for angles in the range of 0° to 15° .

Due to the availability of the experimental data, the validation was only performed for 0° to 15° . For angles of attack larger than 15° , uncertainty is caused by less validation and the strong flow separation, especially for the wedge-tail series. However, these large angles hardly happen at service speed operations, so their impacts on fuel consumption are small. To minimise these uncertainties, the regression formulas of the rudder hydrodynamics to be developed in Section 4.5 are based on the data points in the range of 0° to 10° . The results are shown in the full range of the applied rudder angles (0° to 35°) for manoeuvring simulations to show the tendency of the coefficients, but the uncertainty of the results at the large angles of attack should be noticed.

The presented validation proves the usability of the RANS method for the NACA series. For the IFS series, only low-Reynolds-number results were found in the literature, which was given by Thieme [267]. The validation for the IFS series was not performed with these data which may be affected by the low Reynolds number. Since both the NACA and IFS series are well-streamlined profiles, it is reasonable to assume the method is applicable for the IFS series. Yet, no accurate geometry nor validation data for the wedge-tail rudders was available in the literature. The tail shape may cause stronger flow separation than the NACA and IFS series at large angles of attack while not significantly change the stall angle, which causes uncertainty of using the presented 2D RANS method.

4.2.2. Validation of the 3D RANS method

To validate the 3D RANS method, a model is set up according to the wind-tunnel tests of a spade NACA 0020 rudder carried out by Molland and Turnock [204]. The chord length and the span of the test rudder are 0.667 m and 1 m respectively. The geometric aspect ratio is 1.5. As the gap between the rudder tip and the bottom of the wind tunnel is very small (2.5 mm), the effective aspect ratio of the rudder is 3.0. The wind tunnel is 3.5 m long, 2.5 m wide, and 2.5 m high. The inflow velocity is 20 m s^{-1} . The working fluid is air. The 3D RANS method to validate is configured according to the wind-tunnel tests, except that the domain is larger than the wind tunnel as shown in Figure 4.3. The larger domain is chosen to minimise the influence of the location of the non-physical boundaries on the RANS results.

The rudder tip is connected with the bottom of the domain for simplicity. The viscous effect of the bottom is not accounted in the validation case, but it is accounted in the simulations for the shallow water effect (Section 4.4). Furthermore, the inflow is air at 20 m s^{-1} in the validation case while it is water at a Reynolds number of 6×10^6 for other 3D simulations. Figure 4.6 compares the results of the 3D RANS method and the wind-tunnel tests. In general, the absolute relative differences of the lift, drag, and normal force coefficients are 8 % to 11 %, 6 % to 28 %, and 4 % to 12 % respectively. The accuracy of the method can be improved by changing the turbulence model, increasing the number of cells, and enlarging the domain. However, the computational time may increase significantly.

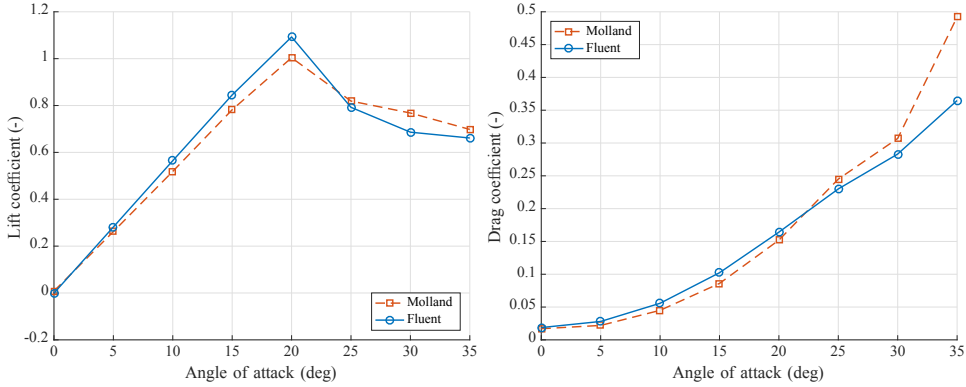


Figure 4.6: Comparison of the 3D Fluent results to the experimental tests.

4.3. 2D RANS study on rudder hydrodynamics

With the validated 2D RANS method, this section studies the hydrodynamic characteristics of single-rudder, twin-rudder, and quadruple-rudder configurations. For each rudder, the force conventions are illustrated in Figure 4.7. In this thesis, counter-clockwise angles are taken as positive.

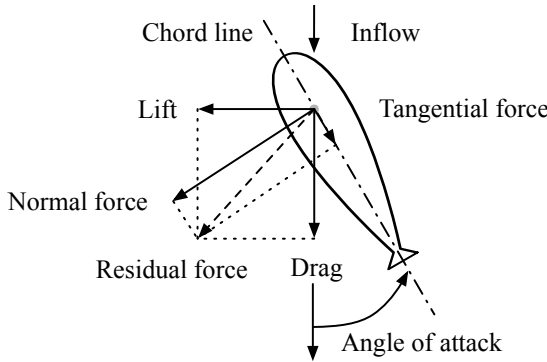


Figure 4.7: Rudder force conventions in RANS simulations.

The relative positions of multiple rudders are defined by the lateral spacing between the rudder stocks, which are shown in Figure 4.8. For twin-rudder configurations, the spacing between the two rudder stocks (y_{TR}) is normally around the value of the propeller diameter (D_P). Additionally, for inland vessels, the rudder chord length (C_R) is commonly not much different from D_P . Therefore, C_R is used as the non-dimensional factor for spacing. A quadruple-rudder configuration can be regarded as a combination of two twin-rudder units with specified spacing between the two inner stocks (y_{TU}). When y_{TR} and y_{TU} are large enough, no interaction effect is expected.

The presented test configurations are listed in Table 4.2. The impacts of the Reynolds number on rudder hydrodynamics (Section 4.3.1), the impacts of profiles on the perfor-

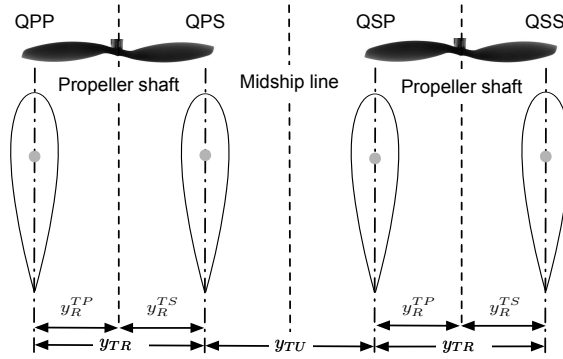


Figure 4.8: Conventions of twin-rudder and quadruple-rudder configurations.

mance of single rudders (Section 4.3.2), the impacts of the spacing on twin rudders (Section 4.3.3), the impacts of the profile on twin rudders (Section 4.3.4), and the impacts of the spacing on quadruple rudders (Section 4.3.5) are studied respectively.

Table 4.2: Test configurations for studies on rudder hydrodynamics in 2D.

Section	Profile	Re (-)	y_{TR} (C_R)	y_{TU} (C_R)
Section 4.3.1	NACA 0012	2×10^5 to 1×10^7	-	-
Section 4.3.2	NACA 0015, NACA 0020, NACA 0025 IFS58 TR15, IFS61 TR25, IFS62 TR25 Wedge-tail 0015, Wedge-tail 0020, Wedge-tail 0025	6×10^6	0.5, 1.0	-
Section 4.3.3	NACA 0018	6×10^6	0.4, 0.5, 0.6, 0.7 0.8, 0.9, 1.0	-
Section 4.3.4	NACA 0015, NACA 0020, NACA 0025 IFS58 TR15, IFS61 TR25, IFS62 TR25 Wedge-tail 0015, Wedge-tail 0020, Wedge-tail 0025	6×10^6	0.5, 0.6 0.7, 0.8 0.9, 1.0	-
Section 4.3.5	NACA 0018	6×10^6	0.5, 0.75, 1.0	0.5, 1.0, 1.5

4.3.1. Impacts of Reynolds numbers on rudder hydrodynamics

The Reynolds number (Re) is defined as the ratio of inertial forces to viscous forces. It represents the similarity among flow patterns and determines the optimal chord-wise and layer-wise mesh sizes. Due to the limited model size and capacity of the test facility, Re of tests in wind tunnels and towing tanks has to be scaled. For CFD methods, full-scale simulations with realistic Re are possible but expensive due to the need for a fine mesh and a large domain.

Experimental results of aerodynamics with a small Mach number can be taken as validation results of incompressible water simulations, as the compressibility effects of a fluid with a Mach number smaller than 0.2 are small. Ladson [155] observed impacts in the lift-curve slope, the maximum lift coefficient, and the maximum lift-drag ratio with increasing Re . Common benchmark wind tunnel tests are carried out at Re in the range of 1×10^5 [267] to 1×10^7 [155]. Nowadays, low-Reynolds-number RANS analysis is still challenging [31, 265] and high-Reynolds-number simulations may be expensive in computation time. The present work tests the NACA0012 profile at Re in a range of 2×10^5 to 1×10^7

as shown in Figure 4.9. These tests are performed with the same grid, boundary conditions, and turbulence model as introduced in Section 4.1.

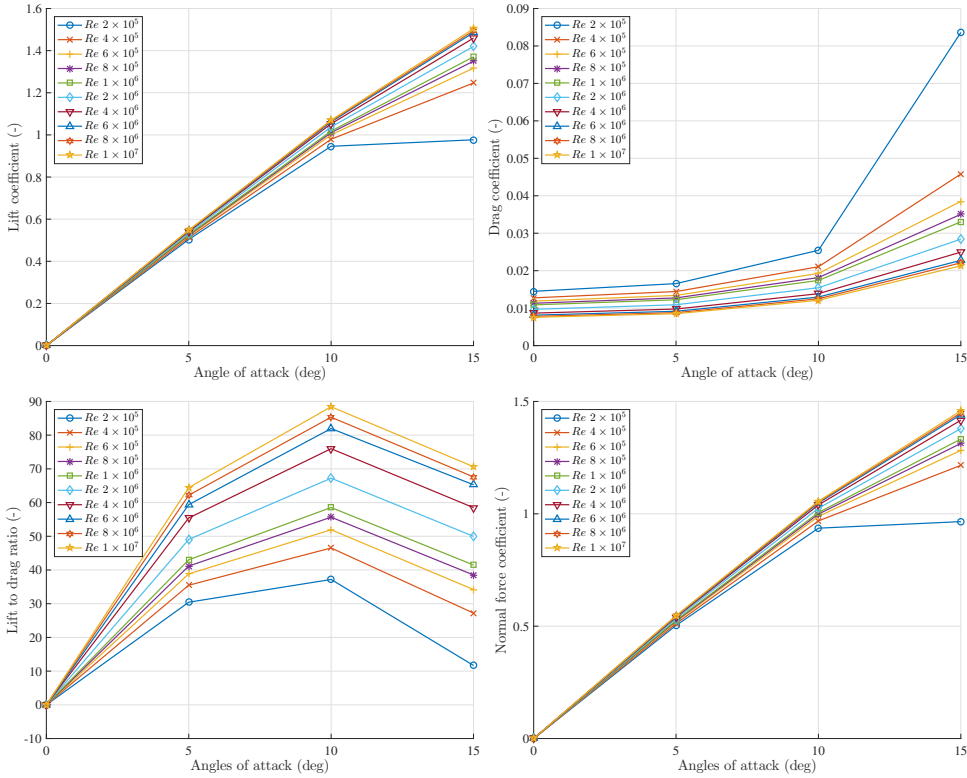


Figure 4.9: Impacts of Reynolds numbers on rudder hydrodynamic coefficients.

The lift curve rises with impacts in Re while the drag curve decreases. Compared to the lift coefficients, the drag coefficients are more sensitive to changes in Re . The drag coefficient under 15° at Re of 1×10^7 is about a quarter of the value at Re of 2×10^5 , whereas the lift coefficient is 1.5 times larger. The differences of lift and drag between low and high Re increase with an increasing angle of attack. Consistent with findings by Ladson [155] and Molland and Turnock [206], a Reynolds number of 6×10^6 can be considered as a threshold value above which little variation may be found.

4.3.2. Impacts of profiles on single-rudder hydrodynamics

2D open water hydrodynamic coefficients of various rudder profiles, which are as the same as the hydrodynamic characteristics of 3D rudders with infinite aspect ratios in open water, are obtained using the 2D RANS method that is validated in Section 4.2.1. Figure 4.10 illustrates the impacts of the profile on rudder efficiency (lift to drag ratios) and effectiveness (normal force coefficients). These RANS results show that the NACA series is most efficient while the wedge-tail series is most effective. However, the NACA series

and the wedge-tail series are least effective and efficient respectively. It not possible to achieve high efficiency (high lift to drag ratios) and high effectiveness (high lift coefficient at a given angle of attack) at the same time. The IFS series, which is initially designed for ships [267], achieves a balance of the efficiency and the effectiveness.

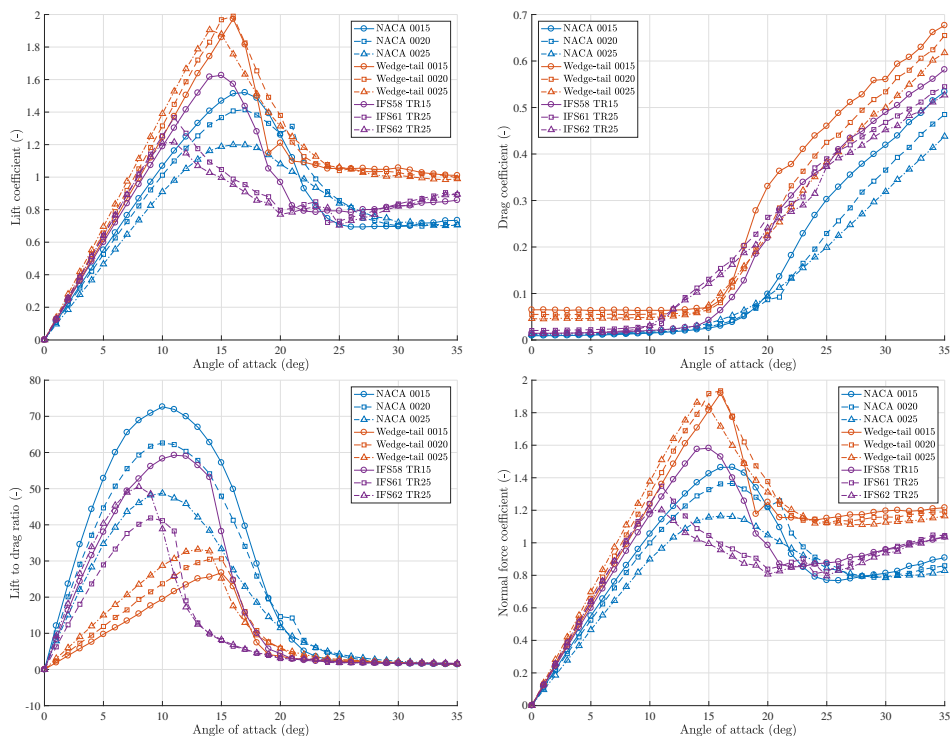


Figure 4.10: 2D open water hydrodynamic coefficients of the tested rudder profiles.

Figure 4.10 also shows that thinner NACA profiles have higher lift and drag coefficients than thicker NACA profiles, resulting in higher normal force coefficients that are dominated more by the lift coefficients than the drag coefficients. The thickness of the NACA profile does not significantly influence the stall angle. Unlike the NACA series, the thinner wedge-tail and IFS profiles have lower lift coefficients than the thicker ones. In addition, thinner wedge-tail and IFS profiles have higher drag coefficients. Due to the change of the profile thickness, the IFS series has a significant change in the lift coefficient and the stall angle. Moreover, a change of the tail thickness extends the stall angles and raises the lift to drag ratios of the IFS profiles. Compared to the NACA and wedge-tail series, thicker IFS profiles have smaller stall angles.

Summarising, various rudder profiles have different hydrodynamic characteristics, which further affect ship manoeuvring performance. The NACA series is most economical. Thus, it is widely applied to ships without critical manoeuvring requirements. The wedge-tail series is most effective but least efficient. Wedge-tail rudders are suggested for ships that need exceptional manoeuvring performance, sail in constrained waterways, or have limited

rudder area, for instance, inland vessels. The IFS series can be a good choice when trying to balance efficiency and effectiveness.

4.3.3. Impacts of spacing on twin-rudder hydrodynamics

The spacing between twin rudders (y_{TR}) affects the pressure distribution around the twin rudders and thus changes the hydrodynamic characteristics. To analyse the impacts of y_{TR} on twin-rudder hydrodynamics, single NACA 0018 rudder and twin NACA 0018 rudders with y_{TR} in the range of $0.4 C_R$ to $1.0 C_R$ at an interval of $0.1 C_R$ are tested. The test range of angles of attack is 0° to 35° . Figure 4.11 illustrates the pressure distributions of twin rudders with different y_{TR} at an angle of attack of 10° .

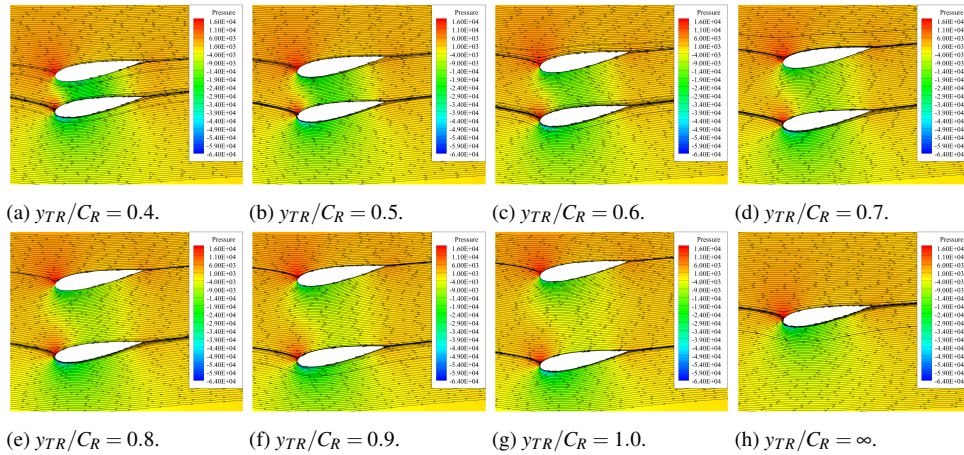


Figure 4.11: Pressure distributions with stream traces of twin NACA 0018 rudders at an angle of attack of 10° with various y_{TR} .

A clear low-pressure region lies between the two rudders. As y_R increases, the pressure difference between the two sides of the port side rudder increases while that of the starboard side rudder decreases, which leads to an increase in the port side lift coefficient and a decrease in the starboard side lift coefficient. The pressure at the leading edge of the port side rudder is decreased while that of the starboard side rudder is increased. This phenomenon explains the changes in the drag coefficients of each rudder. Figure 4.12 compares the lift and drag coefficients of the single rudder and each rudder in the twin-rudder configurations with various y_{TR} .

Compared to the hydrodynamic coefficients of the single rudder, the stall angles of both the port side and the starboard side rudders are increased. Especially, for the starboard side rudders, the sharp decrease of the lift coefficient after the stall angle does not appear. The lift slopes of the port side and starboard side rudders are roughly the same but smaller than that of the single-rudder case. In general, the starboard side rudder has a higher lift coefficient than the port side rudder. However, with y_{TR} of $0.9C$ and $1.0C$, the port side rudder under angles of attack in the range of 10° to 16° has smaller lift coefficient than those of the starboard side rudder.

The drag coefficients of the starboard side and the port side rudders in twin-rudder con-

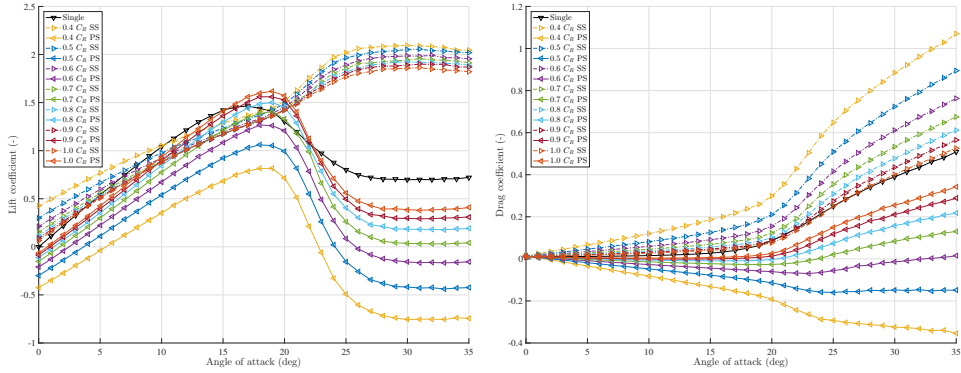


Figure 4.12: Lift and drag coefficients of a single NACA 0018 rudder and either side of twin NACA 0018 rudders with various y_{TR} .

4

figurations are approximately symmetric with the drag coefficient of the single rudder. The drag coefficients at large angles of attack (larger than 15°) are more sensitive to the change of y_{TR} , because the frictional drag is dominant at small angles of attack while the pressure drag is dominant at large angles of attack. It should be noted that the port side rudder may have a negative drag coefficient, which means generating thrust instead of resistance while the starboard side rudder has much higher drag coefficient than the single rudder.

The variation of y_{TR} has larger impacts on the lift coefficient of the port side rudder (C_L^{TP}) than the starboard side rudder (C_L^{TS}). An impacts in y_{TR} leads to an increase in C_L^{TP} and a relatively small decrease in C_L^{TS} . Smaller y_{TR} has larger impacts on the drag coefficient of the port side rudder (C_D^{TP}) and the drag coefficient of the starboard side rudder (C_D^{TS}), more specifically larger differences of C_D^{TP} and C_D^{TS} from the drag coefficient of the single rudder.

Figure 4.13 shows the total hydrodynamic coefficients of the twin rudders with different y_{TR} , where ‘Single’ indicates a single rudder while ‘INF’ means twin rudder with infinite y_{TR} . It is assumed that the hydrodynamic coefficients of ‘INF’ are two times those of ‘Single’. The total lift coefficients of the twin rudders with larger y_{TR} are closer (before the stall angle) but further (after the stall angle) to the total lift coefficient of ‘INF’ than those of twin rudders with smaller y_{TR} . This phenomenon is caused by the stronger interaction that induces a more significant decrease in the lift coefficient on the port side when y_{TR} gets smaller as shown in Figure 4.12.

The total lift coefficients and the total lift slopes increase with an increase in y_{TR} as the interaction effects decrease. An increase in y_{TR} slightly decreases the total drag coefficient at small angles of attack (smaller than 20°) while increases the total drag at large angles of attack. The total lift to drag ratios (C_L/C_D) decrease with a decrease of y_{TR} due to a larger decrease in lift and a smaller decrease in drag. Furthermore, twin rudders with large y_{TR} have higher normal force coefficients than those with small y_{TR} . On the whole, the two cases of the twin rudders with infinite y_{TR} (INF) and zero y_{TR} (Single) set the maximum and minimum bounds of the total twin-rudder hydrodynamic coefficients respectively. With impacts in y_{TR} , both the efficiency (the lift to drag ratio) and the effectiveness (the normal force) of the twin-rudder system in open water increase.

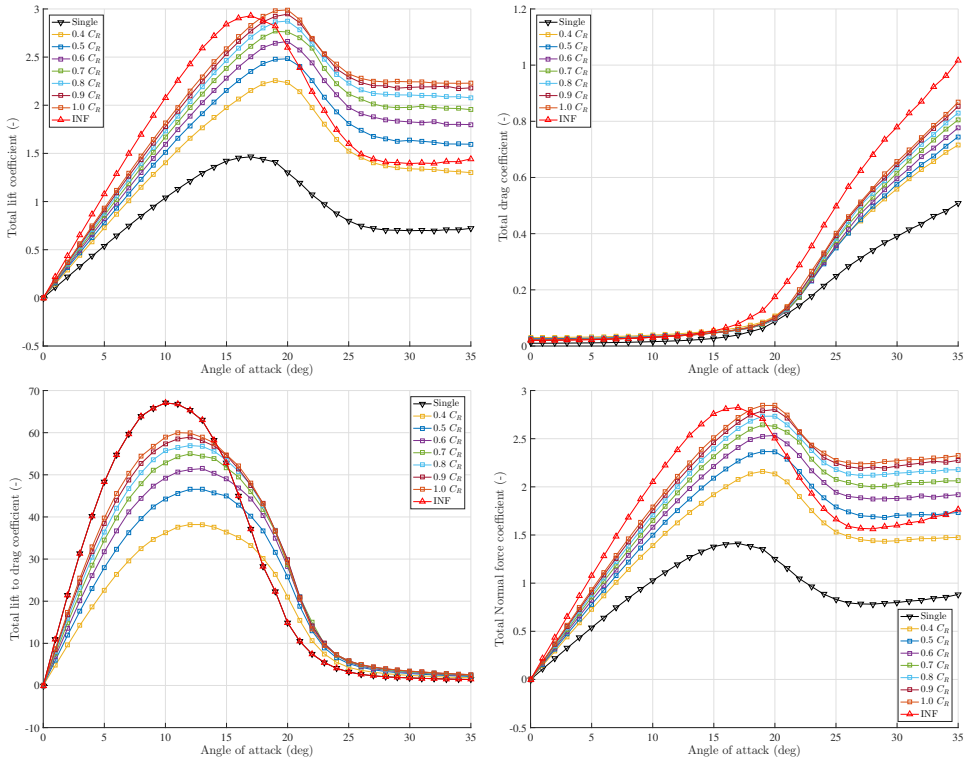


Figure 4.13: Total hydrodynamic coefficients of a single NACA 0018 rudder and twin NACA 0018 rudders with various y_{TR} .

4.3.4. Impacts of profiles on twin-rudder hydrodynamics

To analyse the impacts of the rudder profile on twin-rudder performance, this section presents the test results of 9 profiles from 3 families as listed in Table 4.2. Figure 4.14 and Figure 4.15 present the pressure distributions and the stream traces of the test cases. It is clear that thicker profiles have larger interaction effects as their wake field is larger than those of the thinner profiles. The non-streamlined tails recover the pressure at the trailing edge, increasing the lift but causing more drag. Furthermore, the wedge-tail profiles have larger recirculation than the well-streamlined profiles. In addition, the IFS profiles have a more significant decrease in the pressure at the leading edge, which partly explains their balanced performance in lift and drag.

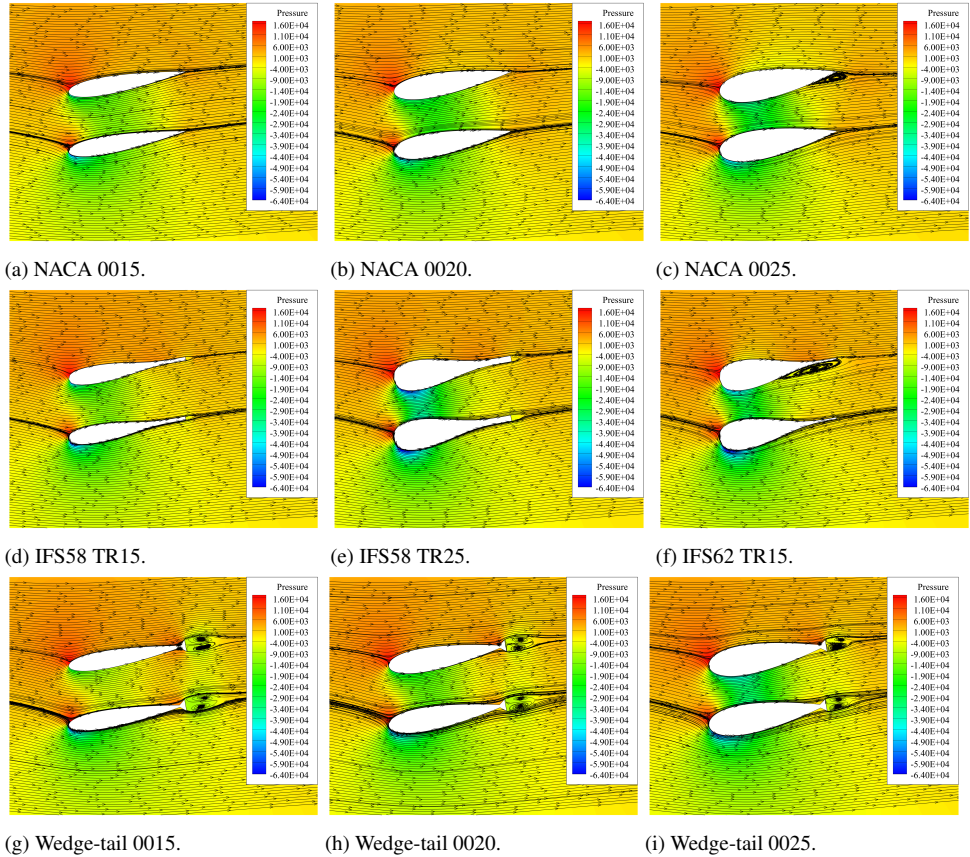


Figure 4.14: Pressure distributions with stream traces of twin-rudder configurations with different profiles at an angle of attack of 10° with $y_{TR} = 0.5 C_R$.

The total lift, total drag, total lift to drag ratios, and total normal force of the tested profiles at y_{TR} of $0.5 C_R$ and $1.0 C_R$ are presented in Figure 4.16 and Figure 4.17 respectively. These two spacings are the common minimum and maximum values for twin-rudder configurations. The impacts of y_{TR} on the hydrodynamic characteristics of different rudder

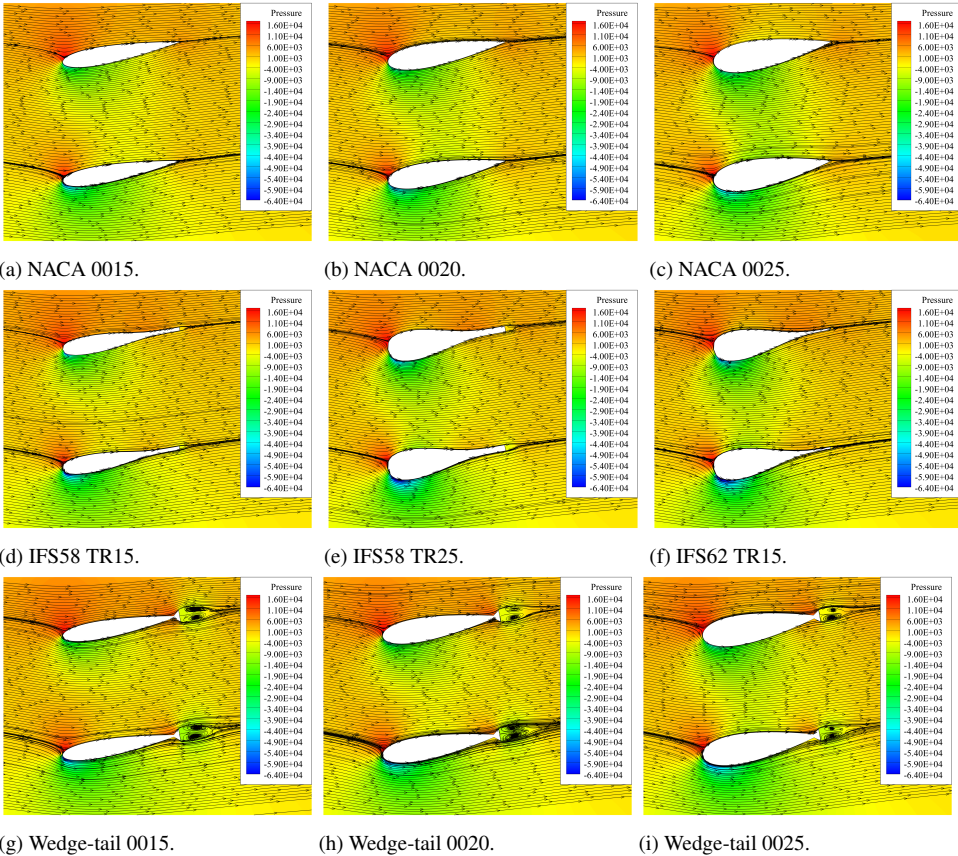


Figure 4.15: Pressure distributions with stream traces of twin-rudder configurations with different profiles at an angle of attack of 10° with $y_{TR} = 1.0 C_R$.

profiles are similar, more specifically impacts in y_{TR} increases the total lift coefficient, the slope of the total lift curves, and the total drag coefficient. Thus, the total normal force becomes larger, which enhances the effectiveness of the twin rudders. Since the increase in the total lift coefficient is larger than the impacts in the total drag coefficient, the total lift to drag ratio gets larger, leading to an improvement of the efficiency of the twin-rudder system.

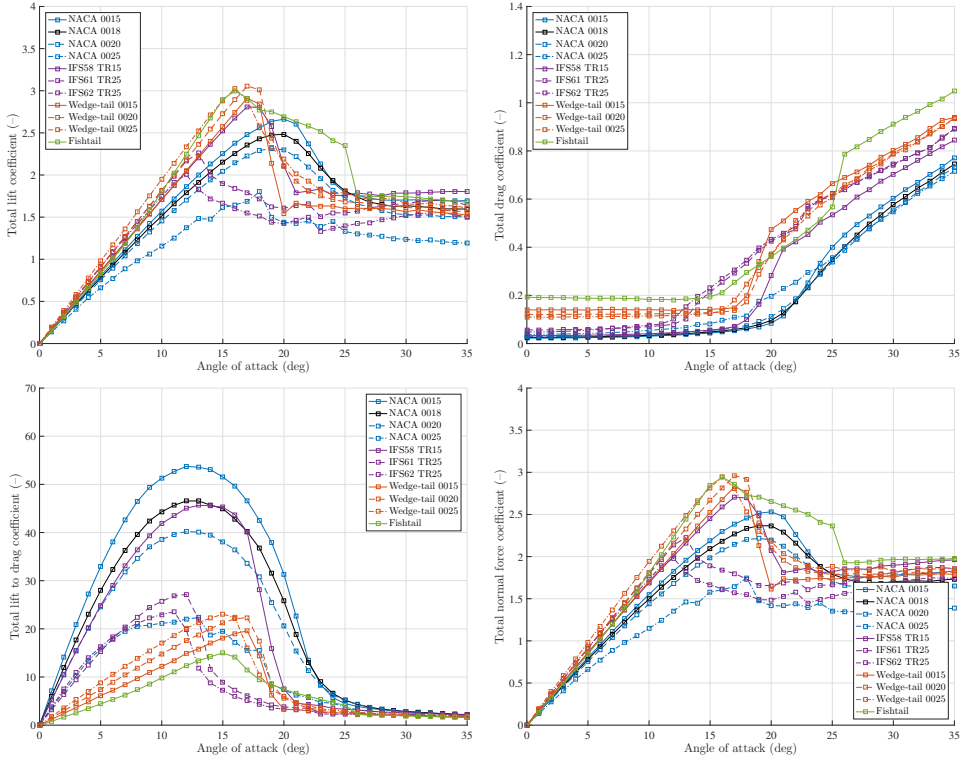


Figure 4.16: Total hydrodynamic coefficients of various twin rudders with $y_{TR} = 0.5 C_R$.

Among the test profiles, in general, wedge-tail is most effective, NACA is most efficient, and IFS is balanced in efficiency and effectiveness. The thinner profiles have better performance than the thicker ones. Commonly, well-streamlined profiles (NACA and IFS) are better than those profiles with non-streamlined appendages (wedge-tail) in the efficiency but worse in the effectiveness. As a summary, the impacts of rudder profiles on the single-rudder and twin-rudder hydrodynamic coefficients are similar.

4.3.5. Impacts of spacing on quadruple-rudder hydrodynamics

To analyse the interaction effects between the two twin-rudder units in quadruple-rudder configurations, y_{TR} and y_{TU} are varied in 3 steps. In total, 9 combinations are tested and compared. The angles of attack are tested in a range of 0° to 15° to reduce the computation time. Figure 4.18 presents the pressure distributions and the stream traces of each case. As

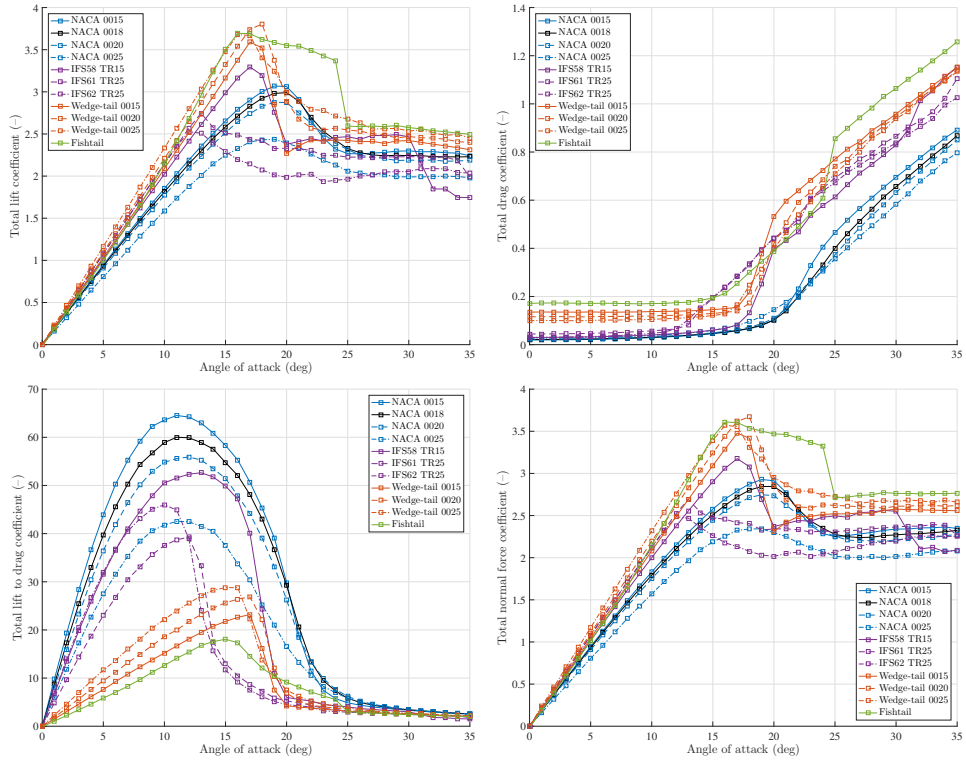


Figure 4.17: Total hydrodynamic coefficients of various twin rudders with $y_{TR} = 1.0 C_R$.

y_{TR} and y_{TU} increase, the pressure distribution of each rudder gets similar to that of the single rudder.

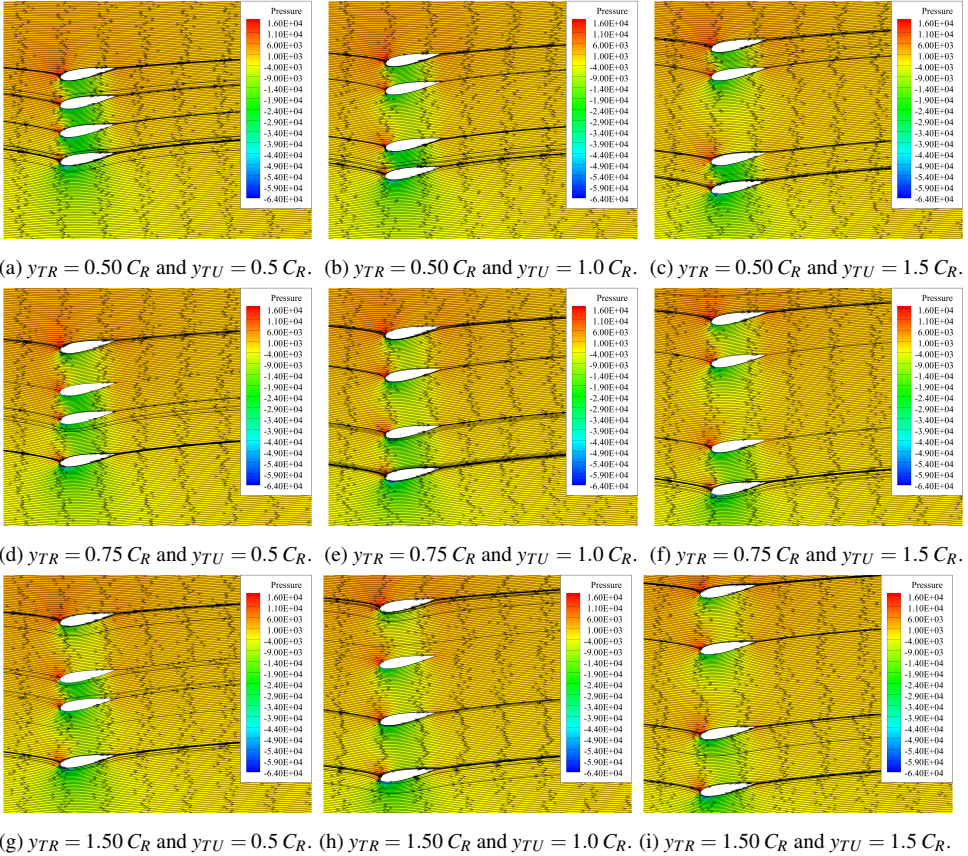
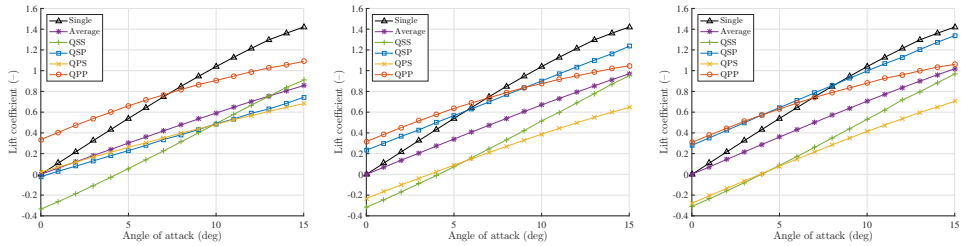


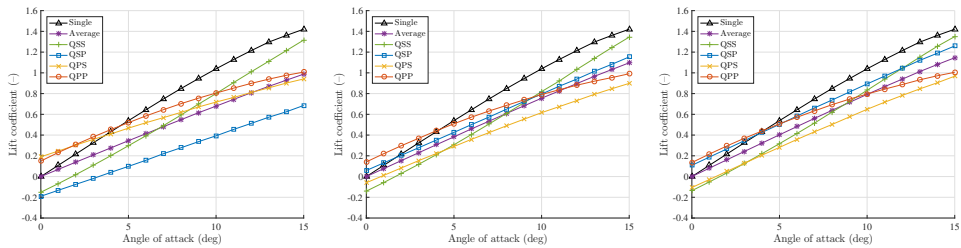
Figure 4.18: Pressure distributions with stream traces of quadruple-rudder configurations at an angle of attack of 10° with different y_{TR} and y_{TU} .

The lift and drag coefficients of each rudder in the quadruple-rudder configurations are compared to the single-rudder coefficients in Figure 4.19 and Figure 4.20. As shown in Figure 4.8, the legends of Single, Average, QSO, QSI, QPI, and QPO stand for the single rudder, the average coefficient of the four rudders, the outer rudder of the starboard side twin-rudder unit, the inner rudder of the starboard side twin-rudder unit, the inner rudder of the port side twin-rudder unit, and the outer rudder of the port side twin-rudder unit respectively. In accordance to the changes in the pressure distribution, the lift and drag coefficients of each rudder in quadruple-rudder configurations get closer to those of the single rudder as spacing among rudders increase.

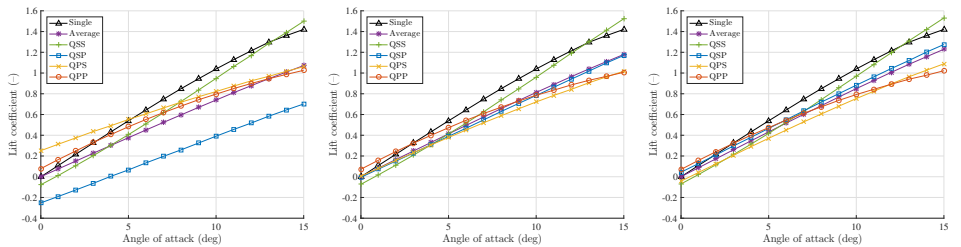
The total hydrodynamic coefficients of the quadruple-rudder configurations are compared in Figure 4.21. With the same y_{TR} , the quadruple-rudder configuration with a larger y_{TU} has higher total C_L and lower total C_D , thus higher total C_L/C_D and total C_N because



(a) $y_{TR} = 0.50 C_R$ and $y_{TU} = 0.5 C_R$. (b) $y_{TR} = 0.50 C_R$ and $y_{TU} = 1.0 C_R$. (c) $y_{TR} = 0.50 C_R$ and $y_{TU} = 1.5 C_R$.



(d) $y_{TR} = 0.75 C_R$ and $y_{TU} = 0.5 C_R$. (e) $y_{TR} = 0.75 C_R$ and $y_{TU} = 1.0 C_R$. (f) $y_{TR} = 0.75 C_R$ and $y_{TU} = 1.5 C_R$.



(g) $y_{TR} = 1.50 C_R$ and $y_{TU} = 0.5 C_R$. (h) $y_{TR} = 1.50 C_R$ and $y_{TU} = 1.0 C_R$. (i) $y_{TR} = 1.50 C_R$ and $y_{TU} = 1.5 C_R$.

Figure 4.19: Lift coefficients of each rudder in a quadruple-rudder configuration compared to the lift coefficient of a single rudder.

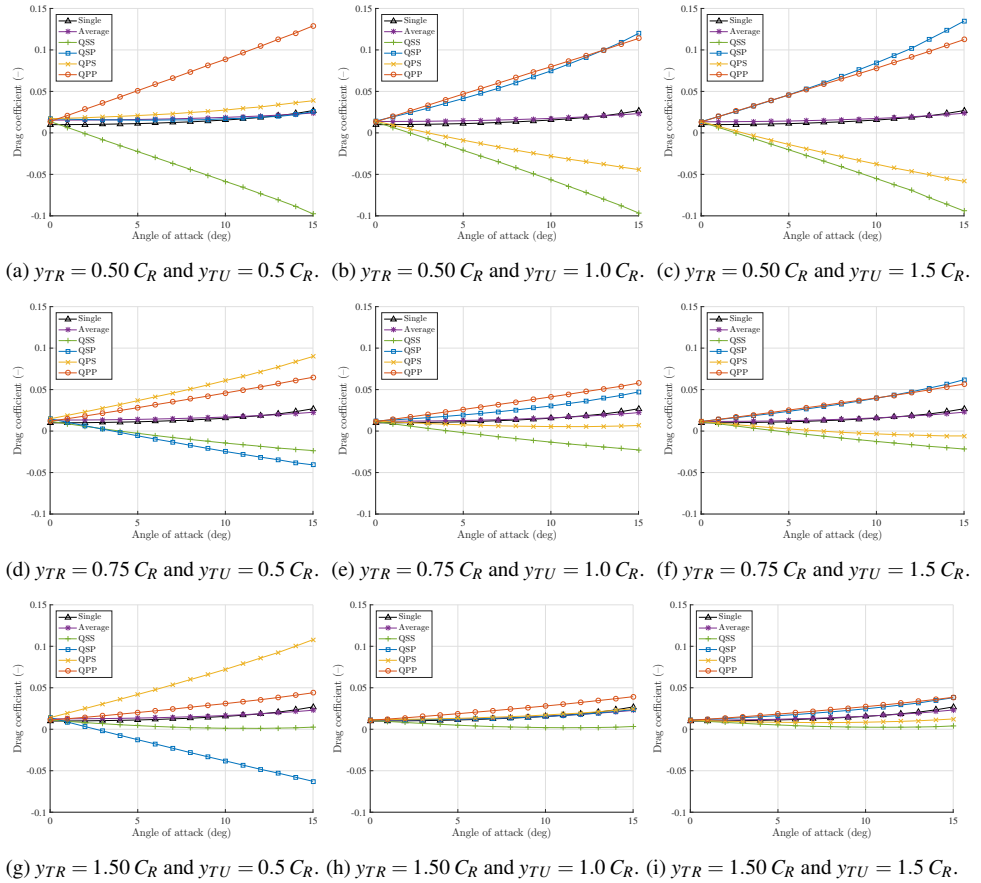


Figure 4.20: Drag coefficients of each rudder in a quadruple-rudder configuration compared to the drag coefficient of a single rudder.

the two inner rudders (QSP and QPS) are in the low-pressure field that is caused by the two outer rudders (QSS and QPP). When y_{TU} is the same, the lift coefficient increases and the drag coefficient decreases as y_{TR} increases. As a summary, the efficiency and the effectiveness of a quadruple-rudder configuration improve as y_{TR} and y_{TU} get larger.

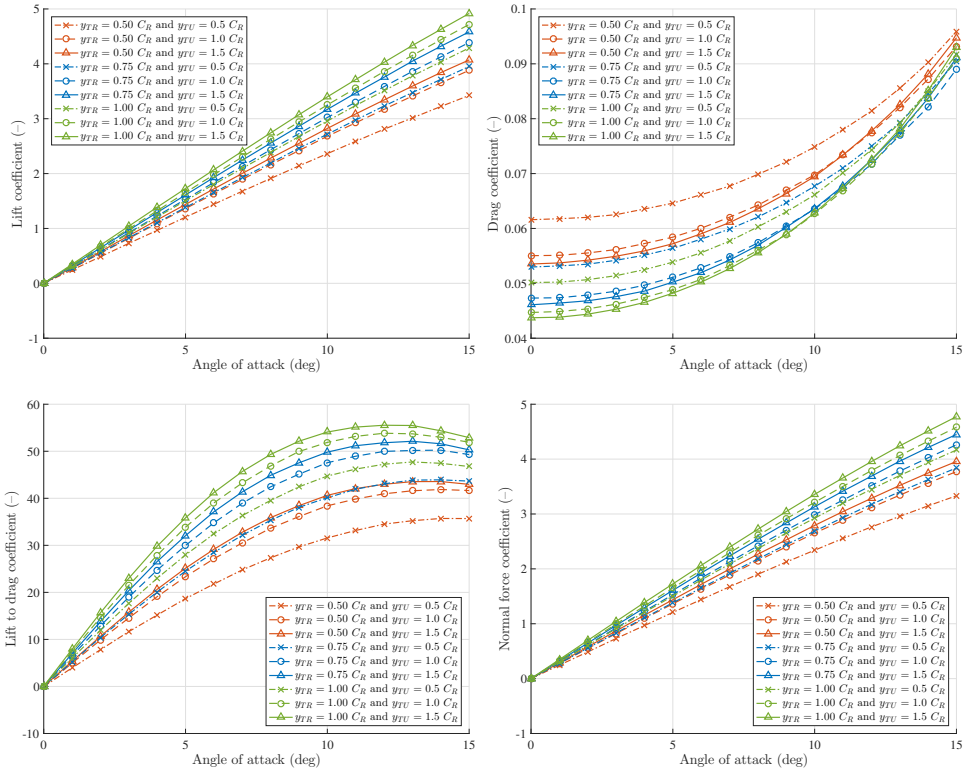


Figure 4.21: Total hydrodynamic coefficients of quadruple NACA 0018 rudders with various y_{TR} and y_{TU} .

4.4. 3D RANS study on rudder hydrodynamics

To analyse the effects of the shallow water and the effective aspect ratio on rudder hydrodynamics, this section presents the results of 3D RANS simulations with a NACA 0020 profile. The 3D RANS method is validated with wind tunnel results in Section 4.2.2. The test configuration is shown in Figure 4.3. Three geometric aspect ratios ($\Lambda_G = 1.2, 1.5, \text{ and } 2.0$) at two non-dimensional tip clearance ($d'_R = 0.2 \text{ and } 0.5$) are tested. Furthermore, the validation case, where ($\Lambda_G = 1.5 \text{ and } d'_R = 0.0$), is included to show the effect of d'_R on the effective aspect ratio. The lift coefficients, the drag coefficients, the lift to drag ratio, and the normal force coefficients of the test cases are presented in Figure 4.22.

With the same non-dimensional tip clearance (d'_R), a decrease in the geometric aspect

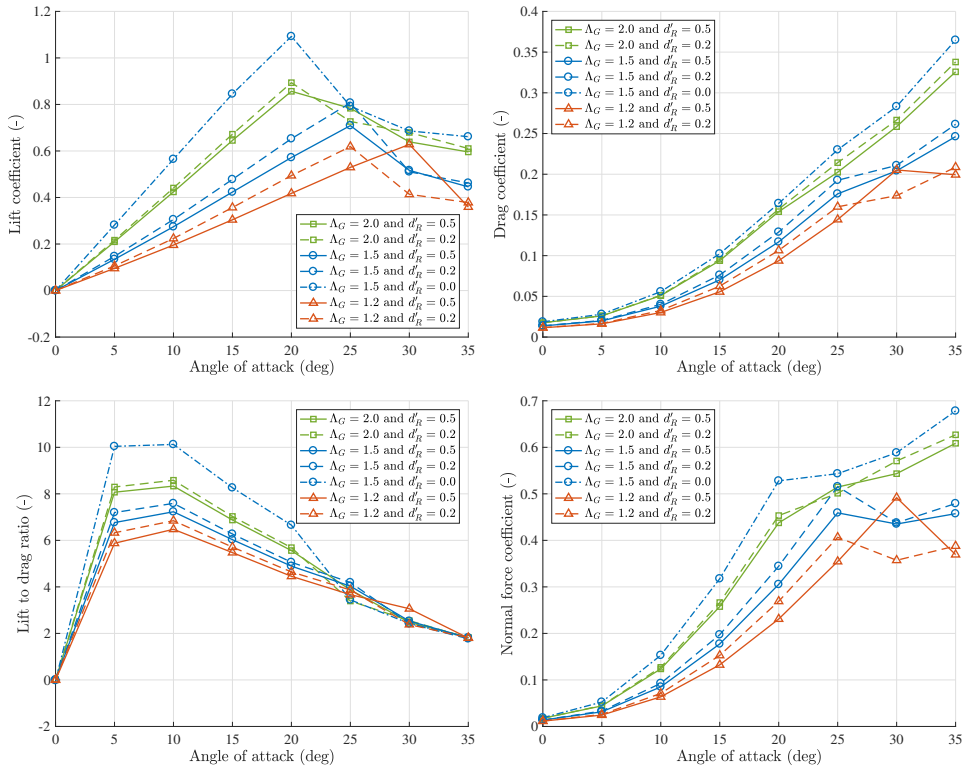


Figure 4.22: Impacts of the shallow water and the effective aspect ratio on rudder hydrodynamic coefficients.

ratio (Λ_G) decreases the slopes of all the four coefficient curves, namely the lift coefficient, the drag coefficient, the lift to drag ratio, and the normal force coefficient while extends the stall angle. Therefore, a large Λ_G improves the rudder efficiency and effectiveness as expected. Owing to the larger stall angles, the rudders with smaller Λ_G may be more effective at larger rudder angles than those with larger Λ_G . With the same Λ_G , the rudders with smaller d'_R have higher slopes of the four coefficient curves. As d'_R gets smaller, the shallow water effect appears, which enlarges the effective aspect ratio of the rudder.

It is known that the ratio of the effective and geometric aspect ratios (Λ_E/Λ_G) is 2 when the rudder tip connects with the bottom, which is the validation case for the 3D RANS method. Λ_E/Λ_G decreases with an increase in d'_R . As d'_R increases from 0.2 to 0.5, the reduction of Λ_E/Λ_G is more noticeable for the rudders with smaller Λ_G than those with larger Λ_G . This phenomenon shows that the shallow water (the small tip clearance), in fact, improves the efficiency and effectiveness of the rudder itself. Furthermore, it shows the benefit of using end plates to enhance the rudder performance, especially for rudders with small geometric aspect ratios.

4.5. Regression study on rudder hydrodynamic coefficients

Series of 2D RANS simulations of single-rudder, twin-rudder, and quadruple-rudder configurations are presented in Section 4.3. Based on these RANS results, rudder hydrodynamic coefficients are obtained considering the rudder profile and the spacing among rudders. New regression formulas of the rudder hydrodynamic coefficients are presented in this section for the proposed manoeuvring model in Chapter 5. The objective is to achieve C_L^{2D} and C_D^{2D} for Equation 5.21 in Section 5.7.2.

4.5.1. Regression study on single-rudder hydrodynamic coefficients

For a single 2D rudder in open water, Table 4.3 presents new regression formulas for various rudder profiles. These regression formulas are derived from the CFD results given in Figure 4.10. The sample points are taken in the range of 0° to 10° . In this range, the accuracy of the RANS results is not significantly affected by the strong flow separation at large angles of attack.

4.5.2. Regression study on twin-rudder hydrodynamics coefficients

In Section 4.3.3, the impacts of the spacing on twin-rudder hydrodynamic characteristics is discussed by modifying y_{TR} . Analysing the data in Figure 4.12, a correlation between the lift and drag coefficients of each rudder in twin-rudder configurations with those of the single-rudder case is found. Therefore, it is proposed to use the single-rudder lift (C_L^{2D}) and drag (C_D^{2D}) coefficients to predict the lift and drag coefficients for starboard and port side rudders (C_L^{TS} , C_L^{TP} , C_D^{TS} , and C_D^{TP}) in the twin-rudder configuration. In the regression study, the data points of twin-rudder configurations with spacing in the range of $0.5 C_R$ and $1.0 C_R$ are selected as it is the commonly applied range in practice.

Considering the impacts of the rudder profile and the spacing on lift and drag coeffi-

Table 4.3: Regression coefficients for the rudder hydrodynamic characteristics of single rudders.

Rudder profile	$\frac{\partial C_N^{2D}}{\partial \sin \alpha_R}$	$\frac{\partial C_L^{2D}}{\partial \sin \alpha_R}$	C_{L0}^{2D}	$\frac{\partial C_D^{2D}}{\partial \sin \alpha_R}$	C_{D0}^{2D}
NACA 0012	6.16	6.24	0.00	0.03	0.01
NACA 0015	6.10	6.18	0.00	0.03	0.01
NACA 0018	5.94	6.01	0.00	0.03	0.01
NACA 0020	5.78	5.85	0.00	0.03	0.01
NACA 0025	5.20	5.26	0.00	0.04	0.01
IFS58 TR15	6.78	6.85	0.00	0.03	0.01
IFS61 TR25	7.19	7.27	0.00	0.05	0.02
IFS62 TR25	7.02	7.10	0.00	0.08	0.01
Wedge-tail 0015	7.12	7.16	0.00	-0.01	0.07
Wedge-tail 0020	7.52	7.57	0.00	0.00	0.06
Wedge-tail 0025	7.94	8.00	0.00	0.01	0.05

icients, the regression formulas are made in the following format:

$$\left. \begin{aligned}
 C_L^{TS,TP} &= \left(k_1^{C_L} \frac{C_R}{y_R^{TS,TP}} \left| \frac{C_R}{y_R^{TS,TP}} \right| + k_2^{C_L} \frac{C_R}{y_R^{TS,TP}} + 1 \right) \frac{\partial C_L^{2D}}{\partial \alpha} \sin \left(k_3^{C_L} \frac{C_R}{y_R^{TS,TP}} \left| \frac{C_R}{y_R^{TS,TP}} \right| + k_4^{C_L} \frac{C_R}{y_R^{TS,TP}} + 1 \right) \alpha \\
 &\quad + k_5^{C_L} \frac{C_R}{y_R^{TS,TP}} \left| \frac{C_R}{y_R^{TS,TP}} \right| + C_{L0}^{2D} \\
 C_D^{TS,TP} &= \left(k_1^{C_D} \frac{C_R}{y_R^{TS,TP}} \left| \frac{C_R}{y_R^{TS,TP}} \right| + k_2^{C_D} \frac{C_R}{y_R^{TS,TP}} + 1 \right) \frac{\partial C_D^{2D}}{\partial \alpha} \sin \left(k_3^{C_D} \frac{C_R}{y_R^{TS,TP}} \left| \frac{C_R}{y_R^{TS,TP}} \right| + k_4^{C_D} \frac{C_R}{y_R^{TS,TP}} + 1 \right) \alpha \\
 &\quad + k_5^{C_D} \frac{C_R}{y_R^{TS,TP}} \left| \frac{C_R}{y_R^{TS,TP}} \right| + C_{D0}^{2D},
 \end{aligned} \right\} \quad (4.2)$$

where

- $\frac{C_R}{y_R^{TS,TP}}$ concerns the relative position of each rudder in a twin-rudder configuration. y_R^{TS} and y_R^{TP} are the relative positions of the starboard side and the port side rudder to the propeller shaft.
- $\frac{\partial C_L^{2D}}{\partial \alpha}$ and $\frac{\partial C_D^{2D}}{\partial \alpha}$ are the slopes of the lift and drag coefficients of a single rudder, which are dependent on the rudder profile as shown in Table 4.3.
- $k_1^{C_L, C_D} \frac{C_R}{y_R^{TS,TP}} \left| \frac{C_R}{y_R^{TS,TP}} \right| + k_2^{C_L, C_D} \frac{C_R}{y_R^{TS,TP}} + 1$ considers the interaction effect on the lift and drag slopes.
- $k_3^{C_L, C_D} \frac{C_R}{y_R^{TS,TP}} \left| \frac{C_R}{y_R^{TS,TP}} \right| + k_4^{C_L, C_D} \frac{C_R}{y_R^{TS,TP}} + 1$ accounts for the interaction effect on the effective angle of attack.
- $k_5^{C_L, C_D} \frac{C_R}{y_R^{TS,TP}} \left| \frac{C_R}{y_R^{TS,TP}} \right|$ represents the interaction effect on the lift and drag coefficients at zero angle of attack.

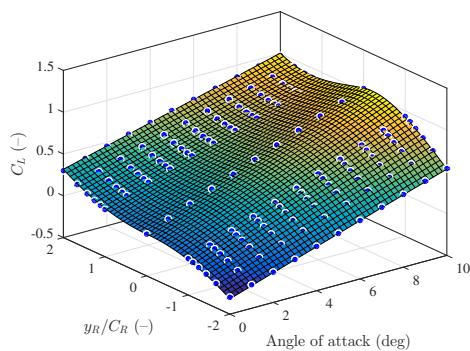
- $C_{L_0}^{2D}$ and $C_{D_0}^{2D}$ are the lift and drag coefficients of a single rudder at zero angle of attack. $C_{L_0}^{2D}$ and $C_{D_0}^{2D}$ can be assumed as zero for symmetric well-streamlined profiles while they should be non-zero when asymmetric profiles are applied.

$\frac{\partial C_L^{2D}}{\partial \alpha}$ and $\frac{\partial C_D^{2D}}{\partial \alpha}$ are determined from the lift and drag coefficients of single-rudder at angles of attack in the range of 0° and 10° . This range is determined to minimise the impacts of the strong flow separation around the stall angle on the RANS simulations. The twin rudders are positioned at equal distances from the propeller shaft, therefore, $y_R^{TS} = \frac{1}{2}y_{TR}$ and $y_R^{TP} = -\frac{1}{2}y_{TR}$. The applied values of $\frac{\partial C_L^{2D}}{\partial \alpha}$, $\frac{\partial C_D^{2D}}{\partial \alpha}$, $C_{L_0}^{2D}$ and $C_{D_0}^{2D}$ for single profile are adapted from Table 4.3. Least squares fitting is performed in the format of Equation 4.2 with the data presented in Figure 4.8. The coefficients of the regression formulas for the lift and drag curves are presented in Table 4.4, where R^2 is R-squared (coefficient of determination) and σ is root mean squared error (standard error) of the regression coefficients.

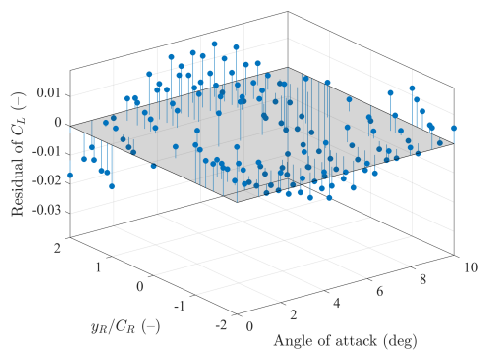
Table 4.4: Regression coefficients of the twin-rudder lift and drag coefficients.

Rudder profile	$k_1^{C_L}$	$k_2^{C_L}$	$k_3^{C_L}$	$k_4^{C_L}$	$k_5^{C_L}$	$R_{C_L}^2$	σ_{C_L}
NACA 0015	0.109	-0.493	-0.069	0.378	0.079	0.999	0.001
NACA 0018	-0.078	0.387	0.118	-0.514	0.067	0.999	0.010
NACA 0020	-0.064	0.372	0.098	-0.475	0.083	0.999	0.012
NACA 0025	-0.073	0.437	0.056	-0.401	0.064	0.993	0.024
IFS58 TR15	0.140	-0.572	-0.095	0.427	0.071	0.999	0.012
IFS61 TR25	0.176	-0.642	-0.076	0.389	0.169	0.999	0.017
IFS62 TR25	-0.729	1.101	0.710	-1.235	0.182	0.969	0.080
Wedge-tail 0015	0.156	-0.620	-0.092	0.437	0.003	0.998	0.015
Wedge-tail 0020	-0.084	0.415	0.167	-0.642	0.065	0.997	0.019
Wedge-tail 0025	-0.068	0.377	0.206	-0.713	0.168	0.996	0.030
Rudder profile	$k_1^{C_D}$	$k_2^{C_D}$	$k_3^{C_D}$	$k_4^{C_D}$	$k_5^{C_D}$	$R_{C_D}^2$	σ_{C_D}
NACA 0015	3.580	-1.524	-0.012	0.045	0.000	0.999	0.001
NACA 0018	2.729	-1.145	-0.002	0.019	0.000	0.999	0.001
NACA 0020	4.221	-1.562	-0.009	0.046	0.000	0.998	0.001
NACA 0025	4.506	-0.990	0.001	0.053	-0.001	0.996	0.002
IFS58 TR15	2.210	-1.360	-0.006	0.026	0.001	0.998	0.001
IFS61 TR25	3.444	-2.630	0.014	0.031	0.002	0.994	0.002
IFS62 TR25	1.749	-1.327	0.265	-0.400	0.003	0.993	0.002
Wedge-tail 0015	-7.663	-7.268	-0.208	0.512	0.001	0.979	0.002
Wedge-tail 0020	38.646	-5.670	-0.161	0.376	0.001	0.947	0.006
Wedge-tail 0025	17.057	-9.379	-0.113	0.274	0.001	0.993	0.003

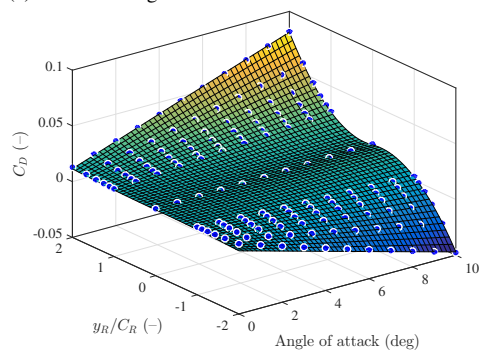
The surface fitting and related residuals of the regression formulas with the coefficients in Table 4.4 are presented in Figure 4.23 for the NACA 0018 profile as an example. The regression formulas are then used for different profiles at $y_{TR} = 0.5 C_R$ and $y_{TR} = 1.0 C_R$ and compared with the RANS results in Figure 4.24, Figure 4.25, Figure 4.26, and Figure 4.27 respectively. The comparison shows the usability of the equations for the test profile series.



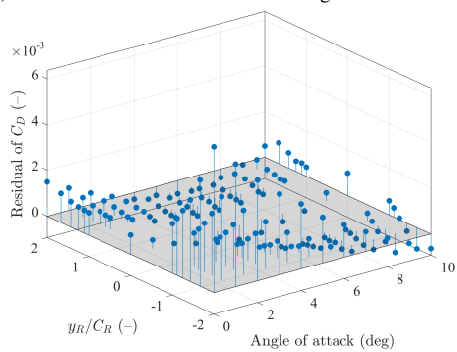
(a) Surface fitting of the lift coefficient.



(b) Residuals of the lift coefficient fitting.



(c) Surface fitting of the drag coefficient.



(d) Residuals of the drag coefficient fitting.

Figure 4.23: Surface fitting of the lift and drag coefficients of the NACA 0018 profile with different spacing.

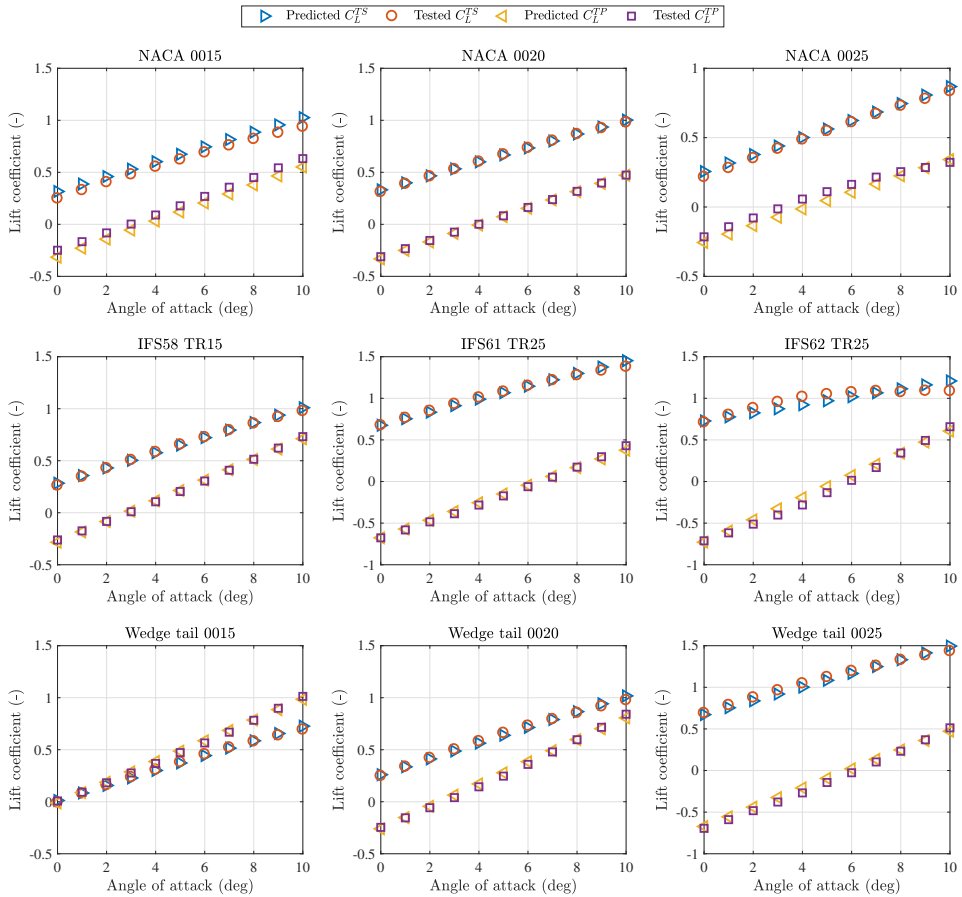


Figure 4.24: Comparison of predicted and tested lift coefficients of different profiles in the twin-rudder configuration with $y_{TR} = 0.5 C_R$.

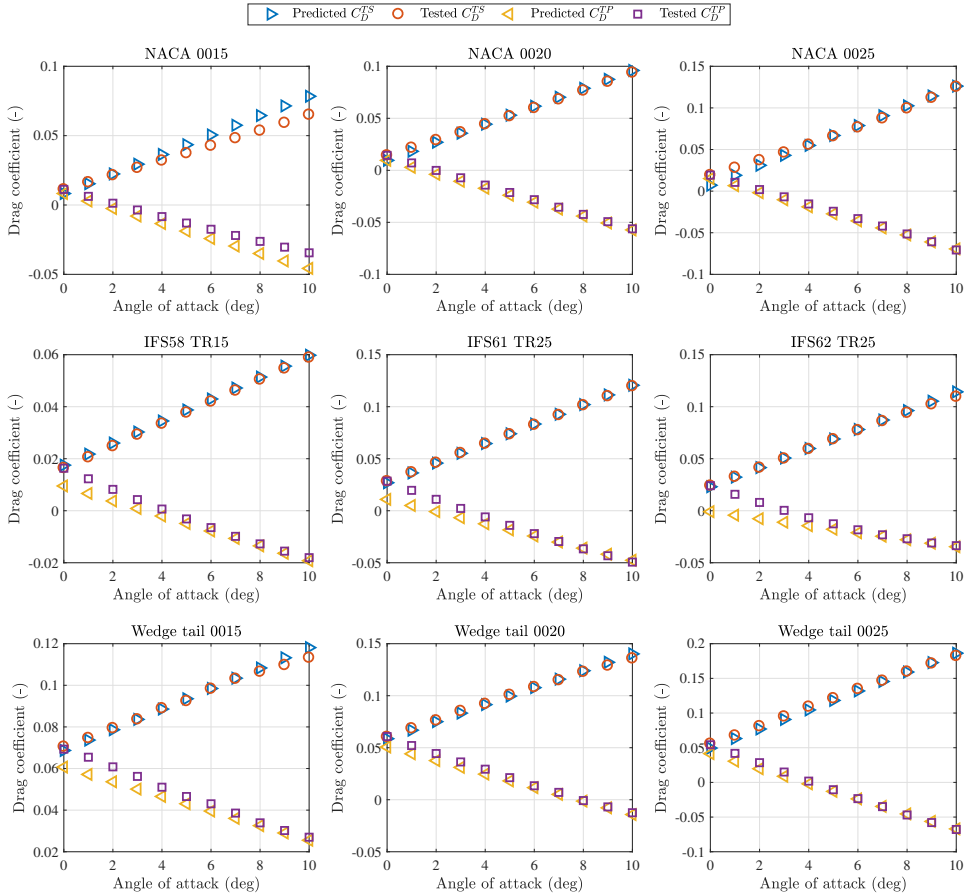


Figure 4.25: Comparison of predicted and tested drag coefficients of different profiles in the twin-rudder configuration with $y_{TR} = 0.5 C_R$.

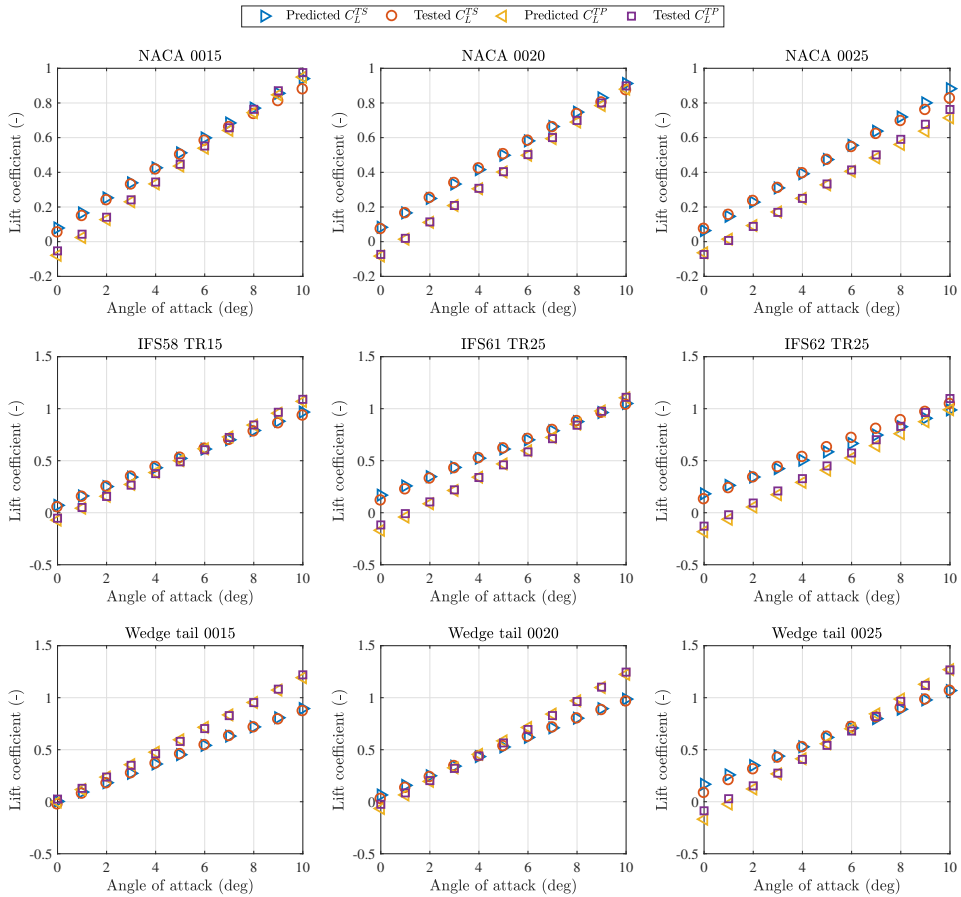


Figure 4.26: Comparison of predicted and tested lift coefficients of different profiles in the twin-rudder configuration with $y_{TR} = 1.0 C_R$.

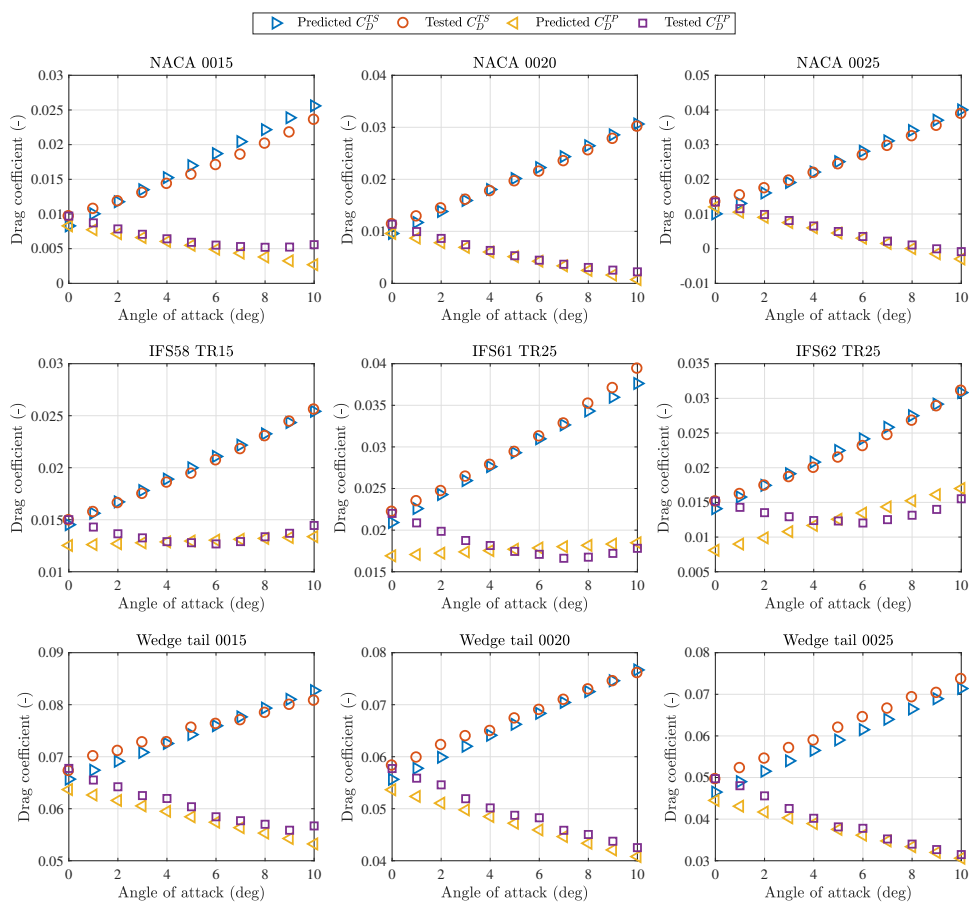


Figure 4.27: Comparison of predicted and tested drag coefficients of different profiles in the twin-rudder configuration with $y_{TR} = 1.0 C_R$.

4.5.3. Limitations of the regression formulas

In the previous sections, regression formulas have been proposed for single and twin rudders on the basis of RANS simulations. These regression formulas are applied in Chapter 5 to build the integrated manoeuvring model for inland vessels. They are also applicable to other research topics related to the rudder hydrodynamics with the following limitations: $|\alpha_R| \leq 35^\circ$ and $0.5 C_R \leq y_{TR} \leq 1.0 C_R$. For $|\alpha_R| > 35^\circ$, the relative differences between the predicted value with the regression formula and the actual value would be enlarged. Normally, y_{TR} cannot be smaller than $0.5 C_R$ from a practical point of view while the interaction effects get less significant when y_{TR} is larger than $1.0 C_R$. Extra check on the usability of the proposed formulas is demanded when they are applied for cases which are out of the limitations.

4.6. Synthesis

This chapter has introduced the applied 2D and 3D RANS methods, which are validated with experimental and numerical test results. The 2D RANS method is used to obtain hydrodynamic characteristics of rudders with infinite aspect ratios in open water. The impacts of the Reynolds numbers, the rudder profiles, and the spacing among multiple rudders on rudder hydrodynamics are analysed. A 3D RANS method is utilised for the impacts of effective aspect ratios and shallow water on rudder hydrodynamics. Conclusions are summarised as follows to answer the second research question in Section 1.3: *How does the rudder configuration affect the rudder hydrodynamic characteristics?*

1. As the Reynolds number increases, the lift curve rises while the drag curve decreases. A Reynolds number of 6×10^6 can be considered as a threshold value above which little impacts on rudder hydrodynamics may be found.
2. Different profiles have different hydrodynamic characteristics. Among the tested profile families, the NACA series is most efficient while the wedge-tail series is most effective. Additionally, the IFS series is a good choice considering the balance of efficiency and effectiveness.
3. An impacts in y_{TR} increases the total lift coefficient, the total drag coefficient, the total lift to drag ratio, and the total normal force coefficient. Therefore, both the efficiency and the effectiveness of the twin-rudder system improve as the rudders are placed further apart.
4. The profile does not significantly affect the impacts of y_{TR} on the twin-rudder hydrodynamics. The significance of the interaction effect is primarily determined by the spacing.
5. The impacts of profiles on single-rudder and twin-rudder hydrodynamic coefficients are similar.
6. As y_{TR} and y_{TU} increase, the total lift coefficient, the total lift to drag coefficient, and the total normal force coefficients of a quadruple-rudder configuration increase while

the total drag coefficient decreases. Therefore, the efficiency and the effectiveness of the quadruple-rudder system improves as y_{TR} and y_{TU} get larger.

7. In the same water depth, the lift coefficient, the drag coefficient, the lift to drag ratio, and the normal force coefficient increase with impacts in the geometric aspect ratio. A large geometric aspect ratio is recommended whenever it is applicable.
8. Shallow water affects the effective aspect ratio of the rudder. A decrease in the rudder tip clearance increases the ratio of the effective geometric aspect ratio to the geometric aspect ratio. This increase is more significant for the rudders with small geometric aspect ratios. However, these shallow-water effects only occur in extraordinary shallow water.
9. It is recommended to use end plates to improve the rudder performance by increasing the effective aspect ratio, especially for the rudders with small aspect ratios. The impacts of the end plates on the rudder hydrodynamic coefficients for manoeuvring will be discussed in Section 5.7.2.

With the results of this chapter, it is now possible to consider the impacts of the rudder configurations on ship manoeuvring performance. Based on the RANS results that are obtained in this chapter, new regression formulas have been proposed and will be integrated into mathematical models for multiple-propeller multiple-rudder ships in Chapter 5. In Chapter 6, this mathematical model will be applied to carry out simulations of the reference ships in the proposed test manoeuvres.

Chapter 5

Mathematical Modelling of Ship Manoeuvrability*

“I am never content until I have constructed a mechanical model of the subject I am studying. If I succeed in making one, I understand; otherwise I do not.”

William Thomson, 1st Baron Kelvin (1824 – 1904)

As reviewed in Chapter 2, inland vessels have more complex rudder configurations than seagoing ships. To analyse inland vessel manoeuvring performance, this chapter describes manoeuvring simulation models for single-rudder, twin-rudder, and quadruple-rudder ships. Section 5.1 introduces the challenges in developing mathematical models for inland vessels. Section 5.2 presents the test benchmark vessels. Section 5.3 describes the mathematical models to be solved for manoeuvring simulations. Section 5.4 calculates the (added) mass and (added) moments of the ship. Section 5.5, Section 5.6, and Section 5.7 express the forces and the moments induced by the hull, the propeller(s), and the rudder(s) respectively. Accordingly, existing methods for each manoeuvring parameter are discussed and some methods are preselected based on theoretical estimation, model test experience, and benchmark values in literature.

Compared to numerical or experimental tests, empirical formulations are the most suitable and least expensive tool to apply, especially in the initial design stage when the details are not settled [51]. Since most of the empirical methods are formed based on databases of seagoing ships, it is questionable to directly apply these methods for inland vessels. Furthermore, there is the absence of validation data as very few studies have been carried out for inland vessels specifically. Section 5.8 determines the most suitable empirical methods for the benchmark inland vessel. Afterwards, Section 5.9 validates the mathematical model by comparing simulated and tested results. Finally, Section 5.10 draws the conclusions of this chapter.

5.1. Introduction to modelling of inland vessels

5.1.1. Degrees of freedom

A lot of effort has been put into the ship manoeuvring models, but current work is primarily evolutionary rather than revolutionary. Ships are free to surge, sway, and heave

*This chapter is based on Liu et al. [181] and Liu et al. [182].

in the direction of axes and roll, pitch, and yaw with respect to axes respectively. As it may affect the speed and accuracy in simulations, the required number of degrees of freedom should be seriously considered according to the navigation conditions and ship particulars.

For inland vessels that rarely encounter severe waves and swell, a model with 3 DOF (Degree Of Freedom), including surge, sway, and yaw motions can give sufficient results. Considering the impacts of sinkage and trim, a 6 DOF model can be more suitable for ships in constrained waterways and shallow water. This thesis takes a 3 DOF model as the goal is to draw general conclusions about the rudder impacts on inland vessel manoeuvrability rather than study a specific ship in specific water depth.

5.1.2. Types of manoeuvring models

In order to solve the equations of motions, expressions are needed for the components of external forces and moments acting on the ship. These forces and moments are caused by the ship hydromechanics and environmental disturbances due to wind, waves, current, and banks. Owing to the different manners of parametrizations for the hydrodynamic forces and moments, the mathematical models are generally divided into two types: the whole ship model [2] and the modular model [218].

According to Abkowitz [2], the whole ship model (so-called Abkowitz model), expresses the hydrodynamic forces and moments as functions of kinematic parameters and rudder angles as the following:

$$\left. \begin{aligned} X &= X(u, v, r, \dot{u}, \dot{v}, \dot{r}, \delta) \\ Y &= Y(u, v, r, \dot{u}, \dot{v}, \dot{r}, \delta) \\ N &= N(u, v, r, \dot{u}, \dot{v}, \dot{r}, \delta) \end{aligned} \right\} \quad (5.1)$$

where u , v , and r are the forward speed, the lateral speed, and the yaw rate in the direction of x -axis, in the direction of y -axis, and around z -axis respectively. These kinematic parameters can be further expressed in Taylor-series. This whole ship model treats the interaction between the hull and the water as a black box and proved to be successful for arbitrary simulations [44, 257].

Represented by Ogawa and Kasai [219], the Mathematical Model Group of the Society of Naval Architects of Japan proposed a modular model, which is also known as the MMG model. The modular model decomposes the hydrodynamic forces and moments into three parts, namely the hull, the propeller, and the rudder, as the following:

$$\left. \begin{aligned} X &= X_H + X_P + X_R \\ Y &= Y_H + Y_P + Y_R \\ N &= N_H + N_P + N_R \end{aligned} \right\} \quad (5.2)$$

where the subscripts H , P , and R indicates the hull, the propeller and the rudder. With the modular model, the contribution of each component and the hull-propeller-rudder interactions to ship manoeuvring performance can be analysed.

Details about the modular model were discussed in a series of papers written by Yasukawa and Yoshimura [304] and Yoshimura [309, 310, 311]. Oltmann and Sharma [223] presented an approximation method of the hull-propeller-rudder interactions. Fujino and Ishiguro [75] showed a remarkable dependence of the rudder effectiveness on the water

depth. Kijima et al. [138, 139] and Kijima and Yasukawa [137] proposed approximation formulas for hydrodynamic coefficients of hull forces in shallow and deep water. Kijima and Nakiri [135], Kijima and Qing [136], and Kijima and Yasukawa [137] applied the MMG model to analyse the interaction forces generated by other ships and banks.

Clarke [39] commented that the whole ship model gives a smooth representation of the manoeuvring forces but has no physical meaning. The whole ship model is more suitable to obtain the overall performance of a manoeuvring ship through free-running tests or system identification methods while the modular model can better express the effects and interactions of each component. Quadvlieg [228] indicated that a modular model is desired to describe the manoeuvring behaviours of inland vessels. In order to analyse the rudder impacts on inland vessel manoeuvrability, this thesis utilises the modular model to perform manoeuvring simulations.

5.1.3. Challenges of the multiple-propeller multiple-rudder model

Seagoing ships are commonly equipped with a single propeller and a single rudder while inland vessels more frequently feature multiple propellers and multiple rudders, particular twin propellers and twin rudders. Furthermore, TPTR ships are preferred in shallow water owing to its superiority manoeuvring performance [134]. Yoshimura and Sakurai [314] showed that a wide-width TPTR ship may have an improved turning ability in shallow water instead of a customarily worsened one for conventional SPSR ships. In general, TPTR vessels are appropriate for ships in shallow water, for instance, inland vessels, and large ships that require extra power and manoeuvrability, as an example, large seagoing container ships.

The interactions among multiple propellers and multiple rudders should be considered in manoeuvring performance analysis. Khanfir et al. [134] noted that TPTR ships are normally wider than single-propeller single-rudder (SPSR) ships. These features, i.e. wide and blunt, are quite typical for inland vessels and may lead to significantly different manoeuvring characteristics from seagoing ships. Previous studies have revealed the lack of experimental or theoretical research for multiple-propeller and multiple-rudder (MPMR) ships, including TPTR ships [77, 132, 165, 314].

Besides studies on the mathematical modelling of MPMR ships [51, 87, 91, 132, 167, 314], several attempts have been made to model the interaction between the hull and the rudder [134], the interaction between the propeller and the rudder [215], and the flow straightening effect of the hull and the propeller on the rudder [205]. A number of studies have been published on the asymmetric manoeuvring behaviour of MPMR ships [43, 54, 125]. Modelling of the single-propeller twin-rudder system is a challenge as the inflow to the rudders is strongly dependent on the propeller action, the ship motion, and the twin-rudder interactions [60, 124]. Thus far, the rudder conflagrations have not been given great attention.

5.2. Reference ships

As previously discussed in Chapter 2, ship particulars and rudder configurations affect ship manoeuvrability and thus influence the choices that are made in the development of the manoeuvring model. This section introduces the applied reference ships. These ships

are the single-propeller single-rudder (SPSR S1) seagoing KVLCC2 tanker, the single-propeller twin-rudder (SPTR R1) and twin-propeller quadruple-rudder (TPQR R2) standard inland vessels on the Rhine River, and the twin-propeller twin-rudder 6700 t bulk carrier (TPTR Y1) and 3500 t tanker (TPTR Y2) from the Yangtze River. Ship particulars and experimental results of the inland vessels are provided by Maritime Research Institute Netherlands (MARIN) [229] and Wuhan Rules and Research Institute, China Classification Society (CCS).

Table 5.1 presents the full-scale particulars of the reference ships. Main particular ratios of the two reference inland vessels from the Yangtze estuary (TPTR Y1 and TPTR Y2) are different from those of the European inland vessels (SPTR R1 and TPQR R2) and common seagoing ships (SPSR S1). Furthermore, the water depth to the ship draught ratio (H/T) of the Yangtze River, especially in the downstream, is commonly much larger than that of the European waterways where H/T is typically around 1.4. Therefore, shallow-water effects are neglected for the reference Yangtze inland vessels while they might be important for European inland vessels.

Table 5.1: Full-scale particulars of the reference ships.

Ship model	SPSR S1	TPTR Y1	TPTR Y2	SPTR R1	TPQR R2
Kind of ship	KVLCC2 tanker	Inland bulk carrier	Inland tanker	Inland tanker	Inland tanker
Environment	Sea	Yangtze River	Yangtze River	Rhine River	Rhine River
Scale	45.71	24.27	22.82	18.00	18.00
V (ms^{-1})	7.97	5.00	5.00	4.47	4.47
L (m)	320.0	107.5	94.6	110.0	110.0
B (m)	58.0	19.2	17.2	11.4	11.4
T (m)	20.8	4.2	4.2	3.5	3.5
S_H (m)	27194	2784.30	2209.30	1866.11	1857.49
∇ (m)	312622	7561.70	5844.82	3876.09	3862.22
C_b (-)	0.8098	0.867	0.855	0.883	0.880
C_m (-)	0.9980	0.999	0.999	0.999	0.999
C_p (-)	0.8120	0.868	0.856	0.884	0.881
D_P (m)	0.71	2.50	2.35	1.80	1.80
P_P/D_P (-)	0.71	0.75	0.68	1.00	1.00
n_P (-)	1	2	2	1	2
n_R (-)	1	2	2	2	4
C_R (m)	0.71	3.05	2.60	1.80	1.80
A_R (m)	115.04	10.51	6.76	3.51	3.51
Λ_G (-)	1.83	1.13	1.00	1.08	1.08
y_{TR}/C_R (-)	-	3.8	4.0	0.89	0.92
y_{TU}/C_R (-)	-	-	-	-	1.75
Rudder profile	NACA 0018	NACA 0015	NACA 0015	Fishtail	Fishtail
Rudder end plate	No	Yes	No	Yes	Yes

Free-running test data of TPTR Y1 and TPTR Y2 are provided by Wuhan Rules and Research Institute, China Classification Society (CCS) to validate the inland vessel manoeuvring model. These two reference ships are different in the hull form and the rudder configuration. TPTR Y1 fits a bulbous bow and a slender stern while TPTR Y2 features a normal bow and a blunt stern. In general, a bulbous bow reduces wave-making resistance over a narrow range of speed and draught, which results in a higher speed for the same power or a lower power for the same speed.

Most of the previous studies focused on the impacts of the bulbous bow on powering while very few studies mentioned its impacts on ship manoeuvrability. Compared to the particulars of TPTR Y1 (a bulbous bow, a slender stern, and rudders without end plates), the features of TPTR Y2 (a normal bow, a blunt stern, and rudders with end plates) are more typical for ships from the Yangtze River. Additionally, inland vessels in Europe are more similar to the arrangements of TPTR Y2 than TPTR Y1.

Regarding the rudder configuration, both vessels equip twin spade type NACA 0015 rudders. However, the rudders of TPTR Y1 have top and bottom end plates while those of TPTR Y2 do not have end plates. The end plates are commonly applied on inland vessels to improve the effective aspect ratios of the rudders and, further, improve the ship manoeuvring performance. Figure 5.1 shows the rudder profile and the end plates.

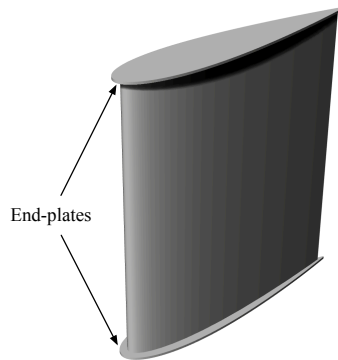


Figure 5.1: The NACA 0015 profile and the end plates of the 6700 t bulk carrier (TPTR Y1).

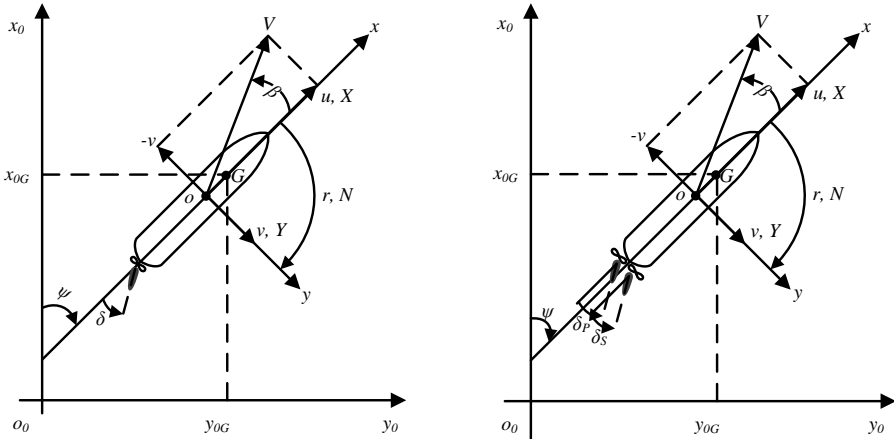
5.3. Mathematical models of ship motions

5.3.1. Coordinate systems

To formulate the mathematical description of ship motions, coordinate systems should be established first. Two right-handed frames of axes are applied in bidirectional earth-fixed and body-fixed coordinate systems. The origin of the earth-fixed coordinate system is commonly located at the start point of the manoeuvring simulation while the origin of the body-fixed coordinate system is set on midship or at the centre of gravity. As highlighted by Yasukawa and Yoshimura [304], midship is more convenient than the centre of gravity considering shipload conditions and thus applied as the origin of the body-fixed coordinate system in this thesis.

Figure 5.2 illustrates the static earth-fixed ($o_0-x_0y_0z_0$) and the dynamic body-fixed ($o-xyz$) coordinate systems for SPSR and TPTR ships as examples. The origin of $o-xyz$ locates on midship. x , y , and z axes are positive to the bow of the ship, the starboard of the ship, and downwards of the water surface respectively. The ship position is determined by the centre of gravity (G) of the ship in $o_0-x_0y_0z_0$, which is $(x_G, 0, 0)$ in $o-xyz$ for the applied three-dimensional model.

If not specified, parameters are defined on midship. Subscript G denotes variables at



(a) Single-propeller single-rudder coordinate systems. (b) Twin-propeller twin-rudder coordinate systems.

Figure 5.2: Earth-fixed and body-fixed coordinate systems.

5

the centre of gravity. Assuming the ship presented in Figure 5.2 is manoeuvring at forward speed (u) and lateral speed (v), the advance speed is $V = \sqrt{u^2 + v^2}$. The heading angle (ψ), longitudinal speed ($u_G = u$), and horizontal speed ($v_G = v + x_G r$) express the ship motion state in $o_0 - x_0 y_0 z_0$. The ship is turning with a rudder angle (δ) at yaw rate ($r = \dot{\psi}$) with a drift angle ($\beta = \arctan(-v/u)$).

In this thesis, prime symbols stand for non-dimensional parameters. Linear velocity (u, v), angular velocity (r), force (X, Y), moment (N), mass (m, m_x, m_y), and moment of inertia (I_z, J_z) are non-dimensionalised as follows:

$$\left. \begin{aligned} u', v' &= \frac{u}{V}, \frac{v}{V} \\ r' &= \frac{rL}{V} \\ X', Y' &= \frac{X}{0.5\rho LTV^2}, \frac{Y}{0.5\rho LTV^2} \\ N' &= \frac{N}{0.5\rho L^2TV^2} \\ m', m'_x, m'_y &= \frac{m}{0.5\rho L^2T}, \frac{m_x}{0.5\rho L^2T}, \frac{m_y}{0.5\rho L^2T} \\ I'_z, J'_z &= \frac{I_z}{0.5\rho L^4T}, \frac{J_z}{0.5\rho L^4T} \end{aligned} \right\} \quad (5.3)$$

where ρ is the water density, L is the ship length between perpendiculars, and T is the ship draught.

5.3.2. Dynamic equations

Dynamic equations for ships with different numbers of propellers and rudders are not that different. Yasukawa and Yoshimura [304] presented a standard MMG model for the KVLCC2 ship. Most of the previous studies on TPTR ship manoeuvrability used similar

modular type MMG models [22, 123, 134, 144, 165, 314], which proves the usability of the MMG model for manoeuvring prediction of TPTR ships in both shallow and deep water by means of adding dynamic characteristics [314]. Owing to different simplifications of the added mass and the location of the body-fixed coordinate system (COG or midship), the equations of motion are not entirely the same in the above-mentioned literature.

According to Yasukawa and Yoshimura [304], this thesis uses a general format of dynamic equations for all the reference ships as follows:

$$\left. \begin{aligned} (m + m_x)\dot{u} - (m + m_y)vr - x_Gmr^2 &= X_H + \sum_{i=1}^{n_P} X_P^i + \sum_{j=1}^{n_R} X_R^j \\ (m + m_y)\dot{v} + (m + m_x)ur + x_Gm\dot{r} &= Y_H + \sum_{i=1}^{n_P} Y_P^i + \sum_{j=1}^{n_R} Y_R^j \\ (I_z + x_G^2m + J_z)\dot{r} + x_Gm(\dot{v} + ur) &= N_H + \sum_{i=1}^{n_P} N_P^i + \sum_{j=1}^{n_R} N_R^j \end{aligned} \right\} \quad (5.4)$$

where the subscripts H, P, R indicate the hull, the propeller, and the rudder, the superscripts i and j refers to each propeller and each rudder respectively, n_P and n_R are the numbers of propellers and rudders respectively, m, m_x, m_y are the ship mass, the added mass in x -direction, and the added mass in y -direction, I_z and J_z are the moment of inertia and the added moment of inertia around the z -axis, u and v are ship forward and lateral speeds, r is ship yaw rate around midship, and the dot notation of u, v , and r denotes the derivative of each parameter. In Equation 5.4, the interactions among the hull, the propeller, and the rudder are not explicitly expressed but included in the calculation of the forces induced by the propeller and the rudder.

5.4. (Added) mass and (added) moment of inertia

5.4.1. Mass and moment of inertia

Ship mass (m) and moment of inertia (I_z) depend on the ship main particulars. Routinely, m is calculated as the following:

$$m = \rho \nabla, \quad (5.5)$$

where ∇ is the ship displacement volume. An estimation of the radius of gyration (i_z) is needed for I_z . Motora [210] estimated I_z as the follows:

$$\left. \begin{aligned} i_z &= 0.2536L \\ I_z &= mi_z^2 \end{aligned} \right\} \quad (5.6)$$

which is widely used in current manoeuvring studies. Since i_z is not very sensitive to the ship type, the Motora [210] method is taken for all the following manoeuvring simulations.

5.4.2. Added mass and added moment of inertia

According to Hooft and Nienhuis [108], the added mass (m_x and m_y) and moment (J_z) can be accurately estimated with the charts given by Motora [210, 211, 212]. Based on these charts, Zhou et al. [317] made regression formulas as follows:

$$\left. \begin{aligned} \frac{m_x}{m} &= \frac{1}{100} \left[0.398 + 11.97C_b \left(1 + 3.73 \frac{T}{B}\right) + 2.89C_b \frac{L}{B} \left(1 + 1.13 \frac{T}{B}\right) \right. \\ &\quad \left. + 0.175C_b \left(\frac{L}{B}\right)^2 \left(1 + 0.54 \frac{T}{B}\right) - 1.107 \frac{L}{B} \frac{T}{B} \right] \\ \frac{m_y}{m} &= 0.882 - 0.54C_b \left(1 - 1.6 \frac{T}{B}\right) - 0.156 \left(1 - 0.673C_b\right) \frac{L}{B} \\ &\quad + 0.826 \frac{T}{B} \frac{L}{B} \left(1 - 0.678 \frac{T}{B}\right) - 0.638C_b \frac{T}{B} \frac{L}{B} \left(1 - 0.669 \frac{T}{B}\right) \\ j_z &= \frac{L}{100} \left[33 - 76.85C_b \left(1 - 0.784C_b\right) + 3.43 \frac{L}{B} \left(1 - 0.63C_b\right) \right] \\ J_z &= m j_z^2. \end{aligned} \right\} \quad (5.7)$$

Originally for seagoing ships, Clarke et al. [40] proposed regression formulas based on Planar Motion Mechanism (PMM) tests for m'_y and J'_z as follows:

$$\left. \begin{aligned} m'_y &= \frac{\pi T}{L} \left[1 + 0.16C_b \frac{B}{T} - 0.51 \left(\frac{B}{L}\right)^2 \right] \\ J'_z &= \frac{\pi T}{L} \left[\frac{1}{12} + 0.017C_b \frac{B}{T} - 0.51 \left(\frac{B}{L}\right)^2 \right]. \end{aligned} \right\} \quad (5.8)$$

Compared to m , m_x is relatively small and Clarke et al. [40] approximated m_x as 3% to 6% of m . The Zhou et al. [317] method and the Clarke et al. [40] method give comparable results. In this thesis, the Zhou et al. [317] method is chosen as it is based on widely used Motora [210, 211, 212] charts.

5.5. Hull forces and moments

The hull induces longitudinal force (X_H), lateral force (Y_H), and yaw moment (N_H), which are commonly expressed in linear or non-linear functions of dimensional or non-dimensional dynamic parameters of the ship, such as u , \dot{u} , v , \dot{v} , r , \dot{r} , and β . The coefficients of such functions are the so-called hydrodynamic derivatives. Traditionally, these derivatives are derived from series of model tests [134, 304]. Fast developments in CFD methods enable the approach of testing model-scale or full-scale ships in a numerical basin [22, 25, 29, 94, 140, 273]. Experimental and numerical tests are expensive in money and time, therefore, commonly not available at the initial design stage.

The longitudinal component of the hull force (X_H) commonly refers to the resistance of the bare hull. X_H can be described as the component due to the straight moving ($X_H(u)$)

and the component due to manoeuvring ($X_H(v', r')$ or $X_H(\beta, r')$). $X_H(u)$ can be obtained through model tests or estimated by the widely used Holtrop and Mennen method [104]. For simplicity or due to lack of data in the initial design stage, $X_H(v', r')$ or $X_H(\beta, r')$ can be neglected [38, 227]. In this thesis, the Holtrop [104] method is used for $X_H(u)$.

Commonly, hydrodynamic coefficients obtained from model tests are used to express $X_H(v', r')$ or $X_H(\beta, r')$ [76, 138, 194, 304]. For initial design, empirical methods are easier and cheaper than experimental methods to apply for quick manoeuvrability prediction. Yoshimura and Ma [312], Kang and Hasegawa [123], and Yoshimura and Masumoto [313] proposed regression formulas for the hydrodynamic coefficients in the expression of $X_H(\beta, r')$. Ankudinov and Jakobsen [9] provided regression formulas to estimate $X_H(v', r')$. With or without $X_H(v', r')$ or $X_H(\beta, r')$, 5 methods for X_H are compared as listed in Table 5.2.

Table 5.2: Compared methods for the hull induced longitudinal force (X_H).

Case	Method for $X_H(u)$	Method for $X_H(\beta, r')$ or $X_H(v', r')$
No. 1	Holtrop [104]	Neglect $X_H(\beta, r')$ or $X_H(v', r')$
No. 2	Holtrop [104]	Yoshimura and Ma [312] for $X_H(\beta, r')$
No. 3	Holtrop [104]	Ankudinov and Jakobsen [9] for $X_H(v', r')$
No. 4	Holtrop [104]	Kang and Hasegawa [123] for $X_H(\beta, r')$
No. 5	Holtrop [104]	Yoshimura and Masumoto [313] for $X_H(\beta, r')$

According to Yoshimura and Sakurai [314], the hydrodynamic derivatives of the hull, the propeller, and the rudder of a TPTR ship are not much different from those of an SPSR ship. Therefore, the existing regression formulas which were developed based on SPSR ships, including, but not limited to, Kijima et al. [138], Matsunaga [194], China Classification Society [38], Kijima and Nakiri [135], Kang and Hasegawa [123], Furukawa et al. [76], and Yoshimura and Masumoto [313], are still applicable for TPTR ships. In this thesis, 8 methods are compared for Y_H and N_H as listed in Table 5.3.

Table 5.3: Compared methods for the hull induced lateral force and yaw moment (Y_H and N_H).

Case	Method for Y_H and N_H
No. 1	Kijima et al. [138]
No. 2	Matsunaga [194]
No. 3	Yoshimura and Ma [312]
No. 4	China Classification Society [38]
No. 5	Kijima and Nakiri [135]
No. 6	Kang and Hasegawa [123]
No. 7	Furukawa et al. [76]
No. 8	Yoshimura and Masumoto [313]

To properly use the empirical methods for hull forces and moments, the applicable ranges of the ship main particulars, such as L/B , B/T , L/T , and C_b should be inspected as most of the empirical formulas are originally formulated based on databases of seagoing ships. Moreover, the dynamic parameters, such as the ship speed (V), the yaw rate (r'), and the drift angle (β) should also be examined.

Table 5.4 lists the static parameters of the reference inland vessels and the applicable ranges of the above-mentioned regression formulas. None of the listed 8 methods perfectly covers the reference inland vessels. In general, the applicable range of the Kijima et al. [138] method, the Matsunaga [194] method, the Furukawa et al. [76], and the Kang and Hasegawa [123] method fit better than the other methods.

Table 5.4: Parameter ranges of the reference ships and the existing regression formulas.

Ship model	L/B	B/T	L/T	C_b
SPSR S1	5.99	2.57	15.38	0.81
TPTR Y1	5.59	4.57	25.64	0.87
TPTR Y2	5.50	4.10	22.53	0.87
SPTR R1	9.65	3.26	31.43	0.88
TPQR R2	9.65	3.26	31.43	0.88
Method	L/B	B/T	L/T	C_b
Kijima et al. [138]	4.51 to 6.89	2.38 to 4.09	13.66 to 25	0.52 to 0.84
Matsunaga [194]	4.51 to 6.89	2.38 to 4.09	13.66 to 25	0.52 to 0.84
Yoshimura and Ma [312]	2.60 to 5.20	2.17 to 2.70	5.65 to 14.05	0.57 to 0.66
China Classification Society [38]	5.71 to 16.67	3.5 to 6.0	20 to 100	-
Kijima and Nakiri [135]	2.60 to 5.20	2.17 to 2.70	5.65 to 14.05	0.57 to 0.66
Kang and Hasegawa [123]	5.00 to 6.13	2.43 to 3.31	13.70 to 18.18	0.78 to 0.83
Furukawa et al. [76]	4.51 to 6.89	2.38 to 4.09	13.66 to 25	0.52 to 0.84
Yoshimura and Masumoto [313]	2.60 to 7.10	2.17 to 4.00	5.65 to 28.40	0.51 to 0.65

Section 5.5 has discussed the available regression methods for the hull forces and moments. Currently, all the regression formulas are made from databases of seagoing ships. No method has been specially generated for inland vessels. Furthermore, the parameter ranges of the reviewed methods do not fit the reference inland vessels as shown in Table 5.4. Table 5.2 and Table 5.3 list the compared 5 methods for X_H and 8 methods for Y_H and N_H . 40 combinations of these methods are made and tested to find the most suitable regression methods for the reference inland vessels. Comparing simulation results of each method to free-running tests, a final selection is made in Section 5.8.

5.6. Propeller forces and moments

Section 5.6 presents the calculation procedures of the forces and moments induced by each propeller (X_p^i , Y_p^i , and N_p^i), which are expressed as the following:

$$\left. \begin{aligned} X_p^i &= (1 - t_p^i) T_p^i \\ Y_p^i &= 0 \\ N_p^i &= -y_p^i (1 - t_p^i) T_p^i \end{aligned} \right\} \quad (5.9)$$

where t_p is the propeller thrust deduction in manoeuvring motions, T_p is the propeller thrust, and y_p is the relative position of the propeller to the centreline of the ship. According to Toxopeus [273, p. 30], the transverse force caused by a propeller rotating in an asymmetrical wake is relatively small and difficult to describe by the existing empirical formulas.

Therefore, the propeller induced side force (Y_p^i) and its contribution to the propeller yaw moment (N_p^i) are assumed to be zero.

Following Equation 5.9, the propeller thrust (T_p) is expressed as follows:

$$T_p^i = \rho (n^i)^2 (D_p^i)^4 K_T^i, \quad (5.10)$$

where n is the propeller revolution rate, D_p is the propeller diameter, and K_T is the propeller thrust coefficient. As the reference ships with multiple propellers have identical propellers rotating at the same constant number of revolutions per second, for simplicity in the following text, $n = n^i$ and $D_p = D_p^i$.

Using a usual format, K_T is calculated by second order polynomials of the propeller advance ratio (J_p) as:

$$K_T^i = k_2^i (J_p^i)^2 + k_1^i J_p^i + k_0^i, \quad (5.11)$$

where k_2 , k_1 , and k_0 are propeller open water characteristics in the representation of K_T . Additionally, these open water characteristics can be assumed to be constant against the water depth [314]. Furthermore, J_p is expressed as:

$$J_p^i = \frac{u(1 - w_p^i)}{nD_p}, \quad (5.12)$$

where w_p is the wake fraction at the propeller position in manoeuvring. Thus far, to resolve Equation 5.9, the question becomes how to get the wake fraction (Section 5.6.1) and the propeller thrust deduction factor (Section 5.6.2) during manoeuvring motions.

5.6.1. Propeller wake fraction

Lee et al. [165] concluded that the propeller's effective wake ($1 - w_p$) during manoeuvring and the flow straightening coefficient of the rudder in port and starboard turning of the ship are the unique parameters of TPTR ships. w_p^P and w_p^S may be different during manoeuvring motions, but it is assumed that $w_p = w_p^i$ here due to lack of information. The wake fraction in manoeuvring motions (w_p) is commonly estimated based on the wake fraction in straight moving (w_{p_0}) or simply assumed to be a constant that is identical to w_{p_0} .

For inland vessels, Kulczyk [154] indicated that for a centre line single propeller with single rudder $w_{p_0} \approx 0.235$ while for twin propellers with a single rudder behind each propeller $w_{p_0} \approx 0.32$. Harvald [90] proposed regression formulas for the wake fraction and the thrust deduction factor. Kristensen and Lützen [153] indicated that the Harvald [90] method may overestimate these values. Accordingly, Kristensen and Lützen [153] derived corrections based on the Harvald [90] method for tankers and bulk carriers. In this thesis, the Kulczyk [154] method is chosen as it is determined based on a database of inland vessels.

The wake fraction during manoeuvring motions (w_p) is complicated and related to the drift angle, the yaw rate, the shape of the stern, the direction of the propeller rotation, and the propeller working load [314]. Kang et al. [124] concluded that the rudder type (single-rudder or twin-rudder) has little influence on w_{p_0} and w_p for a single-propeller ship. w_p can be estimated based on w_{p_0} considering the geometrical inflow angle to the propeller in

manoeuvring (β_P). β_P is defined as the following:

$$\beta_P^i = \beta - \frac{x_P^i}{L} r', \quad (5.13)$$

where x_P is longitudinal position of the propeller. Since $x_P = x_P^i$ for the reference inland vessels, $\beta_P = \beta_P^i$.

Lee et al. [165] showed that $1 - w_P$ of an SPSR ship changes systematically with β_P and reaches a minimum around $\beta_P = 0$. However, $1 - w_P$ of a TPTR ship shows a greatly asymmetric trend with the change of β_P . Hirano [97] expressed the relationship of w_P and w_{P_0} as:

$$\frac{w_P}{w_{P_0}} = \exp(-4\beta_P^2). \quad (5.14)$$

Furthermore, Matsumoto and Sueteru [193] described the relationship of the effective wake fraction $(1 - w_P)/(1 - w_{P_0})$ as the following:

$$\frac{1 - w_P}{1 - w_{P_0}} = 1 + (1 - \cos^2 \beta_P)(1 - |\beta_P|). \quad (5.15)$$

The above-mentioned methods are built up originally for SPSR ships. For simplicity, Yoshimura and Sakurai [314] assumed that $1 - w_P = 1 - w_{P_0}$ for each propeller of a TPTR ship. Kang et al. [124] described the procedure to obtain t_{P_0} , t_P , w_{P_0} , and w_P for an SPTR ship through model tests. This procedure is also usable for TPTR ships but the model tests at initial stage may not be possible. This thesis takes Equation 5.14 as it is recommended by China Classification Society [38].

5.6.2. Propeller thrust deduction factor

A propeller may have different deduction factors in straight moving (t_{P_0}) and manoeuvring motions (t_P). Commonly, t_P is not significantly different from t_{P_0} for SPSR ships and presumed to be a constant [304]. According to Kulczyk [154], for a centre line single propeller with a single rudder $t_{P_0} \approx 0.27$ while for a twin-propeller ship with a single rudder behind each propeller $t_{P_0} \approx 0.2$. Lee et al. [165] showed that t_P of a TPTR ship is similar to that of a SPSR ship. Kang et al. [124] reported that the variation from t_{P_0} to t_P for SPTR ships appeared to be significant in the tested cases. However, additional tests on other ship types are needed to confirm this difference [124].

In this thesis, the assumption of Yoshimura and Sakurai [314] is followed that $t_P = t_{P_0} = t_P^i$. Similar to the calculation of w_P , Kristensen and Lützen [153] indicated that the Harvald [90] method may overestimate t_P and suggested corrections for tankers and bulk carriers. According to Hollenbach [101], the Holtrop and Mennen [106, 107] method is more suitable for twin-screw ships than the Harvald [90] method. Additionally, the Holtrop and Mennen [106, 107] method gives a similar result to the Kulczyk [154] method for the reference ships. Again, the Kulczyk [154] method for t_P is taken as it is the only method that is formed based on inland vessels.

5.7. Rudder forces and moments

Di Mascio et al. [51] pointed out that the rudder forces and moments are very difficult to evaluate as they are strongly affected by the complex flow in the stern region. Commonly, the interactions between the rudders are not considered [314]. However, the hydrodynamic characteristics of each rudder in multiple-rudder configurations are different due to the rudder profiles and the interaction between the twin rudders. Gim [77] showed that the distance between the twin rudders plays an important role in generating the side force and concluded that the critical distance between the rudders should be less than one chord length reducing the turbulence flow and vortices.

Kang et al. [124] concluded that the impact factors on twin-rudder performance are the inflow angle to each rudder, the interactions between the twin rudders, and the decrement of the inflow to the twin rudders. Furthermore, Kang et al. [124] observed that the effective wake fraction, the rudder inflow velocity, and flow straightening factor for the twin rudders are asymmetric during manoeuvring. Kang et al. [125] investigated the inflow characteristics of each rudder on a single-propeller twin-rudder ship, showing that the inflow is not parallel to the ship centre line. This phenomenon leads to asymmetric manoeuvring characteristics, reducing ship manoeuvrability.

Taking the origin on midship, total rudder forces and moments of a TPTR ship (X_R^j , Y_R^j , and N_R^j) are expressed as the following:

$$\left. \begin{aligned} X_R^j &= -(1 - t_R^j)F_X^j \\ Y_R^j &= -(1 + a_H^j)F_Y^j \\ N_R^j &= -(x_R^j + a_H^j x_H^j)F_Y^j + y_R^j(1 - t_R^j)F_X^j \end{aligned} \right\} \quad (5.16)$$

where F_X and F_Y are rudder force components in longitudinal and lateral directions, t_R is the steering resistance deduction factor, a_H is the rudder force increase factor, x_H is the longitudinal coordinate of the acting point of the additional lateral force, x_R and y_R are the longitudinal and lateral positions of the rudder. The applied force and angle conventions are illustrated in Figure 5.3.

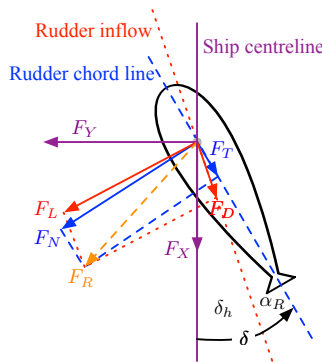


Figure 5.3: Rudder hydrodynamic force convention.

Section 5.7.1 introduces the method to calculate F_X and F_Y by lift and drag forces. Section 5.7.2 describes the applied rudder hydrodynamic coefficients based on the RANS results in Chapter 4. Section 5.7.3 computes the rudder inflow velocity components for the rudder force calculation. In the end, Section 5.7.4 discusses the applied values of the additional parameters, namely a_H , x_H , and t_R in Equation 5.16.

5.7.1. Rudder force components

The longitudinal and lateral components of the rudder force (F_X and F_Y) can either be calculated by the rudder normal and tangential forces (F_N and F_T) or by the rudder lift and drag forces (F_L and F_D). In this thesis, the rudder forces and moments are calculated by using the rudder lift and drag forces as follows:

$$\left. \begin{aligned} F_X^j &= F_L^j \sin \delta_h^j + F_D^j \cos \delta_h^j \\ F_Y^j &= F_L^j \cos \delta_h^j - F_D^j \sin \delta_h^j \end{aligned} \right\} \quad (5.17)$$

where δ_h^j is the hydrodynamic inflow angle of the rudder and expressed as:

$$\delta_h^j = \arctan\left(\frac{v_R^j}{u_R^j}\right), \quad (5.18)$$

where u_R^j and v_R^j are longitudinal and lateral components of the rudder inflow speed as $V_R^j = \sqrt{(u_R^j)^2 + (v_R^j)^2}$, which are discussed in Section 5.7.3.

The rudder hydrodynamic forces (F_L^j and F_D^j) are expressed as follows:

$$\left. \begin{aligned} F_L^j &= 0.5\rho A_R^j C_L^j (V_R^j)^2 \\ F_D^j &= 0.5\rho A_R^j C_D^j (V_R^j)^2 \end{aligned} \right\} \quad (5.19)$$

where C_N^j , C_T^j , C_L^j , and C_D^j are the rudder hydrodynamic coefficients. These coefficients are determined on the effective rudder angle (α_R), which is written as the following:

$$\alpha_R^j = \delta^j - \delta_h^j. \quad (5.20)$$

In this thesis, the general expressions for δ_h and α_R (Equation 5.18 and Equation 5.20) are taken, which were applied by Yoshimura and Ma [312], Yoshimura and Masumoto [313], and Yasukawa and Yoshimura [304] for SPSR ships, Kang et al. [124] for SPTR ships, and Yoshimura and Sakurai [314] for TPTR ships. Other expressions of α_R were described by Nagarajan et al. [213] and Khanfir et al. [134] for different ship types. These methods may improve the accuracy of the prediction but require additional parameters that may not be available at the initial design stage.

5.7.2. Rudder hydrodynamic coefficients

Instead of using the general empirical formulas to estimate the rudder force coefficients, this thesis uses RANS methods to obtain the lift and drag coefficients (C_L and C_D) of

various rudder configurations in Chapter 4. A general format of C_L and C_D for the presented manoeuvring model is written as follows:

$$\left. \begin{aligned} C_L &= k_P \left(\frac{\partial C_L^{2D}}{\partial \sin \alpha_R} \sin \alpha_R + C_{L_0}^{2D} \right) \frac{k_R \Lambda_G}{\Lambda_G + k_\Lambda} \\ C_D &= k_P \left(\frac{\partial C_D^{2D}}{\partial \sin \alpha_R} \sin \alpha_R + C_{D_0}^{2D} \right) \frac{k_R \Lambda_G}{\Lambda_G + k_\Lambda} \end{aligned} \right\} \quad (5.21)$$

where $\frac{\partial C_L^{2D}}{\partial \sin \alpha_R}$, $\frac{\partial C_D^{2D}}{\partial \sin \alpha_R}$, $C_{L_0}^{2D}$, and $C_{D_0}^{2D}$ are calculated with the new regression formulas that are proposed in Section 4.5, k_R is the impact factor of the rudder end plates, k_Λ is impact factor of the rudder aspect ratio, and k_P is the impact factor of the propeller slipstream,. These three impact factors are discussed in the following sections.

End plate effect

The rudders of the reference inland vessels (TPTR Y1, SPTR R1, and TPQR R2) are designed with top and bottom end plates. These end plates are configured to enlarge the effective aspect ratio of the rudder, therefore, improve the rudder effectiveness. To account the effect of the end plates on C_L and C_D , an additional amplify factor k_R is added in Equation 5.21. However, no exact value of k_R was found in the literature. In this thesis, k_R is assumed to be 1.3 based on model test experience.

Effective aspect ratio effect

The presented 2D simulations assume that the rudder has an infinite aspect ratio. As presented in Section 4.4, impacts in the aspect ratio increases the lift slope and reduces the induced drag. Thus, a larger span and aspect ratio is more efficient than a smaller aspect ratio. A large rudder aspect ratio might also achieve a good course keeping with a high lift curve and rapid response while a small rudder aspect ratio may enhance manoeuvring performance with a large stall angle [206, p. 64]. Based on the lifting line theory, k_Λ in Equation 5.21 should be 2. In this thesis, the empirical $k_\Lambda = 2.25$ is taken from the Fujii [72] method.

Propeller slipstream effect

Chapter 4 discussed the rudder hydrodynamics in 2D open water. In reality, ship rudders work in the propeller slipstream. Compared with the rudder working in free stream, Molland and Turnock [202, 203] demonstrated a significant increase in the stall angle when the rudder is working behind a rotating propeller. The propeller slipstream may also have impacts on the rudder hydrodynamic coefficients depending on the propeller working load, the propeller revolution rate, and the arrangement of the propeller and the rudder. These impacts of the propeller-rudder interactions should be accounted for in the calculation of the rudder forces and moments for manoeuvring simulations.

Rudder hydrodynamic characteristics tested in open water are different from those tested in the propeller slipstream. Oppenheim [224] found that the lift curve slope, the maximum lift coefficient, the stall angle, and the drag coefficient increase when the rudder is tested in the propeller slipstream. Kerwin et al. [130] compared the rudder hydrodynamics of a 20% flap rudder in propeller slipstream and in uniform flow indicating that the rudder lift curve slope is increased by about 25% and this increase is constant over the

tested range of longitudinal propeller locations. Nienhuis [216] performed tests for a rudder in open water or in propeller slipstream as compared in Figure 5.4.

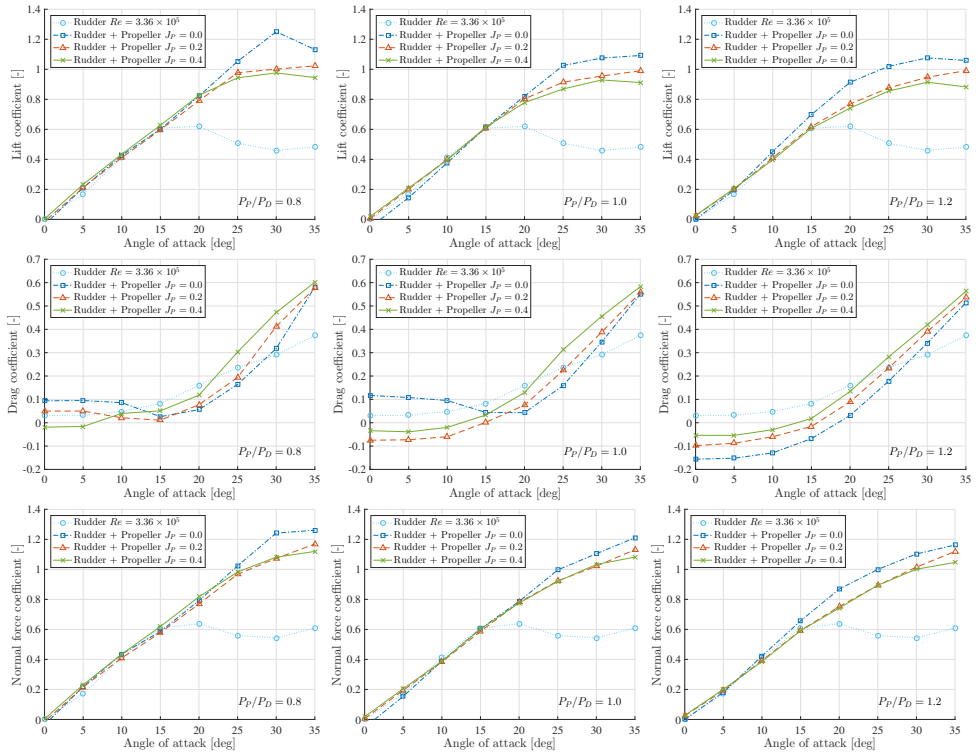


Figure 5.4: Hydrodynamic coefficients of a rudder in open water or in propeller slipstream. Data are adapted from Nienhuis [216].

As shown in Figure 5.4, the propeller slipstream extends the rudder stall angle from the range of 15° to 20° to the range of 30° to 35° . The changes in J_P and P_P/D_P on the lift coefficients are comparatively small to the influence on the drag coefficients. Moreover, as the drag coefficients are relatively small values compared to the lift coefficients, the impacts of these changes are not very significant on the normal force coefficients. According to these results, it is assumed that the effect of the propeller slipstream primarily extends the stall angle without significantly affect the slope of the rudder hydrodynamic coefficients. Therefore, the impact factor of the propeller on the lift and drag slopes (k_P in Equation 5.21) is assumed to be 1.0 in all the presented manoeuvring simulations.

5.7.3. Rudder inflow velocity components

Toxopeus [273, p. 30] concluded that the determination of the rudder inflow velocity and direction as a consequence of the drift angle (β), the yaw rate (r), and the propeller action is one of the most complicated aspects in determining the rudder forces and moments. The longitudinal and lateral inflow velocity components to each rudder (u_R and v_R) affect the amount of the lift and drag forces (Equation 5.19) and the effective rudder angle

(Equation 5.20).

Longitudinal component

According to Yoshimura and Sakurai [314], considering the relative position of the propeller (y_P) for multiple-propeller ships, u_R is expressed as:

$$u_R^j = (1 - w_R^j)(u - y_P^j r) \sqrt{\eta_R \left\{ 1 + \kappa_R \left[\sqrt{\left(1 + \frac{8K_T^i}{\pi(J^i)^2} \right)} - 1 \right] \right\}^2} + (1 - \eta_R), \quad (5.22)$$

where κ_R is a constant that can be 0.5 [304] or 0.55 [313]. Kang et al. [124] assumed that κ_R is the same for both single-rudder and twin-rudder systems as they both have a single propeller. In this thesis, κ_R is estimated by the Yoshimura and Ma [312] method, which considers the ship particulars, as the following:

$$\kappa_R = 0.55 - 0.8C_b \frac{B}{L}. \quad (5.23)$$

Additionally, w_R is the wake fraction at the position of the rudder, η_R is the ratio of the rudder area in the propeller slipstream (A_{RP}) to the area of the rudder movable area (A_R) and η_R is commonly estimated as:

$$\eta_R = \frac{A_{RP}}{A_R} \approx \frac{D_P}{B_R}. \quad (5.24)$$

Equation 5.24 is derived based on the assumption that the trailing edge of the rudder is always in the propeller slipstream. The effect of a part of the rudder that is out of propeller slipstream is not modelled and very little work is available in the literature. Quadvlieg [229] indicated that the rudders of inland vessels are always in the propeller slipstream, and this assumption is followed for the reference inland vessel.

The wake fraction at the position of the rudder during manoeuvring motions (w_R) is commonly estimated based on the wake fraction of the rudder in straight moving (w_{R_0}), the wake fraction at the position of the propeller in straight moving (w_{P_0}) and manoeuvring motions (w_P). According to Kijima et al. [138], w_R is expressed as the following:

$$w_R = w_{R_0} \frac{w_P}{w_{P_0}}. \quad (5.25)$$

Furukawa et al. [76] described w_R as the following:

$$w_R = \zeta_R w_{R_0} \exp \left[-4.0 \left(\beta + \frac{r'}{2} \right)^2 \right], \quad (5.26)$$

where ζ_R is an empirical coefficient and it is assumed to be 1.0 according to China Classification Society [38]. w_{R_0} can be estimated based on the wake fraction ratio (ϵ_R) as proposed by Kijima et al. [138],

$$\epsilon_R = \frac{1 - w_{R_0}}{1 - w_{P_0}} = -156.2 \left(C_b \frac{B}{L} \right)^2 + 41.6 \left(C_b \frac{B}{L} \right) - 1.76. \quad (5.27)$$

In this thesis, the Kijima et al. [138] method (Equation 5.27) is utilised to estimate ε_R for w_{R_0} and the Furukawa et al. [76] method (Equation 5.26) for w_R . These two methods are pure empirical methods and have been widely applied on in previous studies for different ship types. Therefore, they are selected for the present work.

Lateral component

According to Yoshimura and Sakurai [314], Yoshimura and Masumoto [313], and Yasukawa and Yoshimura [304] for TPTR ships and SPSR ships, the lateral component of the rudder inflow velocity (v_R) is written as:

$$v_R^j = \gamma_R^j \beta_R^j, \quad (5.28)$$

where γ_R is the flow straightening factor due to the lateral speed of the ship (v). β_R is the effective inflow angle to the rudder in manoeuvring and expressed as

$$\beta_R^j = \beta - \ell' r', \quad (5.29)$$

where $\ell' = \ell/L$ is the flow-straightening factor due to the yaw rate (r).

The flow straightening coefficient (γ_R) affects the inflow angle to the rudder the further influences the rudder induced forces and moments. Through wind-tunnel tests, Molland and Turnock [205] found that flow straightening effects depend on the type of upstream body, drift angles, and propeller thrust loading. Kang et al. [124] showed that γ_R depends on the effective rudder angle and the drift angle.

Kim et al. [144] indicated that the twin rudders have different inflow angles during manoeuvring. The lee side rudder has larger flow straightening effects than the upwind side rudder. Meanwhile, the flow straightening coefficient γ_R for TPTR ship is smaller to that for the SPSR ship. For SPSR and TPTR ships, γ_R may be slightly asymmetric for port and starboard manoeuvres [124, 134, 165] while for SPTR ships, these asymmetric phenomena become significant [134].

After reviewing the above-mentioned literature, it is assumed that γ_R for SPSR and MPMR ships are similar and not significantly different for port and starboard manoeuvres. For SPSR ships, Kijima et al. [138] proposed such a formula:

$$\gamma_R = -22.2 \left(C_b \frac{B}{L} \right)^2 + 0.02 \left(C_b \frac{B}{L} \right) + 0.68. \quad (5.30)$$

For merchant ships and fishing vessels, Yoshimura and Masumoto [313] proposed:

$$\gamma_R = 2.06 C_b \frac{B}{L} + 0.14. \quad (5.31)$$

According to the experimental results from Yoshimura and Ma [312], Yoshimura and Masumoto [313], and Yasukawa and Yoshimura [304], the possible range of γ_r is 0.4 to 0.6. Therefore, the Kijima et al. [138] method and the Ankudinov et al. [8] method may underestimate γ_R for the reference inland vessel. In this thesis, the Yoshimura and Masumoto [313] method is taken for γ_R as its prediction lies in the reasonable range of values.

Yasukawa and Yoshimura [304] described ℓ as an experimental constant from captive model tests. Kijima et al. [138] expressed $\beta_R = \beta - 2x'_R r'$ and thus $\ell' = 2x'_R \approx -1.0$ in general. Yoshimura and Ma [312] expressed ℓ' as the following:

$$\ell' = 1.7C_b \frac{B}{L} - 1.2. \quad (5.32)$$

For fishing vessels and merchant ships, Yoshimura and Masumoto [313] indicated that $\ell' = -0.90$. Through trial and error, it is found that the manoeuvring performance of the reference inland vessel is not very sensitive to ℓ' . The formula proposed by Yoshimura and Ma [312] is chosen in this thesis as it takes the main particulars of the ship into account.

5.7.4. Additional parameters

In the following paragraphs, additional parameters in Equation 5.16, namely the steering resistance deduction factor (t_R), the rudder force increase factor (a_H), and the longitudinal coordinate of the acting point of the additional lateral force (x_H), are discussed respectively.

Steering resistance deduction factor

According to Matsumoto and Sueteru [193] and Kijima et al. [138], for SPSR ships in deep water, the rudder steering resistance deduction (t_R) can be estimated as the following:

$$t_R = -0.28C_b + 0.45. \quad (5.33)$$

Koh and Yasukawa [146] indicated that the influence of B/T and y_P on t_R is not significant. Furthermore, Yoshimura [309] concluded that the variation of t_R with the change of water depth is negligible. Thus, Equation 5.33 is taken for t_R in this thesis. Additionally, it is assumed that $t_R = t_R^j$.

Rudder force increase factor

Based on the model tests carried out by Kose et al. [150], Yasukawa and Yoshimura [304] indicates the rudder force increase factor (a_H) has a common magnitude of 0.3 to 0.4, which means that the lateral force acting on the ship by steering increases about 30 % to 40 % larger than the rudder normal force component. According to Kijima et al. [138], a regression formula of a_H for SPSR seagoing ships in deep water is made as the following:

$$a_H = 2.0802C_b^2 - 0.6124C_b - 0.0569. \quad (5.34)$$

For inland vessels, Quadvlieg [229] proposed:

$$a_H = 0.627C_b - 0.153. \quad (5.35)$$

For fishing vessels and merchant ships, Yoshimura and Masumoto [313] calculated a_H as the following:

$$a_H = 3.6C_b \frac{B}{L}. \quad (5.36)$$

As shown by Khanfir et al. [134], a_H is dependent on B/T , C_b , and y_P while a_H may be changed significantly by the arrangement of the propellers and rudders. However, little

information was found. From literature [213, 304] and experience, a reasonable value of a_H should be around 0.4. In the presented simulations, the Quadvlieg [229] method is taken for a_H as it is the only method that is intended for inland vessels.

Longitudinal coordinate of the acting point of the additional lateral force

As stated by Khanfir et al. [132], the non-dimensional longitudinal coordinate of the acting point of the additional lateral force (x'_H), where $x'_H = x_H/L$, has a general value of -0.40. Furthermore, Khanfir et al. [134] indicated that x'_H has an almost constant value of -0.37, which is not significantly affected by B/T , C_b , and y_P . Therefore, it is reasonable to assume x_H is not much different for seagoing ships and inland vessels. As specified by Eloot [58], x'_H moves towards midships with decreasing under keel clearance leading to reduced turning ability in shallow water.

According to Kijima et al. [138], a regression formula for x'_H is made as the following:

$$x'_H = 9.5727C_b^2 - 8.0704C_b - 0.0618. \quad (5.37)$$

Lee and Shin [166] proposed formulas of x'_H for low-speed blunt ships with stern bulb and horn type rudders. After neglecting the terms that concern the stern bulb, the Lee and Shin [166] equation becomes:

$$x'_H = -6.054 + 58.18 \frac{B}{L} - 148.44 \left(\frac{B}{L} \right)^2. \quad (5.38)$$

In this thesis, the Lee and Shin [166] is selected to estimate x'_H as it concerns the ship main particulars.

5.8. Selection of the methods for hull forces and moments

Through reviewing the existing methods for the manoeuvring parameters, the pre-selected methods for the reference inland vessels are summarised in Table 5.5. These methods are first used to select the most suitable method for the hull forces and moments in Section 5.8 and then utilised for the manoeuvring validation of the reference inland vessels in Section 5.9. Table 5.2 and Table 5.3 list the tested methods for the longitudinal and lateral hull forces and moments. In total, 40 combinations of the methods for X_H , Y_H , and N_H are compared against free-running tests based on the reference 6700 t bulk carrier (TPTR Y1) and the 6700 t tanker (TPTR Y2).

To compare the performance of each combination, the average absolute deviation of the simulated turning criteria (σ_T) is calculated as the following:

$$\sigma_T = 100\% \times \sum_{i=1}^{n_T} \left(\left| \frac{A_D^{Sim} - A_D^{Exp}}{A_D^{Exp}} \right| + \left| \frac{T_D^{Sim} - T_D^{Exp}}{T_D^{Exp}} \right| + \left| \frac{V_C^{Sim} - V_C^{Exp}}{V_C^{Exp}} \right| + \left| \frac{r_C^{Sim} - r_C^{Exp}}{r_C^{Exp}} \right| \right) / 24, \quad (5.39)$$

where A_D is the advance, T_D is the transfer, V_C is the speed in steady turn, r_C is the yaw rate in steady turn, and n_T is the number of the performed turning manoeuvres. The superscripts 'Sim' and 'Exp' stand for 'Simulation' and 'Experiment'. Furthermore, the average

Table 5.5: Applied methods for the reference inland vessels.

Parameter	Method	Equation
I'_z	Motora [210]	Equation 5.6
$m'_x, m'_y,$ and J'_z	Zhou et al. [317]	Equation 5.7
w_{P_0}	Kulczyk [154]	Constant
w_P	Hirano [97]	Equation 5.14
t_P	Kulczyk [154]	Constant
u_R	Yoshimura and Sakurai [314]	Equation 5.22
$kappa_R$	Yoshimura and Ma [312]	Equation 5.23
w_{R_0}	Kijima et al. [138]	Equation 5.27
w_R	Furukawa et al. [76]	Equation 5.26
v_R	Yasukawa and Yoshimura [304]	Equation 5.28
γ_R	Yoshimura and Masumoto [313]	Equation 5.31
ℓ'	Yoshimura and Ma [312]	Equation 5.32
t_R	Kijima et al. [138]	Equation 5.33
a_H	Quadvlieg [229]	Equation 5.35
x'_H	Lee and Shin [166]	Equation 5.38
C_L and C_D	Section 5.7.2	Equation 5.21

absolute deviation of the simulated zigzag criteria (σ_Z) is written as:

$$\sigma_Z = 100\% \times \sum_{i=1}^{n_Z} \left(\left| \frac{\psi_{O1}^{Sim} - \psi_{O1}^{Exp}}{\psi_{O1}^{Exp}} \right| + \left| \frac{\psi_{O2}^{Sim} - \psi_{O2}^{Exp}}{\psi_{O2}^{Exp}} \right| + \left| \frac{t_{O1}^{Sim} - t_{O1}^{Exp}}{t_{O1}^{Exp}} \right| + \left| \frac{t_{O2}^{Sim} - t_{O2}^{Exp}}{t_{O2}^{Exp}} \right| \right) / 24, \quad (5.40)$$

where ψ_{O1} and ψ_{O2} are the first and second overshoot angles, t_{O1} and t_{O2} are time at first and second overshoot angles, and n_Z is the number of the performed zigzag manoeuvres.

The benchmark free-running tests include 6 turning (15° , 25° , and 35° for starboard and port sides) and 6 zigzag (10° , 15° , and 20° for starboard and port sides) tests. The model-scale initial advance speed (u_0) is slightly different for each test manoeuvre as listed in Table 5.6 and Table 5.7 for the two reference inland vessels. Additionally, the propeller revolution rates (n) are constants of 20.2 s^{-1} and 17.7 s^{-1} for the 6700 t bulk carrier and the 3500 t tanker respectively.

Table 5.6: Model-scale initial speed of each test manoeuvre for the 6700 t bulk carrier (TPTR Y1).

Turning	15°	25°	35°	-15°	-25°	-35°
u_0 [m s^{-1}]	1.09	1.08	1.07	1.14	1.20	1.07
Zigzag	$10^\circ/10^\circ$	$15^\circ/15^\circ$	$20^\circ/20^\circ$	$-10^\circ/-10^\circ$	$-15^\circ/-15^\circ$	$-20^\circ/-20^\circ$
u_0 [m s^{-1}]	1.00	1.03	1.03	1.07	1.00	1.01

Using 40 different combinations of methods for X_H , Y_H , and N_H , the average absolute deviation of the simulated criteria in turning and zigzag manoeuvres (σ_T with Equation 5.39 and σ_Z with Equation 5.40) are calculated and compared in Table 5.8. X_H No. in the first row refers to the methods listed in Table 5.2 while Y_H and N_H No. in the first column

Table 5.7: Model-scale initial speed of each test manoeuvre for the 3500 t tanker (TPTR Y2).

Turning	15°	25°	35°	-15°	-25°	-35°
u_0 [ms ⁻¹]	1.08	1.07	1.06	1.16	1.15	1.05
Zigzag	10°/10°	15°/15°	20°/20°	-10°/-10°	-15°/-15°	-20°/-20°
u_0 [ms ⁻¹]	1.04	1.06	1.03	1.06	1.04	0.59

refers to the methods listed in Table 5.3. Some combinations in Table 5.8 fail to resolve the manoeuvring equations and a few methods do not give reasonable results, which are indicated as 'Fail', due to inaccurate estimation of the hull forces and moments.

Table 5.8: Average absolute deviation of the 6700 t bulk carrier using different combinations of methods for hull forces and moments in turning and zigzag manoeuvres.

	X_H No. 1		X_H No. 2		X_H No. 3		X_H No. 4		X_H No. 5	
	σ_T (%)	σ_Z (%)	σ_T (%)	σ_Z (%)	σ_T (%)	σ_Z (%)	σ_T (%)	σ_Z (%)	σ_T (%)	σ_Z (%)
Y_H and N_H No. 1	6.49	10.59	7.03	10.62	Fail	11.15	12.86	10.57	4.89	10.67
Y_H and N_H No. 2	34.53	60.66	35.34	61.23	Fail	49.41	Fail	59.69	33.15	61.59
Y_H and N_H No. 3	104.74	38.18	32.81	38.48	Fail	33.40	Fail	37.58	35.44	38.84
Y_H and N_H No. 4	29.38	17.37	20.32	17.23	Fail	17.49	40.32	17.36	22.01	17.38
Y_H and N_H No. 5	21.27	46.39	20.23	46.96	Fail	36.25	24.87	45.04	19.98	47.40
Y_H and N_H No. 6	11.71	10.09	8.61	10.13	Fail	10.75	19.66	10.13	8.38	10.13
Y_H and N_H No. 7	21.46	57.77	19.81	58.55	Fail	42.53	25.22	55.36	19.37	59.13
Y_H and N_H No. 8	8.14	13.46	7.56	13.52	Fail	12.53	14.96	13.22	4.86	13.68

As the tested overshoot angles are actually small values, σ_Z is larger than σ_T in Table 5.8. It is supposed that the model with the smallest σ_T and comparable σ_Z is the most suitable combination. Therefore, the combination of X_H No. 5 with Y_H and N_H No. 1 gives the best fit in the prediction of turning and zigzag manoeuvres for the 6700 t bulk carrier. To verify the selection, a similar procedure is carried out for the 3500 t tanker as shown in Table 5.9. Again, the combination of X_H No. 5 with Y_H and N_H No. 1 performs best for the 3500 t tanker. Thus, the selected combination is validated.

Table 5.9: Average absolute deviation of the 3500 t tanker using different combinations of methods for hull forces and moments in turning and zigzag manoeuvres.

	X_H No. 1		X_H No. 2		X_H No. 3		X_H No. 4		X_H No. 5	
	σ_T (%)	σ_Z (%)	σ_T (%)	σ_Z (%)	σ_T (%)	σ_Z (%)	σ_T (%)	σ_Z (%)	σ_T (%)	σ_Z (%)
Y_H and N_H No. 1	9.69	29.81	8.45	29.96	36.76	27.89	14.10	29.51	8.14	30.07
Y_H and N_H No. 2	31.69	97.79	31.91	98.51	Fail	82.75	33.19	95.54	31.58	99.09
Y_H and N_H No. 3	51.23	132.15	42.07	133.87	Fail	103.16	Fail	124.65	43.85	135.66
Y_H and N_H No. 4	34.99	33.01	28.10	32.97	Fail	34.19	46.18	33.18	29.15	33.05
Y_H and N_H No. 5	30.85	162.12	30.66	165.43	Fail	117.01	33.16	152.25	30.55	167.73
Y_H and N_H No. 6	15.14	46.74	13.37	47.01	Fail	40.32	19.95	45.45	13.59	47.30
Y_H and N_H No. 7	32.48	248.50	32.08	259.67	Fail	153.89	34.64	222.69	32.06	262.73
Y_H and N_H No. 8	10.79	24.09	8.16	24.11	40.65	23.56	17.13	24.25	8.35	24.22

Through the comparison, it is determined to use the Holtrop and Mennen [106, 107] method for $X_H(u)$ and the Yoshimura and Masumoto [313] for $X_H(\beta, r')$ (X_H No. 5 in Table 5.2), therefore, $X_H = X_H(u) + X_H(\beta, r')$. Furthermore, Y_H and N_H is calculated by

the Kijima et al. [138] method (Y_H and N_H No. 1 in Table 5.3). This combination is used to perform the manoeuvring simulations in the following sections as it gives the best fit.

5.9. Validation of the manoeuvring model

Section 5.9 introduces the validation of the presented manoeuvring model. Section 5.9.1 validates the mathematical model with a seagoing KVLCC2 tanker (SPSR S1) as most of the applied parameters are from experimental tests. Section 5.9.2 and Section 5.9.3 validate the integrated manoeuvring model with two reference inland vessels (TPTR Y1 and TPTR Y2), which are carried out with the selected empirical methods (from Section 5.4 to Section 5.8) and the RANS results in Chapter 4.

5.9.1. Validation using the seagoing KVLCC2 tanker

The seagoing KVLCC2 (SPSR S1) tanker is utilised as the reference ship to validate the mathematical model (Table 5.1). The KVLCC2 tanker has a single spade-type rudder with a NACA 0018 profile. The free-running model tests carried out by the Maritime Research Institute Netherlands (MARIN) are used as reference [168, 230]. The scale factor is 45.7. Simulations are performed with the model-scale ship particulars as presented in Table 5.10. Then, both results of the model-scale simulations and experiments are transformed to full-scale and compared.

Table 5.10: Applied parameters for the KVLCC2 tanker. Source: Yasukawa and Yoshimura [304].

L	7.0	B_{wl}	1.1688	T	0.455
∇	3.2724	C_b	0.8098	x_G	0.244
m'_x	0.022	m'_y	0.223	J'_z	0.011
u_0	1.179				
R'_0	0.022	Y'_v	-0.315	N'_v	-0.137
X'_{vv}	-0.040	Y'_r	0.083	N'_r	-0.049
X'_{vr}	0.002	Y'_{vvv}	-1.607	N'_{vvv}	-0.030
X'_{rr}	0.011	Y'_{vvr}	0.379	N'_{vvr}	-0.294
X'_{vvvv}	0.771	Y'_{vrr}	-0.391	N'_{vrr}	0.0550
		Y'_{rrr}	0.008	N'_{rrr}	-0.013
D_P	0.216	x'_P	-0.48	n	10.4
k_0	0.2931	k_1	-0.2753	k_2	-0.1385
t_P	0.220	w_{P_0}	0.40		
A_R	0.0539	Λ_G	1.827	x'_R	-0.50
t_R	0.387	a_H	0.312	x'_H	-0.464
C_1	2.0	C_2 ($\beta_P > 0$)	1.6	C_2 ($\beta_P < 0$)	1.1
γ_R ($\beta_R < 0$)	0.395	γ_R ($\beta_R > 0$)	0.640	ℓ'_R	-0.710
ε_R	1.09	κ_R	0.50	δ	15.8

Validation of the seagoing KVLCC2 tanker in turning manoeuvres

Figure 5.5 and Figure 5.6 compare the simulated trajectories and histories to the free-running tests of 35° and -35° turning manoeuvres [168, 230]. The simulated turning trajec-

tories agree well with the free-running tests. The starboard side turning simulation fits better than the port side simulation. It shows that the manoeuvring model underestimates the asymmetry motions of the port and starboard sides manoeuvres. Table 5.11 compares the turning indices of the simulated results (Sim) with the free-running tests (Exp) [168, 230].

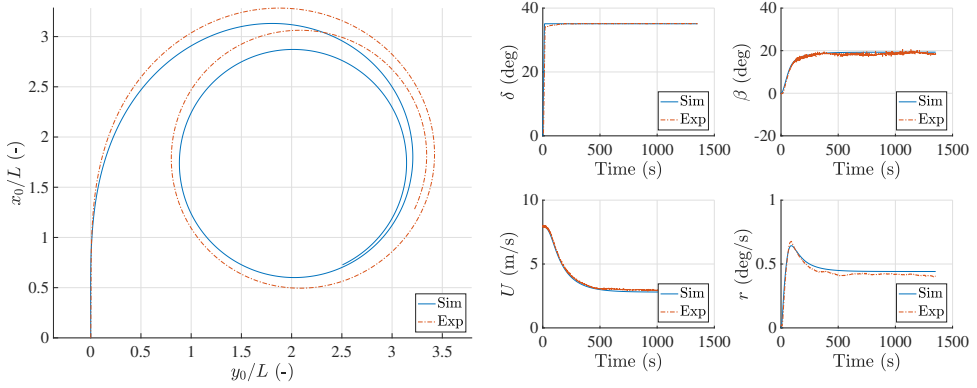


Figure 5.5: Validation of the KVLCC2 tanker in the 35° turning manoeuvre.

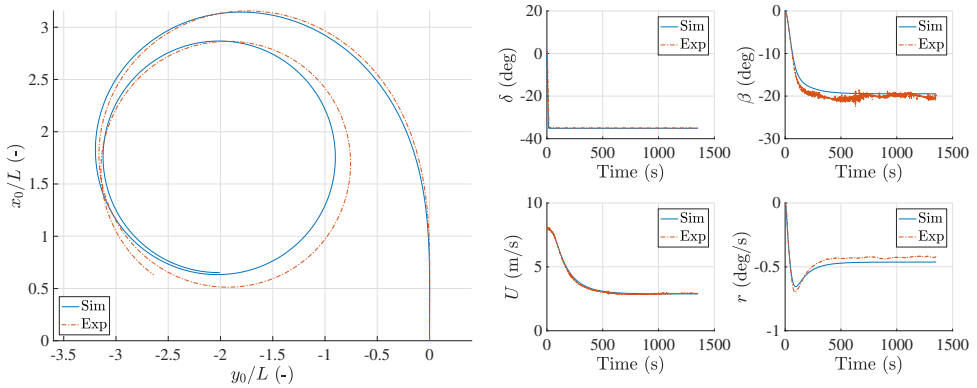


Figure 5.6: Validation of the KVLCC2 tanker in the -35° turning manoeuvre.

Validation of the seagoing KVLCC2 tanker in zigzag manoeuvres

Figure 5.7, Figure 5.8, Figure 5.9, and Figure 5.10 show the trajectories and histories in $10^\circ/10^\circ$, $-10^\circ/-10^\circ$, $20^\circ/20^\circ$, and $-20^\circ/-20^\circ$ zigzag manoeuvres respectively. The simulated results roughly agree with the experimental ship motions in zigzag manoeuvres. A larger speed drop is observed in the simulated time histories than the experiments. The histories of the rudder angle (δ), the drift angle (β), and the turning rate (r) agree well. Table 5.12 compares the simulated overshoot angles to the benchmarks. The manoeuvring indices are underestimated. The largest differences are about 30% in the first and second overshoot angles. It is actually very difficult to predict accurate overshoot angles in degrees.

Table 5.11: Comparison of the simulated turning and the tested turning indices.

Turning criteria	Sim (-)	Exp (-)	Δ (%)	Turning criteria	Sim (-)	Exp (-)	Δ (%)
A'_D ($\delta = 35^\circ$)	3.07	3.07	0.00	A'_D ($\delta = -35^\circ$)	3.09	2.98	3.69
T'_D ($\delta = 35^\circ$)	3.15	3.33	-5.41	T'_D ($\delta = -35^\circ$)	3.14	3.09	1.62

Here, the underestimation is mainly induced by the larger speed decrease, which may be caused by a larger hull damping force calculated in the manoeuvring model.

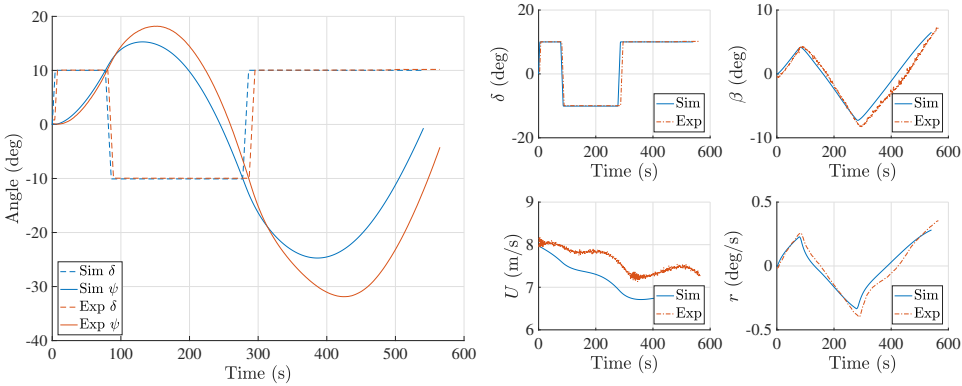


Figure 5.7: Validation of the KVLCC2 tanker in the $10^\circ/10^\circ$ zigzag manoeuvre.

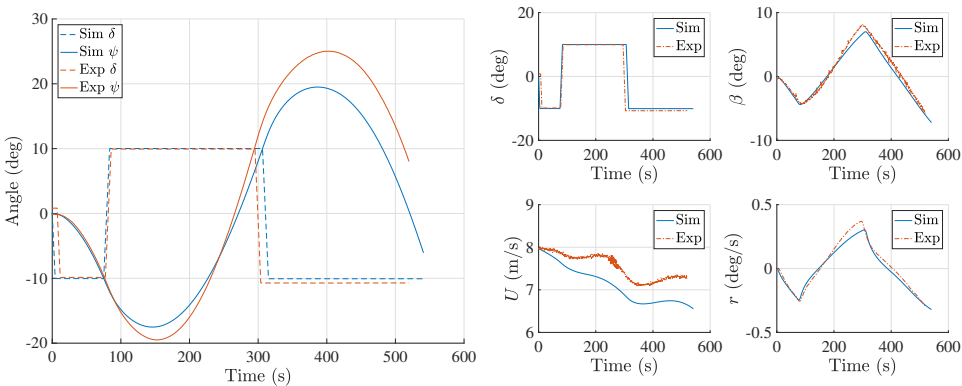


Figure 5.8: Validation of the KVLCC2 tanker in the $-10^\circ/-10^\circ$ zigzag manoeuvre.

Thus far, the applied mathematical model, which is a combination of the standard MMG model [304] and RANS-based rudder normal force coefficients, is validated with free-running tests. The model can capture the manoeuvring motions and related parameters. Underestimations of the asymmetry motions are observed in turning manoeuvres. Apart from the first overshoot angle of $-20^\circ/-20^\circ$ zigzag test, the overshoot angles are underestimated due to a larger speed decrease simulated in the manoeuvring model than

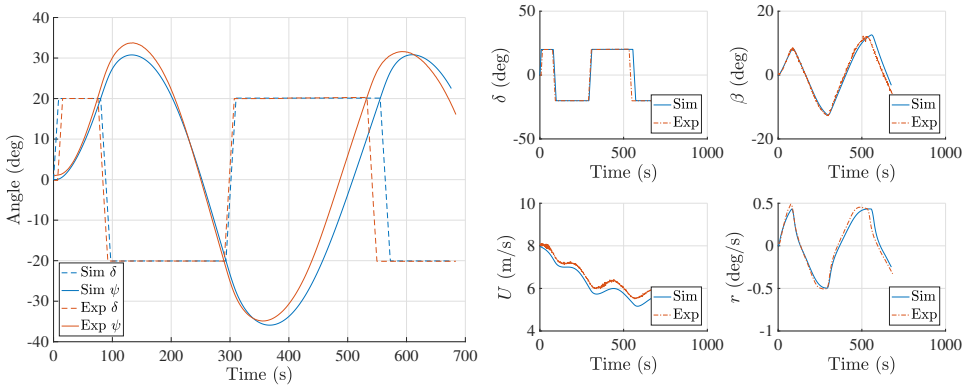


Figure 5.9: Validation of the KVLCC2 tanker in the 20°/20° zigzag manoeuvre.

5

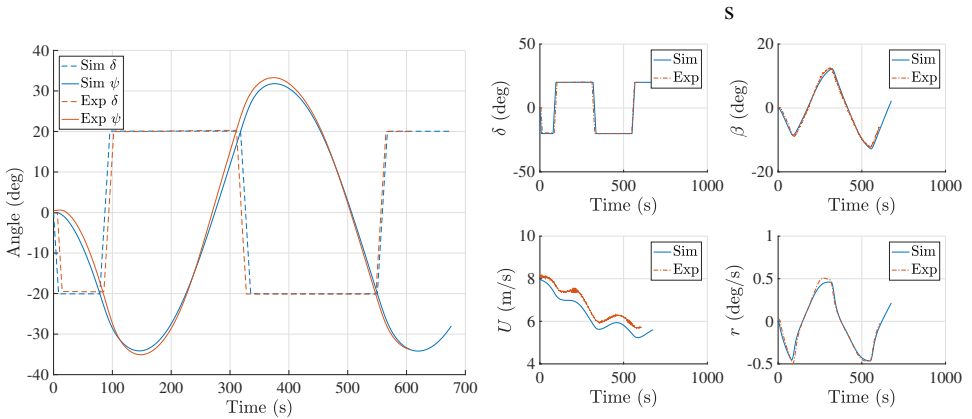


Figure 5.10: Validation of the KVLCC2 tanker in the -20°/-20° zigzag manoeuvre.

Table 5.12: Comparison of the simulated overshoot angles and the tested overshoot angles.

Zigzag criteria	Sim (deg)	Exp (deg)	Δ (%)	Zigzag criteria	Sim (deg)	Exp (deg)	Δ (%)
ψ_{O1} (10°/10°)	5.3	7.9	-33.2	ψ_{O1} (-10°/-10°)	7.5	9.3	-19.1
ψ_{O2} (10°/10°)	14.7	21.6	-31.9	ψ_{O2} (-10°/-10°)	9.5	14.7	-35.4
ψ_{O1} (20°/20°)	10.8	13.3	-19.0	ψ_{O1} (-20°/-20°)	14.1	14.7	-3.9

experiments. Since the rudder forces and moments are calculated based on a specific profile, the model is applicable to investigate the impacts of rudder profiles on manoeuvring performance.

5.9.2. Validation using the inland 6700 t bulk carrier

Manoeuvring simulations of the 6700 t bulk carrier (TPTR Y1) are performed for 15°, 25°, and 35° turning manoeuvres and 10°/10°, 10°/10°, and 10°/10° zigzag manoeuvres on both both port and starboard sides. In the following sections, simulations are performed with model-scale parameters. Then, the simulated and tested results are scaled and compared in full-scale. The simulated and tested results of the trajectories, the rudder angle, the drift angle, the heading angle, the ship speed, and the yaw rates are compared. The drift angles of the experiment are not available. Here, only the simulated drift angles are shown to provide full information on the simulations. Table 5.13 presents the parameters used in the simulations.

Table 5.13: Applied parameters in the simulations of the 6700 t bulk carrier.

L	4.429	B	0.791	T	0.173	∇	0.5290
S	4.665	C_b	0.867	x_G	0.009	m'_x	0.0178
m'_y	0.155	I'_z	0.021	J'_z	0.013	δ	25
$X'_{\beta\beta}$	-0.0019	$X'_{\beta r}$	-0.0608	X'_{rr}	0.0665	$X'_{\beta\beta\beta\beta}$	0.0665
Y'_{β}	0.3395	Y'_r	0.0973	$Y'_{\beta\beta}$	0.5727	Y'_{rr}	-0.0050
$Y'_{\beta rr}$	0.1731	$Y'_{\beta\beta r}$	-0.3656	N'_{β}	0.0781	N'_r	-0.0361
$N'_{\beta\beta}$	0.0381	N'_{rr}	-0.0126	$N'_{\beta rr}$	-0.0448	$N'_{\beta\beta r}$	-0.1295
D_P	0.110	w_{P_0}	0.32	t_P	0.2	x_P	-2.1220
y_P^S	-0.240	y_P^P	0.240	k_2^S	-0.1075	k_1^S	-0.3507
k_0^S	0.3329	k_2^P	-0.1295	k_1^P	-0.3269	k_0^P	0.3307
A_R	0.010	ϵ_R	0.9364	w_{R_0}	0.3633	C_R	0.126
B_R	0.142	Λ_G	1.129	x_R	-2.215	y_R^S	0.240
y_R^P	-0.240	t_R	0.2072	a_H	0.3906	x'_H	-0.3980
γ_R	0.4590	η_R	0.7752	ℓ'_R	-0.937	κ_R	0.426

As discussed in Section 4.3, the interaction between the rudders and shallow water also influences C_L and C_D . However, the spacing between the twin rudders of the reference inland vessels (TPTR Y1 and TPTR Y2) is rather large ($3.81C_R$). It is assumed no significant interaction effect on C_L and C_D of each rudder. The shallow water effect on the rudder itself only applies to extremely small under keel clearance (Section 4.4), therefore, it is neglected. In the end, applied C_L and C_D for TPTR Y1 are described as follows:

$$\left. \begin{aligned} C_L &= 6.175 \sin \alpha_R \frac{1.3\Lambda_G}{\Lambda_G + 2.25} \\ C_D &= 0.032 \sin \alpha_R \frac{1.3\Lambda_G}{\Lambda_G + 2.25} \end{aligned} \right\} \quad (5.41)$$

Validation of the inland 6700 t bulk carrier in turning manoeuvres

Using the methods in Table 5.5 and the parameters in Table 5.13, the trajectories and time histories of simulated and tested motion parameters in the 15° , -15° , 25° , -25° , 35° , and -35° turning manoeuvres are presented in Figure 5.11, Figure 5.12, Figure 5.13, Figure 5.14, Figure 5.15, and Figure 5.16 respectively. Comparing the free-running results of various turning manoeuvres, the starboard side A'_D and T'_D are larger than those of the port side.

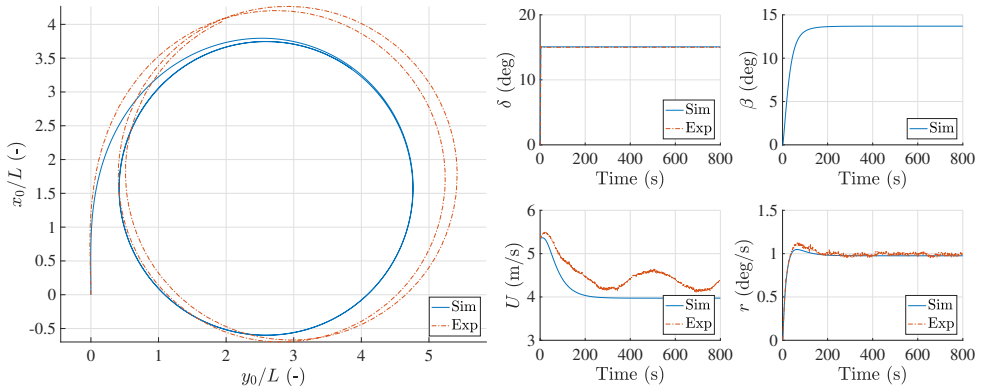


Figure 5.11: Validation of the 6700 t bulk carrier in the 15° turning manoeuvre.

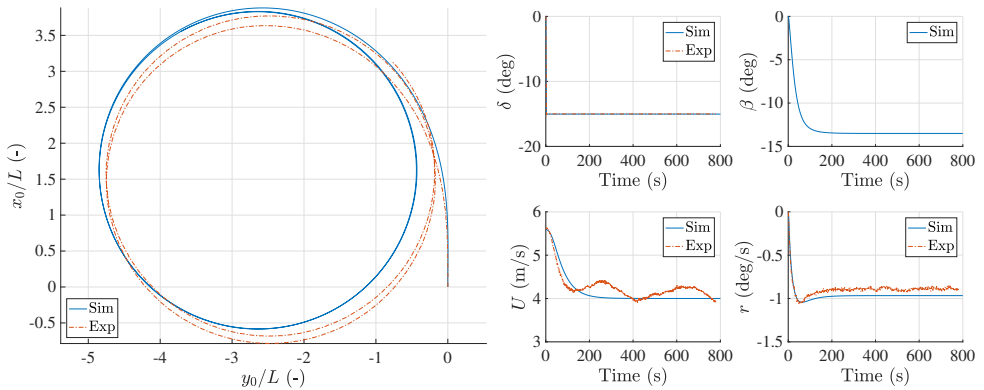


Figure 5.12: Validation of the 6700 t bulk carrier in the -15° turning manoeuvre.

Table 5.14 compares the non-dimensional advance (A'_D), the non-dimensional tactical diameter (T'_D), and the relative deviation in percentage (Δ) of the simulated and tested turning manoeuvres. Asymmetry behaviour is found in the free-running trajectories while it is less obvious in the simulation results. Furthermore, the simulated A'_D and T'_D are mostly smaller on the port side while larger on the starboard side than the tested A'_D and T'_D .

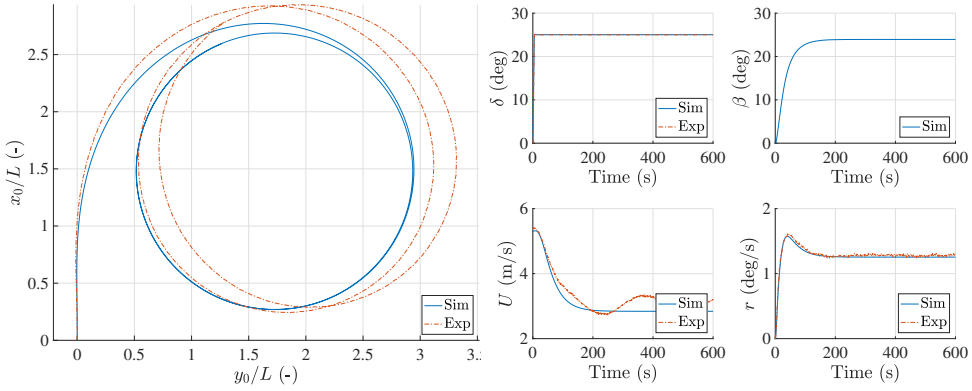


Figure 5.13: Validation of the 6700 t bulk carrier in the 25° turning manoeuvre.

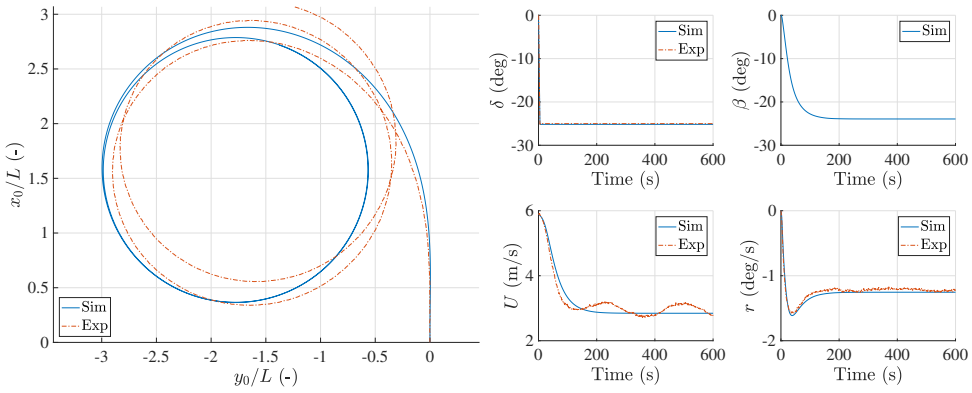


Figure 5.14: Validation of the 6700 t bulk carrier in the -25° turning manoeuvre.

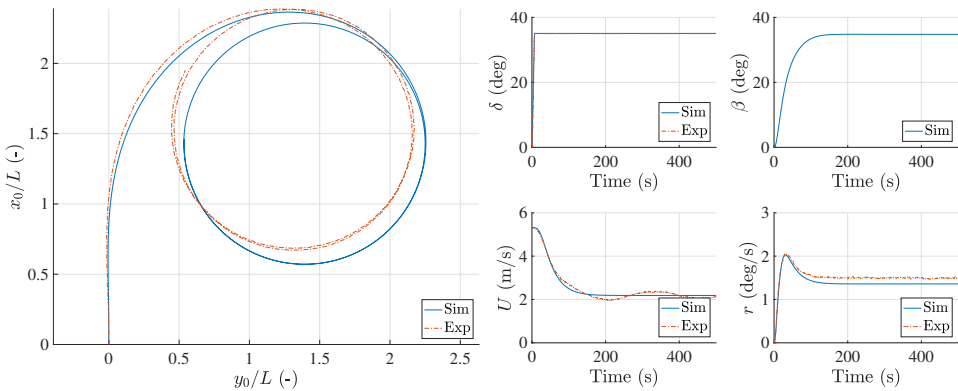


Figure 5.15: Validation of the 6700 t bulk carrier in the 35° turning manoeuvre.

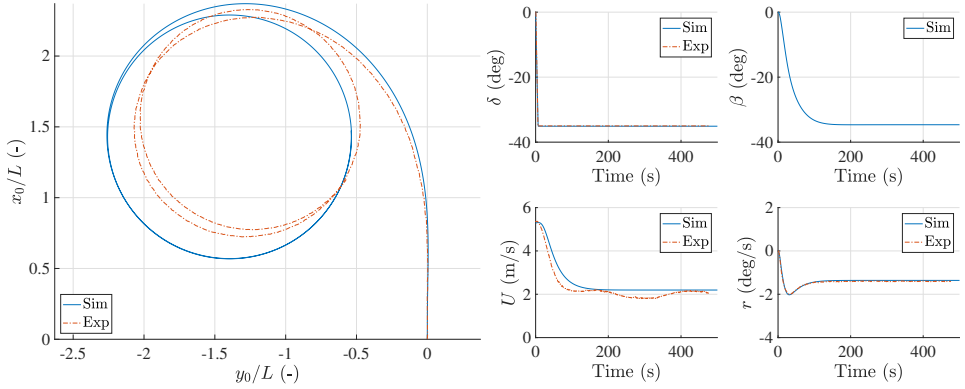


Figure 5.16: Validation of the 6700 t bulk carrier in the -35° turning manoeuvre.

Table 5.14: Comparison of the simulated and tested turning indices of the 6700 t bulk carrier.

Turning criteria	Sim (-)	Exp (-)	Δ (%)	Turning criteria	Sim (-)	Exp (-)	Δ (%)
A'_D ($\delta = 15^\circ$)	3.74	4.08	-8.33	A'_D ($\delta = -15^\circ$)	3.82	3.59	6.41
T'_D ($\delta = 15^\circ$)	4.71	5.08	-7.28	T'_D ($\delta = -15^\circ$)	4.79	4.72	1.48
A'_D ($\delta = 25^\circ$)	2.68	2.83	-5.30	A'_D ($\delta = -25^\circ$)	2.79	2.68	4.10
T'_D ($\delta = 25^\circ$)	2.85	3.02	-5.63	T'_D ($\delta = -25^\circ$)	2.89	2.84	1.76
A'_D ($\delta = 35^\circ$)	2.23	2.27	-1.76	A'_D ($\delta = -35^\circ$)	2.23	2.18	2.29
T'_D ($\delta = 35^\circ$)	2.11	2.05	2.93	T'_D ($\delta = -35^\circ$)	2.11	1.99	6.03

Validation of the inland 6700 t bulk carrier in zigzag manoeuvres

The time histories of simulated and tested motion parameters in the $10^\circ/10^\circ$, $-10^\circ/-10^\circ$, $15^\circ/15^\circ$, $-15^\circ/-15^\circ$, $20^\circ/20^\circ$, and $-20^\circ/-20^\circ$ zigzag manoeuvres are presented in Figure 5.17, Figure 5.18, Figure 5.19, Figure 5.20, Figure 5.21, and Figure 5.22 respectively. Table 5.15 compares the first overshoot angle (ψ_{O1}) and the second overshoot angle (ψ_{O2}) of the simulated and tested zigzag manoeuvres. The simulated ψ_{O1} and ψ_{O2} are mostly larger than the tested ψ_{O1} and ψ_{O2} .

Comparing the results of port and starboard sides, the asymmetric characteristics of the simulated overshoot angles are less significant than the tested ones. The differences in the simulated and tested results are primarily caused by the divergence of the simulated and tested ship speed. The larger speed drop of the simulated results may be caused by the inaccurate prediction of the hull forces.

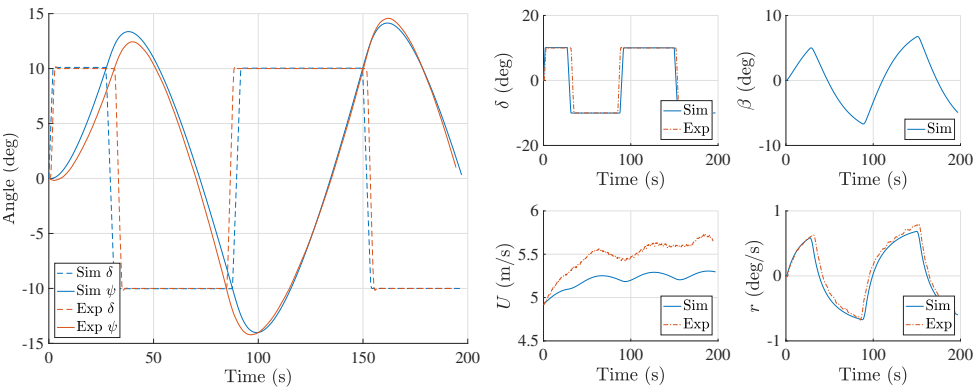


Figure 5.17: Validation of the 6700 t bulk carrier in the $10^\circ/10^\circ$ zigzag manoeuvre.

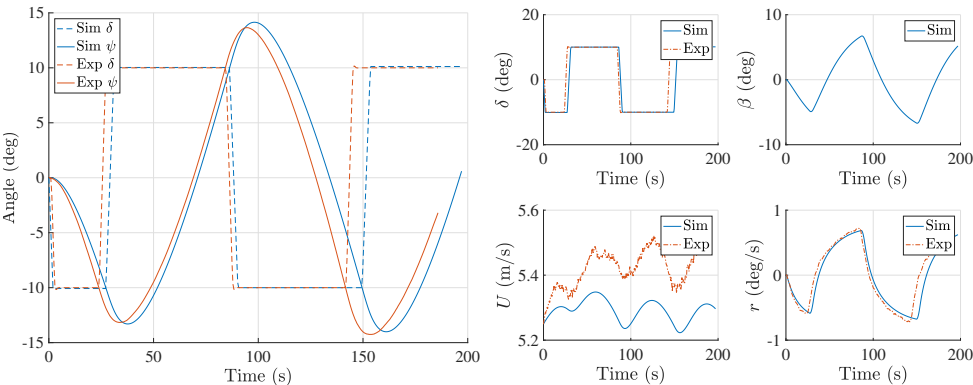


Figure 5.18: Validation of the 6700 t bulk carrier in the $-10^\circ/-10^\circ$ zigzag manoeuvre.

The simulation study shows that the prediction is quite sensitive to the wake fractions (w_P and w_R) and the flow straightening factor (γ_R). The wake fractions affect the inflow

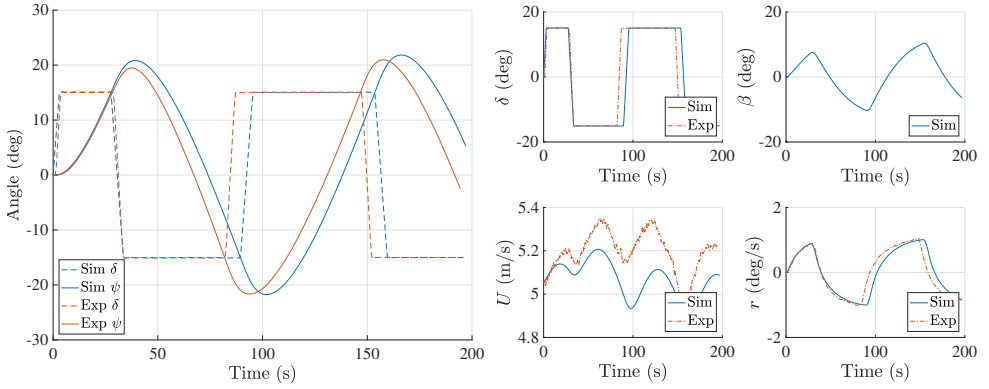


Figure 5.19: Validation of the 6700 t bulk carrier in the 15°/15° zigzag manoeuvre.

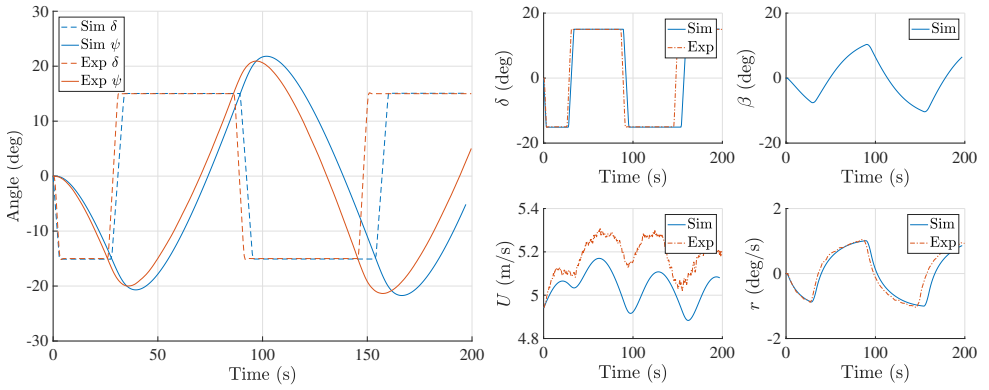


Figure 5.20: Validation of the 6700 t bulk carrier in the -15°/-15° zigzag manoeuvre.

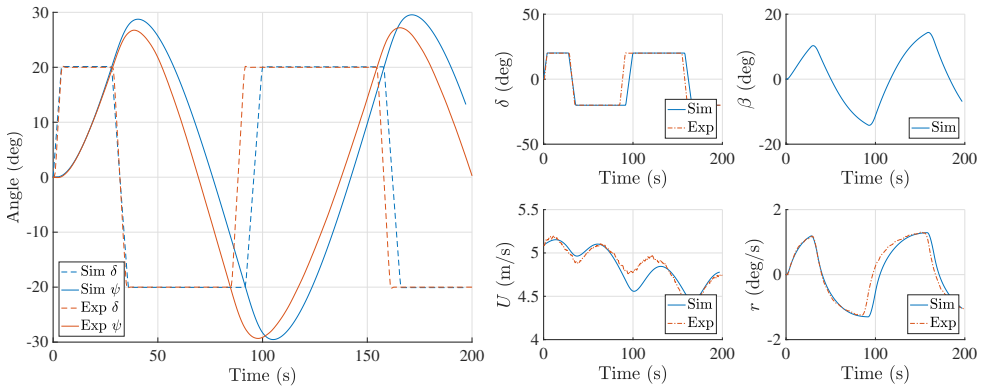


Figure 5.21: Validation of the 6700 t bulk carrier in the 20°/20° zigzag manoeuvre.

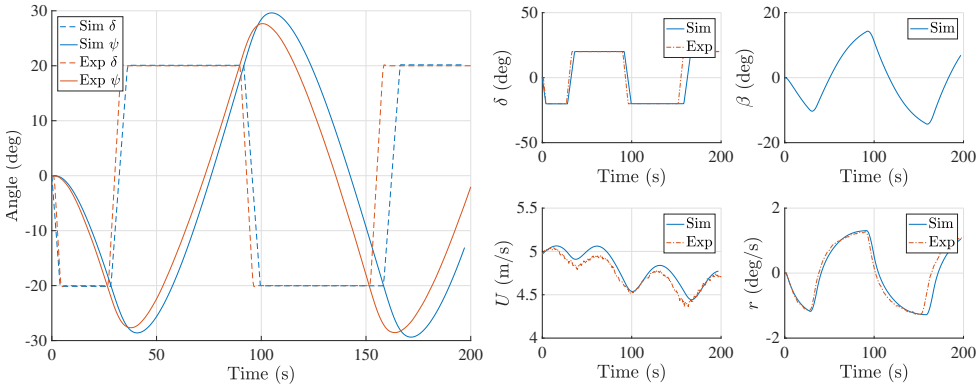


Figure 5.22: Validation of the 6700 t bulk carrier in the $-20^\circ/-20^\circ$ zigzag manoeuvre.

Table 5.15: Comparison of the simulated and the tested overshoot angles of the 6700 t bulk carrier.

Zigzag criteria	Sim (deg)	Exp (deg)	Δ (%)	Zigzag criteria	Sim (deg)	Exp (deg)	Δ (%)
ψ_{O1} ($10^\circ/10^\circ$)	3.36	2.43	38.27	ψ_{O1} ($-10^\circ/-10^\circ$)	3.30	3.16	4.43
ψ_{O2} ($10^\circ/10^\circ$)	4.02	4.17	-3.60	ψ_{O2} ($-10^\circ/-10^\circ$)	4.15	3.65	13.70
ψ_{O1} ($15^\circ/15^\circ$)	5.82	4.49	29.62	ψ_{O1} ($-15^\circ/-15^\circ$)	5.70	4.99	14.23
ψ_{O2} ($15^\circ/15^\circ$)	6.75	6.65	1.50	ψ_{O2} ($-15^\circ/-15^\circ$)	6.81	5.93	14.84
ψ_{O1} ($20^\circ/20^\circ$)	8.75	6.74	29.82	ψ_{O1} ($-20^\circ/-20^\circ$)	8.60	7.66	12.27
ψ_{O2} ($20^\circ/20^\circ$)	9.54	9.33	2.25	ψ_{O2} ($-20^\circ/-20^\circ$)	9.62	7.66	25.59

speed of the propeller and the rudder which, influence the magnitude of the forces and moments of the propeller and the rudder. The flow straightening effect affects the lateral component of the rudder inflow (v_R). Furthermore, it influences the hydrodynamic inflow angle of the rudder (δ_h) and the effective rudder angle (α_R) as shown in Equation 5.18, Equation 5.20, and Equation 5.28. In addition, the model-scale simulations are quite sensitive to the initial status of u_0 and n , which should be carefully matched with the experiments to perform the simulations.

5.9.3. Validation using the inland 3500 t tanker

To further validate the proposed integrated model for inland vessels, this section presents manoeuvring simulations of the 3500 t tanker (TPTR Y2). Table 5.16 presents the parameters used in the simulations. The Holtrop [104], Holtrop and Mennen [107] method is used for $X_H(u)$, the Yoshimura and Masumoto [313] method is used for $X_H(\beta, r')$, and the Kijima et al. [138] method is used for Y_H and N_H . Applied methods for manoeuvring are listed in Table 5.5. Considering the rudder profile, the spacing between the twin rudders, and the end plates, the applied C_L and C_D for TPTR Y2 are written as follows,

$$\left. \begin{aligned} C_L &= 6.175 \sin \alpha_R \frac{\Lambda_G}{\Lambda_G + 2.25} \\ C_D &= 0.032 \sin \alpha_R \frac{\Lambda_G}{\Lambda_G + 2.25} \end{aligned} \right\} \quad (5.42)$$

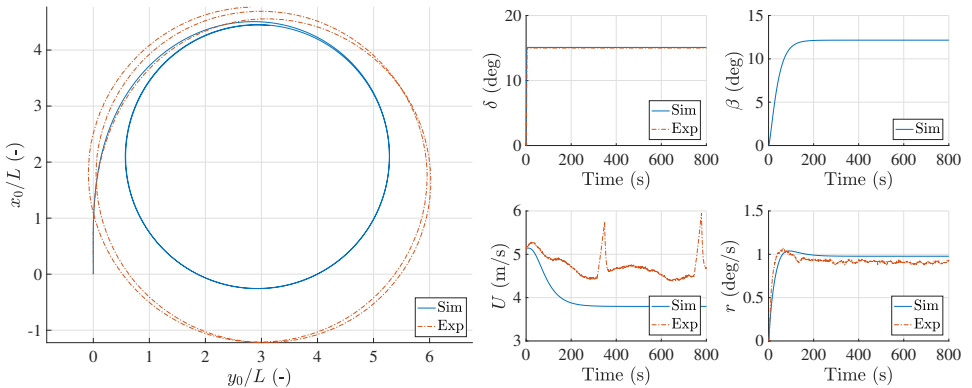
Table 5.16: Applied parameters in the simulations of the 3500 t tanker.

L	4.146	B	0.754	T	0.184	∇	0.492
S	4.244	C_b	0.855	x_G	0.011	m'_x	0.0194
m'_y	0.1708	I'_z	0.02	J'_z	0.0125	δ	25
$X'_{\beta\beta}$	-0.0012	$X'_{\beta r}$	-0.0462	X'_{rr}	0.0663	$X'_{\beta\beta\beta\beta}$	0.0613
Y'_{β}	0.3571	Y'_r	0.0973	$Y'_{\beta\beta}$	0.5885	Y'_{rr}	0.0016
$Y'_{\beta rr}$	0.2105	$Y'_{\beta\beta r}$	-0.3370	N'_{β}	0.0888	N'_r	-0.0401
$N'_{\beta\beta}$	0.0320	N'_{rr}	-0.0123	$N'_{\beta rr}$	-0.0543	$N'_{\beta\beta r}$	-0.1292
D_P	0.11	w_{P_0}	0.32	t_P	0.2	x_P	-2.007
y_P^S	0.228	y_P^P	-0.228	k_2^S	-0.1075	k_1^S	-0.3507
k_0^S	0.3329	k_2^P	-0.1295	k_1^P	-0.3269	k_0^P	0.3307
A_R	0.013	ϵ_R	0.9319	w_{R_0}	0.3663	C_R	0.114
B_R	0.114	Λ_G	1.0	x_R	-2.073	y_R^S	0.22
y_R^P	-0.22	t_R	0.2106	a_H	0.3831	x'_H	-0.3827
γ_R	0.4603	η_R	0.9649	ℓ'_R	-0.9357	κ_R	0.426

5

Validation of the inland 3500 t tanker in turning manoeuvres

Simulations of the 3500 t tanker are carried out in 15° , 25° , and 35° turning manoeuvres on both starboard and port sides, which are presented in Figure 5.23, Figure 5.24, Figure 5.25, Figure 5.26, Figure 5.27, and Figure 5.28 respectively. The non-dimensional turning criteria of the simulated and tested results are compared in Table 5.17. The prediction of the 35° and -35° turning manoeuvres are quite accurate while those of the 15° , -15° , 25° , and -25° turning manoeuvres are not that satisfactory. All the initial turning stages (the first quarters of the turning circles) are well predicted. Therefore, the inaccuracy is primarily caused by the divergence of the steady turn.

Figure 5.23: Validation of the 3500 t tanker in the 15° turning manoeuvre.

Regarding the constant turning stage, the prediction of the T'_D in the 15° , -15° , 25° , and -25° turning manoeuvres is inaccurate while the prediction of T'_D in the 35° and -35° turning manoeuvres is accurate. It shows the defect of the hull force module to estimate

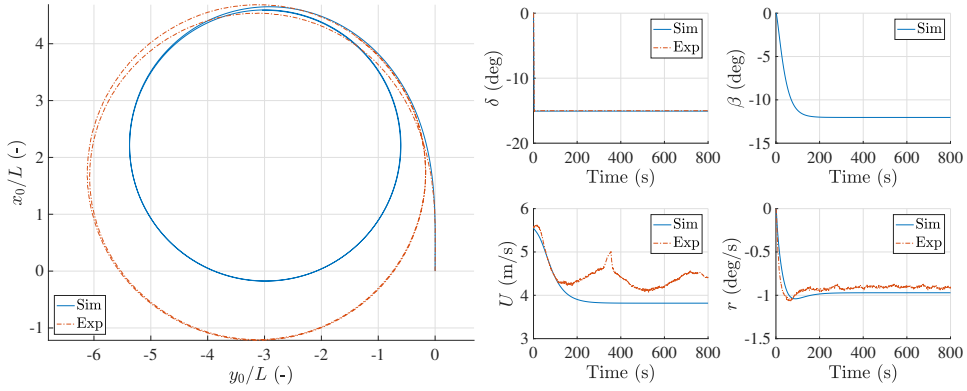


Figure 5.24: Validation of the 3500 t tanker in the -15° turning manoeuvre.

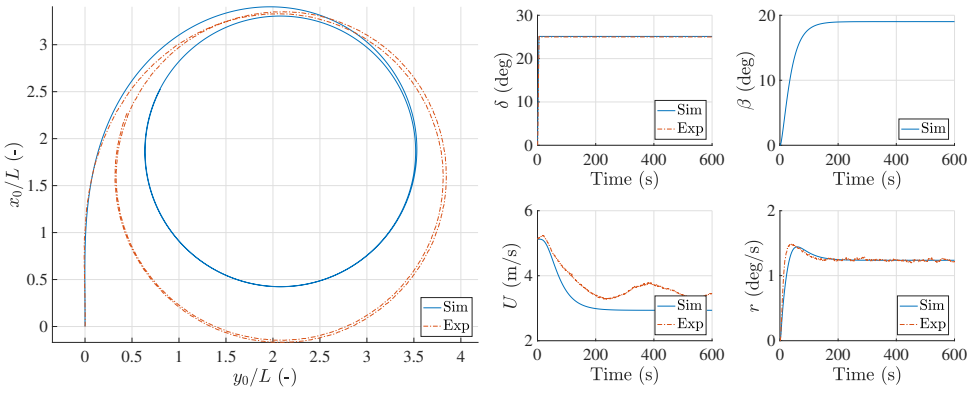


Figure 5.25: Validation of the 3500 t tanker in the 25° turning manoeuvre.

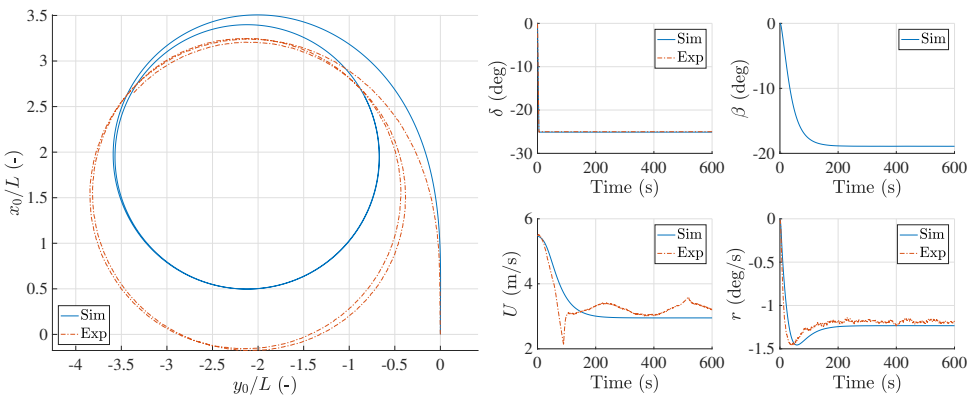
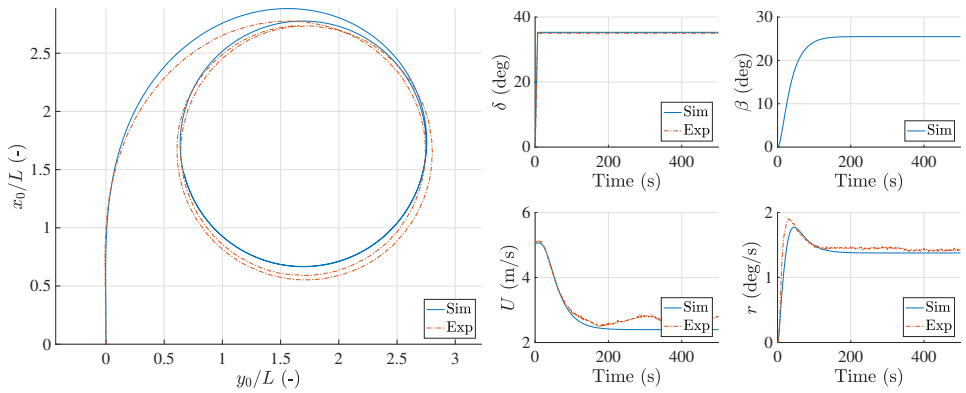


Figure 5.26: Validation of the 3500 t tanker in the -25° turning manoeuvre.

Figure 5.27: Validation of the 3500 t tanker in the 35° turning manoeuvre.

5

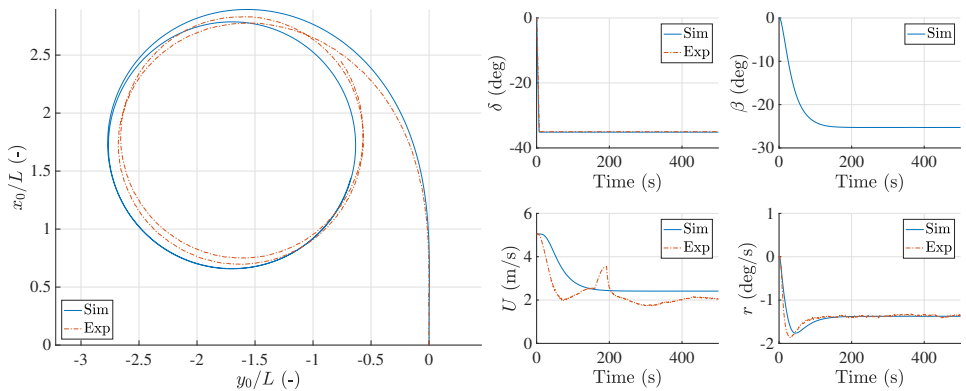
Figure 5.28: Validation of the 3500 t tanker in the -35° turning manoeuvre.

Table 5.17: Comparison of the simulated and the tested turning indices of the 3500 t tanker.

Turning criteria	Sim (-)	Exp (-)	Δ (%)	Turning criteria	Sim (-)	Exp (-)	Δ (%)
A'_D ($\delta = 15^\circ$)	4.46	4.47	-0.22	A'_D ($\delta = -15^\circ$)	4.60	4.43	3.84
T'_D ($\delta = 15^\circ$)	5.23	5.96	-12.25	T'_D ($\delta = -15^\circ$)	5.33	5.97	-10.72
A'_D ($\delta = 25^\circ$)	3.33	3.20	4.06	A'_D ($\delta = -25^\circ$)	3.44	4.01	-14.21
T'_D ($\delta = 25^\circ$)	3.46	3.69	-6.23	T'_D ($\delta = -25^\circ$)	3.51	3.75	-6.40
A'_D ($\delta = 35^\circ$)	2.79	2.63	6.08	A'_D ($\delta = -35^\circ$)	2.80	2.63	6.46
T'_D ($\delta = 35^\circ$)	2.65	2.61	1.53	T'_D ($\delta = -35^\circ$)	2.67	2.64	1.14

the forces and moments when the 3500 t tanker is turning with relatively small drift angles. The drift angles for 15°, 25°, and 35° on starboard and port sides turning are about 12°, 18°, 25° respectively. The 3500 t tanker is fitted with a bulbous bow.

When the ship is turning with a small drift angle, the bulbous bow may significantly influence the flow separation at the bow and further affect the effective rudder angle and the rudder inflow speed. However, most of the previous studies on the bulbous bow focused on its effect on powering and few of them considered its impact on manoeuvring. The impacts of the bulbous bow on manoeuvring forces and moments are not well considered in the presented model and further research is suggested.

Validation of the inland 3500 t tanker in zigzag manoeuvres

The heading angles and rudder angles of the 3500 t tanker in 10°/10°, -10°/-10°, 15°/15°, -15°/-15°, 20°/20°, and -20°/-20° are presented in Figure 5.29, Figure 5.30, Figure 5.31, Figure 5.32, Figure 5.33, and Figure 5.34 respectively. The inaccurate prediction of the speed leads to delays in the time when maximum heading angles are reached.

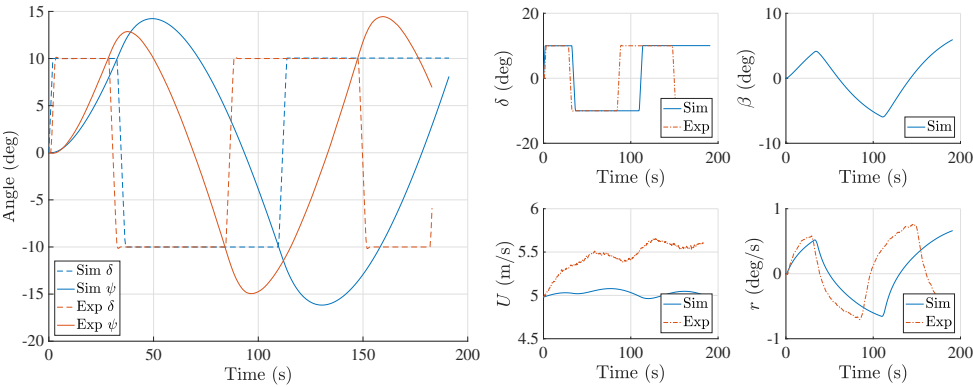


Figure 5.29: Validation of the 3500 t tanker in the 10°/10° zigzag manoeuvre.

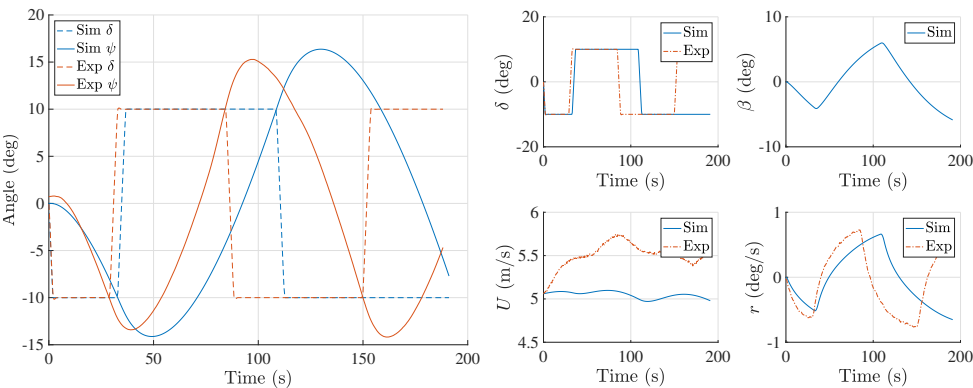


Figure 5.30: Validation of the 3500 t tanker in the -10°/-10° zigzag manoeuvre.

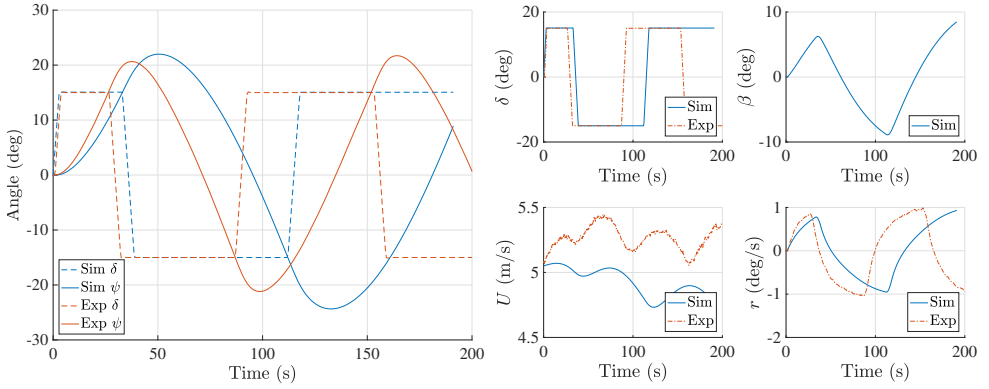


Figure 5.31: Validation of the 3500 t tanker in the $15^\circ/15^\circ$ zigzag manoeuvre.

5

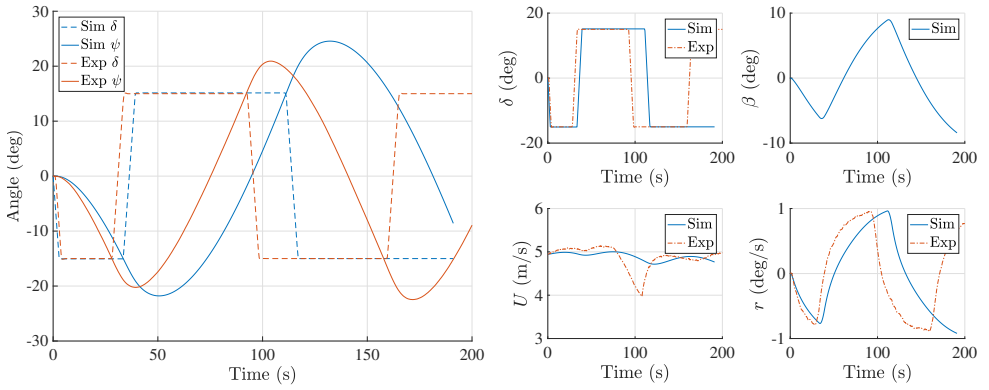


Figure 5.32: Validation of the 3500 t tanker in the $-15^\circ/-15^\circ$ zigzag manoeuvre.

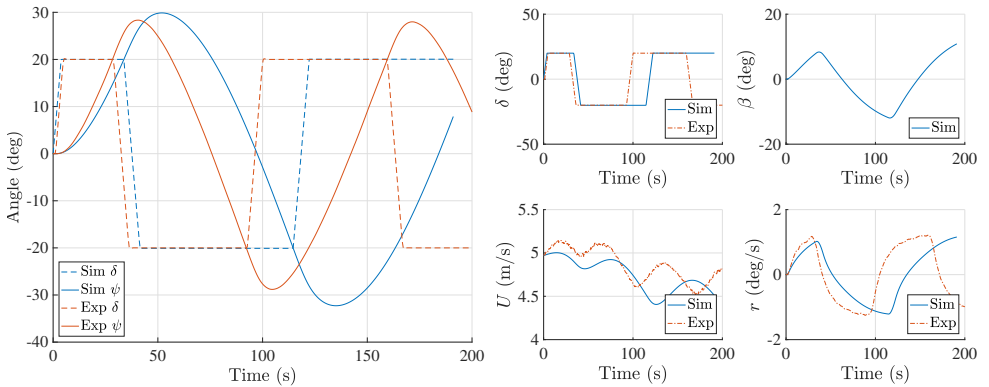


Figure 5.33: Validation of the 3500 t tanker in the $20^\circ/20^\circ$ zigzag manoeuvre.

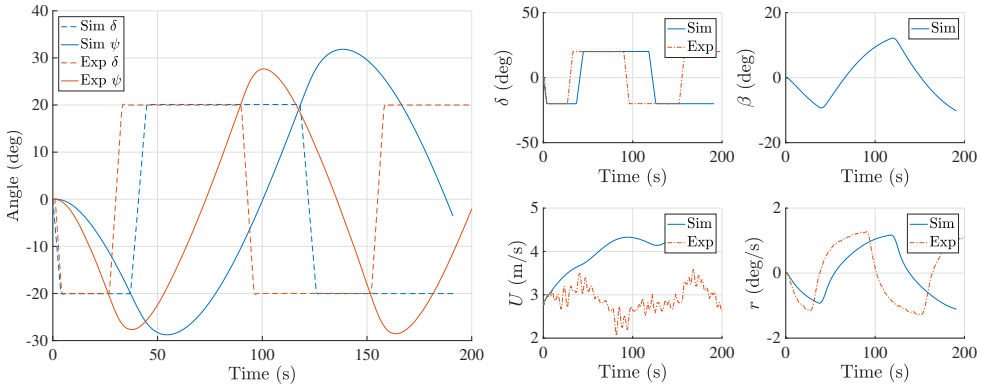


Figure 5.34: Validation of the 3500 t tanker in the $-20^\circ/-20^\circ$ zigzag manoeuvre.

Table 5.18 compares the simulated and tested overshoot angles. Significant speed drops are observed. Similar to the turning manoeuvres, a primary reason for these differences is because the bow effect on the hull forces and moments is not well estimated. The overestimation of the overshoot angles is possibly caused by the fact that the hull damping forces are underestimated. The large predicted speed drop decreases the rudder inflow velocity and reduces the yaw checking force induced by the rudder.

Table 5.18: Comparison of the simulated and the tested overshoot angles of the 3500 t tanker.

Zigzag criteria	Sim (deg)	Exp (deg)	Δ (%)	Zigzag criteria	Sim (deg)	Exp (deg)	Δ (%)
ψ_{O1} ($10^\circ/10^\circ$)	3.82	2.86	33.57	ψ_{O1} ($-10^\circ/-10^\circ$)	3.73	3.42	9.06
ψ_{O2} ($10^\circ/10^\circ$)	5.09	4.95	2.83	ψ_{O2} ($-10^\circ/-10^\circ$)	5.25	5.28	-0.57
ψ_{O1} ($15^\circ/15^\circ$)	6.40	5.64	13.48	ψ_{O1} ($-15^\circ/-15^\circ$)	6.23	5.24	18.89
ψ_{O2} ($15^\circ/15^\circ$)	7.96	6.18	28.80	ψ_{O2} ($-15^\circ/-15^\circ$)	8.06	5.92	36.15
ψ_{O1} ($20^\circ/20^\circ$)	9.27	8.34	11.15	ψ_{O1} ($-20^\circ/-20^\circ$)	8.21	8.34	-1.56
ψ_{O2} ($20^\circ/20^\circ$)	10.69	8.81	21.34	ψ_{O2} ($-20^\circ/-20^\circ$)	10.30	8.81	16.91

5.10. Synthesis

An integrated manoeuvring model with empirical methods and RANS results has been developed for inland vessels through literature surveys, CFD studies, and analysis of combinations of part models. The presented model uses empirical methods that are publicly available to estimate manoeuvring parameters while further improvements can be obtained by carrying out model tests or CFD tests. The regression methods for the hull forces and moment are selected by comparing the simulated and tested manoeuvring indices in various manoeuvres. Furthermore, using 2D open water RANS results, the rudder profile, the spacing between rudders, and the end plate effects on the rudder forces and moments can be considered.

Manoeuvring simulations are performed with one single-propeller single-rudder seagoing KVLCC2 tanker (SPSR S1) and two standard twin-propeller twin-rudder inland vessels (TPTR Y1 and TPTR Y2) from the Yangtze River in various turning and zigzag manoeuvres.

vres on both port and starboard sides. The simulation results are validated with free-running model tests to show the usability of the proposed model. Through the simulation study, it is confirmed that the presented model can roughly capture the manoeuvring characteristics of the reference seagoing and inland vessels.

Chapter 5 partly answers the third research question in Section 1.3: *How does the rudder configuration affect the rudder hydrodynamic characteristics?* Accordingly, conclusions are drawn as follows:

- The seagoing ship oriented methods are usable for inland vessels while additional attention should be paid to large C_b , L/B , and B/T of inland vessels.
- The asymmetric characteristics are not well captured due to inaccurate input parameters, such as w_P , t_P , w_R , and γ_R . These parameters should be different for each propeller and each rudder on starboard and port side manoeuvres.
- The bulbous bow has suspected impacts on the manoeuvring performance of the reference 3500 t tanker, especially for zigzag manoeuvres. However, these impacts are not well covered in the literature.
- The accuracy of the prediction is quite sensitive to the initial status of the simulation, such as the initial speed and the constant propeller revolution rate. Therefore, to properly validate the mathematical model, it is necessary to accurately implement the actual initial states of the validation experiments.

Further investigations and experiments are requested to describe the inland vessel resistance ($X_H(u)$), express the longitudinal component hull forces due to manoeuvring motions ($X_H(v', r')$ or $X_H(\beta, r')$), and collect hydrodynamic derivatives for lateral force (Y_H) and yaw moment (N_H). Moreover, research on the impacts of the bulbous bow on ship manoeuvrability is suggested. Additional tests are needed to determine the impact factor of the propeller (k_P), the rudder (k_R), and the aspect ratio (k_A) on the rudder lift and drag coefficients during manoeuvring motions.

Chapter 6

Impacts of Rudder Configurations on Ship Manoeuvring Performance*

“Shallow men believe in luck or in circumstance. Strong men believe in cause and effect.”

Ralph Waldo Emerson (1803 – 1882)

The performance of ship rudders affects the ship manoeuvrability, including, but not limited to, turning ability, yaw checking ability, and course keeping ability as discussed in Chapter 2. However, the existing empirical formulas for the rudder forces do not cover the impacts of the rudder profile, the rudder parameters, and the rudder interaction. Thus, the applied rudder hydrodynamics were calculated through the presented RANS methods in Chapter 4. Furthermore, an integrated manoeuvring model was introduced in Chapter 5. This chapter discusses the impacts of the rudder configurations, more specifically the rudder profiles (Section 6.1), the spacing between twin rudders (Section 6.2), and the spacing among quadruple rudders (Section 6.3), on ship manoeuvrability through simulations.

Five ship types (Table 5.1) and nine rudder profiles (Figure 2.4) are tested and compared in four chosen manoeuvres from Chapter 3. Four types of manoeuvring tests, namely turning, zigzag, hard turning, and lane changing are selected from the existing and proposed manoeuvres. Reference seagoing and inland ships with different rudder configurations are tested, namely a single-propeller single-rudder KVLCC2 tanker (SPSR S1), a twin-propeller twin-rudder tanker (TPTR Y1) and a twin-propeller twin-rudder cargo vessel (TPTR Y2) from the Yangtze River, and a single-propeller twin-rudder ship (SPTR R1) and a twin-propeller quadruple-rudder ship (TPQR R2) from the Rhine. This chapter concludes insights into the impacts of rudder configurations on ship manoeuvrability. Accordingly, guidance on rudder configurations is provided in Chapter 7.

6.1. Rudder profiles

This section presents the impacts of rudder profiles on ship manoeuvrability. With the proposed integrated manoeuvring model in Chapter 5, the impacts of rudder profiles are illustrated by comparing the manoeuvring indices of ships equipped with different profiles. In addition, the spacing between the twin rudders (y_{TR}) of TPTR Y1 and TPTR Y2 ($3.8 C_R$ and $4.0 C_R$ respectively) are too large to expect significant rudder interactions. Furthermore,

*This chapter is based on Liu et al. [181] and Liu et al. [182].

y_{TR} of SPTR R1 and TPQR R2 is around $0.90 C_R$ and y_{TU} of TPQR R2 is 1.75 where the interactions are not very significant. In Section 6.2 and Section 6.3, the interactions among multiple rudders on ship manoeuvrability are discussed.

6.1.1. Impacts of rudder profiles on turning

Figure 6.1 shows the trajectories of the reference KVLCC2 tanker (SPSR S1) with different rudder profiles in -15° , 15° , -35° and 35° turning manoeuvres as an example for all the ship types. As discussed in Chapter 4, the wedge-tail series can induce larger normal force than the IFS series and the NACA series. Therefore, the turning circles get smaller when the profiles are changed from the NACA series to the wedge-tail series. This reduction of the turning circles is more significant for the -35° and 35° turning manoeuvres than the -15° and 15° ones.

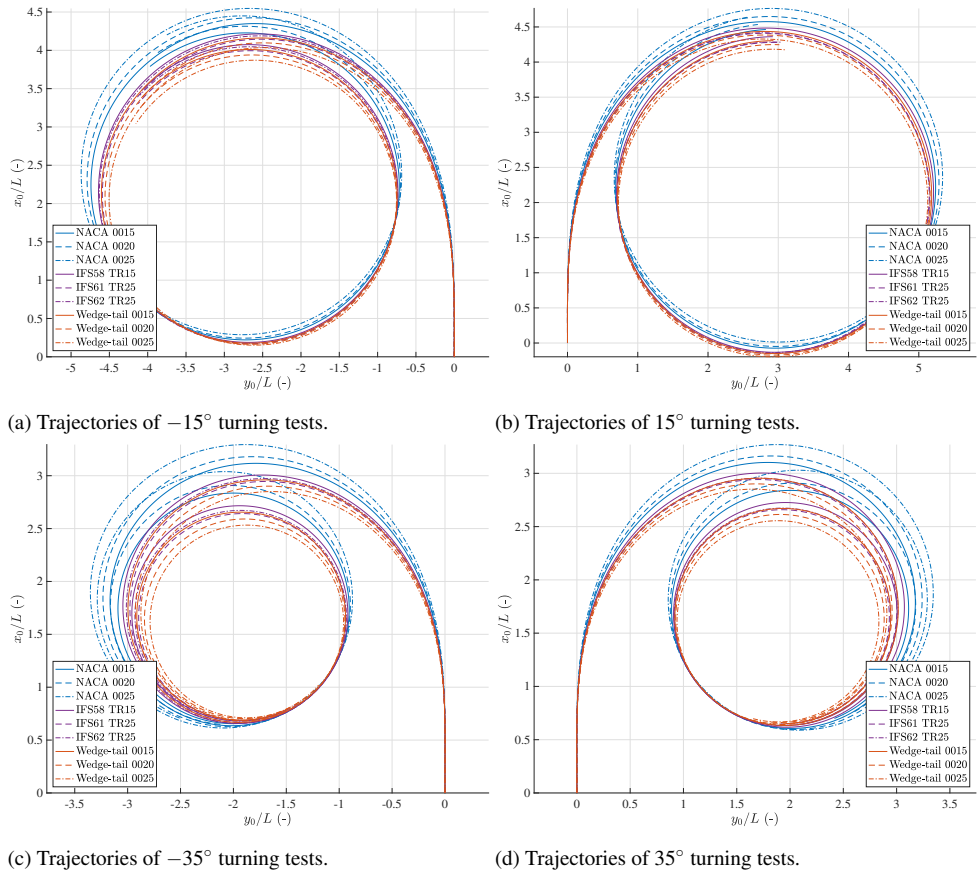
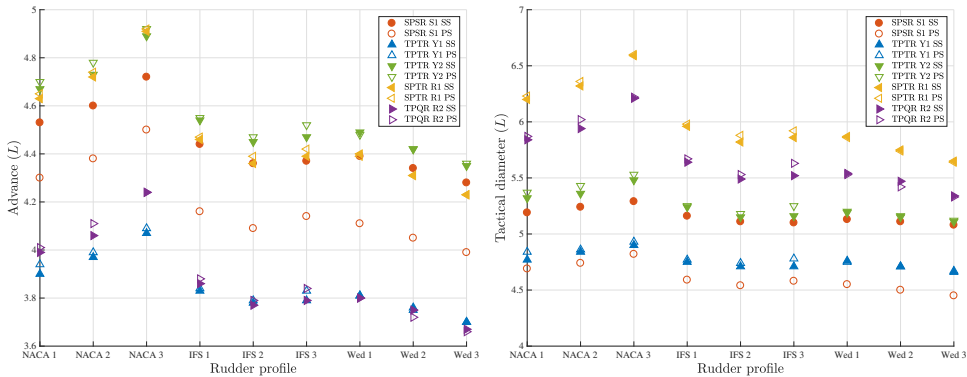


Figure 6.1: Trajectories of the KVLCC2 tanker with different rudder profiles in turning tests.

To improve the turning performance, the advance and the tactical diameter should be minimised and thus the wedge-tail series is the best option for turning. The tactical diameter and the advance of the tested KVLCC2 tanker with the best option of the compared profiles,

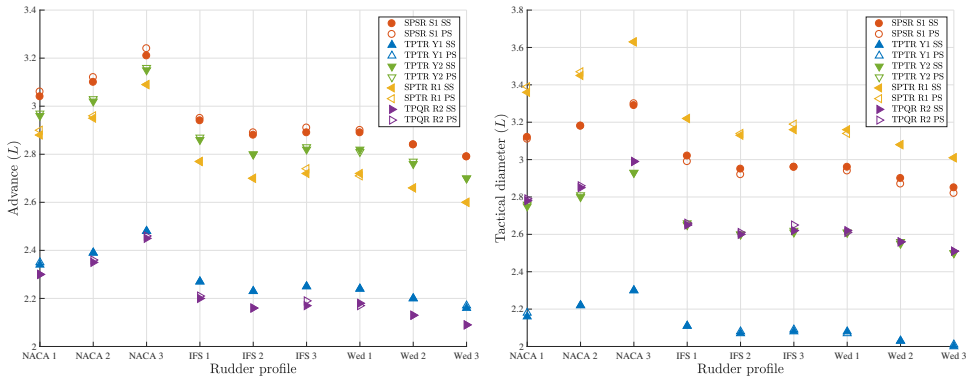
which is the wedge-tail 0025 profile, is about 15 % and 10 % smaller respectively than those with the standard NACA 0018 profile.

Considering the impacts of the rudder profiles on different ships, Figure 6.2 compares the advances and the tactical diameters of the five reference ships with nine profiles. The tendencies of the impacts of the rudder profile on ship manoeuvrability are similar for the tested ships. Effective rudder profiles like the wedge-tail series improve the turning ability of the tested ships. The amounts of improvement in the advances and tactical diameters from the worst case to the best one are similar, which are about 15 % and 10 % respectively.



(a) Advances of ±15° turning tests.

(b) Tactical diameters of ±15° turning tests.



(c) Advances of ±35° turning tests.

(d) Tactical diameters of ±35° turning tests.

Figure 6.2: Turning criteria of the five reference ships with different rudder profiles.

In general, an increase in the number of rudders reduces the advance and the tactical diameter. The differences in the port and the starboard sides turning should be noted due to the asymmetric propeller force (SPSR S1). Additionally, the advances and the tactical diameters of -15° and 15° turning tests are about 1.5 times larger than those of the -35° and 35° tests.

6.1.2. Impacts of rudder profiles on zigzag

Figure 6.3 and Figure 6.4 compare the time histories of rudder angles and heading angles in $-10^\circ/-10^\circ$, $10^\circ/10^\circ$, $-20^\circ/-20^\circ$, and $20^\circ/20^\circ$ zigzag tests of the KVLCC2 tanker (SPSR S1) as a representative of the reference ships. The results show that SPSR S1 with the wedge-tail series responds faster than that with the IFS series and the NACA series. Furthermore, SPSR S1 with the wedge-tail rudders and the IFS rudders have smaller overshoot angles than ships with the NACA rudders. Furthermore, the time that takes from the first overshoot to the second overshoot is decreased significantly.

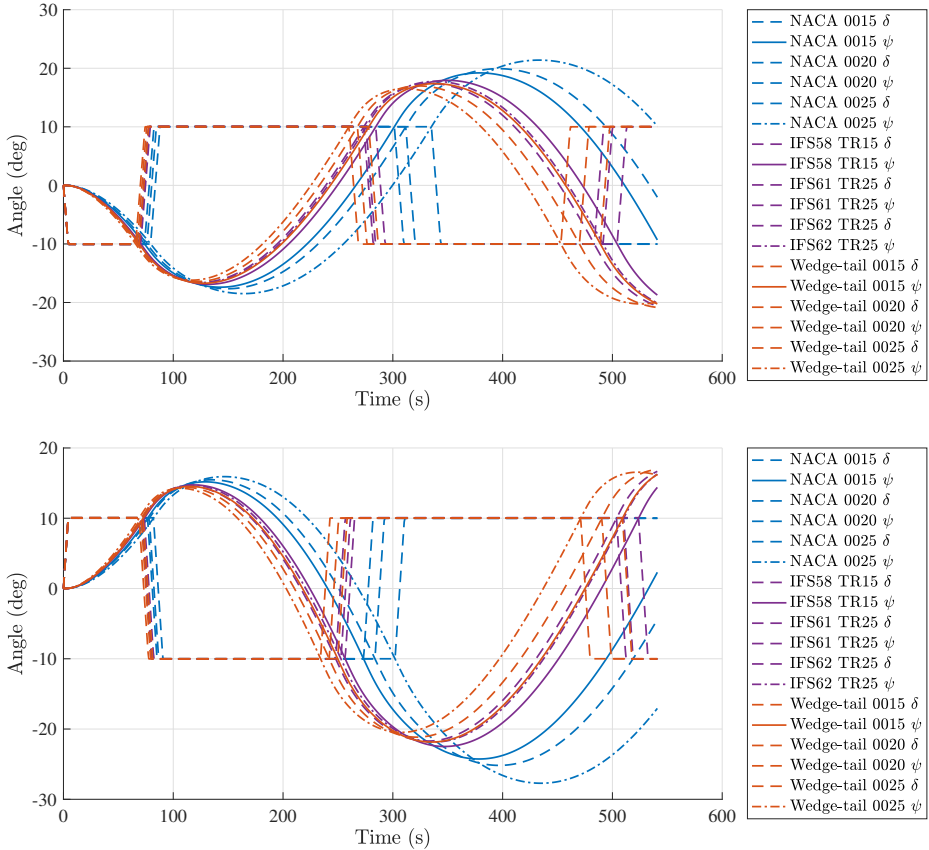


Figure 6.3: Heading angles and rudder angles of the KVLCC2 tanker with different rudder profiles in port and starboard $10^\circ/10^\circ$ zigzag tests.

Figure 6.5 shows the impacts of rudder profiles on the overshoot angles of different ships in various zigzag manoeuvres. The impacts of the ship type is more significant than the rudder profile on zigzag overshoot angles which is logical because the change in the ship types (the number of rudders) increases or decreases the total rudder forces by hundreds of percent while the change in the profiles increases or decreases the total rudder forces by

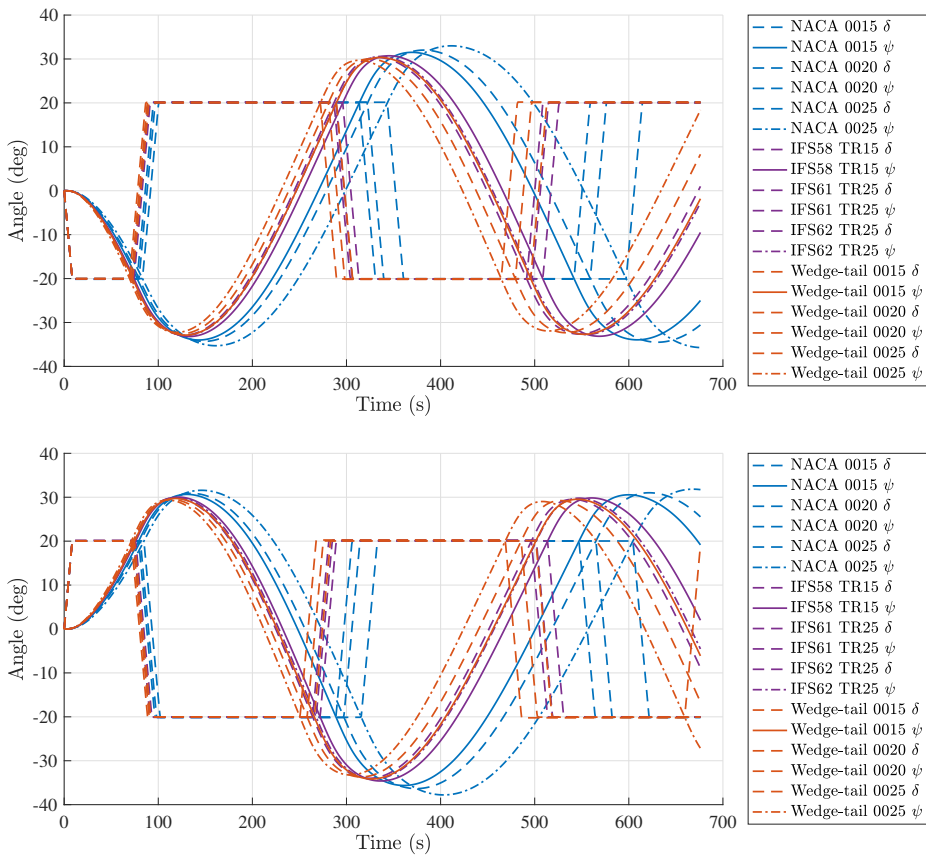
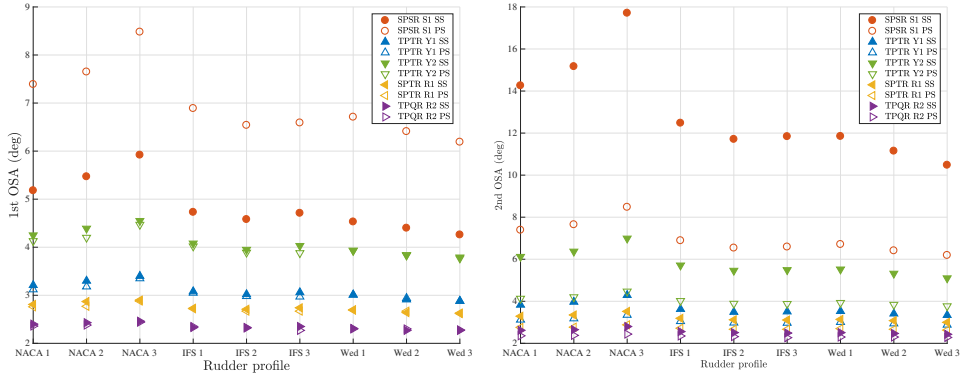
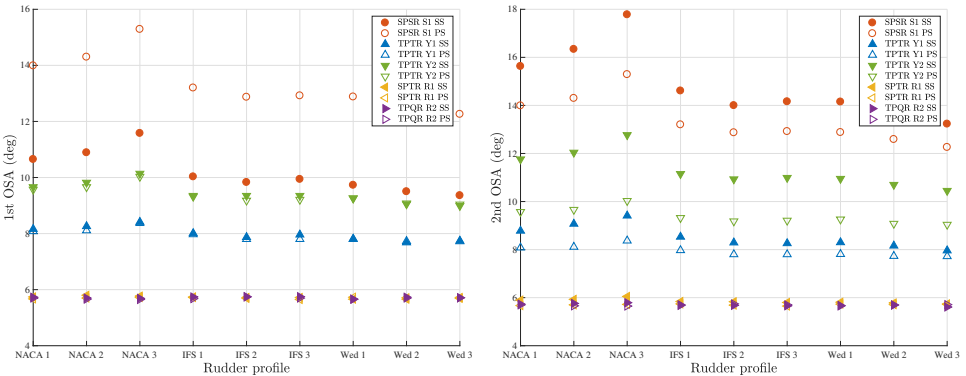


Figure 6.4: Heading angles and rudder angles of the KVLCC2 tanker with different rudder profiles in port and starboard 20°/20° zigzag tests.

tens of percent.



(a) First OSA of $-10^\circ/-10^\circ$ and $10^\circ/10^\circ$ zigzag tests. (b) Second OSA of $-10^\circ/-10^\circ$ and $10^\circ/10^\circ$ zigzag tests.



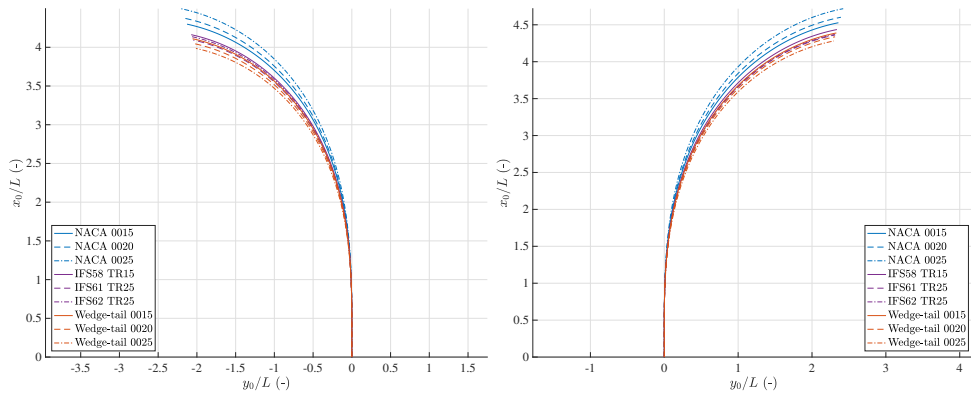
(c) First OSA of $-20^\circ/-20^\circ$ and $20^\circ/20^\circ$ zigzag tests. (d) Second OSA of $-20^\circ/-20^\circ$ and $20^\circ/20^\circ$ zigzag tests.

Figure 6.5: Zigzag criteria of the five reference ships with different rudder profiles.

The SPSR S1 ship shows noticeable differences with different rudder profiles in overshoot angles on port and starboard sides while the differences of other four ships are smaller. Furthermore, the differences caused by the ship type get smaller when the applied rudder angle gets larger. The first and second overshoot angles can be reduced by about 30 % when the most effective profile, wedge-tail 0025, is equipped instead of the standard NACA 0018 profile.

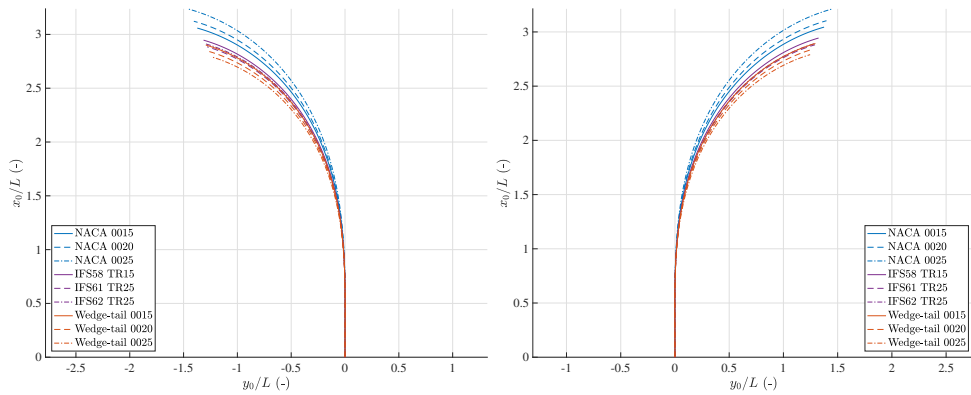
6.1.3. Impacts of rudder profiles on hard turning

Figure 6.6 illustrates the impacts of rudder profiles on the hard turning trajectories of the KVLCC2 tanker. The hard turning manoeuvre is previously defined in Section 3.3.2. The end point of a trajectory is where the ship heading angle changes 90° , which is the advance position of a full turning test. The advance and the transfer increase as the rudder effectiveness decreases. For the KVLCC2 tanker, the advance and the transfer of -15° and 15° hard turning are about 30 % larger than those of -35° and 35° hard turning.



(a) Trajectories of -15° hard turning tests.

(b) Trajectories of 15° hard turning tests.

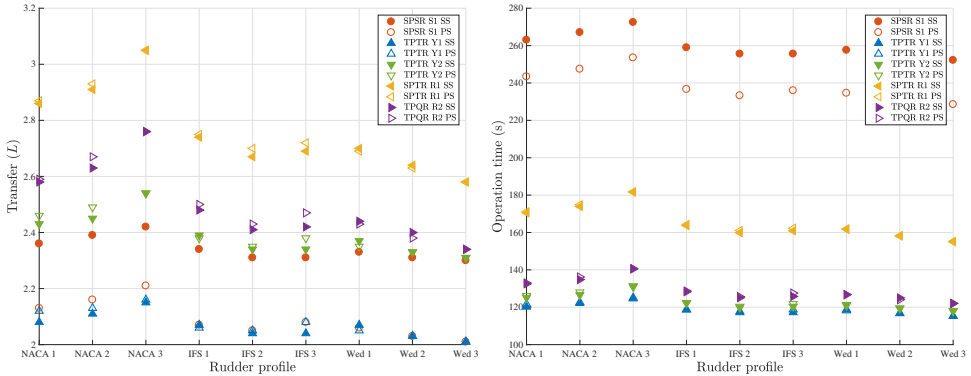


(c) Trajectories of -35° hard turning tests.

(d) Trajectories of 35° hard turning tests.

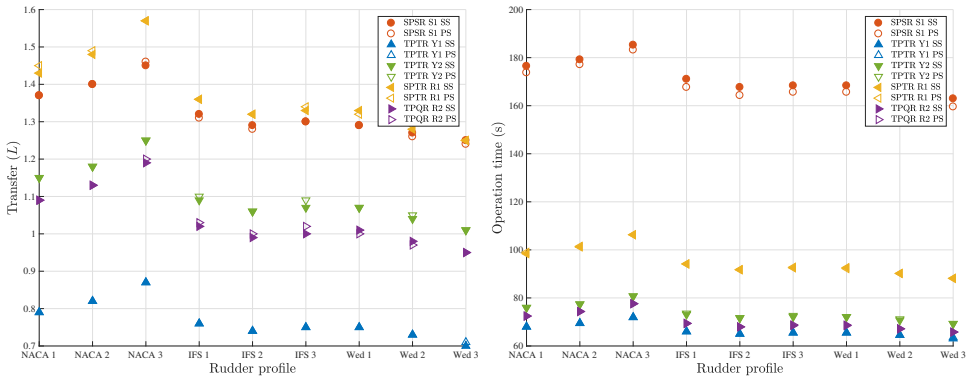
Figure 6.6: Trajectories of the KVLCC2 tanker with different rudder profiles in hard turning tests.

Figure 6.7 presents the impacts of rudder profiles and the ship type on the transfer and the operation time in the hard turning tests. The transfer increases as the profile changes from wedge-tail to NACA and from thin to thick because the rudder forces decrease accordingly. The reference ships take more time to perform hard turning with small rudder angles (-15° and 15°) than those with large rudder angles (-35° and 35°). Furthermore, the operation time is less when more effective profiles are applied like the wedge-tail series. In general, both the transfer and the operation time can be reduced by about 10% through changing the rudder profile.



(a) Transfers of $\pm 15^\circ$ hard turning tests.

(b) Operation time of $\pm 15^\circ$ hard turning tests.



(c) Transfers of $\pm 35^\circ$ hard turning tests.

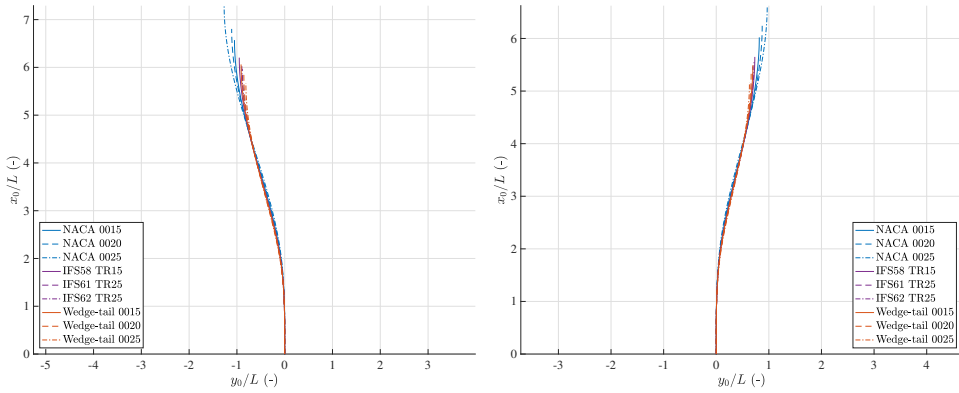
(d) Operation time of $\pm 35^\circ$ hard turning tests.

Figure 6.7: Hard turning criteria of the five reference ships with different rudder profiles.

6.1.4. Impacts of rudder profiles on lane changing

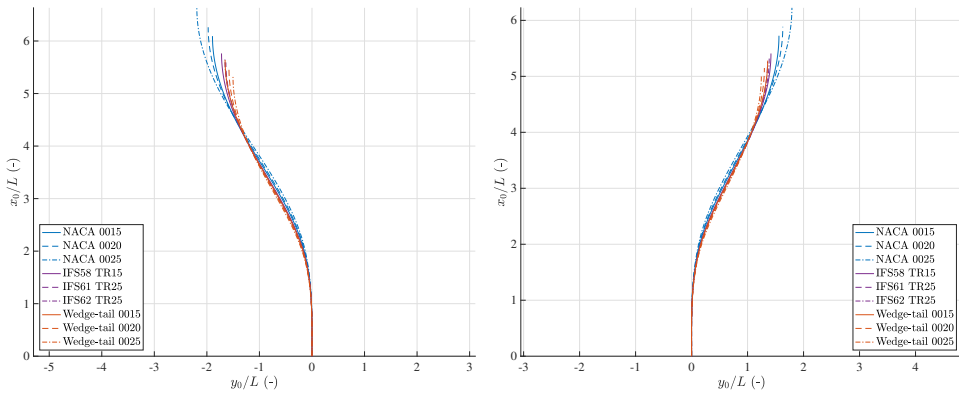
Figure 6.8 shows the trajectories of the KVLCC2 tanker with different profiles in lane changing tests. The lane changing test is defined in Section 3.3.4. The end point of a lane changing trajectory is where the transfer is reached in a normal zigzag test. The transfer should be carefully considered when ships perform lane changing operations like overtaking in narrow waterways. The differences in the trajectories are more significant in the lane

changing tests with larger rudder angles (-20° and 20°) than those with small rudder angles (-10° and 10°).



(a) Trajectories of -10° lane changing tests.

(b) Trajectories of 10° lane changing tests.



(c) Trajectories of -20° lane changing tests.

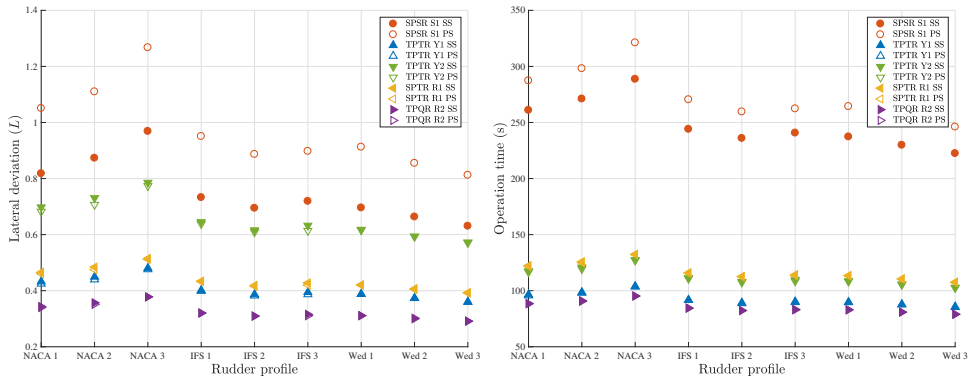
(d) Trajectories of 20° lane changing tests.

Figure 6.8: Trajectories of the KVLCC2 tanker with different rudder profiles in lane changing tests.

Figure 6.9 compares the transfer and the operation time of different ship types with different rudder profiles. Among the reference ships, TPQR R2 achieves the smallest transfer owing to the shortest operation time. A smaller transfer means a lower possibility of ship-bank collision in emergency lane changing operations. Furthermore, a shorter operation time presents a quicker response of the ship to the rudder order, which shows good manoeuvring performance. Depending on the ship and the applied rudder angle for lane changing, the lateral deviations and the operation time can be reduced by about 30 % and 20 % respectively.

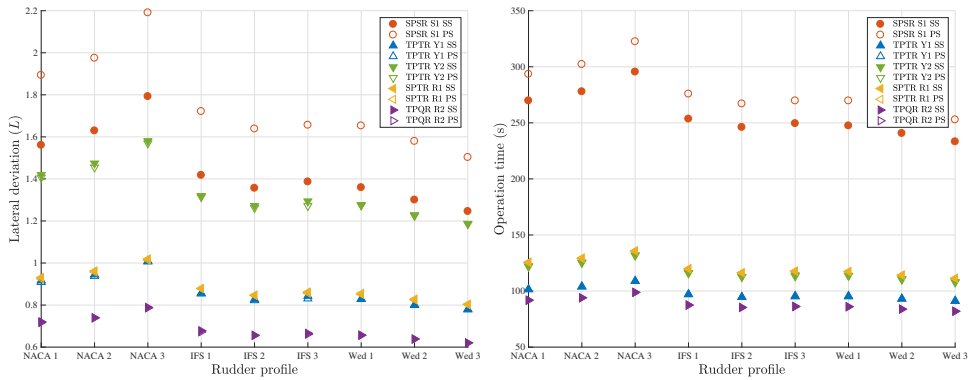
6.1.5. Concluding remarks

Section 6.1 has discussed the impacts of rudder profiles on turning, zigzag, hard turning, and lane changing manoeuvres. The trajectories of the KVLCC2 tanker (SPSR S1) are taken as examples and the manoeuvring criteria of other reference ships are compared.



(a) Lateral deviations of $\pm 10^\circ$ lane changing tests.

(b) Operation time of $\pm 10^\circ$ lane changing tests.



(c) Lateral deviations of $\pm 20^\circ$ lane changing tests.

(d) Operation time of $\pm 20^\circ$ lane changing tests.

Figure 6.9: Lane changing criteria of the five reference ships with different rudder profiles.

In general, reference ships with high-lift profiles like the IFS series and the wedge-tail series commonly have better manoeuvring indices than the more efficient NACA series. For instance, turning indices can be reduced by about 10% by using a thin wedge-tail profile instead of a thick NACA profile.

The impacts of rudder profiles on day-to-day normal operations are not so big, but in an emergency situation, for example, a 35° turn, an effective rudder profile can significantly reduce the tactical diameter, which is important for navigation safety. The impacts of the profiles on the manoeuvring indices of the tested ships are similar. Additionally, ships with more propellers and rudders tend to have better manoeuvring performance than those with fewer propellers and rudders. Therefore, it is recommended to use high-lift profiles and multiple-propeller multiple-rudder configurations from the perspective of good manoeuvrability.

6.2. Spacing between twin rudders

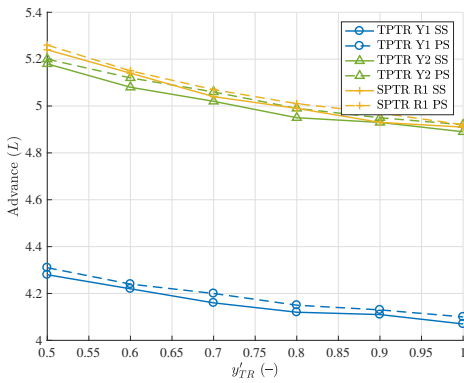
Based on the analyses of the spacing impacts on twin-rudder hydrodynamics in Section 4.3.4, this section presents the impacts of spacing between twin rudders on three reference ships, which are TPTR Y1, TPTR Y2, and SPTR R1 with the NACA 0018 profile. The test range of the non-dimensional spacing between rudders ($y'_{TR} = y_{TR}/C_R$) are $0.5 C_R$ to $1.0 C_R$. Similar to the previous section, manoeuvring simulations are performed in turning (Section 6.2.1), zigzag (Section 6.2.2), hard turning (Section 6.2.3), and lane changing (Section 6.2.4) manoeuvres.

6.2.1. Impacts of spacing between twin rudders on turning

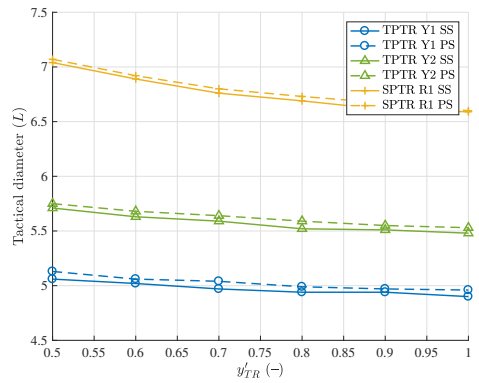
Figure 6.10 illustrates the advances and the tactical diameters of the reference ships with different spacing between the twin rudders (y'_{TR}) in 15° and 35° turning manoeuvres on port and starboard sides. As y'_{TR} increases from 0.5 to 1.0, the advances and the tactical diameters decrease about 5%. The impacts of the spacing on SPTR R1 are slightly more significant than TPTR Y1 and TPTR Y2. Additionally, the ship type does not change the tendency of the impacts of the spacing on the turning indices. Basically, by changing y'_{TR} , both the advances and the tactical diameters of the tested ships in turning manoeuvres can be reduced by about 5%.

6.2.2. Impacts of spacing between twin rudders on zigzag

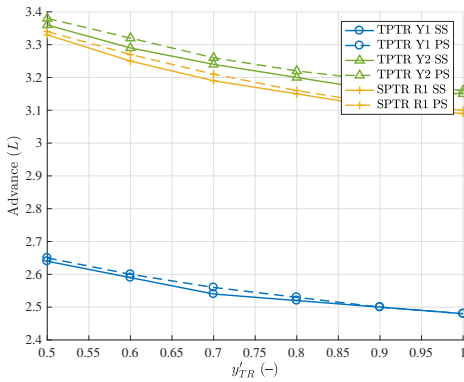
The first and second overshoot angles of TPTR Y1, TPTR Y2, and SPTR R1 with different spacing in 10°/10° and 20°/20° are compared in Figure 6.11. As y'_{TR} decreases, the first and second overshoot angles of the three reference ships get smaller. Changes in overshoot angles are not very significant for TPTR Y1 and SPTR R1 (normal bow and blunt stern) but notable for TPTR Y2 (bulbous bow and slender stern). Additionally, the overshoot angles are almost the same on the starboard and port side zigzag manoeuvres for the tested ships. The presented results show that both the first and the second overshoot angles can be reduced by within 5%.



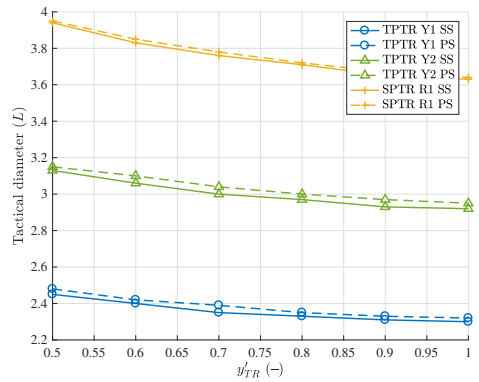
(a) Advances of $\pm 15^\circ$ turning tests.



(b) Tactical diameters of $\pm 15^\circ$ turning tests.

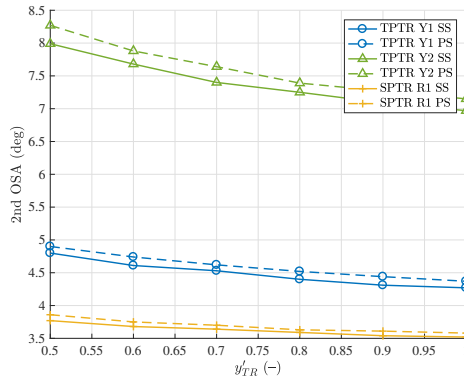
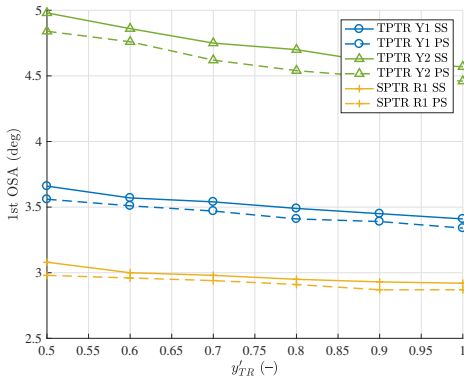


(c) Advances of $\pm 35^\circ$ turning tests.



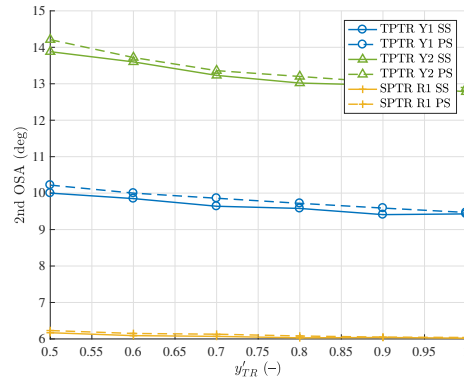
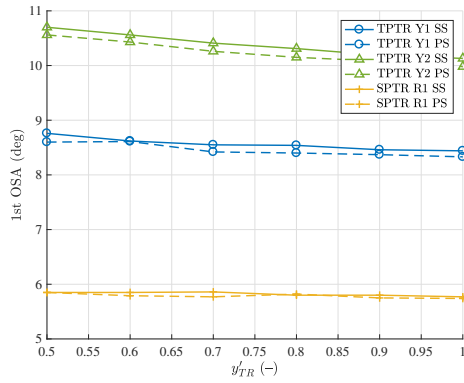
(d) Tactical diameters of $\pm 35^\circ$ turning tests.

Figure 6.10: Turning criteria of twin-rudder ships with different spacing.



(a) First OSA of $-10^\circ/-10^\circ$ and $10^\circ/10^\circ$ zigzag tests.

(b) Second OSA of $-10^\circ/-10^\circ$ and $10^\circ/10^\circ$ zigzag tests.



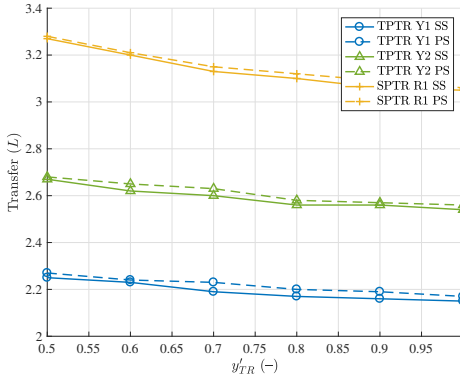
(c) First OSA of $-20^\circ/-20^\circ$ and $20^\circ/20^\circ$ zigzag tests.

(d) Second OSA of $-20^\circ/-20^\circ$ and $20^\circ/20^\circ$ zigzag tests.

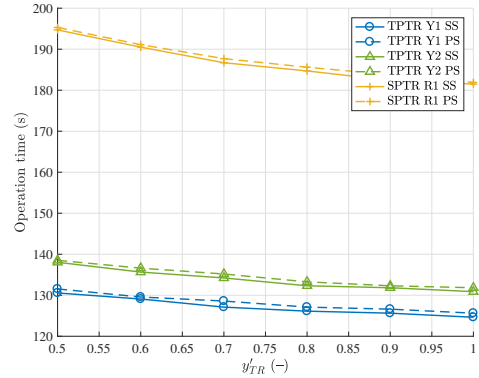
Figure 6.11: Zigzag criteria of twin-rudder ships with different spacing.

6.2.3. Impacts of spacing between twin rudders on hard turning

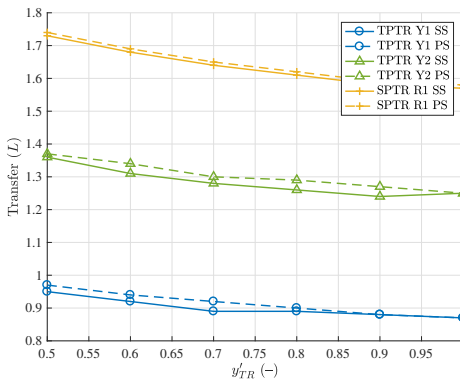
Figure 6.12 presents the transfer and the operation time of different ships with various spacings between twin rudders. As y'_{TR} increases, both the transfer and the operation time decreases. Among the three tested ships, SPTR R1 takes longest time to change the heading angle by 90° , leading to the largest transfer. Considering the transfer and the operation time, TPTR Y1 achieves the best performance of both aspects. After all, Figure 6.12 shows that a 5% reduction in the transfer and the operation time is possible to be achieved by changing y'_{TR} .



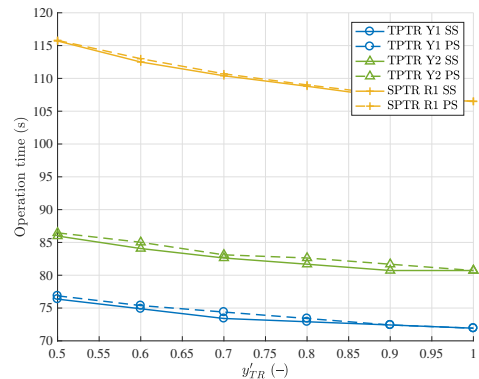
(a) Transfers of $\pm 15^\circ$ hard turning tests.



(b) Operation time of $\pm 15^\circ$ hard turning tests.



(c) Transfers of $\pm 35^\circ$ hard turning tests.



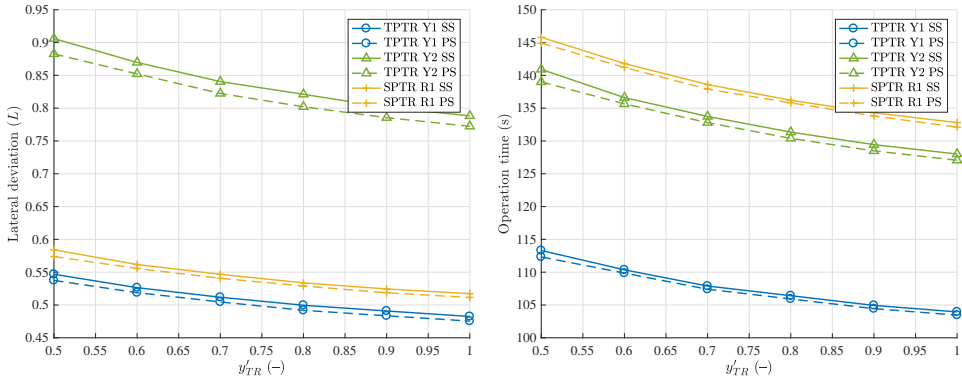
(d) Operation time of $\pm 35^\circ$ hard turning tests.

Figure 6.12: Hard turning criteria of twin-rudder ships with different spacing.

6.2.4. Impacts of spacing between twin rudders on lane changing

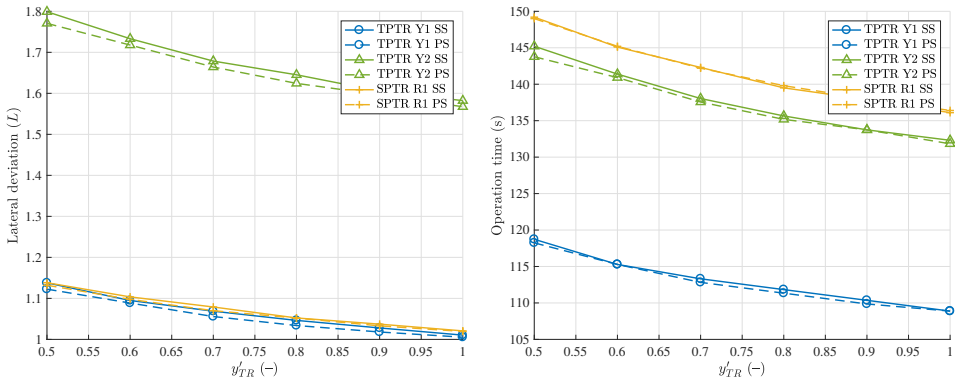
Figure 6.13 compares the lateral deviation and the operation time of three reference ships in lane changing manoeuvres. The lateral deviation decreases as y'_{TR} gets larger, which means safer manoeuvring in restricted waterways. Among the tested ships, TPTR Y2 has the largest lateral deviation but smaller operation time than TPTR Y1, which shows

that TPTR Y2 has a better yaw checking ability and a faster response to the rudder order than TPTR Y1. After all, impacts in y'_{TR} is good for all the tested reference ships as a large spacing can reduce both the lateral deviation and the operation time. Possible reductions in the lateral deviation and the operation time by changing y'_{TR} are about 5 % to 10 %.



(a) Lateral deviations of $\pm 10^\circ$ lane changing tests.

(b) Operation time of $\pm 10^\circ$ lane changing tests.



(c) Lateral deviations of $\pm 20^\circ$ lane changing tests.

(d) Operation time of $\pm 20^\circ$ lane changing tests.

Figure 6.13: Lane changing criteria of twin-rudder ships with different spacing.

6.2.5. Concluding remarks

Section 6.2 has presented the impacts of the spacing between twin rudders on three reference ships in four selected test manoeuvres. In general, as the spacing increases in the range of $0.5 C_R$ to $1.0 C_R$ the reference ships react faster (shorter operation time) and, furthermore, the manoeuvring performance becomes better (smaller advances, transfers, overshoot angles, and lateral deviations). These results are observed with the NACA 0018 profile. Based on the analyse of the profile impacts on ship manoeuvrability in Section 6.1, the spacing impacts with other profiles on ship manoeuvrability are expected to be similar.

6.3. Spacing among quadruple rudders

This section focuses on the impacts of the spacing among quadruple rudders, which are the spacing between the two twin-rudder units (y_{TU}) and the spacing between the twin rudders in each twin-rudder unite (y_{TR}), on quadruple-rudder ship manoeuvrability. Here, the analysis is performed with a 110 m benchmark quadruple-rudder from the Rhine River (TPQR R2) as shown in Table 5.1. Similar to the previous sections, test manoeuvres are turning (Section 6.3.1), zigzag (Section 6.3.2), hard turning (Section 6.3.3), and lane changing (Section 6.3.4). The test profile is NACA 0018. Additionally, y_{TU} and y_{TR} are varied in 3 steps.

6.3.1. Impacts of spacing among quadruple rudders on turning

Figure 6.14 presents the manoeuvring indices of TPQR R2 in 15° and 35° turning tests on port and starboard sides, where y_{TU} and y_{TR} are non-dimensionalised with C_R . As y_{TU} and y_{TR} increase, the rudder hydrodynamic performance gets better as previously discussed in Section 4.3.5. Therefore, the advances and the transfers are reduced with increases in y'_{TU} and y'_{TR} . The impacts of y'_{TU} and y'_{TR} are more significant on the 15° turning manoeuvres than the 35° turning manoeuvres as the operation time of the 15° turning manoeuvres is larger than that of the 35° turning manoeuvres. In general, the advances and the tactical diameters can be reduced about 15 % by enlarging y'_{TU} and y'_{TR} from 0.5 and 0.5 to 1.5 and 1.0 respectively.

6.3.2. Impacts of spacing among quadruple rudders on zigzag

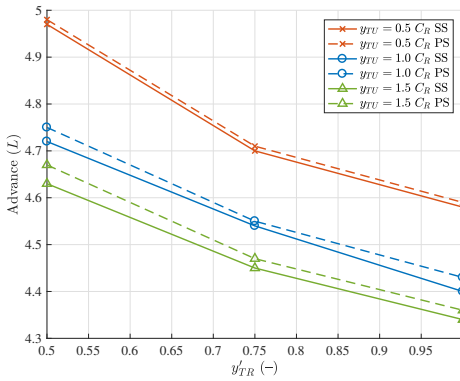
Figure 6.15 presents the first and second overshoot angles of TPQR R2 with different y'_{TU} and y'_{TR} in $-10^\circ/-10^\circ$, $10^\circ/10^\circ$, $-20^\circ/-20^\circ$, and $20^\circ/20^\circ$ zigzag tests. The impacts of y'_{TU} and y'_{TR} on the first overshoot angles are smaller than those on the second overshoot angles, especially for the first overshoot angles of $-20^\circ/-20^\circ$ and $20^\circ/20^\circ$ which are different within 1 %. Basically, as y'_{TU} and y'_{TR} become larger, overshoot angles get smaller. The possible decrease in overshoot angles caused by enlarging y'_{TU} and y'_{TR} can be 5 % to 10 %.

6.3.3. Impacts of spacing among quadruple rudders on hard turning

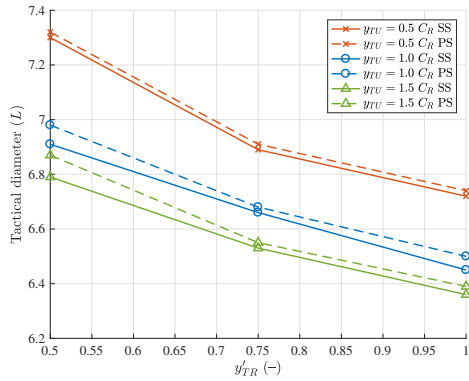
Figure 6.16 shows the transfer and the operation time of TPQR R2 in $\pm 15^\circ$ and $\pm 35^\circ$ hard turning manoeuvres. As y'_{TU} and y'_{TR} get larger, both the transfer and the operation time decrease. With the same y'_{TR} , the differences of the transfer and the operation time are larger by increasing y'_{TU} from $0.5 C_R$ to $1.0 C_R$ than increasing y'_{TU} from $1.0 C_R$ to $1.5 C_R$, which is caused by the stronger interaction effects on the rudder hydrodynamics due to smaller spacings. Additionally, the asymmetry of the port side and the starboard side manoeuvring is not significant. In summary, by enlarging y'_{TU} and y'_{TR} , the transfer and the operation time of the tested quadruple-rudder ship can be reduced by about 10 %.

6.3.4. Impacts of spacing among quadruple rudders on lane changing

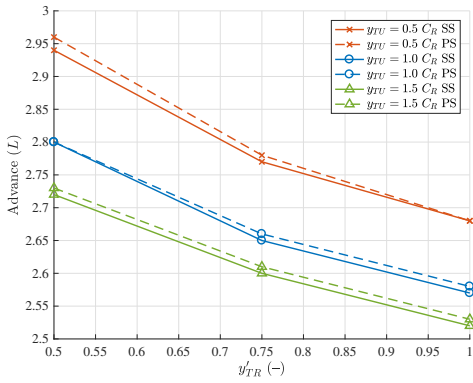
Figure 6.17 shows the impacts of changing y'_{TU} and y'_{TR} on the lateral deviation and the operation time of TPQR R2 in 10° and 20° lane changing on port and starboard sides.



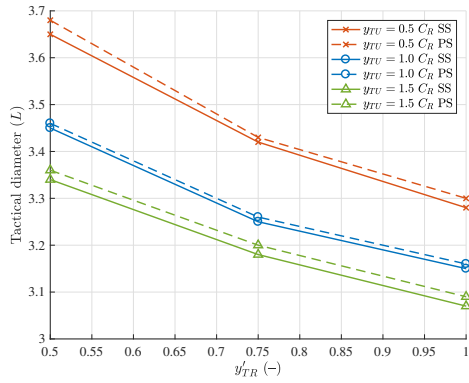
(a) Advances of $\pm 15^\circ$ turning tests.



(b) Tactical diameters of $\pm 15^\circ$ turning tests.

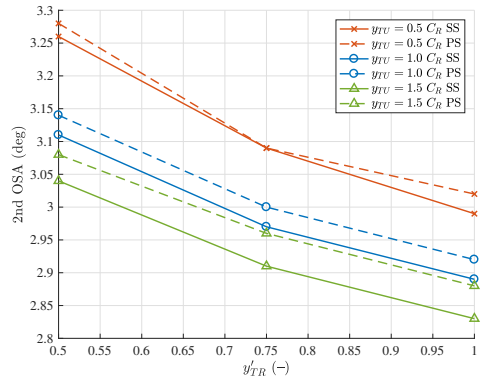
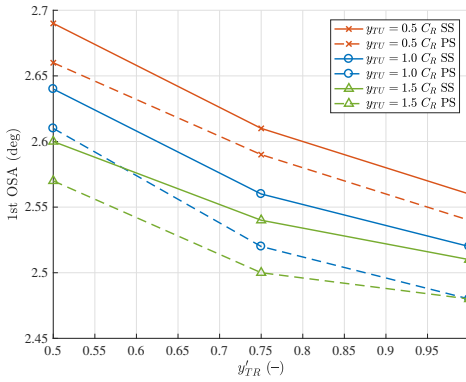


(c) Advances of $\pm 35^\circ$ turning tests.



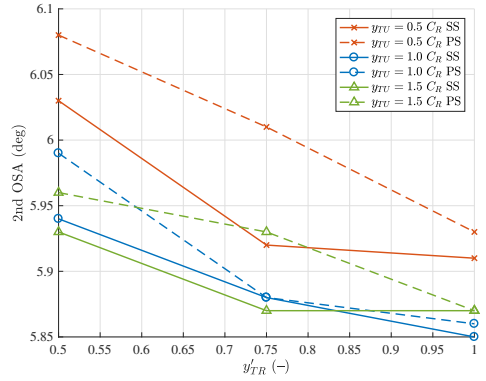
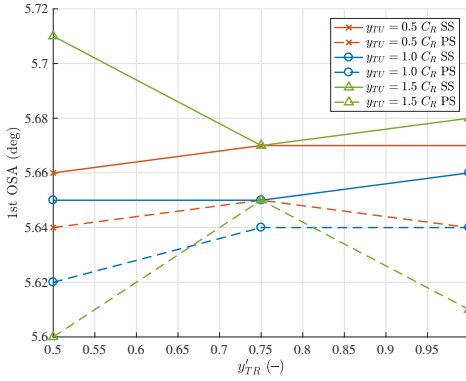
(d) Tactical diameters of $\pm 35^\circ$ turning tests.

Figure 6.14: Turning criteria of quadruple-rudder ships with different spacing.



(a) First OSA of $-10^\circ/-10^\circ$ and $10^\circ/10^\circ$ zigzag tests.

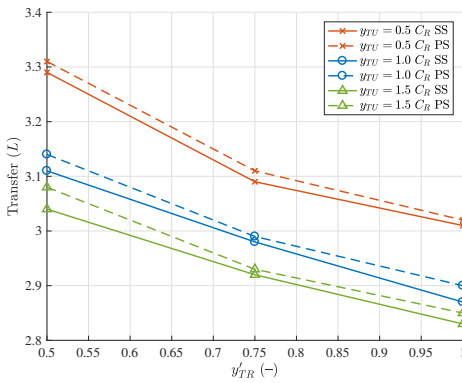
(b) Second OSA of $-10^\circ/-10^\circ$ and $10^\circ/10^\circ$ zigzag tests.



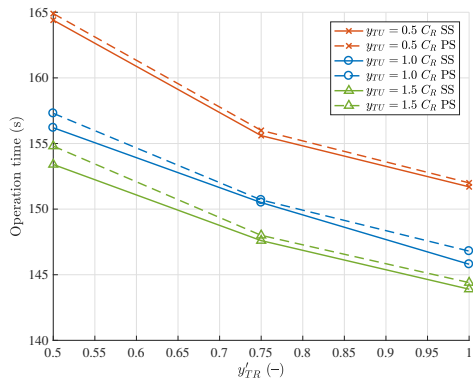
(c) First OSA of $-20^\circ/-20^\circ$ and $20^\circ/20^\circ$ zigzag tests.

(d) Second OSA of $-20^\circ/-20^\circ$ and $20^\circ/20^\circ$ zigzag tests.

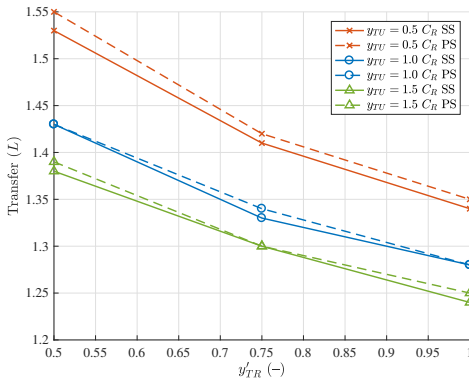
Figure 6.15: Zigzag criteria of quadruple-rudder ships with different spacing.



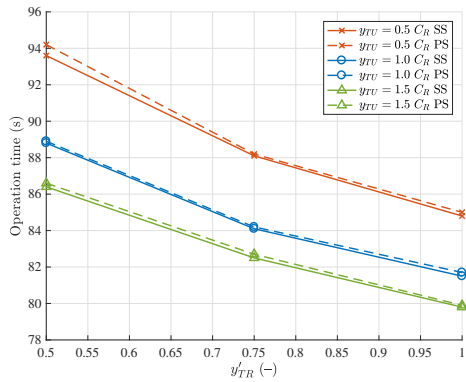
(a) Transfers of $\pm 15^\circ$ hard turning tests.



(b) Operation time of $\pm 15^\circ$ hard turning tests.



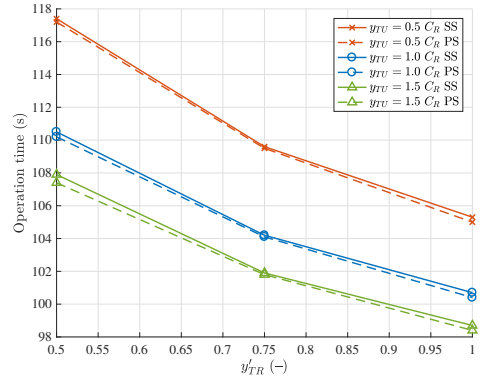
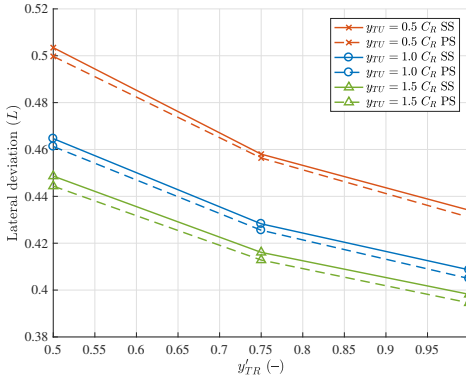
(c) Transfers of $\pm 35^\circ$ hard turning tests.



(d) Operation time of $\pm 35^\circ$ hard turning tests.

Figure 6.16: Hard turning criteria of quadruple-rudder ships with different spacing.

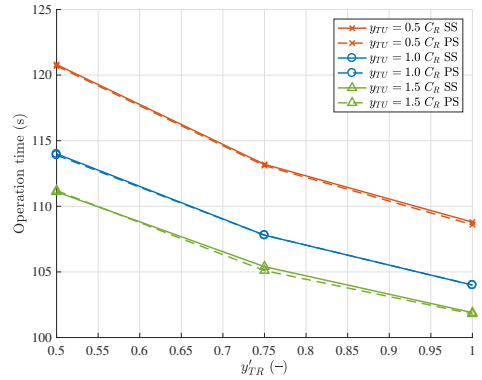
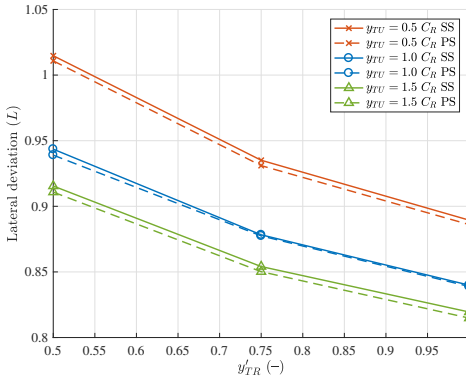
The decrease caused by increasing y'_{TU} and y'_{TR} in the lateral deviation is 10 % to 15 %. Accordingly, the operation time can be reduced by about 10 %. The decreases in the lateral deviation and the operation time can be taken as a reduction of the risks of overtaking in narrow waterways.



(a) Lateral deviations of $\pm 10^\circ$ lane changing tests.

(b) Operation time of $\pm 10^\circ$ lane changing tests.

6



(c) Lateral deviations of $\pm 20^\circ$ lane changing tests.

(d) Operation time of $\pm 20^\circ$ lane changing tests.

Figure 6.17: Lane changing criteria of quadruple-rudder ships with different spacing.

6.3.5. Concluding remarks

Section 6.3 has studied the impacts of spacing among quadruple rudders on the reference ship TPQR R2 in turning, zigzag, hard turning, and lane changing manoeuvres. As the non-dimensional spacing between the twin-rudder units (y'_{TU}) and the spacing between the twin rudders (y'_{TR}) of each unit increase, the manoeuvring criteria like the advance, the tactical diameter, the lateral deviation, and the operation time decrease. Therefore, a better manoeuvring performance is achievable by enlarging y'_{TU} and y'_{TR} .

6.4. Synthesis

This chapter applied the integrated manoeuvring model (Chapter 5) with the rudder hydrodynamic characteristics of different single-rudder, twin-rudder, and quadruple-rudder configurations (Chapter 4) in the classic and proposed turning, zigzag, hard turning, and lane changing manoeuvres (Chapter 3). The presented results show the impacts of rudder configurations and answer the third research question in Section 1.3: *How do changes in the rudder configuration affect the ship manoeuvrability in specific manoeuvres?* Conclusions of this chapter are drawn as follows:

- Various rudder profiles have different hydrodynamic characteristics, which eventually affect ship manoeuvrability. By changing the rudder profile, the manoeuvring indices can be improved by 10 % to 30 % in different manoeuvres.
- Among the tested profiles, the wedge-tail series is most effective and the NACA series is most efficient. The IFS series achieves a balance between the efficiency and effectiveness.
- Basically, profiles with a better hydrodynamic performance will result in a better manoeuvring performance, such as smaller turning circle trajectories, advances, tactical diameters, transfers, overshoot angles, lateral deviations, and operation time.
- As the spacing between twin rudders increase, the twin-rudder reference ships get better manoeuvring performance. The manoeuvring indices can be reduced by 5 % to 15 % by enlarging the spacing.
- As the spacing among quadruple rudders, especially the spacing between the two twin-rudder units, increases, the ship manoeuvring performance improves. Additionally, the possible reduction of the manoeuvring indices is about 10 %.
- With the same rudder profile, ships with more propellers and rudders tend to have better manoeuvring performance than those with fewer propellers and rudders.

Ship rudder design primarily depends on the sailing conditions and the shipping purpose. In Chapter 6, the impacts of the rudder configuration are primarily analysed on ship manoeuvrability, which is one of the important aspects of rudder design. In Chapter 7, the impacts of the rudder configuration on the rudder induced resistance will be briefly discussed. Other aspects should also be considered to choose a proper rudder such as the rudder torque, the rudder impacts on the propeller performance, and the rudder cavitation. Further research is suggested to improve the efficiency of the rudder while maintaining sufficient effectiveness. It should be noted that the above conclusions are achieved based on a small range of benchmark ships.

Chapter 7

Guidance on Rudder Configurations*

*“Thought is the wind, knowledge the sail,
and mankind the vessel.”*

Augustus Hare (1834 – 1903)

This chapter summarises the research of the previous chapters to provide guidance for naval architects to choose a proper rudder configuration. Section 7.1 defines the working conditions of the rudders in practice. Section 7.2, Section 7.3, and Section 7.4 offer guidance on the rudder profile, the rudder parameters, and the rudder type of a rudder configuration respectively. Section 7.5 and Section 7.6 give reference values of the rudder impacts on manoeuvrability and resistance. Section 7.8 draws the conclusions of this chapter.

7.1. Working conditions

As reviewed in Chapter 2, the rudder performance depends on its working conditions, including, but not limited to, the Reynolds number and the angle of attack. Thus, operational profiles of the ship should be considered in the process of the rudder design. A high Reynolds number can be achieved in tests by either enlarging the model size or increasing the inflow speed. Presently, model tests at high-Reynolds-number or full-scale ship tests are not practical for primary studies due to the capacity of the test facilities or high expense. Another possible approach is the high-Reynolds-number CFD study, which is applied in Chapter 4.

Considering the cost of high-Reynolds-number simulations with either model tests or CFD simulations, it is recommended to carry out tests at Reynolds numbers that are as low as possible, without compromising the quality of the results. A Reynolds number of 6×10^6 is recommended, above which the rudder hydrodynamic characteristics are not significantly affected by the change in the Reynolds number. The range of applied rudder angles is -35° to 35° , which should be the main region of interest in the rudder hydrodynamics. Histograms of applied rudder angles and ship speeds like Figure 2.2 are valuable for further studies on ship manoeuvring performance and fuel consumption.

7.2. Rudder profiles

Through the previous reviews (Chapter 2) and CFD studies (Chapter 4), it is clear that different rudder profiles have different hydrodynamic characteristics, namely lift and drag

*This chapter is based on Liu and Hekkenberg [177], Liu et al. [180], and Liu et al. [182].

coefficients, the slope of the lift curve, the stall angle, and the lift to drag ratio. These differences in the characteristics of the profile should be carefully considered in the rudder design. Furthermore, it is recommended to build up a uniform definition of the shapes of wedge-tail and fishtail profiles to make research outcomes easier to verify and expand upon existing research. In general, the choice of the rudder profile should depend on ship particulars, operational requirements of manoeuvring performance, and fuel conservation.

For seagoing ships which sail long distance and commonly have tug assistance for hard manoeuvring in the port area, the efficiency of the rudder may have a higher priority than the effectiveness. Thus, on the prerequisite of sufficient rudder force for course keeping and manoeuvring, highly efficient profiles are suggested, such as NACA, HSVA, and IFS. For ships that mainly sail in constrained waterways like inland vessels, the effectiveness of the rudder is more crucial than efficiency. Therefore, high-lift profiles, including fishtail and wedge-tail, are proposed. Especially, when the applicable rudder area is limited due to ship draught or water depth, high-lift profiles are favourable. If the manoeuvrability of the ship is the key, the effectiveness can be the primary concern while the efficiency can be sacrificed.

As a general rule, thinner rudders have better hydrodynamic performance than thicker ones. The structural requirement and the hydrodynamic performance have to be considered in coincidence with the determination of the rudder thickness. With a prerequisite of the total rudder area, large span means short chord, furthermore, a large geometric aspect ratio, which is desirable for both efficiency and effectiveness. The span, the chord, and the geometric aspect ratio are commonly limited in a routine range, but the effective aspect ratio can be enlarged by adding end plates on the tip and the root of the rudder. All things considered, lift is nearly always gained at the expense of drag. A wise decision of the rudder profile should coincide with the objective of the design of the ship.

7.3. Rudder parameters

Besides the rudder profile, the rudder parameters specify how the rudder is shaped in 3D. The rudder performance is the end product of all these parameters. First of all, the total area should be sufficiently large as it is a determinant factor of the amount of rudder force. The reference values of the total area are given in Table 2.1. When the area of a single rudder is not sufficient, multiple-rudder configurations are recommended for inland vessels because of the limited ship draught due to the enlargement of the ship dimensions. The increase in the total rudder area leads to an improvement in the ship manoeuvrability but makes the rudder induced resistance larger. Therefore, for ships with a large rudder area, the selection of the rudder profile becomes even more crucial. As a summary, to maximise the ship manoeuvrability, large total rudder area, small thickness, large span, short chord, large geometric and effective aspect ratios are recommended.

7.4. Rudder types

Nowadays, conventional propeller-rudder systems still hold a dominant position on merchant ships. Even though active steering devices have been developing rapidly for offshore engineering, the conventional rudders can still provide good performance regarding bol-

lard pull, response times, and cruise behaviour [170]. Following consideration of the rudder type, spade rudders and semi-skeg rudders are primarily contemporary design choices. From the perspective of hydrodynamics, spade rudders are better than semi-skeg rudders for ship manoeuvrability and fuel consumption. Thus, it is proposed to take the spade rudder as a first choice. However, the area of a spade rudder might be limited due to high bending moment. Semi-skeg rudders are recommended for large seagoing ships which require an extraordinary large rudder area.

7.5. Ship manoeuvrability

In Chapter 6, the impacts of rudder configurations on ship manoeuvrability are discussed in details. Table 7.1 provides the average manoeuvring indices of the reference ships (Table 5.1) as indicators, namely the advance (A_D) and the tactical diameter (T_D) that are averaged from $\pm 15^\circ$, $\pm 25^\circ$, $\pm 35^\circ$ turning tests, the first and second overshoot angles (ψ_{O1} and ψ_{O2}) that are averaged from $\pm 10^\circ$, $\pm 15^\circ$, $\pm 20^\circ$ zigzag tests, the transfer (T_r) and the operation time (t_T) that are averaged from $\pm 15^\circ$, $\pm 25^\circ$, $\pm 35^\circ$ hard turning tests, the lateral deviation (L_D) and the operation time (t_L) that are averaged from $\pm 10^\circ$, $\pm 15^\circ$, $\pm 20^\circ$ lane changing tests.

In Table 7.1, the colour legends are marked based on the values of each parameter. The best available configuration among the test cases is the darkest green and the worst is the darkest red. Other colours between the darkest green to the darkest red show the transition. These colour legends are presented to help naval architects to quickly compare the performance of their choice in each aspect of the manoeuvring performance.

Figure 7.1, Figure 7.2, Figure 7.3, and Figure 7.4 present the impacts of the rudder configurations on the averaged manoeuvring criteria in four aspects which are single-rudder profiles, twin-rudder profile, twin-rudder spacing, and quadruple-rudder spacing. These figures show how the ship manoeuvring performance depends on the design of the rudder configuration. Naval architects can use these figures as a reference to quickly access the performance of their initial designs.

As a summary, to achieve a good manoeuvring performance, the rudder configuration should be optimised towards the more effective rudder profiles and larger spacing among rudders. Additionally, the rudder induced resistance or the power consumed by the rudder induced resistance should be considered to have a balance performance in both manoeuvring performance and fuel consumption. Impacts of rudder configurations on ship resistance will be briefly discussed in Section 7.6.

7.6. Ship resistance

In Section 2.3.2, Figure 2.2 presents the probability distributions of the applied rudder angles for an inland vessel that sails from Antwerp, Belgium to Vlaardingen, the Netherlands and then from Vlaardingen, the Netherlands to Hamm, Germany. This inland vessel is almost as the same as one of the reference inland vessels, namely SPTR R1, in Table 5.1. This inland vessel equips a single ducted propeller and twin asymmetric fishtail rudders with top and bottom and plates. Based on Figure 2.2, the probability distributions of the rudder angles in the range of -35° to 35° are refined and shown in Figure 7.5. This range

Table 7.1: Impacts of rudder configurations on the average manoeuvring indices.

Ship	Profile	n_R (-)	y_{TR} (C_R)	y_{TU} (C_R)	\overline{A}_D (L)	\overline{T}_D (L)	$\overline{\psi}_{O1}$ (deg)	$\overline{\psi}_{O2}$ (deg)	\overline{T}_r (L)	\overline{t}_r (L)	\overline{L}_D (L)	\overline{t}_L (s)
SPSR S1	NACA 0012	1	—	—	3.65	3.93	9.28	12.73	1.76	209.37	1.33	276.31
SPSR S1	NACA 0015	1	—	—	3.66	3.94	9.37	12.84	1.76	209.94	1.34	278.11
SPSR S1	NACA 0018	1	—	—	3.69	3.97	9.49	13.19	1.78	211.74	1.37	282.39
SPSR S1	NACA 0020	1	—	—	3.72	4.00	9.66	13.59	1.79	213.43	1.41	287.47
SPSR S1	NACA 0025	1	—	—	3.84	4.09	10.45	15.20	1.84	219.29	1.58	307.41
SPSR S1	IFS58 TR15	1	—	—	3.55	3.85	8.77	11.63	1.72	204.41	1.22	261.10
SPSR S1	IFS61 TR25	1	—	—	3.48	3.79	8.50	11.04	1.69	200.92	1.15	252.31
SPSR S1	IFS62 TR25	1	—	—	3.50	3.81	8.57	11.28	1.70	202.16	1.17	255.46
SPSR S1	Wedge-tail 0015	1	—	—	3.50	3.80	8.52	11.10	1.70	202.27	1.16	254.79
SPSR S1	Wedge-tail 0020	1	—	—	3.44	3.75	8.26	10.62	1.67	199.12	1.11	246.56
SPSR S1	Wedge-tail 0025	1	—	—	3.39	3.70	8.04	10.15	1.65	196.30	1.05	238.67
TPTR Y1	NACA 0015	2	1.0	—	3.03	3.30	5.59	6.37	1.36	90.90	0.67	98.62
TPTR Y1	NACA 0018	2	1.0	—	3.06	3.33	5.62	6.47	1.37	91.80	0.68	99.93
TPTR Y1	NACA 0020	2	1.0	—	3.08	3.35	5.66	6.55	1.38	92.29	0.69	101.08
TPTR Y1	NACA 0025	2	1.0	—	3.18	3.43	5.83	6.89	1.43	94.92	0.74	106.17
TPTR Y1	IFS58 TR15	2	1.0	—	2.95	3.24	5.45	6.08	1.32	88.68	0.63	94.26
TPTR Y1	IFS61 TR25	2	1.0	—	2.90	3.21	5.35	5.89	1.30	87.61	0.60	91.80
TPTR Y1	IFS62 TR25	2	1.0	—	2.92	3.22	5.38	5.98	1.31	88.02	0.61	92.62
TPTR Y1	Wedge-tail 0015	2	1.0	—	2.92	3.22	5.33	5.89	1.31	88.35	0.61	92.54
TPTR Y1	Wedge-tail 0020	2	1.0	—	2.87	3.17	5.25	5.77	1.28	86.87	0.59	90.32
TPTR Y1	Wedge-tail 0025	2	1.0	—	2.83	3.14	5.23	5.62	1.27	85.64	0.57	88.27
TPTR Y1	NACA 0018	2	0.5	—	3.37	1.52	6.10	7.49	1.52	100.26	0.84	115.61
TPTR Y1	NACA 0018	2	0.6	—	3.31	1.49	6.02	7.32	1.49	98.62	0.81	112.66
TPTR Y1	NACA 0018	2	0.7	—	3.26	1.47	5.94	7.18	1.47	97.22	0.78	110.27
TPTR Y1	NACA 0018	2	0.8	—	3.23	1.45	5.91	7.06	1.45	96.40	0.77	108.80
TPTR Y1	NACA 0018	2	0.9	—	3.20	1.44	5.86	6.95	1.44	95.58	0.75	107.32
TPTR Y1	NACA 0018	2	1.0	—	3.18	1.43	5.82	6.89	1.43	95.00	0.74	106.25
TPQR R2	NACA 0018	4	0.5	0.5	3.84	5.25	4.16	4.67	2.31	124.97	0.76	119.05
TPQR R2	NACA 0018	4	0.5	1.0	3.65	4.96	4.12	4.55	2.17	118.50	0.70	112.12
TPQR R2	NACA 0018	4	0.5	1.5	3.56	4.85	4.10	4.51	2.11	115.93	0.68	109.35
TPQR R2	NACA 0018	4	0.8	0.5	3.62	4.93	4.12	4.54	2.15	117.77	0.70	111.30
TPQR R2	NACA 0018	4	0.8	1.0	3.48	4.73	4.07	4.44	2.05	113.07	0.65	105.95
TPQR R2	NACA 0018	4	0.8	1.5	3.41	4.63	4.07	4.41	2.00	110.87	0.63	103.57
TPQR R2	NACA 0018	4	1.0	0.5	3.51	4.77	4.08	4.46	2.07	113.95	0.66	106.93
TPQR R2	NACA 0018	4	1.0	1.0	3.38	4.58	4.06	4.38	1.97	109.70	0.62	102.32
TPQR R2	NACA 0018	4	1.0	1.5	3.32	4.50	4.05	4.36	1.93	107.82	0.61	100.20

Note:

n_R is the number of rudders.

y_{TR} is the spacing between the twin rudders of twin-rudder configurations.

y_{TU} is the spacing between the two twin-rudder units of quadruple-rudder configurations.

\overline{A}_D is the averaged advances of $\pm 15^\circ$, $\pm 25^\circ$, $\pm 35^\circ$ turning tests.

\overline{T}_D is the averaged tactical diameter of $\pm 15^\circ$, $\pm 25^\circ$, $\pm 35^\circ$ turning tests.

$\overline{\psi}_{O1}$ is the averaged first overshoot angle of $\pm 10^\circ$, $\pm 15^\circ$, $\pm 20^\circ$ zigzag tests.

$\overline{\psi}_{O2}$ is the averaged second overshoot angle of $\pm 10^\circ$, $\pm 15^\circ$, $\pm 20^\circ$ zigzag tests.

\overline{T}_r is the averaged transfer of $\pm 15^\circ$, $\pm 25^\circ$, $\pm 35^\circ$ hard turning tests.

\overline{t}_r is the averaged operation time of $\pm 15^\circ$, $\pm 25^\circ$, $\pm 35^\circ$ hard turning tests.

\overline{L}_D is the averaged lateral deviation of $\pm 15^\circ$, $\pm 25^\circ$, $\pm 35^\circ$ lane changing tests.

\overline{t}_D is the averaged operation time of $\pm 10^\circ$, $\pm 15^\circ$, $\pm 20^\circ$ lane changing tests.

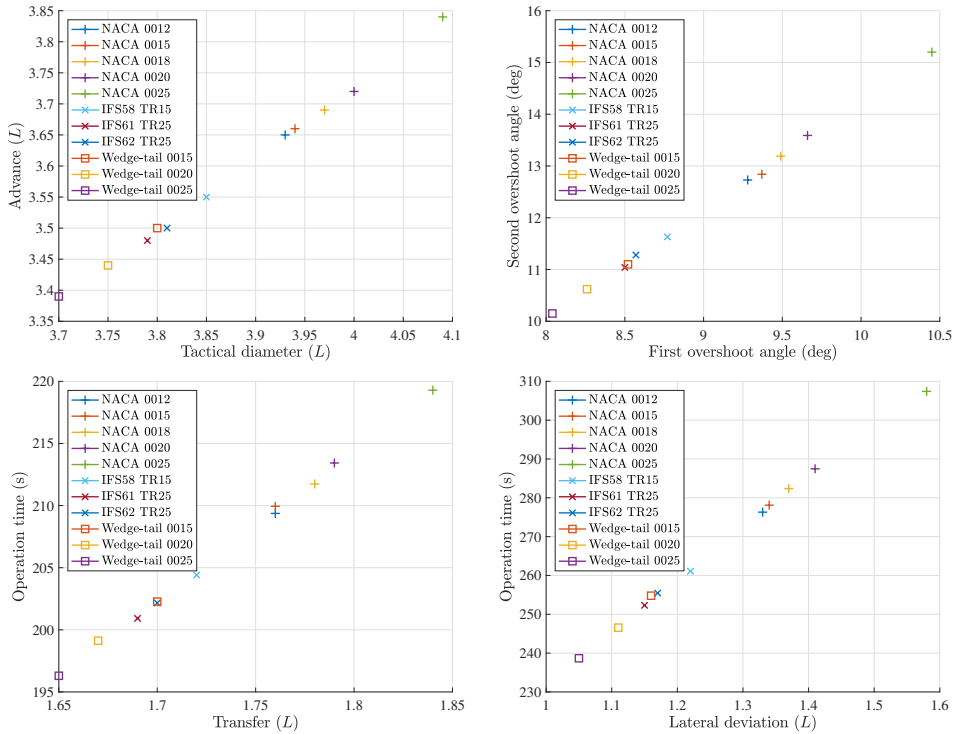


Figure 7.1: Impacts of the rudder profiles on the average manoeuvring criteria of single-rudder ships taking SPSR S1 as an example.

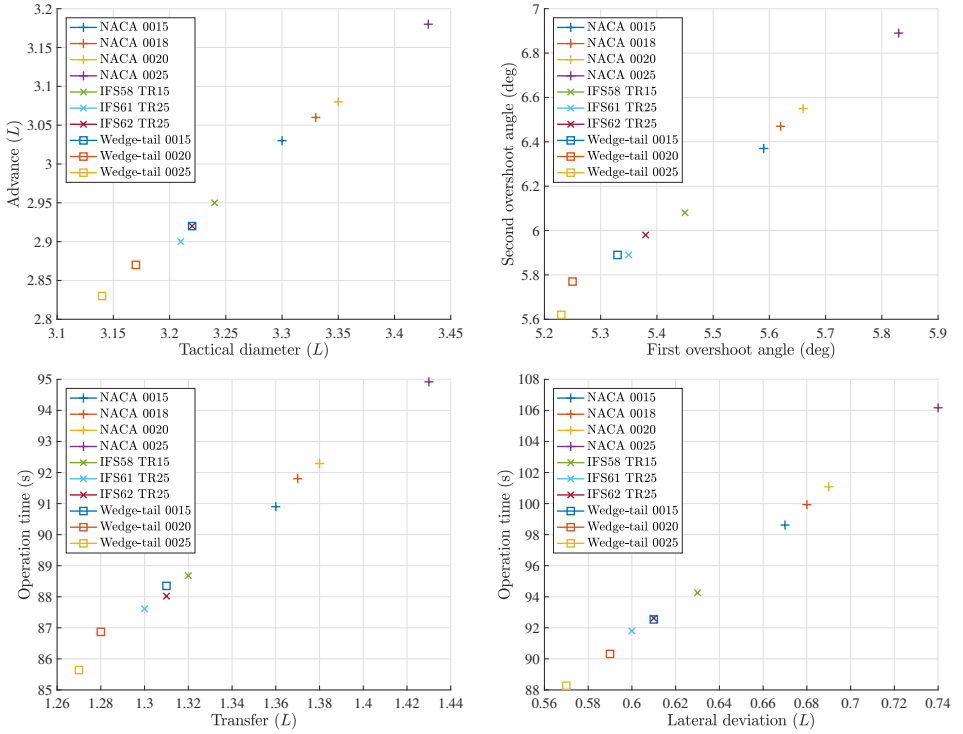


Figure 7.2: Impacts of the rudder profiles on the average manoeuvring criteria of twin-rudder ships taking TPTR Y1 as an example.

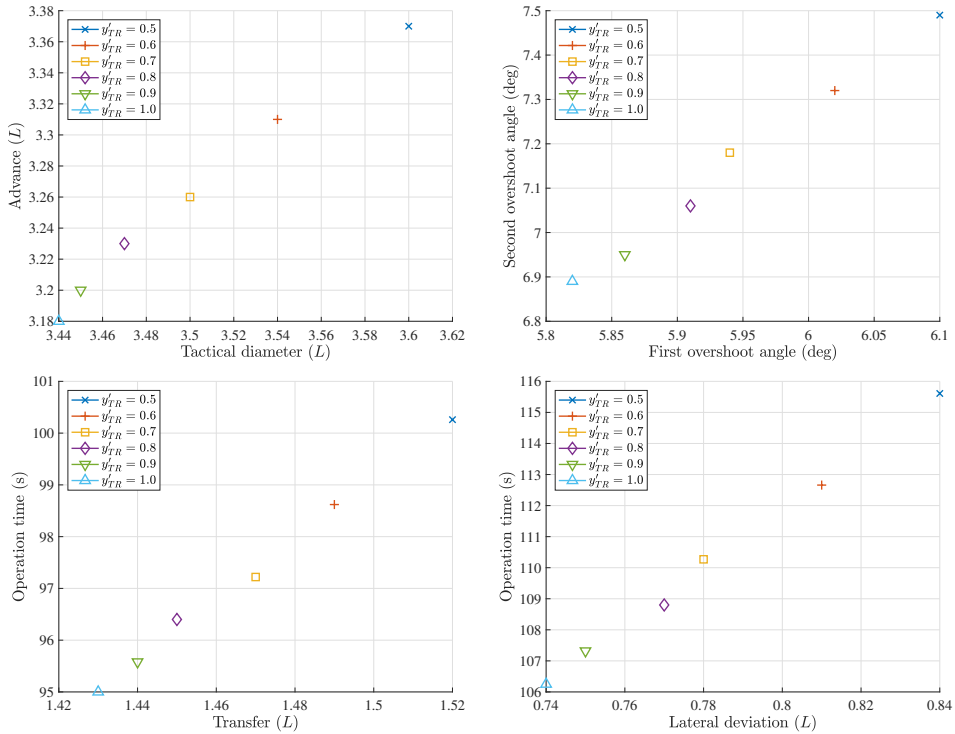


Figure 7.3: Impacts of the spacing between rudders on the average manoeuvring criteria of twin-rudder ships taking TPTR Y1 as an example.

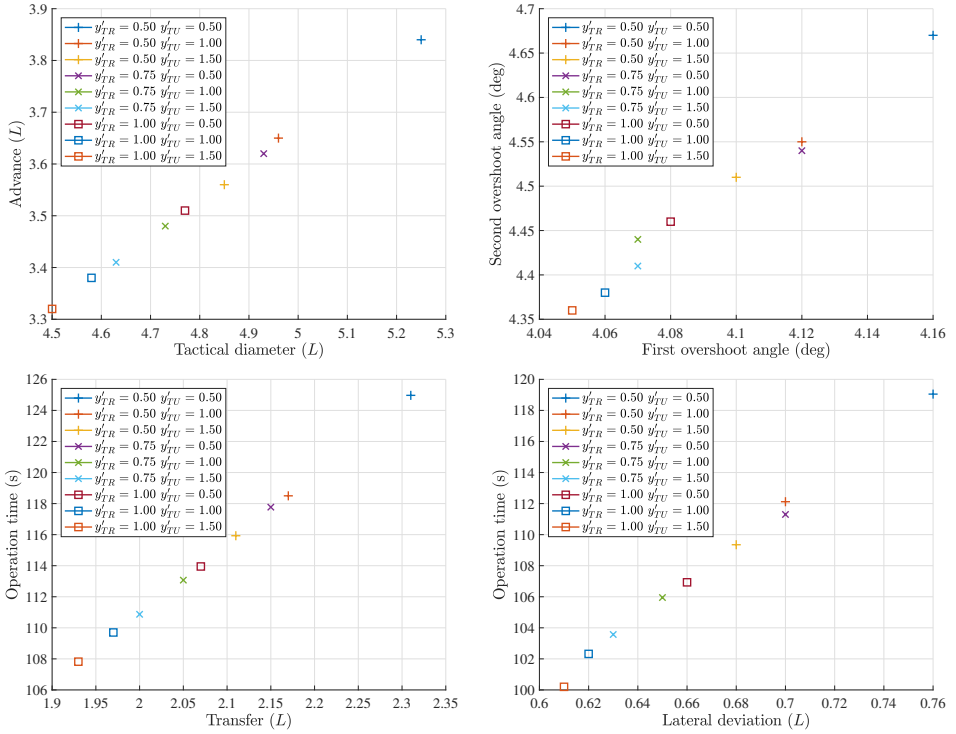


Figure 7.4: Impacts of the spacing among rudders on the average manoeuvring criteria of quad-rudder ships taking TPQR R2 as an example.

of rudder angles is most frequently used in the two journeys, more specifically about 96 % and 93 % of the sailing time respectively, and thus used to consider the impacts of rudder configurations on fuel consumption.

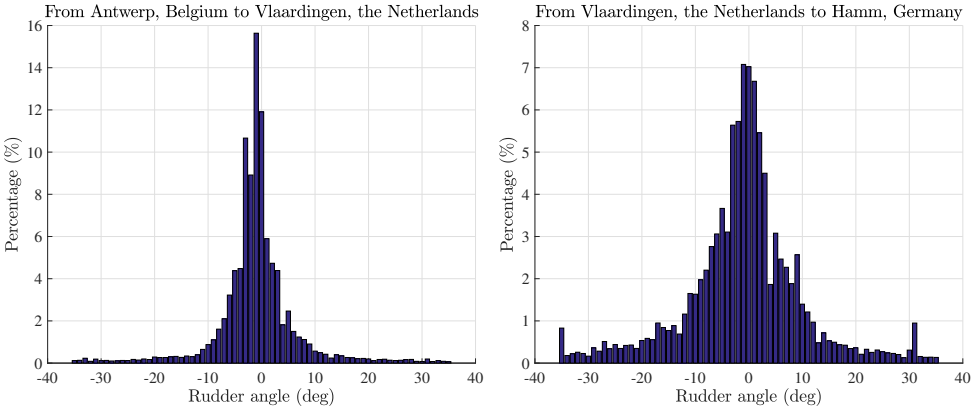


Figure 7.5: Probability distributions of the rudder angles in the range of -35° to 35° .

Based on the probability distributions of each applied rudder angle ($P(\delta)$) in Figure 7.5, the average applied rudder angle ($\bar{\delta}$) is calculated as the following:

$$\bar{\delta} = \sum_{i=1}^{71} P(\delta_i) |\delta_i|, \quad (7.1)$$

Accordingly, the average applied rudder angles for the routes from Antwerp, Belgium to Vlaardingen, the Netherlands ($\bar{\delta}_{AV}$) and from Vlaardingen, the Netherlands to Hamm, Germany ($\bar{\delta}_{VH}$) are 4.66° and 7.66° respectively. Afterwards, these two journeys are simplified as the ship turns with constant $\bar{\delta}_{AV}$ and $\bar{\delta}_{VH}$. This simplification is made because the rudder induced forces are almost linear within the range of -35° to 35° , when the rudder is placed in the propeller slipstream as shown in Figure 5.4.

To analyse the impacts of the rudder configurations on the fuel consumption, the first prerequisite is to ensure all the compared configurations can ensure the reference ship (SPSR R1) has the same manoeuvrability, more specifically the same amount of rudder induced manoeuvring force. In the following study, the lift of each configuration is kept the same to calculate the average applied rudder angle ($\bar{\delta}_{AV}$ and $\bar{\delta}_{VH}$), then the rudder induced resistance is calculated. Additionally, SPTR R1 is taken as the reference ships because it has similar main dimensions to the vessel that is used to log the applied rudder angles.

Based on the hydrodynamic coefficients which are presented in Chapter 4, the average applied angles ($\bar{\delta}_{AV}$ and $\bar{\delta}_{VH}$) are calculated for each rudder configuration assuming it is fitted on SPTR R1. The power consumed by the rudder induced resistance (P), the percentage of the power consumed by the rudder induced resistance to the total power consumed by the hull and the rudder (η), and the relative difference of the power consumed by each configuration compared to the benchmark fishtail configuration ($\Delta(P)$) are calculated and compared in Table 7.2. The colour legends are similar to those for Table 7.1, where the darkest green indicates the best values while the darkest red shows the worst ones.

Table 7.2: Impacts of rudder configurations on the power consumed by the rudder induced resistance.

Ship	Profile	n_R (-)	y_{TR} (C_R)	y_{TV} (C_R)	$\bar{\delta}_{AV}$ (deg)	P_{AV} (kW)	η_{AV} (%)	$\Delta(P_{AV})$ (%)	$\bar{\delta}_{VH}$ (deg)	P_{VH} (kW)	η_{VH} (%)	$\Delta(P_{VH})$ (%)
SPTR R1	Fishtail	2	1.00	—	4.66	16.77	13.25	0.00	7.66	25.79	19.02	0.00
SPSR R1	NACA 0012	1	—	—	8.73	10.64	8.83	-36.57	14.76	28.52	20.62	10.59
SPSR R1	NACA 0015	1	—	—	8.82	10.73	8.90	-36.02	14.91	28.79	20.77	11.63
SPSR R1	NACA 0018	1	—	—	9.05	11.05	9.14	-34.12	15.31	29.57	21.21	14.68
SPSR R1	NACA 0020	1	—	—	9.30	11.42	9.42	-31.93	15.76	30.47	21.72	18.16
SPSR R1	NACA 0025	1	—	—	10.41	12.80	10.44	-23.69	17.63	34.04	23.66	32.01
SPSR R1	IFS58 TR15	1	—	—	7.98	10.19	8.49	-39.28	13.45	26.49	19.43	2.73
SPSR R1	IFS61 TR25	1	—	—	7.51	10.13	8.45	-39.58	12.66	25.60	18.90	-0.73
SPSR R1	IFS62 TR25	1	—	—	7.63	9.97	8.33	-40.54	12.90	25.92	19.10	0.53
SPSR R1	Wedge-tail 0015	1	—	—	7.69	12.92	10.52	-22.99	12.92	28.28	20.48	9.69
SPSR R1	Wedge-tail 0020	1	—	—	7.25	11.84	9.73	-29.42	12.19	26.42	19.39	2.45
SPSR R1	Wedge-tail 0025	1	—	—	6.86	10.82	8.97	-35.52	11.52	24.67	18.35	-4.32
SPTR R1	NACA 0015	2	—	—	5.07	7.21	6.16	-57.00	8.53	17.72	13.89	-31.28
SPTR R1	NACA 0018	2	—	—	5.17	7.46	6.36	-55.53	8.70	18.17	14.20	-29.52
SPTR R1	NACA 0020	2	—	—	5.30	7.71	6.56	-54.03	8.93	18.70	14.55	-27.48
SPTR R1	NACA 0025	2	—	—	5.96	8.79	7.42	-47.57	10.01	21.10	16.12	-18.17
SPTR R1	IFS58 TR15	2	—	—	4.69	7.48	6.38	-55.38	7.86	17.16	13.52	-33.44
SPTR R1	IFS61 TR25	2	—	—	4.42	8.17	6.93	-51.28	7.41	17.34	13.64	-32.74
SPTR R1	IFS62 TR25	2	—	—	4.42	7.30	6.23	-56.50	7.42	16.55	13.09	-35.83
SPTR R1	Wedge-tail 0015	2	—	—	4.58	14.25	11.49	-15.04	7.66	23.44	17.59	-9.10
SPTR R1	Wedge-tail 0020	2	—	—	4.32	12.70	10.37	-24.26	7.24	21.44	16.33	-16.87
SPTR R1	Wedge-tail 0025	2	—	—	4.09	11.38	9.39	-32.18	6.84	19.68	15.20	-23.68
SPTR R1	NACA 0018	2	—	—	6.20	8.94	7.53	-46.68	10.45	21.74	16.53	-15.67
SPTR R1	NACA 0018	2	—	—	5.87	8.44	7.13	-49.70	9.90	20.57	15.78	-20.22
SPTR R1	NACA 0018	2	—	—	5.63	8.08	6.85	-51.82	9.48	19.72	15.22	-23.53
SPTR R1	NACA 0018	2	—	—	5.44	7.82	6.65	-53.39	9.16	19.07	14.80	-26.04
SPTR R1	NACA 0018	2	—	—	5.29	7.61	6.48	-54.63	8.91	18.57	14.46	-27.99
SPTR R1	NACA 0018	2	—	—	5.17	7.46	6.36	-55.53	8.70	18.17	14.20	-29.52
TPQR R1	NACA 0018	4	—	0.50	3.97	8.81	7.43	-47.45	6.68	17.11	13.48	-33.64
TPQR R1	NACA 0018	4	—	1.00	3.51	7.84	6.66	-53.26	5.90	15.20	12.16	-41.07
TPQR R1	NACA 0018	4	—	1.50	3.32	7.53	6.41	-55.13	5.59	14.52	11.68	-43.70
TPQR R1	NACA 0018	4	—	0.50	3.46	7.64	6.50	-54.47	5.81	14.88	11.93	-42.30
TPQR R1	NACA 0018	4	—	1.00	3.11	6.85	5.87	-59.18	5.23	13.40	10.87	-48.05
TPQR R1	NACA 0018	4	—	1.50	2.96	6.60	5.67	-60.67	4.98	12.85	10.48	-50.16
TPQR R1	NACA 0018	4	—	0.50	3.17	7.11	6.08	-57.61	5.33	13.79	11.16	-46.53
TPQR R1	NACA 0018	4	—	1.00	2.88	6.41	5.51	-61.79	4.85	12.51	10.23	-51.49
TPQR R1	NACA 0018	4	—	1.50	2.75	6.19	5.34	-63.10	4.64	12.04	9.88	-53.31

Note:

n_R is the number of rudders.

y_{TR} is the spacing between the twin rudders of twin-rudder configurations.

y_{TV} is the spacing between the two twin-rudder units of quadruple-rudder configurations.

AV denotes the route from Antwerp, Belgium to Vlaardingen, the Netherlands.

VH denotes the route from Vlaardingen, the Netherlands to Hamm, Germany.

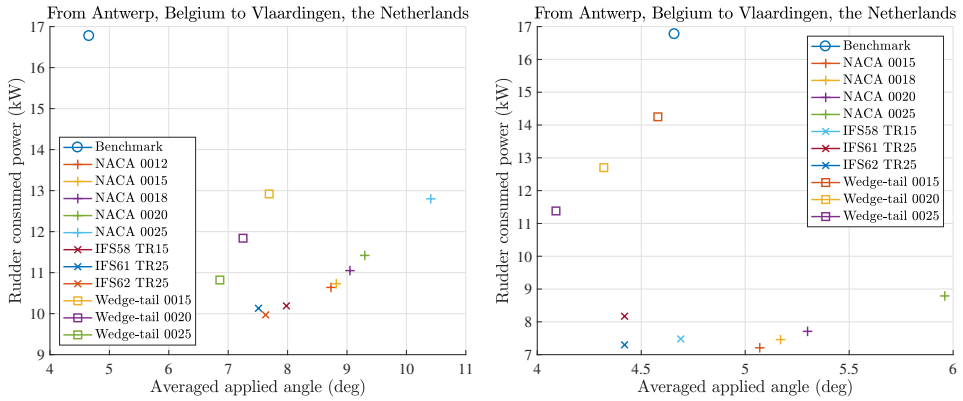
$\bar{\delta}$ is the average applied angles.

P is the power consumed by the rudder induced resistance.

η is the percentage of the power consumed by the rudder induced resistance to the total consumed power.

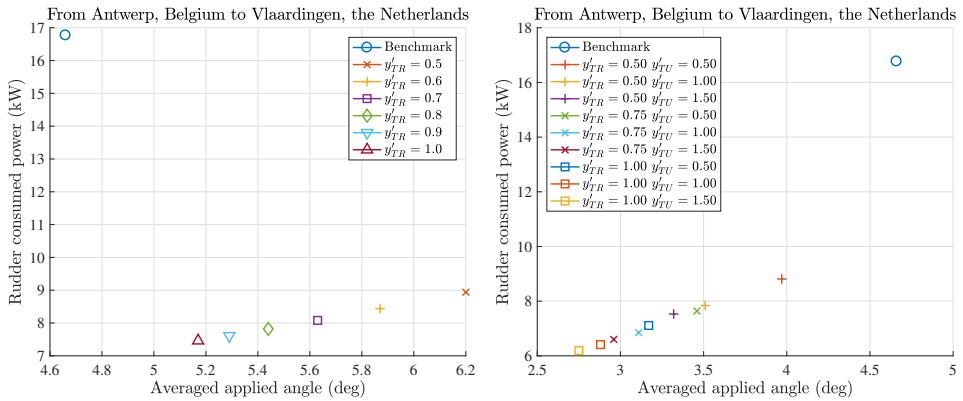
$\Delta(P)$ is the relative difference of the power consumed by each configuration compared to the benchmark configuration.

Comparing the two routes from Antwerp, Belgium to Vlaardingen, the Netherlands and from Vlaardingen, the Netherlands to Hamm, Germany, the first one is easier for a ship to sail than the second one because small angles are more frequently applied in the first route than the second one (Figure 7.5). Therefore, these two routes are taken as examples of which the rudder is moderately used and heavily used respectively. Accordingly, Figure 7.6 and Figure 7.7 show the impacts of the rudder configuration on the average applied angle and the power consumed by the rudder induced resistance when the rudder is moderately and heavily used.



(a) Impacts of single-rudder profiles.

(b) Impacts of twin-rudder profiles.

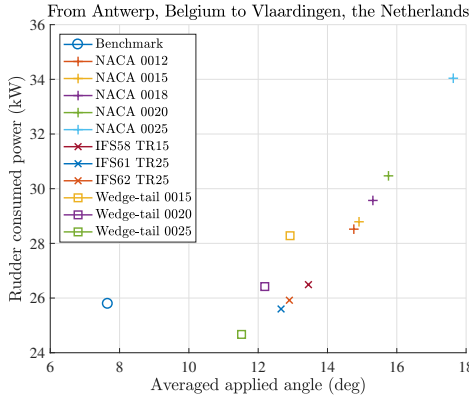


(c) Impacts of twin-rudder spacing.

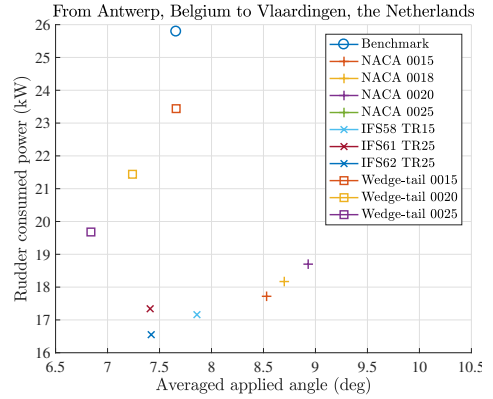
(d) Impacts of quadruple-rudder spacing.

Figure 7.6: Impacts of the rudder configuration on the average applied angle and the power consumed by the rudder induced resistance when the rudder is moderately used.

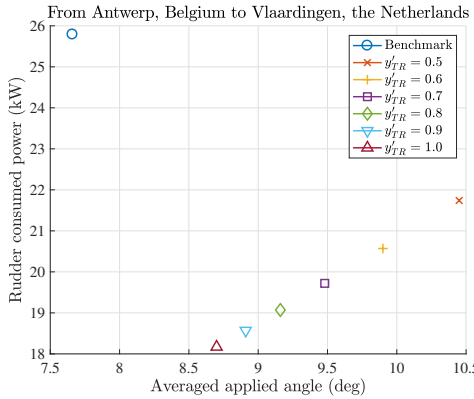
When the rudder configuration gets more efficient hydrodynamic characteristics, larger rudder angles have to be applied than those of configurations with more effective hydrodynamic characteristics to provide sufficient manoeuvring forces. Therefore, an efficient configuration from the hydrodynamic point of view may consume more power than that of an effective configuration, more specifically the navigation efficiency is reduced. It is sug-



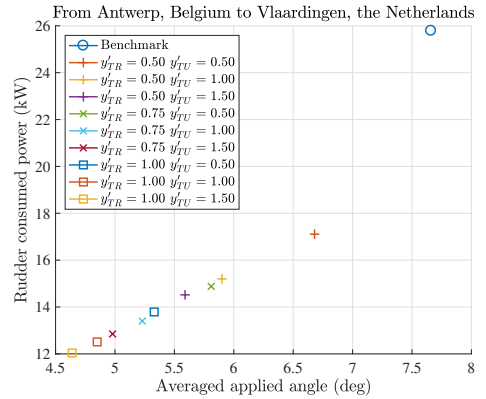
(a) Impacts of single-rudder profiles.



(b) Impacts of twin-rudder profiles.



(c) Impacts of twin-rudder spacing.



(d) Impacts of quadruple-rudder spacing.

Figure 7.7: Impacts of the rudder configuration on the average applied angle and the power consumed by the rudder induced resistance when the rudder is heavily used.

gested to preselect a range of options based on the manoeuvrability requirements and then optimise the design to get lower power consumption. The values given in Table 7.2 can be used as indicators of how to choose a proper design while Figure 7.6 and Figure 7.7 show the tendency of the rudder configuration impacts on the power consumed by the rudder-induced resistance. Furthermore, the tendencies of these impacts are expected to be similar to other reference ships.

7.7. Design flow

The proposed design flow of a rudder configuration is described in Figure 7.8. The presented hierarchy of design choices is suggested considering the effectiveness of the modification, but it is not mandatory. The design of a rudder configuration starts from the default rudder configuration, which depends on the navigation environment and the operation profile of the ship. If the ship frequently sails in bendy waterways, where the rudder has to be heavily used, the wedge-tail 0025 profile is suggested, because it is the most effective profile among the tested cases to generate the required rudder forces at relatively smaller angles. Otherwise, if the ship is designed for mostly straight moving, the NACA 0015 profile is the best choice among the studied rudder profiles because it has the lowest drag with small angles. In between, the IFS61 TR25 profile is an alternative because it achieves a balance in effectiveness and efficiency.

The structural requirements should be checked in the selection of the rudder profile, for instance, using a thicker NACA 0018 profile instead of the thinner NACA 0015 profile. Commonly, a thicker rudder means more drag and lower hydrodynamic efficiency. A single spade type rudder with the above-mentioned default profile will be the first configuration to be considered. The default rudder area should be decided based on the reference values listed in Table 2.1 according to the type of operation. Furthermore, the rudder span should be maximised to get the largest possible aspect ratios, and then the rudder chord length is determined corresponding to the rudder area and the rudder span. In default, end plates are not applied.

After each step, the manoeuvring performance of the ship should be checked against the manoeuvrability standards. If the default configuration cannot satisfy the requirements, the area of the single rudder is suggested to be increased first. The increase of rudder area should be limited to 30 % because the increase of rudder area makes the aspect ratios smaller (without changing the rudder span) and the rudder heavier, which reduce the performance of the rudder and put more burden on the steering gear. After increasing the rudder area, end plates can be applied, which may increase the lift and drag by about 30 % at the same time.

If a single-rudder single-propeller system cannot satisfy the manoeuvring requirements, more specifically a single rudder cannot provide sufficient manoeuvring forces or an excessively large area is needed, multiple rudders should be applied, which may increase the amount of rudder forces by hundreds of percent. A multiple-rudder configuration may have a larger investment and maintenance cost than a single-rudder system. However, a ship with multiple rudders may retain part of manoeuvrability in case that one of the rudders is not functional, thus enhancing navigation safety. When multiple rudders are applied, the spacing between rudders should be maximised. However, the rudder should not be located

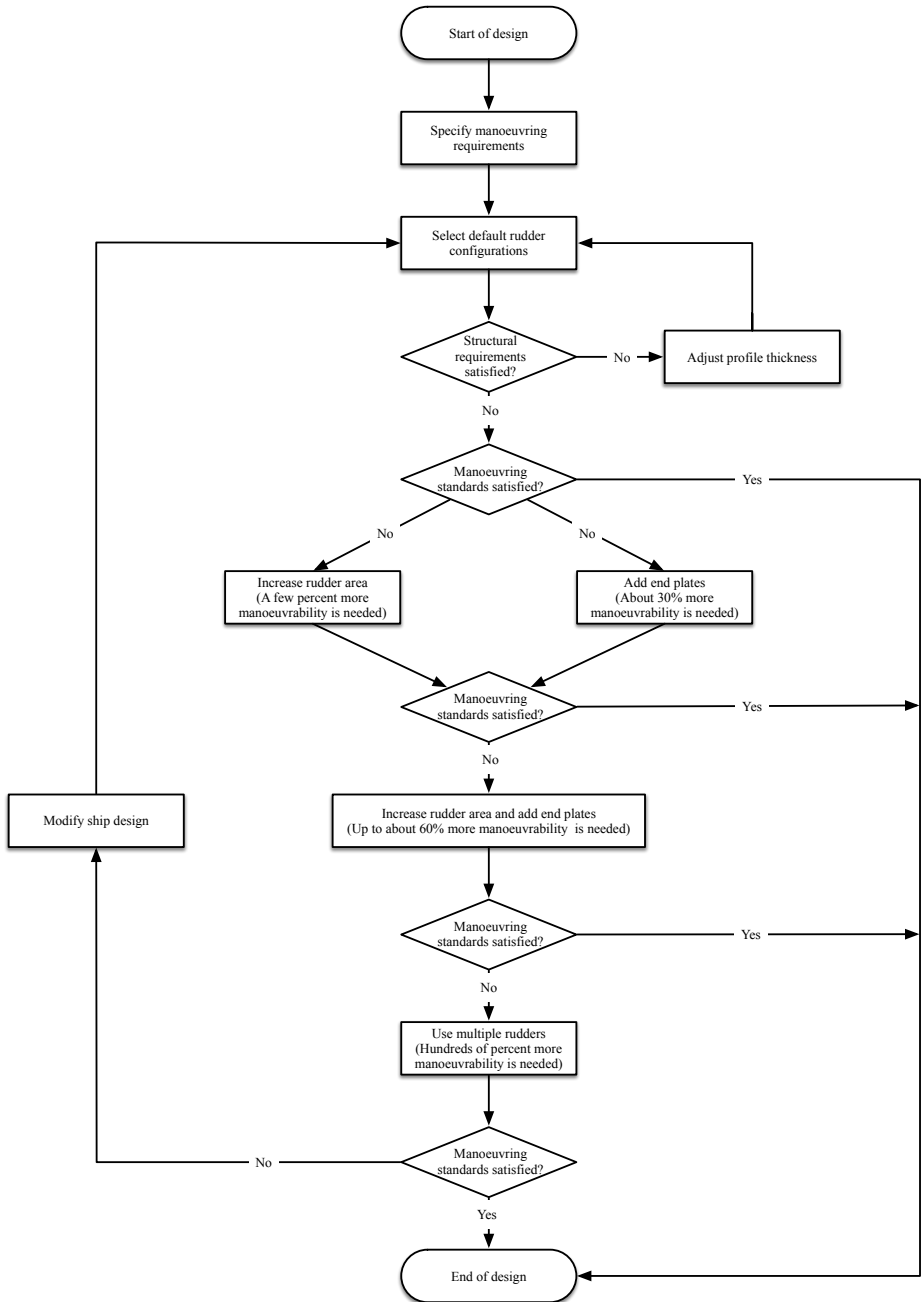


Figure 7.8: Design flow of rudder configurations.

out of the propeller slipstream. Otherwise, the rudder effectiveness drops sharply. If this still does not lead to sufficient manoeuvrability, the ship design has to be modified, namely by applying a second propeller.

7.8. Synthesis

The keys to improving the effectiveness of the rudder in ship manoeuvrability are increasing the rudder inflow velocity or the percentage of the rudder area in the propeller slipstream, enlarging the total rudder area, and improving the rudder hydrodynamic characteristics by changing the profile, the parameters, and the type. However, the improvement in the ship manoeuvrability in all calculated cases comes at the expense of extra rudder induced resistance. As a summary, this chapter answers the fourth research question in Section 1.3: *How to choose a proper rudder configuration according to the required manoeuvring performance?* Conclusions of this chapter are drawn as follows:

- The working conditions should be carefully defined before choosing a configuration. The navigation conditions should be studied to estimate the probability distributions of the applied rudder angles, for instance the probability distributions as shown in Figure 7.5. According to the actual use of rudder angles, the configuration can be optimised to balance the manoeuvring performance and the fuel consumption.
- The rudder profile, the rudder parameters, and the rudder type should be considered as a whole because each choice of the rudder configuration affects its hydrodynamic characteristics, leading to a change in the rudder induced manoeuvring forces and resistance.
- To improve the ship manoeuvring performance, the configuration should be optimised towards larger rudder induced side force, such as using effective profiles, enlarging the total rudder area, and increasing spacing among the rudders.
- The rudder configuration should be first determined according to the requirements of manoeuvrability and then refined to have lower rudder induced resistance. Based on the design flow that is presented in Figure 7.8, a proper rudder configuration can be determined accordingly considering the purpose of the ship.
- The navigation efficiency of ships with more efficient but less effective configurations from a hydrodynamic point of view may be lower than those with more effective but less efficient configurations because larger rudder angles have to be applied to provide sufficient manoeuvring forces.

Chapter 8

Conclusions and Recommendations*

“In three words I can sum up everything I’ve learned about life: it goes on.”

Robert Frost (1874 – 1963)

This thesis investigates the impacts of the rudder configuration on inland vessel manoeuvrability. Several aspects of a rudder configuration have been discussed in the previous chapters, such as the rudder profile, the rudder parameters, the rudder type, and the spacing among multiple rudders. As a concluding chapter, Section 8.1 summarises the main findings and answers the research questions of this thesis. Section 8.2 discusses the remaining open issues and suggests the directions for future research.

8.1. Answers to research questions

In this thesis, the following main research question is addressed: *What are the proper rudder configurations to achieve well manoeuvrable inland vessels without significant loss of navigation efficiency?* To invest this subject, the hydrodynamic characteristics of different rudder configurations are analysed through CFD simulations (Chapter 4), which are used in an integrated mathematical model for inland vessels (Chapter 5). With the new manoeuvring model, the impacts of the rudder configuration on the manoeuvring performance of ships are studied (Chapter 6). Accordingly, guidance on the rudder configurations is provided in Chapter 7.

Following the main research question, the following four key research questions (Section 1.3) are answered as follows:

Q1. *What are the practical manoeuvres to evaluate and compare the manoeuvring performance of inland vessels?*

Chapter 2 reviews the impact factors on ship manoeuvring performance and identifies the differences between seagoing ships and inland vessels. It is clear that the requirements of inland manoeuvrability should be more critical than seagoing ships due to a more complex environment and design factors. Accordingly, Chapter 3 presents the existing test manoeuvres and criteria for seagoing ships and inland vessels. It is clear that the requirements of inland manoeuvrability should be more elaborate than they are now.

*This chapter is based on Liu and Hekkenberg [177] and Liu et al. [180].

The classic turning and zigzag manoeuvres are useful but not sufficient to present a full vision of inland vessel manoeuvrability. Therefore, new test manoeuvres, namely hard turning, T-junction, lane changing, stopping with rudder corrections, and stopping with clam shell angles, are proposed in Chapter 3. Hard turning and lane changing manoeuvres are taken as examples in Chapter 6. T-junction tests can be regarded turning or hard-turning with boundaries, which should be determined by authorities or designers.

The proposed manoeuvres can be used as supplementary means with the classic manoeuvres. More information can be obtained from the traditional turning and zigzag tests, for instance, the maximum values in the manoeuvres. Further research is required to formulate detailed criteria for each proposed test manoeuvres. Additionally, safe operation margins should be studied to properly configure the proposed T-junction manoeuvres.

Q2. *How does the rudder configuration affect the rudder hydrodynamic characteristics?*

A rudder configuration consists of several aspects, such as the profile, the parameters, and the type, as discussed in Chapter 2. Using RANS simulations, different rudder configurations are tested to obtain insights into the correlation of the rudder configuration and its hydrodynamic characteristics. Detailed information is presented in Chapter 4. Furthermore, new regression formulas of the rudder hydrodynamic coefficients are proposed to predict the rudder induced forces and moments in manoeuvring.

Q3. *How do changes in the rudder configuration affect the ship manoeuvrability in specific manoeuvres?*

To resolve this key research question, the rudder induced forces and moments should be accurately calculated considering the rudder configuration. The hydrodynamic characteristics of different configurations are obtained in Chapter 4. Furthermore, an integrated manoeuvring model for inland vessels is built through validation studies of reference inland vessels in Chapter 5.

In Chapter 6, the impacts of the rudder configuration on ship manoeuvring performance are analysed using five reference ships in four test manoeuvres. In general, manoeuvring indices can be improved by 5 % to 30 % through optimising the rudder configuration. The improvements can be achieved by using effective rudder profiles, increasing the spacing between rudders, applying multiple rudders, and fitting end plates.

Q4. *How to choose a proper rudder configuration according to the required manoeuvring performance?*

The possible rudder configurations should be first selected according to the manoeuvrability requirements and then optimised to reduce the rudder induced resistance (consumed power). The profile, the parameter, and the type of a rudder configuration should be considered as a whole to improve its hydrodynamic performance. Chapter 7 gives guidance for naval architects to make proper choices of the rudder configuration. Additionally, reference manoeuvring indices and consumed power are

given in Chapter 7 to quickly access the performance of a configuration at the initial design stage.

In summary, a brief answer to the main research question is made as the following:

A proper rudder configuration should be determined under the prerequisite that sufficient manoeuvring forces can be induced. The rudder profile, the rudder parameters, and the rudder type of a configuration should be considered as a whole to optimise its hydrodynamic characteristics, leading to a good manoeuvring performance. Furthermore, among the calculated cases, the navigation efficiency is not significantly affected when the manoeuvring performance is improved. After all, multiple rudders with effective profiles, large spacing, and end plates are suggested for inland vessels.

8.2. Recommendations for future research

To get even more reliable estimates of manoeuvring performance of inland vessels, additional validation data are needed for the applied CFD methods and the mathematical model. Further investigations are also required, which are listed as the research directions in the following sections. These further research directions are given in the perspectives of the rudder hydrodynamics, the rudder design, the manoeuvring modelling, shallow-water effects on ship manoeuvring, and the interactions among the hull, the propeller, and the rudder as follows:

- **Rudder hydrodynamics**

More operational data of different ships with various rudder configurations in inland waterways or open sea are needed. Moreover, studies on the rudder performance for very slow moving ships, more specifically at Reynolds numbers lower than usual, with uncustomary large rudder angles are suggested.

- **Rudder design**

Future research is suggested on the investigation of energy saving methods of the rudders such as the twisted rudders and the energy saving bulbs. Considering cavitation, whole-body profiles and types like the spade rudder with a NACA profile have advantages over the separated ones like the semi-skeg rudder with a flapped profile. Even though for common commercial ships, the effectiveness and efficiency of the rudder get higher priority than the cavitation in the design process, a final check of the rudder performance in the cavitation cannot be neglected.

- **Manoeuvring modelling**

Further investigations and experiments are requested to describe the inland vessel resistance ($R(u)$), express the longitudinal component hull forces due to manoeuvring motions ($R(v', r')$ or $R(\beta, r')$), and collect hydrodynamic derivatives for (Y_H and N_H). Additional tests are needed to determine the impact factor of the propeller (ϵ) and the rudder (ϵ_R) on the rudder lift and drag coefficients during manoeuvring motions. Furthermore, the estimation of the wake factors of the propeller (w_P) and the rudder (w_R) needs to be improved.

- **Slow-speed and birthing performance**

This thesis mainly focused on the manoeuvring performance of inland vessels at service speed. Due to the limited time and data, slow-speed manoeuvring and birthing performance were not thoroughly discussed. In slow-speed and birthing situations, the hydrodynamic coefficients of the hull, the propeller, and the rudder may be changed. For instance, the rudder will be ineffective owing to the slow inflow to it. The proposed integrated manoeuvring model can be improved by adding additional terms to consider the impacts of slow speed, which needs additional tests for conducting the data and validating the model in the future.

- **Shallow water effects on ship manoeuvring**

To predict the manoeuvring performance of inland vessels in shallow/confined water, further research is recommended for the estimation of the hull forces and moments. Additionally, the wake factors at the positions of the propeller and the rudder may also be affected by shallow water. Furthermore, it is recommended to study how the flow straightening factor and the effective rudder angle are changed by the variation in water depth.

- **Ship-bank and ship-ship interactions**

As previously reviewed in Chapter 2, ship-bank and ship-ship interactions are important for inland vessels. Up to now, these effects are still hard to quantify and, thus, not extensively studied in this thesis. Ship-bank and ship-ship interactions become significant as the distance among them gets smaller. Precise estimation of the start and the amount of the interactions is meaningful to ensure the safety of inland navigation and fully utilise the capacity of inland waterways. Therefore, research on ship-bank and ship-ship interactions of inland vessels is suggested for the future.

- **Interactions among the hull, the propeller, and the rudder**

As a rule, the interactions among the hull, the propeller, and the rudder affect the rudder hydrodynamic characteristics. The flow straightening effect influences the effective rudder angle, which is important for the calculation of the rudder induced force in manoeuvring simulations. However, in the existing literature, the flow straightening factor is primarily determined by model tests. More research is needed to better understand the roles of the impact factors on the flow straightening effect. Furthermore, it is proposed to generate regression formulas of the flow straightening factor through series of benchmark tests.

The propeller slipstream mainly delays the stall angle. It may maintain or change the slope of the lift curve depending on the working load of the propeller. Further research in this field would be of great help in manoeuvring simulations. The relative position of the propeller and the rudder influences the performance of both the propeller and the rudder. With extra consideration of cavitation, it is recommended to put the rudder as close as possible to the propeller. Moreover, interaction among multiple rudders requires further study, which is particularly meaningful for inland vessels.

Bibliography

- [1] Abbott, I. H. and Von Doenhoff, A. E. *Theory of Wing Sections: Including a Summary of Airfoil Data*. Dover Publications, New York, USA, 1 edition, 1959.
- [2] Abkowitz, M. A. Lectures on Ship Hydrodynamics Steering and Maneuverability. Technical report, Hydro and Aerodynamic Laboratory, Lyngby, Denmark., 1964.
- [3] Abkowitz, M. A. Measurement of hydrodynamic characteristics from ship maneuvering trials by system identification. *SNAME Transactions*, 88:283–318, 1980.
- [4] Ahn, K., Choi, G. H., Son, D. I., and Rhee, K. P. Hydrodynamic characteristics of X-Twisted rudder for large container carriers. *International Journal of Naval Architecture and Ocean Engineering*, 4(3):322–334, 2012.
- [5] Alte, R. and Baur, M. V. Propulsion Handbuch der Werften (in German). *Hansa*, 18: 132, 1986.
- [6] American Bureau of Shipping. Guide for Vessel Maneuverability, Mar. 2006.
- [7] Amos, P., Jia, D., Ning, T., Sun, J., and Fei, W. Sustainable Development of Inland Waterway Transport in China. Technical report, The World Bank and The Ministry of Transport, People’s Republic of China, 2009.
- [8] Ankudinov, V., Kaplan, P., and Jacobsen, B. K. Assessment and principal structure of the modular mathematical model for ship maneuverability prediction and real-time maneuvering simulations. In *International Conference on Marine Simulation and Ship Manoeuvrability (MARSIM '93)*, St. John’s, Newfoundland, Canada, Sept. 1993.
- [9] Ankudinov, V. K. and Jakobsen, B. K. Physically based maneuvering model for simulations and test evaluations. In *International Conference on Marine Simulation and Ship Maneuverability (MARSIM '06)*, Terschelling, the Netherlands, June 2006.
- [10] Araki, M., Sadat-Hosseini, H., Sanada, Y., Tanimoto, K., Umeda, N., and Stern, F. Estimating maneuvering coefficients using system identification methods with experimental, system-based, and CFD free-running trial data. *Ocean Engineering*, 51:63–84, 2012.
- [11] Badoe, C. E., Phillips, A. B., and Turnock, S. R. Influence of drift angle on the computation of hull-propeller-rudder interaction. *Ocean Engineering*, 103:64–77, 2015.
- [12] Barr, R. A., Miller, E. R., Ankudinov, V., and Lee, F. C. Technical Basis for Maneuvering Performance Standards. Technical report, U.S. Department of Transportation, U.S. Coast Guard, Office of Merchant Marine Safety, Dec. 1981.

- [13] Barrass, B. *Ship Design and Performance for Masters and Mates*. Elsevier Butterworth-Heinemann, Oxford, UK, 1st edition, 2004.
- [14] Batten, W. M. J., Bahaj, A. S., Molland, A. F., and Chaplin, J. Hydrodynamics of marine current turbines. *Renewable Energy*, 31(2):249–256, 2006.
- [15] Batten, W. M. J., Bahaj, A. S., Molland, A. F., and Chaplin, J. R. The prediction of the hydrodynamic performance of marine current turbines. *Renewable Energy*, 33(5):1085–1096, 2008.
- [16] Baudu, H. *Ship Handling*. DOKMAR Maritime Publishers BV, Enkhuizen, the Netherlands, 1 edition, 2014.
- [17] Belenky, V. and Falzarano, J. Rating-based maneuverability standards. In *SNAME Annual Meeting Conference*, number 1994, pages 227–246, Florida, USA, 2006.
- [18] Bertagnolio, F., Sørensen, N. N., Johansen, J., and Fuglsang, P. Wind Turbine Airfoil Catalogue. Denmark. Forskningscenter Risoe. Risoe-R; No. 1280 (EN), 2001.
- [19] Bertram, V. *Practical Ship Hydrodynamics*. Elsevier, Oxford, UK, 2 edition, 2012.
- [20] Bhattacharyya, A., Krasilnikov, V., and Steen, S. Scale effects on open water characteristics of a controllable pitch propeller working within different duct designs. *Ocean Engineering*, 112:226–242, 2016.
- [21] Biancardi, C. G. Integrating ship manoeuvrability with safety. In *International Conference on Marine Simulation and Ship Maneuverability (MARSIM '93)*, volume 1, pages 33–47, St. John's, Newfoundland, Canada, Sept. 1993.
- [22] Bonci, M., Viviani, M., Broglia, R., and Dubbioso, G. Method for estimating parameters of practical ship manoeuvring models based on the combination of RANSE computations and System Identification. *Applied Ocean Research*, 52:274–294, 2015.
- [23] Brennen, C. E. *Cavitation and Bubble Dynamics*. Cambridge University Press, Oxford, UK, 1995.
- [24] Brix, J. *Manoeuvring Technical Manual*. Seehafen Verlag, Hamburg, Germany, 1993.
- [25] Broglia, R., Dubbioso, G., Durante, D., and Di Mascio, A. Simulation of turning circle by CFD: Analysis of different propeller models and their effect on manoeuvring prediction. *Applied Ocean Research*, 39:1–10, 2013.
- [26] Broglia, R., Dubbioso, G., Durante, D., and Di Mascio, A. Turning ability analysis of a fully appended twin screw vessel by CFD, Part I: Single rudder configuration. *Ocean Engineering*, 105:275–286, 2015.
- [27] Bureau Veritas. Rules for the Classification of Inland Navigation Vessels, Nov. 2011.

- [28] Carlton, J. S., Radosavljevic, D., and Whitworth, S. Rudder-propeller-hull interaction: The results of some recent research, in-service problems and their solutions. In *1st Symposium on Marine Propulsors*, Trondheim, Norway, June 2009.
- [29] Carrica, P. M., Mofidi, A., Eloot, K., and Delefortrie, G. Direct simulation and experimental study of zigzag maneuver of KCS in shallow water. *Ocean Engineering*, 112:117–133, 2016.
- [30] Castro, A. M., Carrica, P. M., and Stern, F. Full scale self-propulsion computations using discretized propeller for the KRISO container ship KCS. *Computers & Fluids*, 51:35–47, 2011.
- [31] Catalano, P. and Tognaccini, R. RANS analysis of the low-Reynolds number flow around the SD7003 airfoil. *Aerospace Science and Technology*, 15(8):615–626, 2011.
- [32] Central Commission for the Navigation of the Rhine. The Rhine Vessel Inspection Regulations, 1995.
- [33] Central Commission for the Navigation of the Rhine. Reglement Onderzoek Schepen op de Rijn (in Dutch), 2012.
- [34] Central Commission for the Navigation of the Rhine. The Inland Navigation Market in 2012, 2013.
- [35] Champlain, J. G. Analysis of Flapped Rudder Gap Effects. Master thesis, Massachusetts Institute of Technology, May 1971.
- [36] Chau, S. W. *Numerical investigation of free-stream rudder characteristics using a multi-block finite volume method*. PhD thesis, University of Hamburg, 1997.
- [37] Chen, H. C., Lin, W. M., and Hwang, W. Y. Application of Chimera RANS method for multiple-ship interactions in a navigation canal. In *20th International Offshore and Polar Engineering Conference*, volume 3, pages 330–337, Kitakyushu, Japan, May 2002.
- [38] China Classification Society. Guidelines for Inland Vessel Manoeuvrability (in Chinese), 2003. Guidance Notes GD-2003.
- [39] Clarke, D. The foundations of steering and manoeuvring. In *IFAC Conference on Manoeuvring and Control of Marine Craft (MCMC 2003)*, Girona, Spain, Sept. 2003.
- [40] Clarke, D., Gedling, P., and Hine, G. Application of manoeuvring criteria in hull design using linear theory. *Transactions of the Royal Institution of Naval Architect*, 125:45–68, 1983.
- [41] Clement, E. P. Scale Effect on the Drag of a Typical Set of Planing Boat Appendages. Technical report, David Taylor Model Basin, Bethesda, Maryland, USA, Aug. 1957.

- [42] Cleynen, O. Airfoil nomenclature. Accessed on December 30, 2015, retrieved from <https://en.wikipedia.org/wiki/Airfoil>, 2011.
- [43] Coraddu, A., Dubbioso, G., Mauro, S., and Viviani, M. Analysis of twin screw ships' asymmetric propeller behaviour by means of free running model tests. *Ocean Engineering*, 68:47–64, 2013.
- [44] Crane, C. L. Maneuvering safety of large tankers: Stopping, turning and speed selection. *SNAME Transactions*, 81:218–242, 1973.
- [45] Daidola, J. C., Lundy, W., and Barr, R. Evolution of the IMO standards for maneuverability. *SNAME Transactions*, 110:395–411, 2002.
- [46] Dand, I. Low-speed manoeuvring criteria: Some considerations. In *International Conference on Marine Simulation and Ship Maneuverability (MARSIM '03)*, Kanazawa, Japan, Aug. 2003.
- [47] Date, J. C. *Performance Prediction of High Lift Rudders Operating Under Steady and Periodic Flow Conditions*. PhD thesis, University of Southampton, July 2001.
- [48] De Koning Gans, H. Squat results from calculations of panel methods. In *International Maritime-Port Technology and Development Conference*, Singapore, 2005.
- [49] Del Estado, P. Recommendations for the Design of the Maritime Configuration of Ports, Approach Channels and Harbour Basins, Nov. 2000. ROM 3.1-99.
- [50] Det Norske Veritas. Hull equipment and appendages: Stern frames, rudders and steering gears. *Rules for Classification of Steel Ships*, (Part 3, Chapter 3, Section 2): 6–28, Jan. 2000.
- [51] Di Mascio, A., Dubbioso, G., Notaro, C., and Viviani, M. Investigation of twin-screw naval ships maneuverability behavior. *Journal of Ship Research*, 55(4):221–248, 2011.
- [52] Dijkhuis, T., Van Toorenburg, J. C. K., and Verkerk, F. New manoeuvring criteria for the river Rhine. In *International Conference on Marine Simulation and Ship Maneuverability (MARSIM '93)*, volume 1, pages 77–86, St. John's, Newfoundland, Canada, Sept. 1993.
- [53] Dubbioso, G. and Viviani, M. Aspects of twin screw ships semi-empirical maneuvering models. *Ocean Engineering*, 48:69–80, 2012.
- [54] Dubbioso, G., Mauro, S., and Ortolani, F. Experimental and numerical investigation of asymmetrical behaviour of rudder/propeller for twin screw Ships. In *International Conference on Marine Simulation and Ship Maneuverability (MARSIM '15)*, Newcastle upon Tyne, UK, Sept. 2015.
- [55] Dubbioso, G., Durante, D., Mascio, A. D., and Broglia, R. Turning ability analysis of a fully appended twin screw vessel by CFD, Part II: Single vs. twin rudder configuration. *Ocean Engineering*, 117:259–271, 2016.

- [56] El Moctar, O. Numerical computations of flow forces in ship manoeuvring. *Ship Technology Research*, 48(3):98–123, 2001.
- [57] Eleni, D. C., Athanasios, T. I., and Dionissios, M. P. Evaluation of the turbulence models for the simulation of the flow over a National Advisory Committee for Aeronautics (NACA) 0012 airfoil. *Journal of Mechanical Engineering Research*, 4(3): 100–111, 2012.
- [58] Eloot, K. *Selection, Experimental Determination and Evaluation of a Mathematical Model for Ship Manoeuvring in Shallow Water*. PhD thesis, Ghent University, 2006.
- [59] Eloot, K. and Vantorre, M. Prediction of low speed manoeuvring based on captive model tests: Opportunities and limitations. In *International Marine Simulation Forum (IMSF): Annual General Meeting 2004*, pages 13–17, Antwerp, Belgium, 2004.
- [60] Eloot, K. and Vantorre, M. Ship behaviour in shallow and confined water: An overview of hydrodynamic effects through EFD. *Assessment of Stability and Control Prediction Methods for NATO Air and Sea Vehicles*, pages 1–20, 2011. RTO-MP-AVT-189.
- [61] Eloot, K., Verwilligen, J., and Vantorre, M. A methodology for evaluating the controllability of a ship navigating in a restricted channel. *Archives of Civil and Mechanical Engineering*, 7(3):91–104, 2007.
- [62] Eloot, K., Delefortrie, G., and Vantorre, M. Inland navigation: Assessing the manoeuvring behaviour for real-time simulation purposes. In *International Conference on Marine Simulation and Ship Maneuverability (MARSIM '12)*, pages 1–12, Singapore, Apr. 2012.
- [63] European Commission. Commission Directive 2008/126/EC of 19 December 2008 Amending Directive 2006/87/EC of the European Parliament and of the Council Laying down Technical Requirements for Inland Waterway Vessels, Dec. 2008.
- [64] European Commission. COM/2011/0144 final White Paper ‘Roadmap to a Single European Transport Area – Towards a Competitive and Resource Efficient Transport System’, Mar. 2011.
- [65] European Conference of Ministers of Transport. Resolution No. 92/2 on New Classification of Inland Waterways, June 1992.
- [66] European Court of Auditors. Special Report No 1/2015 ‘Inland Waterway Transport in Europe: No significant improvements in modal share and navigability conditions since 2001’, Mar. 2015.
- [67] Eurostat. Modal split of freight transport. Accessed on November 20, 2015, retrieved from <http://ec.europa.eu/eurostat/data/database>, 2015.
- [68] Eurostat. Inland waterway transport statistics. Accessed on September 30, 2016, retrieved from http://ec.europa.eu/eurostat/statistics-explained/index.php/Inland_waterway_transport_statistics, 2016.

- [69] Fach, K. and Bertram, V. High-performance simulations for high-performance ships. *Ships and Offshore Structures*, 2(2):105–113, 2007.
- [70] Federal Ministry of Transport and Digital Infrastructure. Waterways as transport routes. Accessed on September 30, 2016, retrieved from <http://www.bmvi.de/SharedDocs/EN/Artikel/WS/waterways-as-transport-routes.html>, 2016.
- [71] Fink, M. P. and Lastinger, J. L. Aerodynamic Characteristics of Low-Aspect-Ratio Wings in Close Proximity to the Ground. Technical report, Langley Research Center, Washington, DC, USA, 1961.
- [72] Fujii, H. Experimental researches on rudder performance (1) (in Japanese). *Journal of Zosen Kiokai*, (107):105–111, 1960.
- [73] Fujii, H. and Tsuda, T. Experimental researches on rudder performance (2) (in Japanese). *Journal of Zosen Kiokai*, (110):31–42, 1961.
- [74] Fujii, H. and Tsuda, T. Experimental researches on rudder performance (3) (in Japanese). *Journal of Zosen Kiokai*, (111):51–58, 1962.
- [75] Fujino, M. and Ishiguro, T. A study of the mathematical model describing manoeuvring motions in shallow water. *Journal of the Society of Naval Architects of Japan*, 156:180–192, 1984.
- [76] Furukawa, Y., Nakiri, Y., Kijima, K., and Hiroshi, I. The prediction of the manoeuvrability of KVLCC1 and KVLCC2. In *SIMMAN 2008: Workshop on Verification and Validation of Ship Manoeuvring Simulation Methods*, pages 9–14, Copenhagen, Denmark, Apr. 2008.
- [77] Gim, O. S. Assessment of flow characteristics around twin rudder with various gaps using PIV analysis in uniform flow. *Ocean Engineering*, 66:1–11, 2013.
- [78] Goundar, J. N., Rafiuddin Ahmed, M., and Lee, Y. H. Numerical and experimental studies on hydrofoils for marine current turbines. *Renewable Energy*, 42:173–179, 2012.
- [79] Gray, W. O., Waters, J., Blume, A., and Landsburg, A. C. Channel design and vessel maneuverability: Next steps. *Marine Technology*, 40(2):93–105, 2003.
- [80] Gregory, D. and Beach, T. Resistance Measurements of Typical Planing Boat Appendages. Technical report, David Taylor Model Basin, Bethesda, Maryland, USA, 1979.
- [81] Gregory, N. and O'Reilly, C. L. Low-Speed Aerodynamic Characteristics of NACA 0012 Aerofoil Section, including the Effects of Uppers-Surface Roughness Simulating Hoar Frost. Technical report, Ministry of Defence, London, UK, 1970.
- [82] Greitsch, L. Prognosis of rudder cavitation risk in ship operation. In *11th Numerical Towing Tank Symposium*, Brest, France, Sept. 2008.

- [83] Greitsch, L., Eljardt, G., and Krueger, S. Operating conditions aligned ship design and evaluation. In *1st International Symposium on Marine Propulsors*, Trondheim, Norway, Sept. 2009.
- [84] Grochowalski, S. Investigation into the Physics of Ship Capsizing by Combined Captive and Free-Running Model Tests. Technical report, National Research Council Canada, St. John's, Newfoundland, Canada, 1989.
- [85] Gronarz, A. A mathematical model for manoeuvring simulation on shallow water. In *International Conference on Marine Simulation and Ship Maneuverability (MARSIM '93)*, pages 143–153, St. John's, Newfoundland, Canada, Aug. 1993.
- [86] Gronarz, A. *Numerical Simulation of the Ships Motion in Manoeuvres with Special Consideration of the Dependency of the Water Depth*. PhD thesis, University of Duisburg, 1997.
- [87] Hamamoto, M. and Enomoto, T. Maneuvering performance of a ship with VecTwin rudder system. *Journal of the Society of Naval Architects of Japan*, (181):197–204, 1997.
- [88] Han, J. M., Kong, D. S., Song, I. H., and Lee, C. S. Analysis of the cavitation flow around the horn-type rudder in the race of a propeller. In *4th International Symposium on Cavitation*, Pasadena, CA, USA, June 2001.
- [89] Harris, C. D. Two-Dimensional Aerodynamic Characteristics of the NACA 0012 Airfoil in the Langley 8 Foot Transonic Pressure Tunnel. Technical report, Langley Research Center, Hampton, Virginia, USA, 1981.
- [90] Harvald, S. A. *Resistance and Propulsion of Ships*. John Wiley & Sons, New York, USA, 1983.
- [91] Hasegawa, K., Kang, D., Sano, M., and Nabeshima, K. Study on the maneuverability of a large vessel installed with a mariner type Super VecTwin rudder. *Journal of Marine Science and Technology*, 11(2):88–99, 2006.
- [92] Hasegawa, K., Kang, D., Sano, M., Nagarajan, V., and Yamaguchi, M. A study on improving the course-keeping ability of a pure car carrier in windy conditions. *Journal of Marine Science and Technology*, 11:76–87, 2006.
- [93] Hasegawa, K., Nagarajan, V., and Kang, D. H. Performance evaluation of Schilling rudder and Mariner rudder for Pure Car Carriers (PPC) under wind condition. In *International Conference on Marine Simulation and Ship Maneuverability (MARSIM '06)*, number M5, pages 1–10, Terschelling, the Netherlands, June 2006.
- [94] He, S., Kellett, P., Yuan, Z., Incecik, A., Turan, O., and Boulougouris, E. Manoeuvring prediction based on CFD generated derivatives. *Journal of Hydrodynamics, Ser. B*, 28(2):284–292, 2016.
- [95] Hekkenberg, R. *Inland Ships for Efficient Transport Chains*. PhD thesis, Delft University of Technology, 2013.

- [96] Hekkenberg, R. and Liu, J. Developments in inland waterway vessels. In Wiegman, B. and Konings, R., editors, *Inland Waterway Transport: Challenges and Prospects*, number 6 in Routledge Studies in Transport Analysis, chapter 7, pages 142–167. Taylor & Francis, July 2016.
- [97] Hirano, M. A practical calculation method of ship maneuvering motion at initial design stage. *Naval Architecture and Ocean Engineering*, 147:68–80, 1980.
- [98] Hochkirch, K. and Bertram, V. Engineering options for more fuel efficient ships. In *1st International Symposium on Fishing Vessel Energy Efficiency*, Vigo, Spain, 2010.
- [99] Hoerner, S. F. *Fluid-Dynamic Drag: Practical Information on Aerodynamic Drag and Hydrodynamic Resistance*. Hoerner Fluid Dynamics, Bakersfield, CA, USA, 2 edition, 1965.
- [100] Hofman, M. and Kozarski, V. Shallow water resistance charts for preliminary. *International Shipbuilding Progress*, 47(449):61–76, Jan. 2000.
- [101] Hollenbach, K. U. Estimating resistance and propulsion for single-screw and twin-screw ships in the preliminary design. In *10th International Conference on Computer Applications in Shipbuilding (ICCAS)*, volume 2, pages 237–250, Cambridge, Massachusetts, USA, June 1999.
- [102] Hollenbach, U. and Friesch, J. Efficient hull forms: What can be gained? In *1st International Conference on Ship Efficiency*, Hamburg, Germany, 2007.
- [103] Hollenbach, U. and Reinholz, O. Hydrodynamic trends in optimizing propulsion. In *2nd International Symposium on Marine Propulsors*, Hamburg, Germany, June 2011.
- [104] Holtrop, J. A statistical re-analysis of resistance and propulsion data. *International Shipbuilding Progress*, 31(363):272–276, 1984.
- [105] Holtrop, J. Extrapolation of propulsion tests for ships with appendages and complex propulsors. *Marine Technology*, 38(3):145–157, 2001.
- [106] Holtrop, J. and Mennen, G. G. J. A statistical power prediction method. *International Shipbuilding Progress*, 25:253–256, 1978.
- [107] Holtrop, J. and Mennen, G. G. J. An approximate power prediction method. *International Shipbuilding Progress*, 29(335):166–170, 1982.
- [108] Hooft, J. P. and Nienhuis, U. The prediction of the ship's manoeuvrability in the design stage. *SNAME Transactions*, 102:419–445, 1994.
- [109] Hwang, W., Jakobsen, B., Barr, R., Ankudinov, V., Fuller, N., Vest, L., Morris, M., McGovern, A., and Landsburg, A. An exploratory study to characterize ship manoeuvring performance at slow speed. In *International Conference on Marine Simulation and Ship Maneuverability (MARSIM '03)*, volume 3, Kanazawa, Japan, Aug. 2003.

- [110] Im, N. K. and Seo, J. H. Ship manoeuvring performance experiments using a free running model ship. *International Journal of Marine Navigation and Safety of Sea Transportation*, 4(1):29–33, Mar. 2010.
- [111] International Maritime Organization. Standards for Ship Manoeuvrability, 2002. Resolution MSC.137(76), adopted on December 4, 2002.
- [112] International Maritime Organization. Explanatory Notes to the Standards for Ship Manoeuvrability, 2002. MSC/Circ.1053, adopted on December 16, 2012.
- [113] International Maritime Organization. Amendments to the Annex of the Protocol of 1997 to Amend the International Convention for the Prevention of Pollution from Ships, 1973, as Modified by the Protocol of 1978 Relating Thereto, 2011. Resolution MEPC.203(62), adopted on July 16, 2011.
- [114] International Maritime Organization. SOLAS Consolidated Edition 2012: Consolidated Text of the International Convention for the Safety of Life at Sea, 1974, and its Protocol of 1988: Articles, Annexes and Certificates, 2012.
- [115] International Towing Tank Conference. ITTC Recommended Procedures and Guidelines 7.5-04-02-01: Full Scale Measurements Manoeuvrability Full Scale Manoeuvring Trials, 2002.
- [116] International Towing Tank Conference. ITTC Recommended Procedures and Guidelines 7.5-02-03-02.1: Testing and Extrapolation Methods Propulsion, Propulsor Open Water Test, 2008.
- [117] International Towing Tank Conference. ITTC Recommended Procedures and Guidelines 7.5-01-01-01: Ship Models, 2011.
- [118] ITTC Manoeuvring Committee. Final Report and Recommendations to the 25th ITTC. In *25th International Towing Tank Conference*, Fukuoka, Japan, 2008.
- [119] ITTC Manoeuvring Committee. Final Report and Recommendations to the 26th ITTC. In *26th International Towing Tank Conference*, pages 123–181, Rio de Janeiro, Brazil, 2011.
- [120] ITTC Manoeuvring Committee. Final Report and Recommendations to the 27th ITTC. In *27th International Towing Tank Conference*, volume 1, pages 128–194, Copenhagen, Denmark, 2014.
- [121] Jachowski, J. Assessment of ship squat in shallow water using CFD. *Archives of Civil and Mechanical Engineering*, 8(1):27–36, 2008.
- [122] Jurgens, A. J. Static and dynamic effects of rudder-hull-propeller interaction on fast monohulls. In *8th International conference on Fast Sea Transportation (FAST 2005)*, St. Petersburg, Russia, June 2005.
- [123] Kang, D. and Hasegawa, K. Prediction method of hydrodynamic forces acting on the hull of a blunt-body ship in the even keel condition. *Journal of Marine Science and Technology*, 12(1):1–14, 2007.

- [124] Kang, D., Nagarajan, V., Hasegawa, K., and Sano, M. Mathematical model of single-propeller twin-rudder ship. *Journal of Marine Science and Technology*, 13(3):207–222, 2008.
- [125] Kang, D., Nagarajan, V., Gonno, Y., Uematsu, Y., Hasegawa, K., and Shin, S. C. Installing single-propeller twin-rudder system with less asymmetric maneuvering motions. *Ocean Engineering*, 38:1184–1196, 2011.
- [126] Karim, M. M. and Ahmmed, M. S. Numerical study of periodic cavitating flow around NACA 0012 hydrofoil. *Ocean Engineering*, 55:81–87, 2012.
- [127] Kelecyc, F. J. Coupling momentum and continuity increases CFD robustness. *ANSYS Advantage*, 2(2):49–51, 2008.
- [128] Kervezee, I. Inland Waterway Transport in the Pearl River Basin. Technical report, Consulate-General of the Kingdom of the Netherlands in Guangzhou, Guangzhou, China, 2011.
- [129] Kerwin, J. E., Mandel, P., and Lewis, S. D. An experimental study of a series of flapped rudders. *Journal of Ship Research*, 16:221–239, Dec. 1972.
- [130] Kerwin, J. E., Lewis, S. D., and Oppenheim, B. W. Experiments on rudders with small flaps in free-stream and behind a propeller. Technical report, Cambridge, MA, USA, Oct. 1974.
- [131] Kerwin, J. W., Mandel, P., and Lewis, S. D. Hydrodynamic characteristics of flapped rudders. *Journal of Mechanical Engineering Science*, 14(7):142–149, 1972.
- [132] Khanfir, S., Hasegawa, K., Lee, S. K., Jang, T. S., Lee, J. H., and Cheon, S. J. Mathematical model for maneuverability and estimation of hydrodynamic coefficients of twin-propeller twin-rudder ship. In *The Japan Society of Naval Architects and Ocean Engineers*, number 7K, pages 57–60, Osaka, Japan, Nov. 2008. 2008K-G4-3.
- [133] Khanfir, S., Nagarajan, V., Hasegawa, K., and Lee, S. K. Estimation of mathematical model and its coefficients of ship manoeuvrability for a twin-propeller twin-rudder ship. In *International Conference on Marine Simulation and Ship Maneuverability (MARSIM '09)*, volume 8, pages 159–166, Panama City, Panama, 2009.
- [134] Khanfir, S., Hasegawa, K., Nagarajan, V., Shouji, K., and Lee, S. K. Manoeuvring characteristics of twin-rudder systems: Rudder-hull interaction effect on the manoeuvrability of twin-rudder ships. *Journal of Marine Science and Technology*, 2011(16): 472–490, 2011.
- [135] Kijima, K. and Nakiri, Y. On the practical prediction method for ship manoeuvrability in restricted water (in Japanese). *Journal of the Japan Society of Naval Architects and Ocean Engineers*, (107):37–54, 2004.
- [136] Kijima, K. and Qing, H. Manoeuvring motion of a ship in the proximity of bank wall. *Journal of the Society of Naval Architects of Japan*, 162:125–132, 1988.

- [137] Kijima, K. and Yasukawa, H. Manoeuvrability of ships in narrow waterway. *Journal of the Society of Naval Architects of Japan*, 23(3):25–37, 1985.
- [138] Kijima, K., Katsuno, T., Nakiri, Y., and Furukawa, Y. On the manoeuvring performance of a ship with the parameter of loading condition. *Journal of the Society of Naval Architects of Japan*, (168):141–148, Nov. 1990.
- [139] Kijima, K., Tanaka, S., Matsunga, M., and Hori, T. Manoeuvring characteristics of a ship in deep and shallow waters as a function of loading condition. In *2nd International Conference on Manoeuvring and Control of Marine Craft*, pages 73–86, Southampton, UK, July 1992.
- [140] Kim, H., Akimoto, H., and Islam, H. Estimation of the hydrodynamic derivatives by RANS simulation of planar motion mechanism test. *Ocean Engineering*, 108: 129–139, 2015.
- [141] Kim, H. C. and Moss, J. L. Research in Resistance and Propulsion, Part III: Blockage Correction in a Ship Model Towing Tank and Scale Effect on Propulsive Parameters. Technical report, University of Michigan, Michigan, USA, 1963.
- [142] Kim, H. J., Kim, S. H., Oh, J. K., and Seo, D. W. A proposal on standard rudder device design procedure by investigation of rudder design process at major Korean shipyards. *Journal of Marine Science and Technology*, 20(4):450–458, 2012.
- [143] Kim, J. H., Choi, J. E., Choi, B. J., and Chung, S. H. Twisted rudder for reducing fuel-oil consumption. *International Journal of Naval Architecture and Ocean Engineering*, 6(3):715–722, 2014.
- [144] Kim, Y. G., Kim, S. Y., Kim, H. T., Lee, S. W., and Yu, B. S. Prediction of the maneuverability of a large container ship with twin propellers and twin rudders. *Journal of Marine Science and Technology*, 12(3):130–138, 2007.
- [145] Koç, S. T., Yılmaz, S., Erdem, D., and Kavsaoğlu, M. Ş. Experimental Investigation of a Ducted Propeller. In *Proceedings of the 4th European Conference for Aerospace Sciences*, Saint Petersburg, Russia, July 2011.
- [146] Koh, K. K. and Yasukawa, H. Comparison study of a pusher-barge system in shallow water, medium shallow water and deep water conditions. *Ocean Engineering*, 46:9–17, 2012.
- [147] Koh, K. K., Yasukawa, H., and Hirata, N. Hydrodynamic derivatives investigation of unconventionally arranged pusher-barge systems. *Journal of Marine Science and Technology*, 13(3):256–268, 2008.
- [148] Koh, K. K., Yasukawa, H., and Hirata, N. Shallow water effect on turning motion of a pusher-barge system. In *4th Asia-Pacific Workshop on Marine Hydrodynamics*, volume 3, pages 16–18, Taipei, June 2008.

- [149] Koh, K. K., Yasukawa, H., Hirata, N., and Kose, K. Maneuvering simulations of pusher-barge systems. *Journal of Marine Science and Technology*, 13(2):117–126, 2008.
- [150] Kose, K., Yumuro, A., and Yoshimura, Y. Concrete of mathematical model for ship manoeuvring (in Japanese). In *3rd Symposium on Ship Manoeuvrability*, Society of Naval Architects, pages 27–80, 1981.
- [151] Kracht, A. M. Rudder in the slipstream of a propeller. In *International Symposium on Ship Resistance and Powering Performance*, pages 261–270, Shanghai, China, Apr. 1989.
- [152] Krasilnikov, V., Ponkratov, D., and Crepier, P. A numerical study on the characteristics of the system propeller and rudder at low speed operation. In *2nd International Symposium on Marine Propulsors*, Hamburg, Germany, June 2011.
- [153] Kristensen, H. O. and Lützen, M. Prediction of Resistance and Propulsion Power of Ships. Technical report, University of Southern Denmark and Technical University of Denmark, Denmark, Oct. 2012.
- [154] Kulczyk, J. Propeller-hull interaction in inland navigation vessel. *Transactions on the Built Environment*, 11:73–89, 1995.
- [155] Ladson, C. L. Effects of Independent Variation of Mach and Reynolds Numbers on the Low-Speed Aerodynamic Characteristics of the NACA 0012 Airfoil Section. Technical report, Langley Research Center, Hampton, Virginia, USA, 1988.
- [156] Ladson, C. L., Hill, A. S., and Sproles, D. Computer Program to Obtain Ordinates for NACA Airfoils. Technical Report NASA Technical Memorandum 4741, Langley Research Center, Hampton, Virginia, USA, Dec. 1996.
- [157] Landsburg, A. C., Barr, R. A., Daggett, L., Hwang, W. Y., Jakobsen, B., Morris, M., and Vest, L. Critical needs for ship maneuverability: Lessons from the Houston ship channel full-scale maneuvering trials. *Marine Technology*, 42(1):11–20, 2005.
- [158] Langley Research Center. Turbulence Modeling Resource. Accessed on September 10, 2014, retrieved from http://turbmodels.larc.nasa.gov/naca0012_val.html, 2014.
- [159] Lataire, E., Vantorre, M., and Delefortrie, G. Captive model testing for ship-to-ship operations. In *International Conference on Marine Simulation and Ship Maneuverability (MARSIM '09)*, Panama City, Panama, Aug. 2009.
- [160] Lataire, E., Vantorre, M., Vandenbroucke, J., and Eloot, K. Ship to ship interaction forces during lightering operations. In *2nd International Conference on Ship Manoeuvring in Shallow and Confined Water: Ship to Ship Interaction*, pages 211–221, Trondheim, Norway, May 2011.
- [161] Launder, B. E. and Spalding, D. B. The numerical computation of turbulent flows. *Computer Methods in Applied Mechanics and Engineering*, 3(2):269–289, 1974.

- [162] Lee, C. K. and Lee, S. G. On the ship manoeuvring characteristics in shallow water. *Transactions of The West-Japan Society of Naval Architects*, (109):135–142, 2005.
- [163] Lee, C. K. and Lee, S. G. Hydrodynamic forces between vessels and safe maneuvering under wind-effect in confined waters. *Journal of Mechanical Science and Technology*, 21(5):837–843, 2007.
- [164] Lee, C. K. and Lee, S. G. Investigation of ship maneuvering with hydrodynamic effects between ship and bank. *Journal of Mechanical Science and Technology*, 22(6):1230–1236, 2008.
- [165] Lee, H., Kinnas, S. A., Gu, H., and Natarajan, S. Numerical modeling of rudder sheet cavitation including propeller/rudder interaction and the effects of a tunnel. In *5th International Symposium on Cavitation*, Osaka, Japan, Nov. 2003.
- [166] Lee, H. Y. and Shin, S. S. The prediction of ship's manoeuvring performance in initial design stage. In *Practical Design of Ships and Other Floating Bodies Conference*, pages 633–639, The Hague, the Netherlands, 1998.
- [167] Lee, S. K. and Fujino, M. Assessment of a mathematical model for the manoeuvring motion of a twin-propeller twin-rudder ship. *International Shipbuilding Progress*, 50(1-2):109–123, 2003.
- [168] Lee, S. W., Toxopeus, S. L., and Quadvlieg, F. Free Sailing Manoeuvring Tests on KVLCC1 and KVLCC2. Technical report, Maritime Research Institute Netherlands (MARIN), Wageningen, the Netherlands, 2007.
- [169] Lehmann, D. Improved propulsion with tuned rudder systems. In *1st International Conference on Ship Efficiency*, Hamburg, Germany, 2007.
- [170] Lehmann, D. Station keeping with High-Performance Rudders. In *Dynamic Positioning Conference 2012*, Houston, USA, Oct. 2012.
- [171] Li, Y., Landsburg, A. C., Barr, R. A., and Calisal, S. M. Improving ship maneuverability standards as a means for increasing ship controllability and safety. In *MTS/IEEE OCEANS 2005*, pages 1972–1981, Washington, DC, USA, Sept. 2005.
- [172] Lima, D., Sutulo, S., and Soares, C. G. Study of ship-to-ship interaction in shallow water with account for squat phenomenon. In *3rd International Conference on Maritime Technology and Engineering (MARTECH 2016)*, pages 333–338, Lisbon, Portugal, July 2016.
- [173] Liu, J. and Hekkenberg, R. Hydrodynamic characteristics of twin-rudders at small attack angles. In *12th International Marine Design Conference (IMDC)*, pages 177–188, Tokyo, Japan, May 2015.
- [174] Liu, J. and Hekkenberg, R. Interaction effects on hydrodynamic characteristics of twin rudders. In *2016 International Conference on Maritime Technology (ICMT 2016)*, pages 1–7, Harbin, China, July 2016.

- [175] Liu, J. and Hekkenberg, R. 3D RANS simulations of shallow water effects on rudder hydrodynamic characteristics. In *2016 International Conference on Maritime Technology (ICMT 2016)*, pages 35–39, Harbin, China, July 2016.
- [176] Liu, J. and Hekkenberg, R. Suitable mesh properties for RANS analyses of aerofoils: A case study of ship rudders. *Submitted for journal publication*, 2016.
- [177] Liu, J. and Hekkenberg, R. Sixty years of research on ship rudders: Effects of design choices on rudder performance. *Ships and Offshore Structures*, pages 1–18, 2016.
- [178] Liu, J., Xu, Y., and Liu, M. Flow field simulation of bridge group area considering cross-bridge opening. In *International Conference on Marine Simulation and Ship Maneuverability (MARSIM '12)*, Singapore, 2012.
- [179] Liu, J., Hekkenberg, R., and Rotteveel, E. A proposal for standard manoeuvres and parameters for the evaluation of inland ship manoeuvrability. In *European Inland Waterway Navigation Conference*, Budapest, Hungary, Sept. 2014.
- [180] Liu, J., Hekkenberg, R., Rotteveel, E., and Hopman, H. Literature review on evaluation and prediction methods of inland vessel manoeuvrability. *Ocean Engineering*, 106:458–471, Sept. 2015.
- [181] Liu, J., Quadvlieg, F., and Hekkenberg, R. Impacts of rudder profiles on ship manoeuvrability. In *International Conference on Marine Simulation and Ship Maneuverability (MARSIM '15)*, Newcastle upon Tyne, UK, Sept. 2015.
- [182] Liu, J., Quadvlieg, F., and Hekkenberg, R. Impacts of the rudder profile on manoeuvring performance of ships. *Ocean Engineering*, 124:226–240, 2016.
- [183] Liu, J., Hekkenberg, R., Quadvlieg, F., and Hopman, H. An integrated empirical manoeuvring model for inland vessels. *Submitted for journal publication*, 2017.
- [184] Liu, J., Hekkenberg, R., Rotteveel, E., and Hopman, H. Hydrodynamic characteristics of multiple-rudder configurations. *Ships and Offshore Structures*, pages 1–19, 2017.
- [185] Lo, D. C. Numerical simulation of hydrodynamic interaction produced during the overtaking and the head-on encounter process of two ships. *Engineering Computations*, 29(1):83–101, 2012.
- [186] Loftin, L. K. and Smith, H. A. Aerodynamic Characteristics of 15 NACA Airfoil Sections at Seven Reynolds Numbers from 0.7×10^6 to 9.0×10^6 . Technical report, National Advisory Committee for Aeronautics, Washington, DC, USA, Oct. 1949.
- [187] Longo, J., Stern, F., and Toda, Y. Mean-flow measurements in the boundary layer and wake and wave field of a Series 60 CB = 0.6 ship model, Part 2: Scale effects on near-field wave patterns and comparisons with inviscid theory. *Journal of Ship Research*, 37(1):16–24, 1993.

- [188] Lübke, L. Investigation of a semi-balanced rudder. *Ship Technology Research*, 56 (2):69–86, 2009.
- [189] Luo, W. and Zhang, P. Evaluating the maneuverability of a new type of self-propelled barge. *Journal of Marine Science and Application*, 6(4):44–47, 2007.
- [190] Maimun, A., Priyanto, A., Muhammad, A. H., Scully, C. C., and Awal, Z. I. Manoeuvring prediction of pusher barge in deep and shallow water. *Ocean Engineering*, 38:1291–1299, 2011.
- [191] Mandel, P. *Ship Maneuvering and Control*. PhD thesis, Stevens Institute of Technology, 1967.
- [192] MARNET-CFD. Best Practice Guidelines for Marine Applications of Computational Fluid Dynamics. Accessed on December 3, 2014, retrieved from <https://pronet.atkinsglobal.com/marnet/guidelines/guide.html>, 2002.
- [193] Matsumoto, K. and Sueteru, K. The prediction of manoeuvring performances by captive model tests. *Journal of the Kansai Society of Naval Architects*, (176):11–22, 1980.
- [194] Matsunaga, M. Method of predicting ship manoeuvrability in deep and shallow waters as a function of loading condition. *Technical Bulletin of Nippon Kaiji Kyokai*, 11:51–59, 1993.
- [195] McCroskey, W. J. A Critical Assessment of Wind Tunnel Results for the NACA 0012 Airfoil. Technical report, National Aeronautics and Space Administration, Moffett Field, CA, USA, 1987.
- [196] Menter, F. R. Two-equation eddy-viscosity turbulence models for engineering applications. *AIAA journal*, 32(8):1598–1605, 1994.
- [197] Mewis, F. and Klug, H. The challenge of very large container ships: A hydrodynamic view. In Keil, H. and Lehmann, E., editors, *9th Symposium on Practical Design of Ships and Other Floating Structures*, pages 173–181, Luebeck Travemuende, Germany, Sept. 2004.
- [198] Minchev, A., Schmidt, M., and Schnack, S. Contemporary bulk carrier design to meet IMO EEDI Requirements. In Binns, J., Brown, R., and Bose, N., editors, *3rd International Symposium on Marine Propulsors*, pages 283–291, Launceston, Tasmania, Sept. 2013.
- [199] Ministry of Transport of the People’s Republic of China. Layout Planning of China Waterways and Ports (in Chinese). Accessed on November 20, 2015, retrieved from http://www.gov.cn/gzdt/2007-07/20/content_691664.htm, 2007.
- [200] Molland, A. F. The Free-Stream Characteristics of a Semi-Balanced Ship Skeg-Rudder. Technical report, University of Southampton, Southampton, UK, 1977.

- [201] Molland, A. F. Further Free-Stream Characteristics of Semi-Balanced Ship Skeg-Rudders. Technical report, University of Southampton, Southampton, UK, 1978.
- [202] Molland, A. F. and Turnock, S. R. Wind Tunnel Investigation of the Influence of Propeller Loading on Ship Rudder Performance. Technical report, University of Southampton, Southampton, UK, Mar. 1991.
- [203] Molland, A. F. and Turnock, S. R. Further Wind Tunnel Investigation of the Influence of Propeller Loading on Ship Rudder Performance. Technical report, University of Southampton, Southampton, UK, 1992.
- [204] Molland, A. F. and Turnock, S. R. Wind Tunnel Tests on the Influence of Propeller Loading on Ship Rudder Performance: Four Quadrant Operation, Low and Zero Speed Operation. Technical report, University of Southampton, Southampton, UK, 1993.
- [205] Molland, A. F. and Turnock, S. R. Flow straightening effects on a ship rudder due to upstream propeller and hull. *International Shipbuilding Progress*, 49(3):195–214, 2002.
- [206] Molland, A. F. and Turnock, S. R. *Marine Rudders and Control Surfaces: Principles, Data, Design and Applications*. Elsevier Butterworth-Heinemann, Oxford, UK, 1 edition, 2007.
- [207] Molland, A. F., Turnock, S. R., and Smithwick, J. E. T. Wind Tunnel Tests on the Influence of Propeller Loading and the Effect of a Ship Hull on Skeg-Rudder Performance. Technical report, University of Southampton, Southampton, UK, 1995.
- [208] Molland, A. F., Bahaj, A. S., Chaplin, J. R., and Batten, W. M. J. Measurements and predictions of forces, pressures and cavitation on 2-D sections suitable for marine current turbines. *Proceedings of the Institution of Mechanical Engineers, Part M: Journal of Engineering for the Maritime Environment*, 218(2):127–138, June 2004.
- [209] Morgan, W. B. and Lin, W. C. Predicting ship hydrodynamic performance in today's world. *Naval Engineers Journal*, 110:91–98, 1998.
- [210] Motora, S. On the measurement of added mass and added moments of inertia for ship motions (in Japanese). *Journal of the Society of Naval Architects of Japan*, 105: 83–89, 1959.
- [211] Motora, S. On the measurement of added mass and added moments of inertia for ship motions, Part 2: Added mass for the longitudinal motions (in Japanese). *Journal of the Society of Naval Architects of Japan*, 106:59–62, 1960.
- [212] Motora, S. On the measurement of added mass and added moments of inertia for ship motions, Part 3: Added mass for the transverse motions (in Japanese). *Journal of the Society of Naval Architects of Japan*, 106:63–68, 1960.

- [213] Nagarajan, V., Kang, D. H., Hasegawa, K., and Nabeshima, K. Comparison of the mariner Schilling rudder and the mariner rudder for VLCCs in strong winds. *Journal of Marine Science and Technology*, 13:24–39, 2008.
- [214] Nagarajan, V., Kang, D. H., Hasegawa, K., Nabeshima, K., and Ariei, T. A proposal for propulsion performance prediction of a single-propeller twin-rudder ship. *Journal of Marine Science and Technology*, 14:296–309, 2009.
- [215] Nakatake, K., Ando, J., Kataoka, K., Sato, T., and Yamaguchi, K. Study on the propulsive performance of twin screw ship: Interaction between propeller and rudder in a uniform flow (in Japanese). *Transactions of The West-Japan Society of Naval Architects*, 78:49–57, 1989.
- [216] Nienhuis, U. Passieve Manoeuvrerhulpmiddelen: Open Water Proeven met Roer (in Dutch). Technical report, Maritime Research Institute Netherlands (MARIN), Wageningen, the Netherlands, July 1987.
- [217] Nobukawa, T., Kato, T., Motomura, K., and Yoshimura, Y. Studies on manoeuvrability standards from the viewpoint of marine pilots. In *International Conference on Marine Simulation and Ship Maneuverability (MARSIM '90)*, Tokyo, Japan, June 1990.
- [218] Norrbin, N. H. Theory and observation on the use of a mathematical model for ship maneuvering in deep and confined waters. In *8th Symposium on Naval Hydrodynamics*, pages 807–904, Pasadena, California, 1970.
- [219] Ogawa, A. and Kasai, H. On the mathematical model of manoeuvring motion of ships. *International Shipbuilding Progress*, 25(292):306–319, Dec. 1978.
- [220] Oh, H. W. *Advanced Fluid Dynamics*. InTech, 2012.
- [221] Olson, C. R. Effects of Various Linkage Ratios on the Free-Stream Hydrodynamic Characteristics of an All-Movable Flapped Rudder. Technical report, David Taylor Model Basin, Washington, DC, USA, Sept. 1955.
- [222] Oltmann, P. On the influence of speed on the manoeuvring behaviour of a container carrier. In *International Conference on Marine Simulation and Ship Maneuverability (MARSIM '96)*, pages 515–523, Copenhagen, Denmark, Sept. 1996.
- [223] Oltmann, P. and Sharma, S. D. Simulation of combined engine and rudder maneuvers using an improved model of hull-propeller-rudder interactions. In *15th Symposium on Naval Hydrodynamics*, pages 1–24, Hamburg, Germany, 1984.
- [224] Oppenheim, B. W. A Theoretical and Experimental Investigation of the Performance of Flapped Rudders. Master thesis, Massachusetts Institute of Technology, 1974.
- [225] Oyan, E. Speed and Powering Prediction for Ships Based on Model Testing. Master thesis, Norwegian University of Science and Technology, Nov. 2012.

- [226] Pelletier, A. and Mueller, T. J. Low Reynolds Number aerodynamics of low-aspect-ratio, thin/flat/cambered-plate wings. *Journal of Aircraft*, 37(5):825–832, 2000.
- [227] Pérez, F. L. and Clemente, J. A. The influence of some ship parameters on manoeuvrability studied at the design stage. *Ocean Engineering*, 34:518–525, 2007.
- [228] Quadvlieg, F. Mathematical models for the prediction of manoeuvres of inland ships: Does the ship fit in the river? In Rigo, P. and Wolters, M., editors, *Smart Rivers 2013*, pages 1871–1879, Liège, Belgium/Maastricht, the Netherlands, Sept. 2013. PIANC.
- [229] Quadvlieg, F. Theoretische Berekening van Simulatiemodellen voor Binnenvaartschepen ten Behoeve van Maatgevende Manoeuvres (in Dutch). Technical report, Maritime Research Institute Netherlands (MARIN), Wageningen, the Netherlands, 2013.
- [230] Quadvlieg, F. and Brouwer, J. KVLCC2 benchmark data including uncertainty analysis to support manoeuvring predictions. In *4th International Conference on Computational Methods in Marine Engineering (MARINE 2011)*, Lisbon, Portugal, 2011.
- [231] Quadvlieg, F. and Van Coevorden, P. Manoeuvring criteria: More than IMO A751 requirements alone! In *International Conference on Marine Simulation and Ship Maneuverability (MARSIM '03)*, volume 2, pages 1–8, Kanazawa, Japan, Aug. 2003.
- [232] Quérard, A., Temarel, P., and Turnock, S. R. Influence of viscous effects on the hydrodynamics of ship-like sections undergoing symmetric and anti-symmetric motions using RANS. In *ASME 2008 27th International Conference on Offshore Mechanics and Arctic Engineering*, volume 5, pages 683–692, Estoril, Portugal, 2008.
- [233] Ram, B. R. R., Surendran, S., and Lee, S. K. Computer and experimental simulations on the fin effect on ship resistance. *Ships and Offshore Structures*, 10(2):121–131, May 2015.
- [234] Reichel, M. Influence of rudder location on propulsive characteristics of a single screw container ship. In Koushan, K. and Steen, S., editors, *1st International Symposium on Marine Propulsors*, pages 1–6, Trondheim, Norway, 2009. Norwegian Marine Technology Research Institute (MARINTEK).
- [235] Rhee, S. H., Lee, C., Lee, H. B., and Oh, J. Rudder gap cavitation: Fundamental understanding and its suppression devices. *International Journal of Heat and Fluid Flow*, 31(4):640–650, 2010.
- [236] Rigo, P. and Wolters, M. PIANC - SMART Rivers Conference 2013. In Rigo, P. and Wolters, M., editors, *PIANC - SMART Rivers Conference 2013*, Liège, Belgium and Maastricht, the Netherlands, Sept. 2013. PIANC.
- [237] Rijkswaterstaat. Waterway Guidelines 2011, Dec. 2011.
- [238] Rijkswaterstaat. Supplement Rchtlijnen Vaarwegen 2011 (in Dutch), Nov. 2013.

- [239] Rotteveel, E. Investigation of Inland Ship Resistance, Propulsion and Manoeuvring Using Literature Study and Potential Flow Calculations. Master thesis, Delft University of Technology, Sept. 2013.
- [240] Rotteveel, E., Hekkenberg, R., and Liu, J. Design guidelines and empirical evaluation tools for inland ships. In *European Inland Waterway Navigation Conference*, Budapest, Hungary, Sept. 2014.
- [241] Sarasquete, A., Collazo, A. C., Coache, S., Meis, M., and Ruiz, V. Increased energy efficiency of the fishing fleet due to improved hydrodynamic performance. In *2nd International Symposium on Fishing Vessel Energy Efficiency*, Vigo, Spain, May 2012.
- [242] Sathaye, S. S. Lift Distributions on Low Aspect Ratio Wings at Low Reynolds Numbers. Master thesis, Worcester, MA, USA, 2004.
- [243] Schilling, K. Rudder Control Arrangement. United States Patent Office, 3,101,693, Aug. 1963.
- [244] Schilling, K. and Rathert, H. Dual Rudder Assembly. United States Patent Office, 4,085,694, Apr. 1978.
- [245] Schneekluth, H. and Bertram, V. *Ship Design for Efficiency and Economy*. Elsevier Butterworth-Heinemann, Oxford, UK, 2 edition, 1998.
- [246] Shen, Y. T., Jiang, C. W., and Remmers, K. D. A twisted rudder for reduced cavitation. *Journal of Ship Research*, 41(4):260–272, 1997.
- [247] Shen, Y. T., Remmers, K. D., and Jiang, C. W. Effects of ship hull and propeller on rudder cavitation. *Journal of Ship Research*, 41(3):172–180, Sept. 1997.
- [248] Sheno, R. R., Krishnankutty, P., and Selvam, R. P. Study of manoeuvrability of container ship by static and dynamic simulations using a RANSE-based solver. *Ships and Offshore Structures*, pages 1–19, 2014.
- [249] Shih, T. H., Liou, W. W., Shabbir, A., Yang, Z., and Zhu, J. A new $k-\epsilon$ eddy viscosity model for high Reynolds number turbulent flows. *Computers & Fluids*, 24(3):227–238, 1995.
- [250] Söding, H. Prediction of ship steering capabilities. *Schiffstechnik*, 29(1):3–29, 1982.
- [251] Spalart, P. R. and Allmaras, S. R. A one equation turbulence model for aerodynamic flows. *Recherche Aerospaciale*, (1):5–21, 1994.
- [252] Spyrou, K. J. A general model of ship manoeuvrability assessment based on decisions' analysis, and its practical application. *Journal of the Society of Naval Architects of Japan*, 176:267–280, 1994.
- [253] Stern, F., Wilson, R. V., Coleman, H. W., and Paterson, E. G. Verification and Validation of CFD Simulations. Technical report, Iowa Institute of Hydraulic Research, Iowa City, USA, Sept. 1999.

- [254] Stern, F., Wilson, R. V., Coleman, H. W., and Paterson, E. G. Comprehensive approach to verification and validation of CFD simulations, Part I: Methodology and procedures. *Journal of Fluids Engineering*, 123:793–802, Dec. 2001.
- [255] Stierman, E. J. The influence of the rudder on the propulsive performance of ships, Part I. *International Shipbuilding Progress*, 36(407):303–334, 1989.
- [256] Stierman, E. J. The influence of the rudder on the propulsive performance of ships, Part II. *International Shipbuilding Progress*, 36(407):303–334, 1989.
- [257] Strom Tejsen, J. and Chislett, M. S. A Model Testing Technique and Method of Analysis for the Prediction of Steering and Manoeuvring Qualities of Surface Vessels. Technical report, Hydro and Aerodynamics Lab, Washington, DC, USA, 1966.
- [258] Stuck, A., Turnock, S., and Bressloff, N. An Evaluation of the RANS Method for the Prediction of Steady Ship Rudder Performance Compared to Wind Tunnel Measurements. Technical report, University of Southampton, Southampton, UK, 2004.
- [259] Surendran, S. and Kiran, V. Technical note Studies on the feasibilities of control of ship roll using fins. *Ships and Offshore Structures*, 1(4):357–365, 2006.
- [260] Surendran, S. and Kiran, V. Control of ship roll motion by active fins using fuzzy logic. *Ships and Offshore Structures*, 2(1):11–20, 2007.
- [261] Tabaczek, T. Numerical simulation of planar motion of a twin-screw inland waterway vessel in shallow water. In *18th International Conference on Hydrodynamics in Ship Design, Safety and Operation*, pages 37–50, Gdansk, Poland, May 2010.
- [262] Tabaczek, T., Kulczyk, J., and Zawiślak, M. Analysis of hull resistance of pushed barges in shallow water. *Polish Maritime Research*, 14:10–15, 2007.
- [263] Takekoshi, Y., Kawamura, T., Yamaguchi, H., Maeda, M., Ishii, N., Kimura, K., Taketani, T., and Fujii, A. Study on the design of propeller blade sections using the optimization algorithm. *Journal of Marine Science and Technology*, 10(2):70–81, 2005.
- [264] Tamura, K. Study on the blockage correction. *Journal of the Society of Naval Architects of Japan*, (131):17–28, 1972.
- [265] Tang, L. Reynolds-Averaged Navier-Stokes simulation of low-Reynolds-number airfoil aerodynamics. *Journal of Aircraft*, 45(3):848–856, 2008.
- [266] Tezdogan, T., Demirel, Y. K., Kellett, P., Khorasanchi, M., Incecik, A., and Turan, O. Full-scale unsteady RANS CFD simulations of ship behaviour and performance in head seas due to slow steaming. *Ocean Engineering*, 97:186–206, 2015.
- [267] Thieme, H. Design of Ship Rudders (Zur Formgebung von Schiffsrudern). Technical report, Shipbuilding Institute, University of Hamburg, Washington, DC, USA, 1965.

- [268] Timmer, W. A. Aerodynamic characteristics of wind turbine blade airfoils at high angles-of-attack. In *3rd EWEA Conference-Torque 2010: The Science of making Torque from Wind*, pages 71–78, Heraklion, Crete, Greece, June 2010.
- [269] Toda, Y., Stern, F., and Longo, J. Mean-flow measurements in the boundary layer and wake and wave field of a Series 60 CB = 0.6 ship model, Part 1: Froude numbers 0.16 and 0.316. *Journal of Ship Research*, 36(4):360–378, 1992.
- [270] Todd, F. H. Some further experiments on single screw merchant ship forms - Series 60. *SNAME Transactions*, 61, 1953.
- [271] Todd, F. H. Series 60 Methodical Experiments with Models of Single-Screw Merchant Ships. Technical report, David Taylor Model Basin, Washington, USA, July 1963.
- [272] Torres, G. E. and Mueller, T. J. Low-aspect-ratio wing aerodynamics at low Reynolds Numbers. *AIAA Journal*, 42(5):865–878, 2004.
- [273] Toxopeus, S. *Practical Application of Viscous-Flow Calculations for the Simulation of Manoeuvring Ships*. PhD thesis, Delft University of Technology, 2011.
- [274] Tuck, E. O. and Taylor, P. J. Shallow water problems in ship hydrodynamics. In *8th Symposium on Naval Hydrodynamics*, pages 627–659, Washington, DC, USA, 1970.
- [275] Turnock, S. R. *Prediction of Ship Rudder-Propeller Interaction Using Parallel Computations and Wind Tunnel Measurements*. PhD thesis, University of Southampton, 1993.
- [276] Tyagi, A. and Sen, D. Calculation of transverse hydrodynamic coefficients using computational fluid dynamic approach. *Ocean Engineering*, 33:798–809, 2006.
- [277] Ueno, M. and Tsukada, Y. Rudder effectiveness and speed correction for scale model ship testing. *Ocean Engineering*, 109:495–506, 2015.
- [278] Ueno, M., Tsukada, Y., and Kitagawa, Y. Rudder effectiveness correction for scale model ship testing. *Ocean Engineering*, 92:267–284, 2014.
- [279] Van Beek, T. Technology guidelines for efficient design and operation of ship propulsors. *Marine News, Wärtsillä Propulsion, Netherlands BV*, 1:14–19, 2004.
- [280] Van Leeuwen, G. and Journée, J. M. J. Prediction of Ship Manoeuvrability Making Use of Model Tests. Technical report, Ship Hydromechanics Laboratory, Delft University of Technology, Delft, the Netherlands, Apr. 1970.
- [281] Van Nguyen, T. and Ikeda, Y. Hydrodynamic characteristic of rudder sections with high lift force. *Journal of the Japan Society of Naval Architects and Ocean Engineers*, (19):403–406, 2013.
- [282] Van Nguyen, T. and Ikeda, Y. Development of fishtail rudder sections with higher maximum lift coefficients. In *24th International Ocean and Polar Engineering Conference*, pages 940–947, Busan, Korea, 2014.

- [283] Van Nguyen, T. and Ikeda, Y. Hydrodynamic characteristic of rudder sections with high lift force, Part 2: The wedge tail shapes. *Journal of the Japan Society of Naval Architects and Ocean Engineers*, (18):171–174, 2014.
- [284] Van Nguyen, T. and Ikeda, Y. Hydrodynamic characteristic of rudder sections with high lift force, Part 3: The trailing edge with flat plate. *Journal of the Japan Society of Naval Architects and Ocean Engineers*, (18):171–174, 2014.
- [285] Van Nguyen, T. and Ikeda, Y. Development of marine high lift performance rudders with wedge tails: Effect of reynolds number on hydrodynamic forces. In *International Conference on Transportation Mechanical Engineering and Sustainable Development*, Danang, Vietnam, Sept. 2015.
- [286] Vantorre, M. Accuracy and optimization of captive ship model tests. In *PRADS '92: 5th International Symposium on Practical Design of Ships and Mobile Units*, volume 1, pages 190–203, Newcastle, UK, May 1992.
- [287] Vantorre, M. Stationary and non-stationary open water rudder tests. In Kijima, K., editor, *Mini Symposium on Prediction of Ship Manoeuvring Performance*, pages 103–111, Tokyo, Japan, Oct. 2001.
- [288] Vantorre, M. Review of practical methods for assessing shallow and restricted water effects. In *International Conference on Marine Simulation and Ship Maneuverability (MARSIM '03)*, pages 1–11, Kanazawa, Japan, Aug. 2003.
- [289] Vantorre, M. and Eloot, K. Requirements for standard harmonic captive manoeuvring tests. *Control Engineering Practice*, 6:643–652, 1998.
- [290] Vantorre, M., Verzhbitskaya, E., and Laforce, E. Model test based formulations of ship-ship interaction forces. *Ship Technology Research*, 49:124–141, 2002.
- [291] Vantorre, M., Delefortrie, G., Eloot, K., and Laforce, E. Experimental investigation of ship-bank interaction forces. In *International Conference on Marine Simulation and Ship Maneuverability (MARSIM '03)*, pages 1–9, Kanazawa, Japan, Aug. 2003.
- [292] Versteeg, H. K. and Malalasekera, W. *An Introduction to Computational Fluid Dynamics: The Finite Volume Method*. Pearson Education, 2 edition, 2007.
- [293] Wang, H. Z. and Zou, Z. J. Numerical study on hydrodynamic interaction between a berthed ship and a ship passing through a lock. *Ocean Engineering*, 88:409–425, 2014.
- [294] Wasberg, C. E. and Reif, B. A. P. Hydrodynamical Simulations in Fluent. Technical report, Norwegian Defence Research Establishment (FFI), Kjeller, Norway, Apr. 2010.
- [295] Whicker, L. F. and Fehlner, L. F. Free-Stream Characteristics of a Family of Low-Aspect-Ratio, All-Movable Control Surfaces for Application to Ship Design. Technical report, David Taylor Model Basin, Washington, DC, USA, 1958.

- [296] Wilcox, D. C. Reassessment of the scale-determining equation for advanced turbulence models. *AIAA journal*, 26(11):1299–1310, 1988.
- [297] Wilcox, D. C. Formulation of the kw turbulence model revisited. *AIAA journal*, 46(11):2823–2838, 2008.
- [298] Wilson, R. V., Stern, F., Coleman, H. W., and Paterson, E. G. Comprehensive approach to verification and validation of CFD simulations, Part 2: Application for RANS simulation of a cargo/container ship. *Journal of Fluids Engineering*, 123: 803, Dec. 2001.
- [299] World Wide Inland Navigation Network. China Inland Waterways. Accessed on November 25, 2015, retrieved from <http://www.w Winn.org/china-inland-waterways>, 2015.
- [300] World Wide Inland Navigation Network. USA Inland Waterways. Accessed on November 25, 2015, retrieved from <http://www.w Winn.org/us-inland-waterways>, 2015.
- [301] Yakhot, V., Orszag, S. A., Thangam, S., Gatski, T. B., and Speziale, C. G. Development of turbulence models for shear flows by a double expansion technique. *Physics of Fluids A: Fluid Dynamics*, 4(7):1510–1520, 1992.
- [302] Yang, H., Lee, J., and Kim, K. Numerical and Experimental study on the rudder force of a twisted rudder. In *International Conference on Marine Simulation and Ship Maneuverability (MARSIM '15)*, Newcastle upon Tyne, UK, Sept. 2015.
- [303] Yasukawa, H. and Kobayashi, E. Shallow water model experiments on ship turning performance. In *Mini Symposium on Ship Manoeuvrability*, pages 72–83, Fukuoka, Japan, May 1995.
- [304] Yasukawa, H. and Yoshimura, Y. Introduction of MMG standard method for ship maneuvering predictions. *Journal of Marine Science and Technology*, 20(1):37–52, 2014.
- [305] Yılmaz, S., Erdem, D., and Kavsaoğlu, M. Ş. Effects of duct shape on a ducted propeller performance. In *51st AIAA Aerospace Sciences Meeting including the New Horizons Forum and Aerospace Exposition*, pages 1–11, Grapevine, Texas, USA, Jan. 2013.
- [306] Yoo, W. J., Yoo, B. Y., and Rhee, K. P. An experimental study on the maneuvering characteristics of a twin propeller/twin rudder ship during berthing and unberthing. *Ships and Offshore Structures*, 1(3):191–198, 2006.
- [307] Yoon, H. K. and Rhee, K. P. Identification of hydrodynamic coefficients in ship maneuvering equations of motion by estimation-before-modeling technique. *Ocean Engineering*, 30:2379–2404, 2003.

- [308] Yoon, H. K., Son, N. S., and Lee, G. J. Estimation of the roll hydrodynamic moment model of a ship by using the system identification method and the free running model test. *IEEE Journal of Oceanic Engineering*, 32(4):798–806, 2007.
- [309] Yoshimura, Y. Mathematical model for the manoeuvring ship motion in shallow water (in Japanese). *Journal of the Kansai Society of Naval Architects, Japan*, (200): 41–51, 1986.
- [310] Yoshimura, Y. Mathematical model for the manoeuvring ship motion in shallow water (2nd report): Mathematical model at slow forward speed. *Journal of the Japan Society of Naval Architects and Ocean Engineers*, pages 77–84, 1988.
- [311] Yoshimura, Y. Mathematical model for manoeuvring ship motion (MMG Model). In *Workshop on Mathematical Models for Operations Involving Ship-Ship Interaction*, pages 1–6, Tokyo, Japan, Aug. 2005.
- [312] Yoshimura, Y. and Ma, N. Manoeuvring prediction of fishing vessels. In *International Conference on Marine Simulation and Ship Maneuverability (MARSIM '03)*, Kanazawa, Japan, Aug. 2003.
- [313] Yoshimura, Y. and Masumoto, Y. Hydrodynamic database and maneuvering prediction method with medium high-speed merchant ships and fishing vessels. In *International Conference on Marine Simulation and Ship Maneuverability (MARSIM '12)*, Singapore, Apr. 2012.
- [314] Yoshimura, Y. and Sakurai, H. Mathematical model for the manoeuvring ship motion in shallow water (3rd report): Manoeuvrability of a twin-propeller twin-rudder ship. *Journal of the Kansai Society of Naval Architects, Japan*, 211:115–126, Mar. 1989.
- [315] Yoshimura, Y., Kose, K., and Hiraguchi, T. Criteria for yaw-checking and course-keeping abilities in IMO's interim standards for ship manoeuvrability. In *International Conference on Marine Simulation and Ship Maneuverability (MARSIM '00)*, pages 389–400, Orlando, USA, 2000.
- [316] Zhang, X. G. and Zou, Z. J. Identification of Abkowitz model for ship manoeuvring motion using ϵ -support vector regression. *Journal of Hydrodynamics*, 23(3):353–360, 2011.
- [317] Zhou, Z., Yan, S., and Feng, W. Manoeuvring prediction of multiple-purpose cargo ships (in Chinese). *Ship Engineering*, 6:21–36, 1983.
- [318] Zou, L. and Larsson, L. Computational Fluid Dynamics (CFD) prediction of bank effects including verification and validation. *Journal of Marine Science and Technology*, 18(3):310–323, 2013.

Curriculum Vitae

Jialun Liu was born on March 23, 1987, in Fushun, Liaoning, China. From 2006 to 2010, he studied at Wuhan University of Technology, Wuhan, China, specialising in Navigation Technology. From 2008 to 2010, he minored in Japanese at Huazhong University of Science and Technology, Wuhan, China. He obtained his BSc and BA degrees in 2010. After that, he was then recommended to continue master education at Wuhan University of Technology in Traffic Engineering and Control. In 2012, he was founded by China Scholarship Council and started his PhD research at Delft University of Technology, Delft, the Netherlands. In 2013, he received his MSc degree.

From 2012 to 2017, Jialun Liu worked at the section of Ship Design, Operation, and Production in the department of Marine and Transportation Technology. His PhD project, which is presented in this thesis, is about the impacts of rudder configurations on inland vessel manoeuvrability. He used Computational Fluid Dynamic (CFD) methods to study the hydrodynamic characteristics of different rudder configurations and applied these CFD results to build an integrated mathematical model for inland vessel manoeuvring studies. His research interests include ship manoeuvrability, rudder design, autonomous ships, and CFD applications in maritime engineering. His publications during PhD are as follows:

13. **Jialun Liu**, Robert Hekkenberg, Frans Quadvlieg, Hans Hopman, Bingqian Zhao, 2016. [An integrated empirical manoeuvring model for inland vessels](#). *Submitted for journal publication*.
12. **Jialun Liu**, Robert Hekkenberg, Erik Rotteveel, Hans Hopman, 2017. [Hydrodynamic characteristics of multiple-rudder configurations](#). *Ships and Offshore Structures*.
11. **Jialun Liu**, Robert Hekkenberg, 2016. [Suitable mesh properties for RANS analyses of aerofoils: A case study of ship rudders](#). *Submitted for journal publication*.
10. **Jialun Liu**, Frans Quadvlieg, Robert Hekkenberg, 2016. [Impacts of rudder profiles on manoeuvring performance of ships](#). *Ocean Engineering* 124, pp. 226-240.
9. **Jialun Liu**, Robert Hekkenberg, 2016. [Sixty years of research on ship rudders: Effects of design choices on rudder performance](#). *Ships and Offshore Structures*, pp. 1-18.
8. **Jialun Liu**, Robert Hekkenberg, 16-18 July, 2016. [Interaction effects on hydrodynamic characteristics of twin rudders](#), in *2016 International Conference on Maritime Technology (ICMT 2016)*. Harbin, China, pp. 1-7.
7. **Jialun Liu**, Robert Hekkenberg, 16-18 July, 2016. [3D RANS simulations of shallow-water effects on rudder hydrodynamic characteristics](#), in *2016 International Conference on Maritime Technology (ICMT 2016)*. Harbin, China, pp. 35-39.

6. Robert Hekkenberg, **Jialun Liu**, 2016. [Developments in inland waterway vessels](#). in Bart Wiegman and Rob Konings (Ed.), *Inland Waterway Transport: Challenges and Prospects*. No. 6 in Routledge Studies in Transport Analysis. Taylor & Francis, Ch. 7, pp. 142-167.
5. **Jialun Liu**, Frans Quadvlieg, Robert Hekkenberg, 8-11 September, 2015. [Impacts of rudder profiles on ship manoeuvrability](#), in *International Conference on Marine Simulation and Ship Manoeuvrability (MARSIM'15)*. Newcastle upon Tyne, UK.
4. **Jialun Liu**, Robert Hekkenberg, Erik Rotteveel, Hans Hopman, 2015. [Literature review on evaluation and prediction methods of inland vessel manoeuvrability](#). *Ocean Engineering*, 106, pp. 458-471.
3. **Jialun Liu**, Robert Hekkenberg, 11-14 May, 2015. [Hydrodynamic characteristics of twin-rudders at small attack angles](#), in *The 12th International Marine Design Conference (IMDC)*. Tokyo, Japan, pp. 177-188.
2. **Jialun Liu**, Robert Hekkenberg, Erik Rotteveel, 10-12 September, 2014. [A proposal for standard manoeuvres and parameters for the evaluation of inland vessel manoeuvrability](#), in *European Inland Waterway Navigation Conference (EIWN)*. Budapest, Hungary.
1. Erik Rotteveel, Robert Hekkenberg, **Jialun Liu**, 10-12 September, 2014. [Design guidelines and empirical evaluation tools for inland vessels](#), in *European Inland Waterway Navigation Conference (EIWN)*. Budapest, Hungary.